

THESE
c.1



28226945



This is to certify that the

dissertation entitled

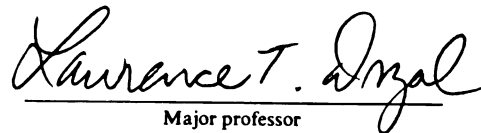
THE INFLUENCE OF PROCESSING, CHEMISTRY,
AND INTERPHASE MICROSTRUCTURE ON THE
ADHESION OF CARBON FIBERS TO THERMOSET
AND THERMOPLASTIC MATRICES

presented by

MARK CORNELL WATERBURY

has been accepted towards fulfillment
of the requirements for

PH.D degree in MATERIALS SCIENCE



Major professor

Date AUGUST 7, 1991

**PLACE IN RETURN BOX to remove this checkout from your record.
TO AVOID FINES return on or before date due.**

DATE DUE	DATE DUE	DATE DUE
MAY 2 1995	_____	_____
_____	_____	_____
_____	_____	_____
_____	_____	_____
_____	_____	_____
_____	_____	_____
_____	_____	_____

MSU Is An Affirmative Action/Equal Opportunity Institution

c:\crl\data\due.pm3-p.1

**THE INFLUENCE OF PROCESSING, CHEMISTRY, AND INTERPHASE
MICROSTRUCTURE ON THE ADHESION OF CARBON FIBERS
TO THERMOSET AND THERMOPLASTIC MATRICES**

By

Mark Cornell Waterbury

A DISSERTATION

**Submitted to
Michigan State University
in partial fulfillment of the requirements
for the degree of**

DOCTOR OF PHILOSOPHY

Department of Metallurgy, Mechanics, and Materials Science

1991

ABSTRACT

THE INFLUENCE OF PROCESSING, CHEMISTRY, AND INTERPHASE MICROSTRUCTURE ON THE ADHESION OF CARBON FIBERS TO THERMOSET AND THERMOPLASTIC MATRICES

By

Mark Cornell Waterbury

The adhesion of surface treated PAN-based carbon fibers to DGEBA epoxy, a thermoset polymer, BPA-polycarbonate, an amorphous thermoplastic, and Nylon 6,6, a semicrystalline thermoplastic was investigated with an integrated set of surface analysis and mechanical tests. Intermediate modulus Hercules IM6 carbon fibers with different amounts of electrochemical oxidative surface treatment were subjected to XPS surface composition analysis and micro-Wilhelmy surface energy measurements, and, along with treated and sized fibers, single fiber fragmentation tests, interlaminar shear, transverse flexural, and mode II fracture toughness tests.

Increasing surface treatment increased surface oxygen, polar surface free energy, and interfacial shear strength. Mode II fracture toughness increased with increasing treatment, and with sizing. Interlaminar shear and transverse flexural strengths increased with initial surface treatment, but leveled off as treatment proceeded.

Carbon fiber adhesion to thermoplastic matrices was investigated with the single fiber fragmentation test, and by observation of the failure modes by polarized light microscope for amorphous polycarbonate, and by Confocal Scanning Optical Microscopy (CSOM) for semicrystalline Nylon 6,6. Polycarbonate specimens were fabricated by solvent deposition and by hot pressing, Nylon 6,6 specimens by hot pressing.

Carbon fiber adhesion to Lexan was found to reach a limiting value, regardless of processing. Solvent deposition specimens showed very poor adhesion. Pure

Mark Cornell Waterbury

polycarbonate specimens showed adhesion increasing with consolidation time and temperature.

Carbon fiber adhesion to Nylon 6,6 increased with development of a transcrystalline sheath and with fiber surface treatment. CSOM observations of fragmentation specimens revealed radial matrix cracks that interacted with the interphase and spherulitic microstructure.

An experimental method was developed to measure fiber volume fractions in unidirectional composites by an image analysis technique, Optical Numeric Volume Fraction Analysis (ONVfA). An In Situ Fiber Strength test (ISFS) was developed to accurately measure the strengths of fibers at short gage lengths, in situ.

An analysis of the single fiber fragmentation process was performed, failure modes were discussed, and reproducible parameters associated with interfacial properties were identified.

DEDICATION

To all who came before, for all who will follow.

TABLE OF CONTENTS

LIST OF TABLES		x
LIST OF FIGURES		xi
1.0	THE INFLUENCE OF THE FIBER-MATRIX INTERFACE ON THE PROPERTIES OF FIBER REINFORCED COMPOSITE	1
1.1	<u>SYNOPSIS</u>	1
1.2	<u>INTRODUCTION</u>	1
1.3	<u>COMPOSITE PERFORMANCE AND INTERFACE PROPERTIES</u> ..	2
1.4	<u>CHEMISTRY OF THE FIBER/MATRIX INTERFACE</u>	3
1.5	<u>MATERIALS SCIENCE OF THE FIBER/MATRIX INTERFACE</u> ..	4
1.5.1	SCALE EFFECTS ON INTERPHASE PROPERTIES	5
1.5.2	CONSTRAINT EFFECTS ON INTERPHASE PROPERTIES	5
1.5.3	MICROSTRUCTURAL EFFECTS ON INTERPHASE PROPERTIES .	6
1.6	<u>EXPERIMENTAL PROGRAM OVERVIEW</u>	7
1.6.1	ANALYSIS OF THE FRAGMENTATION TEST	8
1.6.2	IN SITU FIBER STRENGTH TESTING	8
1.6.3	OPTICAL NUMERIC VOLUME FRACTION ANALYSIS	9
1.6.4	FIBER SURFACE TREATMENT EFFECTS ON IM6/EPOXY	10
1.6.5	AMORPHOUS THERMOPLASTIC, BPA-POLYCARBONATE	11
1.6.6	SEMICRYSTALLINE THERMOPLASTIC, NYLON 6,6	12
2.0	ON THE ACQUISITION AND INTERPRETATION OF INFORMATION FROM THE SINGLE FIBER FRAGMENTATION INTERFACIAL SHEAR STRENGTH TEST	14
2.1	<u>FRAGMENTATION TEST SYNOPSIS</u>	14
2.2	<u>FRAGMENTATION TEST INTRODUCTION</u>	14
2.3	<u>OVERVIEW OF THE SINGLE FIBER FRAGMENTATION TEST</u> ..	15
2.4	<u>FRAGMENTATION TEST FAILURE MODES</u>	20
2.4.1	INTERFACIAL FAILURE	20
2.4.2	RADIAL MATRIX CRACKING	24
2.4.3	INTERPHASE YIELDING	25
2.5	<u>FIBER STRENGTH DISTRIBUTION EFFECTS</u>	26
2.6	<u>FAILURE MODE INTERACTIONS</u>	31
2.7	<u>SFF SPECIMEN FABRICATION EFFECTS</u>	31
2.7.1	FIBER SURFACE CONTAMINATION	32
2.7.2	FIBER DAMAGE	32
2.7.3	STRESSES INDUCED BY MATRIX COOLING AND CURING	33
2.8	<u>MEASURABLE FRAGMENTATION TEST PARAMETERS</u>	33
2.9	<u>STRESS BIREFRINGENCE PATTERN OBSERVATION AND RECORDING</u>	35

2

2

2

3

3

3

3

3

3

3

3

3

3

3

3

3

4

4

4

4

4

4

4

4

4

5

5

5

5

5

5

5

5

5

5

5

5

5

5

5

5

5

2.10	<u>RAPID SINGLE FIBER FRAGMENTATION</u>	
	<u>TEST DATA ACQUISITION</u>	42
2.11	<u>RELATIONSHIP TO OTHER INTERFACIAL ADHESION TESTS</u> . .	43
2.12	<u>FRAGMENTATION TEST CONCLUSIONS</u>	55
3.0	ON THE DETERMINATION OF FIBER STRENGTHS	
	BY IN-SITU FIBER STRENGTH TESTING	56
3.1	<u>IN-SITU FIBER STRENGTH TEST SYNOPSIS</u>	56
3.2	<u>ISFS INTRODUCTION</u>	56
3.3	<u>ISFS EXPERIMENTAL PROCEDURE</u>	58
3.3.1	<u>SINGLE FIBER FRAGMENTATION TEST</u>	58
3.3.2	<u>IN-SITU FIBER STRENGTH TEST</u>	59
3.3.3	<u>ISFS SPECIMEN FABRICATION</u>	61
3.3.4	<u>ISFS DATA ACQUISITION</u>	62
3.3.5	<u>ISFS CALCULATIONS</u>	64
3.3.6	<u>COMPUTER TENSION TEST SIMULATION</u>	65
3.3.7	<u>ACOUSTIC EMISSION DETECTION</u>	66
3.4	<u>ISFS RESULTS AND DISCUSSION</u>	68
3.5	<u>COMPARISON OF ISFS AND CONVENTIONAL TENSION TESTS</u> .	74
3.6	<u>ISFS CONCLUSIONS</u>	75
4.0	DETERMINATION OF FIBER VOLUME FRACTIONS BY	
	OPTICAL NUMERIC VOLUME FRACTION ANALYSIS (ONVfA) .	76
4.1	<u>ONVfA SYNOPSIS</u>	76
4.2	<u>ONVfA INTRODUCTION</u>	76
4.3	<u>ONVfA EXPERIMENTAL</u>	83
4.4	<u>ONVfA EQUIPMENT</u>	84
4.5	<u>ONVfA SAMPLE CALCULATIONS</u>	85
4.6	<u>ONVfA RESULTS AND DISCUSSION</u>	86
4.7	<u>FUTURE ONVFA WORK</u>	91
4.8	<u>ONVFA CONCLUSIONS</u>	92
5.0	EFFECTS OF OXIDATIVE SURFACE TREATMENTS ON FIBER	
	SURFACE CHEMISTRY, FIBER-MATRIX ADHESION AND	
	COMPOSITE MECHANICAL PROPERTIES OF INTERMEDIATE	
	MODULUS IM6 CARBON FIBERS IN DGEBA/MPDA EPOXY	93
5.1	<u>IM6 SYNOPSIS</u>	93
5.2	<u>IM6 INTRODUCTION</u>	94
5.3	<u>IM6 EXPERIMENTAL PROGRAM</u>	97
5.3.1	<u>IM6 EXPERIMENTAL MATERIALS</u>	97
5.3.2	<u>CHARACTERIZATION OF FIBER SURFACE PROPERTIES</u>	100
5.3.2.1	<u>XPS Surface Composition Analysis</u>	100
5.3.2.1.1	<u>Chemical Composition</u>	101
5.3.2.1.2	<u>Chemical Group Deconvolution</u>	101
5.3.2.2	<u>Micro-Wilhelmy Surface Energy Measurements</u>	101
5.3.2.2.1	<u>Micro-Wilhelmy Balance System</u>	105
5.3.2.2.2	<u>Micro-Wilhelmy Experimental Program</u>	108
5.3.2.3	<u>Fiber Surface and Cross Section Examination</u>	108
5.3.3	<u>IM6 MECHANICAL TESTING</u>	109
5.3.3.1	<u>Fiber Tensile Strength Tests</u>	109
5.3.3.2	<u>Interfacial Shear Strength Tests</u>	110
5.3.3.2.1	<u>Fragmentation Specimen Fabrication</u>	111

5.3.3.3	Fabrication of Composite Specimens	113
5.3.3.4	Volume Fraction Analysis by ONVfA	116
5.3.3.5	Mode II Fracture Toughness Tests	116
5.3.3.6	Transverse Bending Tests	116
5.3.3.7	Short Beam Shear Tests	116
5.3.3.8	SEM Fractography of Mode II and Trasverse Flexure Surfaces	117
5.3.3.9	Birefringence Evolution Sequence Acquisition	117
5.4	<u>IM6 RESULTS AND INTERPRETATION</u>	120
5.4.1	<u>FIBER SURFACE ANALYSIS RESULTS</u>	120
5.4.1.1	Surface Chemical Composition Results	120
5.4.1.2	Chemical Group Deconvolution Results	124
5.4.1.3	Micro-Wilhelmy Surface Energy Results	126
5.4.1.4	Fiber Surface and Cross Section Examination Results	130
5.4.2	<u>MECHANICAL TEST RESULTS</u>	133
5.4.2.1	Fiber Tensile Strength Results	133
5.4.2.2	Fiber Volume Fractions and Distributions	135
5.4.2.3	Interfacial Shear Strength Results	139
5.4.2.3.1	Birefringence Evolution Sequence Interpretations	144
5.4.2.4	Mode II Fracture Toughness Results	153
5.4.2.5	Transverse Flexural Results	155
5.4.2.6	Interlaminar Shear Strength Results	158
5.4.2.7	SEM Fractographic Analysis	160
5.5	<u>IM6 CONCLUSIONS</u>	171
6.0	<u>THE INFLUENCE OF PROCESSING TIME, TEMPERATURE, AND MATRIX COMPOSITION ON THE ADHESION OF CARBON FIBERS TO BISPHENOL-A POLYCARBONATE</u>	176
6.1	<u>POLYCARBONATE SYNOPSIS</u>	176
6.2	<u>POLYCARBONATE INTRODUCTION</u>	176
6.3	<u>POLYCARBONATE EXPERIMENTAL MATERIALS</u>	178
6.4	<u>POLYCARBONATE EXPERIMENTAL PROCEDURE</u>	179
6.4.1	HOT PRESSED SPECIMEN FABRICATION	179
6.4.2	SOLVENT DEPOSITED SPECIMEN FABRICATION	182
6.4.3	DATA ACQUISITION AND ANALYSIS	182
6.4.4	BIREFRINGENT IMAGE ACQUISITION	183
6.5	<u>POLYCARBONATE RESULTS AND DISCUSSION</u>	183
6.5.1	SOLVENT PROCESSED SPECIMENS	183
6.5.2	SOLVENT-FREE SPECIMENS	186
6.5.3	INTERPRETATION OF BIREFRINGENCE PATTERNS	189
6.6	<u>POLYCARBONATE CONCLUSIONS</u>	195
7.0	<u>THE INFLUENCE OF FIBER NUCLEATED CRYSTALLIZATION ON INTERFACIAL SHEAR STRENGTHS AND FAILURE MODES OF CARBON FIBERS IN NYLON 6,6</u>	196
7.1	<u>NYLON 6,6 SYNOPSIS</u>	196
7.2	<u>NYLON 6,6 INTRODUCTION</u>	196
7.3	<u>NYLON 6,6 EXPERIMENTAL PROCEDURE</u>	199
7.3.1	NYLONN 6,6 EXPERIMENTAL MATERIALS	199
7.3.2	FABRICATION OF NYLON 6,6 ISS SPECIMENS	200
7.3.3	NYLON 6,6 FRAGMENTATION TESTING	201
7.4	<u>NYLON 6,6 RESULTS AND DISCUSSION</u>	202
7.4.1	NYLON 6,6 ISS RESULTS	202

7.
7.
7.

8.
8.
8.
8.
8.
8.
8.
8.

A

A
F

A
S

A
V

A
E

E

7.4.2	MICROSTRUCTURE AND FAILURE MODE OBSERVATIONS . . .	205
7.4.3	HEATED STAGE MICROSCOPE OBSERVATIONS	221
7.5	<u>NYLON 6.6 CONCLUSIONS</u>	221
8.0	CONCLUSIONS	222
8.1	<u>FRAGMENTATION TEST CONCLUSIONS</u>	222
8.2	<u>ISFS CONCLUSIONS</u>	223
8.3	<u>ONVFA CONCLUSIONS</u>	223
8.4	<u>IM6 CONCLUSIONS</u>	223
8.5	<u>POLYCARBONATE CONCLUSIONS</u>	224
8.6	<u>NYLON 6.6 CONCLUSIONS</u>	225
8.7	<u>THERMOSET AND THERMOPLASTIC MATRIX CONCLUSIONS</u> .	225

APPENDICES

APPENDIX A. SOURCE CODE FOR FIBERTRACK, SINGLE FIBER FRAGMENTATION TEST DATA ACQUISITION AND ANALYSIS SYSTEM .	228
APPENDIX B. SOURCE CODE FOR FIBERLINK, IN SITU FIBER STRENGTH FRAGMENTATION TEST DATA ANALYSIS SYSTEM	245
APPENDIX C. SOURCE CODE FOR OPTICAL NUMERIC VOLUME FRACTION ANALYSIS SYSTEM	263
APPENDIX D. SOURCE CODE FOR WILHELMY WETTING BALANCE DATA ACQUISITION AND ANALYSIS SYSTEMS	294
REFERENCES	312

LIST OF TABLES

Table 1.	Flaws per 25 mm @ strain increment for AS4 fibers.	68
Table 2.	In situ and ex situ AS4 fiber strengths.	72
Table 3.	Volume fractions by ONVfA and acid digestion.	87
Table 4.	Void volume fractions by areal analysis and acid digestion.	90
Table 5.	Properties of IM6 carbon fibers summarized from Hercules data sheet.	98
Table 6.	Surface oxygen, nitrogen, and functional groups on IM6 fibers.	121
Table 7.	Polar, dispersive, and total surface free energy on IM6 fibers.	127
Table 8.	Critical lengths, L_c/D 's, tensile strengths, and ISS for IM6 fibers.	135
Table 9.	Fiber and void volume fractions by ONVfA.	136
Table 10.	Mode II fracture toughness for IM6/epoxy composites.	154
Table 11.	Transverse flexural strengths and moduli for IM6/epoxy composites.	157
Table 12.	Interlaminar shear strengths for IM6/epoxy composites.	159
Table 13.	Properties of Lexan 141 polycarbonate resin.	179
Table 14.	Matrix type, processing, L_c/D 's, and ISS for AS4 in Lexan 141.	184
Table 15.	Matrix type, processing, L_c/D 's, and ISS for AS4 in PC.	187
Table 16.	Processing, L_c/D , and ISS for Nylon 6,6 matrices.	204

LIST OF FIGURES

Figure 1.	Cross sectional diagram of fiber, interphase, and matrix.	13
Figure 2.	Diagram of single fiber fragmentation specimen.	16
Figure 3.	Approximate tensile stress distribution in fragmentation test.	17
Figure 4.	Slightly more realistic tensile stress distribution in fragmentation test.	18
Figure 5.	Interfacial failure by stick-slip Mode II cracking.	22
Figure 6.	Fiber failure strain energy effects on interfacial failure.	28
Figure 7.	Fiber strain energy effects at higher coupon strain.	28
Figure 8.	Diagram of fiber strain energy effects on shear stress transfer.	29
Figure 9.	Diagram of fiber failure strain effects on interphase yielding.	30
Figure 10.	Birefringence patterns for 8 breaks in AS4 fiber, 1.3% coupon strain.	36
Figure 11.	Birefringence patterns for 8 breaks in AS4 fiber, 1.5% coupon strain.	36
Figure 12.	Birefringence patterns for 8 breaks in AS4 fiber, 1.8% coupon strain.	37
Figure 13.	Birefringence patterns for 8 breaks in AS4 fiber, 2.0% coupon strain.	37
Figure 14.	Birefringence patterns for 8 breaks in AS4 fiber, 2.3% coupon strain.	38
Figure 15.	Birefringence patterns for 8 breaks in AS4 fiber, 2.5% coupon strain.	38
Figure 16.	Birefringence patterns for 8 breaks in AS4 fiber, 2.7% coupon strain.	39
Figure 17.	Birefringence patterns for 8 breaks in AS4 fiber, 3.0% coupon strain.	39
Figure 18.	Rasterized integration of birefringence patterns to detect yielding.	41
Figure 19.	Symmetric mode II crack in homogeneous material.	45
Figure 20.	Asymmetry of mode II crack between dissimilar materials.	45
Figure 21.	Crack growth habits for 4 crack initiation and loading conditions.	47
Figure 22.	Symmetry of interfacial cracking for fragmentation test.	49
Figure 23.	Symmetry of interfacial cracking for pullout test.	51
Figure 24.	Symmetry of interfacial cracking for droplet pullout test.	52
Figure 25.	Symmetry of interfacial cracking for short fiber.	53
Figure 26.	Symmetry of interfacial cracking for indentation test.	54
Figure 27.	Fragmention stresses and polling lengths.	59
Figure 28.	Straining stage for single fiber fragmentation test.	60
Figure 29.	Block functional diagram of FiberTrack/FiberLink.	63
Figure 30.	Fiber break positions recorded by FiberTrack.	64
Figure 31.	AE trace from carbon fiber failure.	67
Figure 32.	Flaws vs strain increment by specimen in PC.	69
Figure 33.	Flaws vs strain for AS4 fibers in PC and epoxy.	70
Figure 34.	Flaws vs strain and exponential curves.	71
Figure 35.	In-situ and ex-situ fiber strengths.	72
Figure 36.	Digitized image of graphite/epoxy composite.	79
Figure 37.	Same image with fibers counted and tagged.	79
Figure 38.	Boxes shaded to indicate number of fibers.	80
Figure 39.	Fiber map, one white pixel per fiber.	81
Figure 40.	Block areal density map, (fibers/box).	82
Figure 41.	Fiber areal density distribution function.	82
Figure 42.	Fiber maps and distributions for HP1, 2, and 3.	88

Figure 43.	Fiber maps and distributions for AC1, 2, and 3.	89
Figure 44.	Fiber fractions by ONVfA and Acid Digestion.	91
Figure 45.	Chemical structures of epoxy precursors.	99
Figure 46.	Surface tension influence on contact angles.	102
Figure 47.	Fiber wetting force and contact angle measurement.	104
Figure 48.	Block diagram of micro-Wilhelmy wetting balance.	106
Figure 49.	Single fiber fragmentation test specimen.	111
Figure 50.	Mechanical test specimen diagrams.	115
Figure 51.	Surface oxygen percentage by XPS.	122
Figure 52.	Surface nitrogen percentage by XPS.	123
Figure 53.	Surface functional groups versus surface treatment.	125
Figure 54.	Fiber surface free energy versus surface treatment.	127
Figure 55.	Polar free energy versus surface oxygen percentage.	129
Figure 56.	SEM of fiber surface morphology #1.	131
Figure 57.	SEM of fiber surface morphology #2.	131
Figure 58.	SEM of fiber cross-section, #1.	132
Figure 59.	SEM of fiber cross-section, #2.	132
Figure 60.	Extrapolation of fiber tensile strengths to critical lengths.	134
Figure 61.	Fiber volume fractions and distributions for 24 ply laminates.	137
Figure 62.	Fiber volume fractions and distributions for 12 ply laminates.	138
Figure 63.	Interfacial shear strengths for IM6 fibers.	140
Figure 64.	Interfacial shear strengths for IM6 and A4.	141
Figure 65.	ISS versus surface oxygen and polar surface free energy.	142
Figure 66.	ISS and functional groups versus surface treatment.	143
Figure 67.	Birefringence sequence for Untreated IM6 fiber.	147
Figure 68.	Birefringence sequence for 20%ST IM6 fiber.	148
Figure 69.	Birefringence sequence for 100%ST IM6 fiber.	149
Figure 70.	Birefringence sequence for 200%ST IM6 fiber.	150
Figure 71.	Birefringence sequence for 600%ST IM6 fiber.	151
Figure 72.	Birefringence sequence for 100GST IM6 fiber.	152
Figure 73.	Mode II fracture toughness for IM6 composites.	154
Figure 74.	Transverse flexural strengths for IM6 composites.	157
Figure 75.	Interlaminar shear strengths for IM6 composites.	159
Figure 76.	SEM @ 200X, untreated mode II fracture.	161
Figure 77.	SEM @ 200X, 20% treated mode II fracture.	161
Figure 78.	SEM @ 200X, 100% treated mode II fracture.	162
Figure 79.	SEM @ 200X, 200% treated mode II fracture.	162
Figure 80.	SEM @ 200X, 600% treated mode II fracture.	163
Figure 81.	SEM @ 200X, 100% GST sized mode II fracture.	163
Figure 82.	SEM @ 1000X, untreated mode II fracture.	164
Figure 83.	SEM @ 1000X, 20% treated mode II fracture.	164
Figure 84.	SEM @ 1000X, 100% treated mode II fracture.	165
Figure 85.	SEM @ 1000X, 200% treated mode II fracture.	165
Figure 86.	SEM @ 1000X, 600% treated mode II fracture.	166
Figure 87.	SEM @ 1000X, 100% GST sized mode II fracture.	166
Figure 88.	SEM @ 500X, Untreated transverse flexural fracture.	168
Figure 89.	SEM @ 500X, 20%ST transverse flexural fracture.	168
Figure 90.	SEM @ 500X, 100%ST transverse flexural fracture.	169
Figure 91.	SEM @ 500X, 200%ST transverse flexural fracture.	169
Figure 92.	SEM @ 500X, 600%ST transverse flexural fracture.	170
Figure 93.	SEM @ 500X, 100GST transverse flexural fracture.	170
Figure 94.	Mode II fracture toughness versus ISS.	172

Figure 95.	Interlaminar shear strength versus ISS.	174
Figure 96.	Summary of mechanical test results versus surface treatment.	175
Figure 97.	Chemical structure of BPA polycarbonate.	179
Figure 98.	Fixture for hot pressing single fiber specimens.	181
Figure 99.	Spin coating fixture for solvent deposition specimen fabrication.	182
Figure 100.	Interfacial shear strengths for AS4 in Lexan 141.	185
Figure 101.	Interfacial shear strengths for AS4 in pure polycarbonate.	186
Figure 102.	Solvent deposited Lexan matrix birefringence pattern.	191
Figure 103.	Fast cooled Lexan matrix birefringence pattern.	191
Figure 104.	Slow cooled Lexan matrix birefringence pattern.	191
Figure 105.	Pure polycarbonate matrix birefringence pattern.	191
Figure 106.	Surface of annealed polycarbonate.	192
Figure 107.	Possible polycarbonate crystalline sheath around AS4 fiber.	193
Figure 108.	Crazed polycarbonate fragmentation specimen.	194
Figure 109.	Chemical structure of Nylon 6,6 - poly(hexamethyl adipamide).	200
Figure 110.	Interfacial shear strengths of carbon fibers in Nylon 6,6.	204
Figure 111.	Four CSOM micrographs of transcrystallinity in Nylon 6,6.	206
Figure 112.	TOM of AU4 breaks in Nylon 6,6.	208
Figure 113.	TOM of AS4 break in rapidly cooled Nylon 6,6.	209
Figure 114.	TOM of AS4 break in Nylon 6,6 slowly cooled from 275 °C.	210
Figure 115.	TOM of AS4 in Nylon 6,6 cons. @ 275 °C, iso-xtal @ 225 °C.	211
Figure 116.	TOM of AS4 in Nylon 6,6 cons. @ 300 °C, iso-xtal @ 225 °C.	212
Figure 117.	Interfacial shear strength versus radial crack diameter.	214
Figure 118.	CSOM of AS4 break initiated interspherulitic crack #1.	215
Figure 119.	CSOM of AS4 break initiated interspherulitic crack #2.	215
Figure 120.	CSOM of AS4 break initiated intraspherulitic cracks #1.	216
Figure 121.	CSOM of AS4 break initiated intraspherulitic cracks #2	216
Figure 122.	CSOM of AS4 break initiated transcrystalline crack #1.	217
Figure 123.	CSOM optical section of AS4 break in Nylon 6,6, Z= 2.35.	218
Figure 124.	CSOM optical section of AS4 break in Nylon 6,6, Z= 3.6.	218
Figure 125.	CSOM optical section of AS4 break in Nylon 6,6, Z= 4.8.	219
Figure 126.	CSOM optical section of AS4 break in Nylon 6,6, Z= 6.0.	219
Figure 127.	CSOM optical section of AS4 break in Nylon 6,6, Z= 7.2.	220
Figure 128.	CSOM optical section of AS4 break in Nylon 6,6, Z= 8.45	220
Figure 129.	ISS of AU4 and AS4 fibers in thermoset and thermoplastic matrices.	226

CHAPTER 1

THE INFLUENCE OF THE FIBER-MATRIX INTERFACE ON THE PROPERTIES OF FIBER REINFORCED COMPOSITES

1.1 SYNOPSIS

An outline of the research program, and its motivation is given in this section. The background of the research effort in this area is briefly described.

1.2 INTRODUCTION

The fiber/matrix interface may be thought of as the center of a composite material. Since a composite is, by definition, a material with at least two distinct phases, separated by an interface, all composites rely upon some degree of interfacial adhesion. Depending on the desired properties, the optimal value of this adhesion for a given composite application may be as high as possible, or it may be much lower to deliberately facilitate debonding. An intermediate level of interfacial adhesion that provides good strength values while preventing brittle failure modes is commonly the most desirable compromise.

The complexity of failures in composites, even under the idealized conditions of carefully controlled laboratory tests, makes the understanding of composite failure in terms of basic mechanisms extremely difficult. Since the interface lies at the core of the most complex interactions within the composite, interfacial effects are even more difficult to adequately model than those involving failure initiated within the fibers or matrix.

While the motivation for this research is driven partly by the necessity to improve the understanding of the linkage between interface and composite properties to insure adequate and predictable composite performance, there are also opportunities

to achieve

1.3 Q

interfere

have

comp

made

macro

[Ma

cha

inst

occ

stre

rep

in

re

sy

e

f

l

f

t

to achieve significant property improvements which are not yet fully exploited.

1.3 COMPOSITE PERFORMANCE AND INTERFACE PROPERTIES

The relationship between the performance of composite materials and interfacial properties is under intensive investigation. Composite behavior models have often met with little quantitative success, however, due to the inherent complexity of the mechanics and failure of multiphase materials. Attempts have been made to develop performance models based on integrated micromechanical and macromechanical criteria, developed along the lines of Griffith's criterion for failure [Mahishi, 1986], and using finite element method models [Kolle, 1990]

A more common, and less ambitious approach is based on the investigation of changes in composite failure mode with differences in interfacial adhesion. For instance, Shih [1986] found that a change from compressive to flexural failure occurred in unidirectional composites subjected to four point bending when interfacial strengths were reduced. A failure mode transition diagram was constructed to represent this process.

Another approach to understanding composite performance has been to perform integrated sets of mechanical tests on a range of composites [Curtis, 1987]. By noting relationships between the fiber, matrix and interface characteristics of a variety of systems and the resultant composite performance, conclusions about the influence of each were drawn.

Numerous researchers have used the single fiber fragmentation test to evaluate failure mode transitions along with interfacial shear strengths, including [Dibenedetto, 1985, 1986], [Drzal, 1980 (B), 1982], [Wimolkiatisak, 1989] and many others. While fragmentation test failure modes may, or may not, directly correspond to changes in behavior of the macroscale composite, due to the differences in loading conditions,

thi

1.

ex

ad

bo

di

lit

ca.

(K

ma

ad

suc

gen

deg

fi

me

whi

and

prop

rein

equi

insta

poly

this technique allows composite failures to be studied in microcosm.

1.4 CHEMISTRY OF THE FIBER/MATRIX INTERFACE

The chemistry of the fiber/matrix interface region has been the object of extensive investigation and is the basis for many of the models of fiber/matrix adhesion. Chemically based fiber/matrix bonding may involve primary chemical bonds, hydrogen bonding, or the various forms of dispersion bonding (dipole-dipole, dipole-induced dipole, etc.). There have been numerous attempts reported in the literature to resolve adhesion into these components.

The reinforcing fibers used in modern composites include the PAN-based carbon fibers investigated in this study, glass fibers, liquid crystal polymer fibers (Kevlar), other polymer fibers (UHMW polyethylene), and inorganic, crystalline materials, (silicon carbide, alumina, etc.). Each class of fiber presents its own set of adhesion challenges. In some cases these challenges have largely been met, i.e., the success of silane coupling agents with glass fibers. In others interfacial adhesion is generally sufficient, as with metal matrix composites, but other problems such as fiber degradation by diffusion of the matrix continue to present problems. For carbon fibers the adhesion issue presents a "moving target" as a result of changing processing methods for the fibers continue to increase the axial properties, strength and modulus, while tending to degrade the transverse properties, such as interlaminar shear strength and toughness.

A general model of adhesion of polymers to inorganic surfaces has been proposed by Plueddemann, based on the behavior of silane coupling agents and glass reinforcements [Plueddemann, 1970]. This model proposes that a dynamic equilibrium exists at the interface and that resistance to an aqueous environment, for instance, results from the equilibrium favoring coupling of polar groups within the polymer to the surface.

C

a

t

[

s

[

D

p

st

d:

Ra

ed

ba

in

de

by

att

mo

1.5

"in

extr

extr

The nature of bonding to fibers is the object of extensive investigation and debate. Fibers treated with bromine, have been shown to have improved adhesion and to change in electrical conductivity. These changes have been attributed both to the formation of an intercalant with bromine situated between graphite planes, [Jaworske, 1986] and to primary chemical bond formation, [Jaworske, 1987]. The structure of carbon fibers involves some degree of microporosity, [Denison, 1988], [Hughes, 1990], as indicated by a somewhat lower density than that for solid graphite. Denison, et al have suggested that these micropores may absorb polymer chains and promote bonding. With polymer chains sufficiently deeply absorbed, interfacial shear strengths may approach those expected for primary chemical bonds even when only dispersion type forces are active.

The chemical properties of graphite edge planes have been investigated by Raman spectroscopy, [Katagiri, 1988]. They have found that Raman spectra from the edges of graphite planes differ from those of the cleaved basal planes in displaying bands at 1355 cm^{-1} and 1620 cm^{-1} . They attribute this difference to the discontinuity in the structure, and suggest that Raman spectra may serve as an indication of the degree of graphitization.

The acid-base properties of surface treated carbon fibers have been investigated by [Wesson, Allred, 1990], [Watts, 1991] and many others. Adhesion may also be attributed to London dispersion forces, especially with thermoset matrices where small monomer units can interact with a high proportion of surface sites.

1.5 MATERIALS SCIENCE OF THE FIBER/MATRIX INTERFACE

The understanding of the properties of the fiber/matrix interface region, or "interphase" or "mesophase" as it is now called, is largely dependent upon extrapolation of material properties measured in macro-scale specimens. This extrapolation is complicated by differences in chemical composition, size, constraint

co

d:

se

co

sig

the

of

eff

1.5

with

inte

at d

in m

MPa

stren

resul

at th

the s

matr

1.5.2

high

the m

conditions, and microstructure that are often unknown and immeasurable. As discussed in the previous section, differences in chemical composition can arise from segregation to or away from the interface, or physisorption or chemisorption of matrix constituents by the fiber surface. These differences can lead to an interphase with significantly changed basic material properties from the bulk material.

Even in the absence of compositional differences, however, the properties of the matrix in the vicinity of a surface may be substantially different. Some sources of these differences include scale effects, constraint effects, and microstructural effects. These influences are discussed in the following sections.

1.5.1 SCALE EFFECTS ON INTERPHASE PROPERTIES

The limiting properties of composite interphases have often been compared with the strength and other failure characteristics of the bulk matrix. This interpretation neglects the changes in material behavior that occur in identical systems at different size scales, because smaller specimens tend to have smaller flaws. Glass in macroscopic form, for example, is extremely brittle and low in strength, 7 to 140 MPa for "off the shelf" glass rods. Surface defect free silica, in contrast, shows strengths in the 3-5 GPa range [Kelley, 1986]. While this strength increase does not result from smaller specimens [Kelley, 1986] but from the greater stress concentration at the tip of larger defects [Griffith, 1921, 1924], similar effects appear to influence the strength and extent of plastic deformation of adhesives [Stringer, 1985] and matrices [Bascom, 1985].

1.5.2 CONSTRAINT EFFECTS ON INTERPHASE PROPERTIES

The constraint imposed on the low modulus polymeric matrix by the much higher modulus fiber causes a change in material properties within the "interphase", the matrix material in close proximity to the fiber. The thickness of this interphase

f
m
S
li
ad
of
na
de;
the
thes
mak
*tran

depends to some degree upon how it is defined, that is, on how much different its properties must be from the bulk matrix material. A theoretical approach to determining the interphase thickness has been proposed, however, and may be used to analytically evaluate this thickness and compare it with experimental properties [Theocaris, 1985, 1986]. This model is based on measurements of the moduli of the fiber, matrix, and composite along with basic assumptions about the continuity of properties between the interphase, the fiber, and the bulk matrix. The interphase thickness has also been evaluated by a thermal analysis technique, [Sideridis, 1988] which is based upon measurements of discontinuities in the heat capacity at the glass transition temperature that result from the decreased mobility of the polymer chains in the vicinity of the fiber.

1.5.3 MICROSTRUCTURAL EFFECTS ON INTERPHASE PROPERTIES

Although the surfaces of carbon fibers generally appear to be smooth, except for axial striations, at all size scales visible by either optical or scanning electron microscopy, at smaller scales considerable topographic roughness is evident. Scanning tunneling microscope (STM) of carbon fibers are beginning to appear in the literature and should help to clarify the role of mechanical interlocking in fiber/matrix adhesion. Hoffman, Elings, and Gurley [Hoffman, 1988] have published STM images of pitch-based Amoco P-55 carbon fibers at size scales ranging from the tens of nanometers to atomic scales. The apparent roughness was found to vary considerably depending on size, being very rough at the nanometer scale, and much smoother as the image came to include only the surface of a single graphite crystallite. Although these images were very difficult to produce, the increased availability of STMs should make their application to comparative studies of carbon fibers commonplace.

Semicrystalline thermoplastics generally develop what has been termed a "transcrystalline" interphase resulting from nucleation of polymer crystals by the

1

2

u

an

in

se

in

cl

de

pro

use

by

met

dist

fiber

poly

surface of the fiber or by shear strains along the fiber surface. This interphase has a strongly oriented structure with anisotropic moduli and strengths. These values may not be determined by measurement of bulk material properties due to the fundamentally different microstructures.

Microstructural changes also occur as a result of segregation of low molecular weight components of the matrix toward the interface. The decrease in chain mobility of these components in the fiber vicinity is less than that of the higher Mw constituents, resulting in a free energy driving force. This segregation may occur for thermosets during the curing process, and for amorphous or semicrystalline thermoplastics during consolidation.

1.6 EXPERIMENTAL PROGRAM OVERVIEW

This section provides an overview of the experimental and theoretical program undertaken for this work and attempts to show how the several parts of the program are directed toward an improved understanding of the influence of fiber/matrix interface characteristics on composite performance. The program consists of three sections that are intended to enhance the experimental tools available for composite interface research, and three sections that are applications of these tools to different classes of matrices. The experimental tools investigated are the fragmentation test described in Chapter 2 which is used as a probe of the fiber/matrix interphase properties and failure modes, the in situ fiber strength test in Chapter 3 which can be used to obtain information on the short gage length fiber strengths that are required by models of composite properties, and the optical numeric volume fraction analysis method in Chapter 4 that can be used to investigate the influence of fiber fraction and distribution on composite properties. The applications consist of investigations of fiber/matrix adhesion for carbon fibers to thermoset epoxy (Chapter 5), to polycarbonate, an amorphous thermoplastic (Chapter 6), and to Nylon 6,6, a

se

the

un

ca

fo

l.

b

c

sy

c

in

in

in

f

b

n

l

n

n

is

u

semicrystalline thermoplastic (Chapter 7). These systems were chosen to represent the three most common classes of polymer matrices in an effort to develop an understanding of the similarities and differences in fiber/matrix adhesion for these cases.

The motivation and background for these investigations are outlined in the following sections.

1.6.1 ANALYSIS OF THE FRAGMENTATION TEST

The single fiber fragmentation interfacial shear strength test has formed the basis of many fiber/matrix interface studies in recent years, and is exploited in the current work as well. Although its principal advantage is the relative simplicity of a system comprised of only a single fiber compared with vastly more complex composite systems, there is still enough complexity to generate a wide range of interpretations among researchers.

In the course of these investigations the author has developed his own interpretations and insights into the mechanisms involved in the fragmentation test and into the kinds of information that may be available from it. This analysis of the fragmentation test is intended to convey these insights in the hopes that they will benefit future work. The analysis is not intended to be a complete review of the method, which is beyond the scope of this work.

1.6.2 IN SITU FIBER STRENGTH TESTING

Perhaps the most fundamental of the properties of the constituents of composite materials is the strength of the reinforcing fibers. The remarkably high strengths of modern, low defect fibers is the foundation on which the entire composites industry is built. The development of models of the strength of composites usually depends upon information about fiber strengths at the shortest gage lengths that can be fully

loaded through the interface. The Weibull analysis of fragmentation tests also requires information about short gage length fiber strengths.

In addition to theoretical interest, direct measurements of fiber strengths in situ may prove to be a powerful tool for process optimization. Although the fibers in polymer matrix composites are generally only damaged to a minimal degree by handling during the fabrication process, in metal matrix composites fiber surfaces are subjected to diffusion and attack by the melt as an integral part of the consolidation process. Indeed, the development of good interfacial strength is dependent upon the same diffusional penetration of the fiber by the matrix that eventually leads to the degradation of fiber strength. The in situ strengths of fibers in such systems will, in general, be significantly different from their ex situ, virgin values. A great deal of work has been done to develop coatings to protect metal matrix reinforcement fibers from diffusional damage. The assessment of the performance of these coatings requires that the fiber strengths be measured in situ, following the complete consolidation process.

Numerous researchers, including the author, have recently independently suggested that fiber strength information is available from the fragmentation test [Waterbury, 1990], [Wagner, 1989], [Henstenburg, 1989], [Figuroa, 1990]. A theoretical development of a simple, robust experimental technique for single fiber fragmentation in situ fiber strength testing and an experimental verification of this approach appears in Chapter 3.

1.6.3 OPTICAL NUMERIC VOLUME FRACTION ANALYSIS

The distribution of fibers within the matrix material must be sufficiently uniform for the translation of the high performance properties of the fibers to the composite material to be efficient. High performance aerospace-grade composites require a high volume fraction of well distributed fibers with low void content and

minimal direct fiber-fiber contact.

Fiber volume fractions have largely been measured by digestion of the matrix material by an acid or other solvent, providing only averaged values with no information on the distribution of fibers and voids. Optical numeric volume fraction analysis (ONVfA) measures volume fractions by counting the numbers of fibers in optical microscope images of composite cross sections. These measurements are accurate and reproducible, and provide information on the volume fraction distribution at the finest possible scale, that of the fibers. By comparisons with the distribution of voids measured by areal image analysis, it is possible to develop a complete mapping of the fibers, voids, and matrix components in a composite. These data may be used in the interpretation of mechanical test results to gain an improved understanding of the influence of matrix rich areas, voids, and other distribution effects on composite performance.

1.6.4 FIBER SURFACE TREATMENT EFFECTS ON IM6/EPOXY

The carbon fiber/epoxy resin interface has been one of the most extensively studied composite interfaces. This activity has been motivated by the difficulty of achieving adequate bonding to a fiber surface that is mostly comprised of extremely unreactive graphitic carbon, and by the wide usage of these materials as high performance composites. Although the problem is far from intractable, many effective surface treatments having been developed, no completely successful approach, such as the use of silane coupling agents with glass fibers, has been developed. Moreover, changes in carbon fiber production methods have tended toward higher moduli, higher strength fibers with more highly oriented graphitic carbon surfaces that are more difficult to adhere to.

The core of this research effort consists of an integrated set of micromechanical and macromechanical tests on intermediate modulus, Hercules

Magnamite® IM6 fibers with different surface treatments, coupled with measurements of the fiber surface atomic and molecular compositions and free energies. The surface treatments investigated include a series of electrochemical oxidative treatments that are proprietary to Hercules® and so cannot be fully reported, but which represent different extents of the standard commercial preparation for these fibers.

1.6.5 AMORPHOUS THERMOPLASTIC, BPA POLYCARBONATE

Although most current composite matrices are thermoset polymers, there are numerous advantages to thermoplastic materials for this application. Chief among these is a substantial reduction in fabrication time, an essential development for the use of composites in high volume, low cost applications. An additional advantage involves the greater toughness of thermoplastics compared with thermosets. The exploitation of this advantage requires that improvements are made in fiber/matrix adhesion for thermoplastic matrix systems.

Adhesion in thermoset matrix composites may involve the formation of primary chemical bonds between the fiber surface, or chemisorbed surface species, and the highly reactive matrix precursors. Thermoplastics, in contrast, have already undergone polymerization and are much less reactive. Primary chemical bond formation is therefore extremely unlikely. Adhesion is probably dependent entirely upon physisorption driven by dispersion forces and upon mechanical interlocking. Mechanical interlocking may be significantly augmented by the possibility of partial intercalation of the polymer chains into the graphitic "mosaic" structure, however. Levels of adhesion in thermoplastics that approach those of thermoset matrices have been reported.

by

by

bo

ini

ex

ar

aj

se

in

f

1.6.6 SEMICRYSTALLINE THERMOPLASTIC, NYLON 6,6

Fiber/matrix adhesion in semicrystalline thermoplastic matrices is complicated by the intricate morphology of the spherulitic microstructures of the bulk matrix and by the influence of fiber-nucleated crystallization of the matrix. Failure modes within both macro and micro composites must interact in some way with this anisotropic and inhomogeneous interphase. Even in the absence of failure, changes may still be expected in the transfer of shear stresses between the fiber and matrix because of the anisotropy in the moduli of the oriented transcrystalline structure.

A schematic "cartoon" of some of the factors involved in fiber/matrix adhesion appears in Figure 1. Adhesion may be effected by primary chemical bonds, secondary, London dispersion forces or acid-base interactions, mechanical interlocking, the stiffness of the interphase region, or any combination of these factors. An attempt to elucidate the roles of these factors comprises this dissertation.

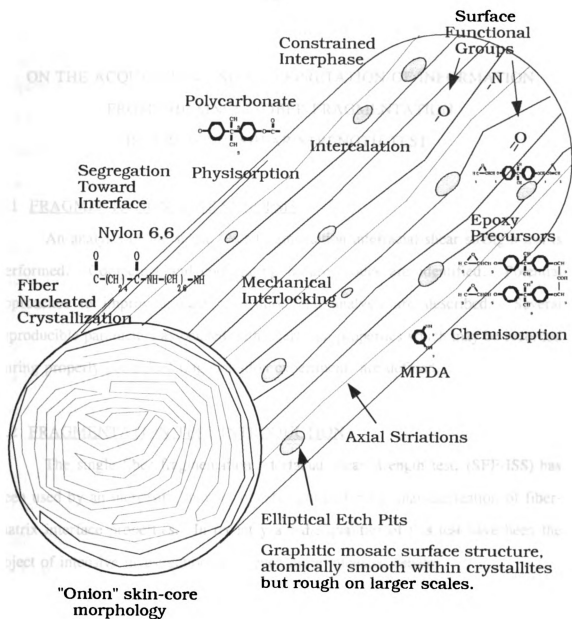


Figure 1. Cross sectional diagram of fiber, interphase, and matrix.

CHAPTER 2

ON THE ACQUISITION AND INTERPRETATION OF INFORMATION FROM THE SINGLE FIBER FRAGMENTATION INTERFACIAL SHEAR STRENGTH TEST

2.1 FRAGMENTATION TEST SYNOPSIS

An analysis of the single fiber fragmentation interfacial shear strength test is performed. Competing and cooperating failure modes are identified. Potential approaches to improving data acquisition and analysis are described. Several reproducible parameters associated with interfacial properties which may be recorded during properly controlled fragmentation experiments are defined.

2.2 FRAGMENTATION TEST INTRODUCTION

The single fiber fragmentation interfacial shear strength test, (SFF-ISS) has been used by an increasing number of laboratories for the characterization of fiber-matrix interface properties. In recent years the qualities of this test have been the object of intensive investigation, and even more intensive debate.

Each of the current interfacial shear strength testing techniques, including pullout testing, droplet pullout, indentation testing, and fragmentation testing, suffers from its own set of experimental limitations. Many of these result from the small size and brittleness of modern reinforcing fibers, factors which are increasing with the trend toward higher moduli and smaller diameters.

Numerous experimental factors complicate the performance of fragmentation tests and the interpretation of results. While some of these complications are widely appreciated, if not fully understood, others have received little or no attention in the literature. Failure to adequately control all relevant experimental variables can lead

to g

fre

The

ext

pro

wh

in

th

co

is

as

c

e

s

t

n

:

to generation of misleading and confusing data.

The final average fragment length and the fragment length distribution are frequently subjected to sophisticated statistical analyses based upon idealized models. The validity of these analyses is compromised by the differences in the failure modes exhibited by real microcomposites with varying surface treatments, matrices, and processing conditions.

The SFF-ISS test proceeds as a complex admixture of simultaneous failures which compete in some cases, cooperate in others, and which sometimes involve the interface, and sometimes do not. All failures that occur during the test contribute to the final microcomposite defect structure. These defects tend to accommodate the coupon tensile strain, influencing the fiber fragment lengths. The final critical length is a function of the material properties of the fiber, matrix, interphase, and interface, and of the failure modes operative in them.

A more complete understanding of the failure processes in single fiber composites can improve the application of this tool for the study of methods to enhance composite performance. This paper is a review of some of the possible single fiber fragmentation test failure modes and an assessment of their influence on the final test results. An attempt will also be made to identify viable approaches to refining SFF-ISS information acquisition and analysis.

2.3 OVERVIEW OF THE SINGLE FIBER FRAGMENTATION TEST

As described in numerous other publications [Fraser, 1983], [DiBenedetto, 1986], [Drzal, 1980] the single fiber fragmentation test proceeds as follows.

Separated single fibers are embedded in a small tensile coupon of epoxy or other, usually transparent matrix, parallel to the gage section (Figure 2). As the coupon is raised to a strain level greater than the failure strain of the fiber, the fiber repeatedly fails. This fragmentation process stops when the lengths of the remaining

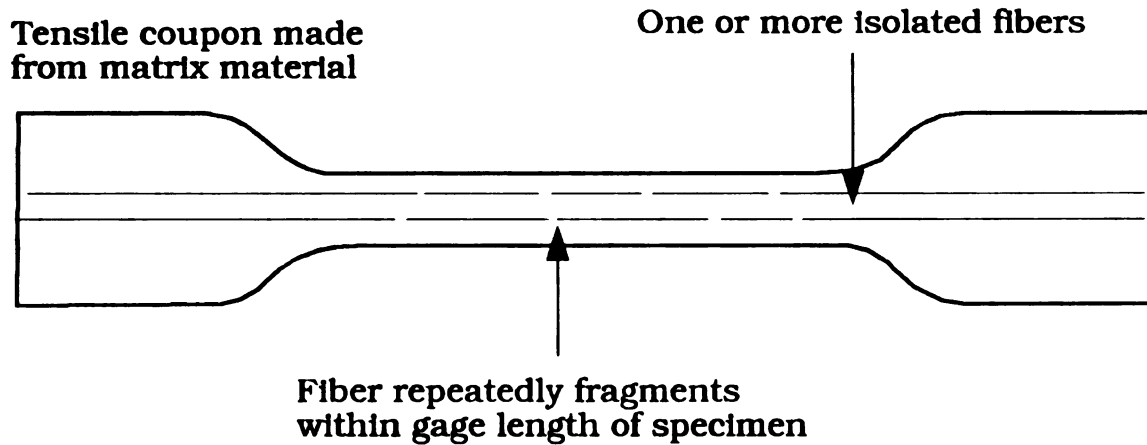


Figure 2. Diagram of single fiber fragmentation specimen.

fragments approach an average limiting value, often called the critical length, L_c . This length, along with the strengths of the fiber fragments, forms the basis of the single fiber fragmentation interfacial shear strength test.

A diagram of the approximate normal stresses in fiber fragments appears in Figure 3. This simple diagram is based on a constant shear stress transfer along the entire length of the fragments. The constant stress distribution is derived from the assumption of a perfectly bonded interface to a perfectly plastic matrix. The matrix is assumed to yield at all highly stressed regions until shear tractions equalling the shear strength of the matrix are uniformly attained. A shear lag model in which the tensile strength of the final fragments multiplied by the fiber cross sectional area is taken to be equal to the interfacial shear strength multiplied by the surface area of each half of the fragment is then used to calculate the ISS. Since a fragment can fail at any point greater than $L_c/2$ from the end, the final range of fragment lengths ranges from $L_c/2$ to L_c . A constant term of $3/4$ is therefore sometimes introduced to compensate for this.

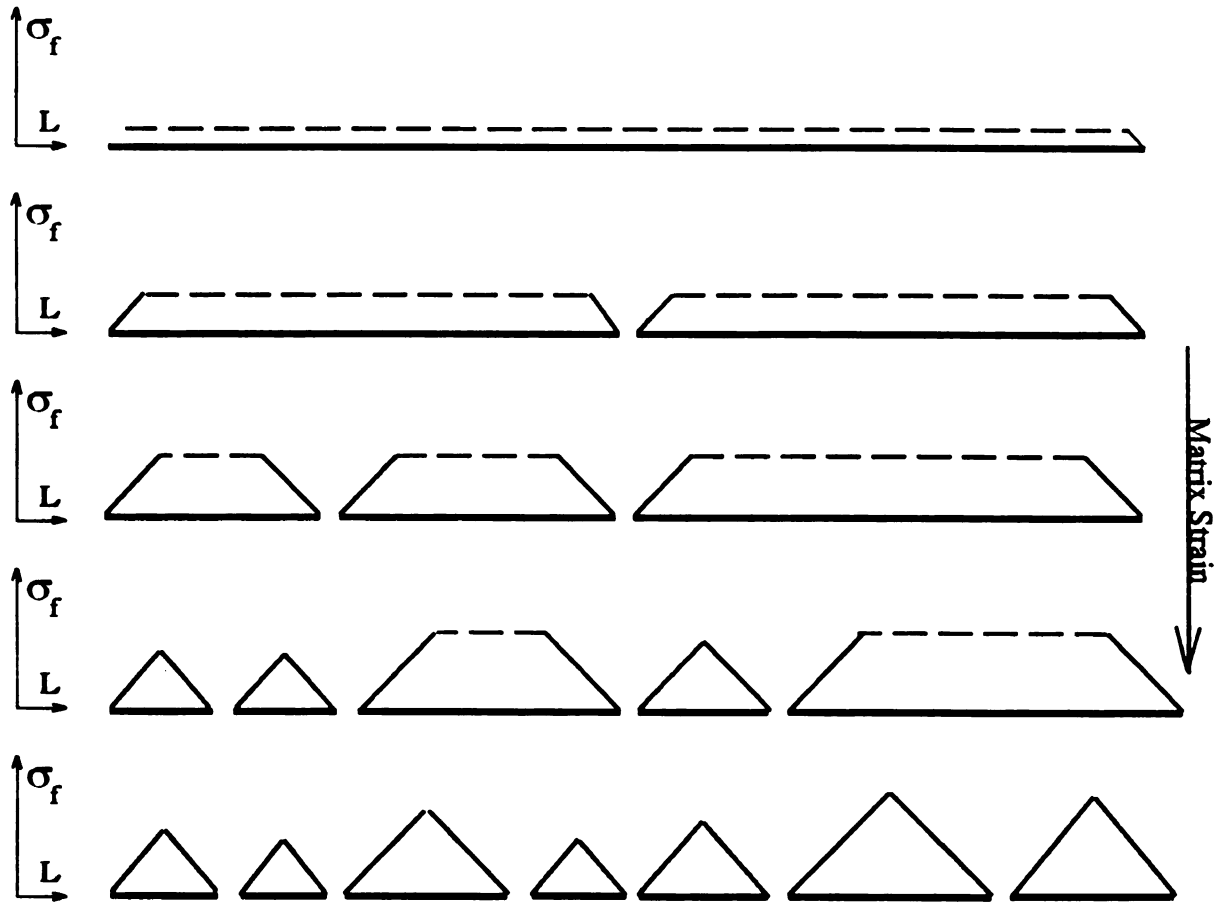


Figure 3. Approximate tensile stress distribution in fragmentation test.

A constant shear traction never occurs in actual fragmentation tests that always involve some combination of elastic and plastic behavior and often include some degree of interfacial debonding. The constant traction assumption has, nevertheless, played an integral role in most of the data reduction methods in use. A slightly more realistic distribution of tensile stresses is shown in Figure 4. Allowance is made for some indeterminate amount of interfacial failure at the fragment ends and for the lack of shear stress at the fragment midpoints.

In one improvement on the shear lag analysis, a Poisson-Weibull treatment, developed for use with optical fibers [Medrano, 1987], has been applied to allow for the distribution of fiber strength [Drzal, 1980]. This treatment corrects for the fact that fiber fracture occurs over a range of stress levels, rather than at a unique

1
a
th
ai
tr
str

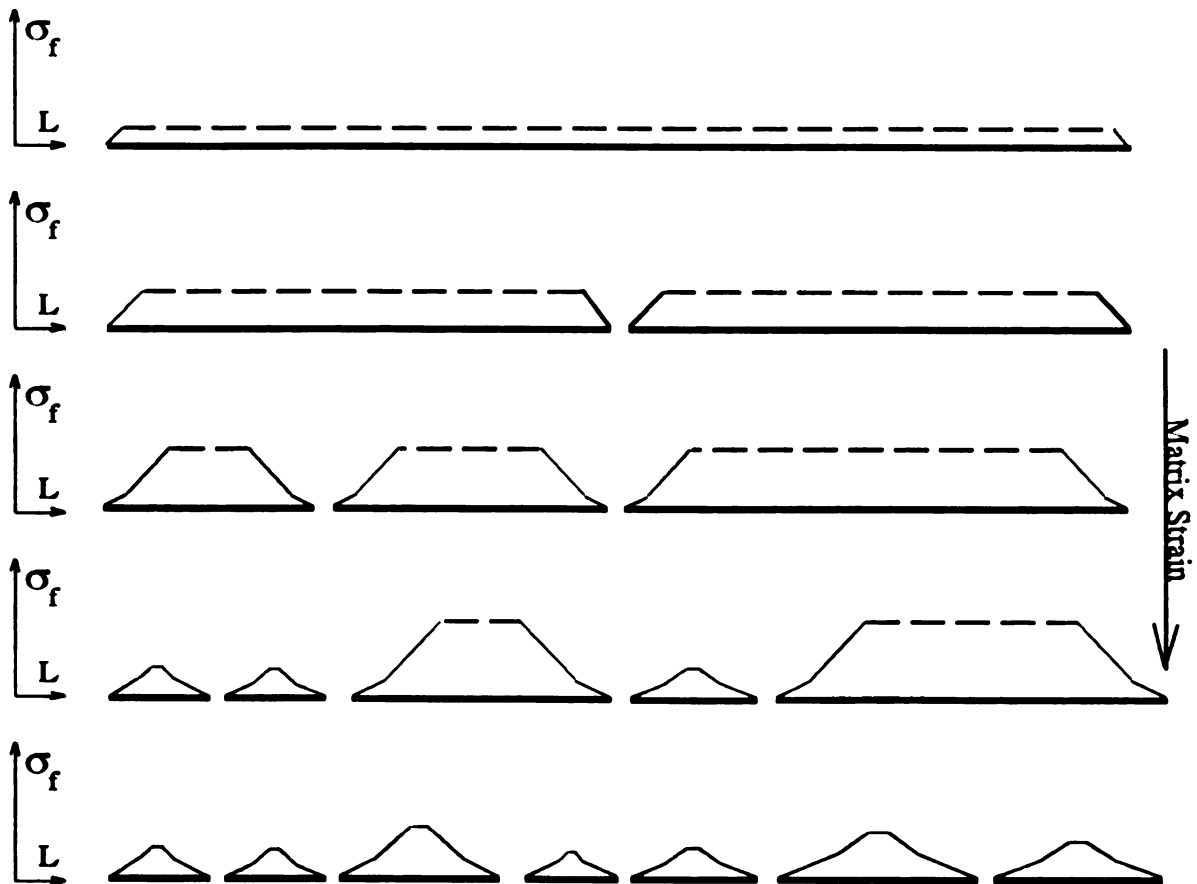


Figure 4. Slightly more realistic tensile stress distribution in fragmentation test.

strength. Although the Poisson-Weibull analysis has the considerable advantage of being applicable to all SFF-ISS specimens, regardless of failure mode, there are a number of approximations made in this treatment. Some of the more important of these are the following:

- 1) The assumption that tractions equal to the interfacial shear strength are uniformly attained along the fragment length. Interfacial debonding near the fiber ends reduces the maximum possible tractions within these regions to those transferred by friction alone. The low moduli of matrices compared with fibers also limit their stress transfer abilities even without debonding. Transverse matrix cracks can further reduce stress transfer near fiber ends. Near the fragment midpoints, shear stresses approach

zero because of symmetry.

2) The assumption that the entire fiber fragment is subject to failure when, near the completion of the test, only a narrow region at the midpoint is highly stressed. Fiber strengths as a function of length are based on the largest flaw present within the entire gage length. The fully stressed regions in SFF fragments are vanishingly small, and yet the strength at critical length is the value used in the equation.

3) The use of the strength of a randomly selected fiber with a gage length equal to the critical length in the analysis. In fact the fragments remaining at the end of the SFF test are non-random segments without any large flaws, which would have failed in the course of the test. This proof testing of fibers has been described in detail [Fraser, 1980]. A computer program which corrects this difference to perform in-situ fiber strength measurements has also been developed (see Chapter 3) [Waterbury, 1991].

Determinations of more accurate shear traction distributions have been attempted by a number of researchers. A detailed analysis of stress transfer in single fiber composites by a finite difference approach was performed by Termonia [1987]. This analysis found that stress transfer is a function of the ratio of Young's moduli for the case of perfect interfacial bonding. For the case of interfacial failure, a non-linear relationship between interfacial adhesion and critical length was predicted. A very large increase in critical length was predicted for interfacial bonding less than 30% of the matrix strength.

Shear tractions have been determined experimentally by the use of the Raman optical strain gage [Galiotis, 1989]. This technique measures shifts in Raman spectra of carbon or Kevlar fibers to produce plots of the tensile stresses along the lengths of fragments during the course of the test. These stresses can be differentiated as a function of length to determine the actual shear traction. This extremely promising

experimental technique can be used to directly verify the predictions of finite element and other theoretical mechanics predictions. The maximum shear tractions measured by this method can be interpreted as the shear strength of the interface with much less ambiguity.

2.4 FRAGMENTATION TEST FAILURE MODES

Several different failure modes occur within fragmentation specimens, depending upon the interface and other properties, sometimes within the same specimen. A list of the basic modes and some comments about them comprises this section.

2.4.1 INTERFACIAL FAILURE

The most common mode of failure in fragmentation tests is interfacial failure by the propagation of mode II cracks starting at the ends of fragments and advancing some distance along the fiber. When a fiber breaks the freed ends snap back and subject the fiber-matrix interface to both a sudden shock wave of shear stresses and to continued stress after the passage of the shock. Interfacial cracking may be initiated either by this shock wave or, statically, by the increasing interfacial stresses as coupon strain is raised throughout the test.

Interfacial failure may occur either extremely close to the actual, atomically-thin interface or at some small distance within the interphase. Distinguishing between these nearly identical failure modes is the object of some interest. Crasto, et al, detected and correlated emissions of photons and even electrons with acoustic events accompanying fiber failures in model composites with 1 to 300 fibers [Crasto, 1987]. The photon emissions were taken to be indications of adhesive failures, since the light was probably emitted when dissimilar materials with different electron affinities were separated.

f

c

a

r

t

t

i

s

f

c

s

g

b

th

o

co

st

si

st

be

size

bir

The locus of interfacial failure may also be distinguished by microtomy of fragmentation test specimens and subsequent TEM observations [Drzal, 1983]. In the case of failure within the fiber surface, fiber surface fragments may be seen to be adhering to the matrix material, while interfacial failure within the interphase or matrix leaves some matrix material adhered to the fiber and a gap between this and the bulk matrix.

Following the initial failure of the fiber/matrix interface adjacent to fiber breaks, shear tractions continue to be transmitted to the fiber across the failed interface by friction. These tractions have a maximum value limited by the interfacial static coefficient of friction. The actual traction is effected by the displacement of the fiber during interfacial failure. For a small amount of failure and a low sliding coefficient of friction, the fiber end may be almost completely moved to a relaxed state, resulting in negligible tractions until coupon strain is significantly increased.

Mechanical interlocking after interfacial failure may occur as a result of the generation of irregular fracture surfaces, or from relief structures etched into fibers by surface treatments. Ismael and Vangsness [Ismael, 1987] for instance, have found the presence of elliptical pits aligned with the fiber axis after high temperature oxidative surface treatment. The smoother surface of Hercules AS4 fibers in comparison with AS1 fibers has been found to lead to a reduction in interfacial shear strength, as measured by the fragmentation test of approximately 10% [Drzal, 1983].

Piggot [1986] has claimed that interfacial failure accompanies virtually all single fiber failures, and that the test only provides an indication of frictional shear strengths as a result.

For many fiber/matrix combinations, interfacial failure proceeds by what has been called "stick-slip" behavior. Stick-slip debonding is usually associated with un-sized fibers, and with higher modulus fibers with poor interfacial shear strengths. A birefringence sequence of a typical stick-slip debonding crack appears in Figure 5.

1
2
3
4
5
6
7
8
9
10
11
12
13
14
15
16
17
18
19
20
21
22
23
24
25
26
27
28
29
30
31
32
33
34
35
36
37
38
39
40
41
42
43
44
45
46
47
48
49
50
51
52
53
54
55
56
57
58
59
60
61
62
63
64
65
66
67
68
69
70
71
72
73
74
75
76
77
78
79
80
81
82
83
84
85
86
87
88
89
90
91
92
93
94
95
96
97
98
99
100

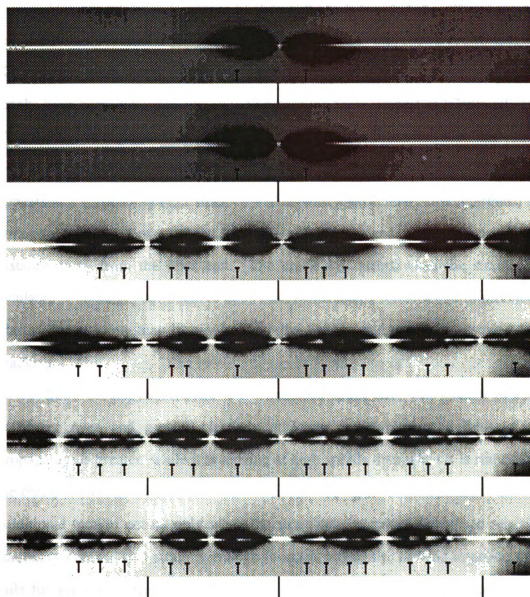


Figure 5. Interfacial failure by stick-slip mode II cracking.

This failure mode is related to stick-slip crack advance in isotropic materials, and is a consequence of the difference between the crack initiation fracture toughness, K_{ic} and the crack arrest fracture toughness, K_{ac} . The characteristics of stick-slip cracks have been measured and used to determine these properties [Cantwell, 1989]. This method may prove to be valid and valuable in fragmentation data analysis.

As coupon strain is increased, a break in the fiber occurs. If this break appears at a sufficiently high strain in a fiber with a sufficiently low interfacial shear strength, a crack at or near the interface will initiate and rapidly propagate some distance away from the fiber end. The crack will arrest when the strain energy available is no longer sufficient to create the two fracture surfaces and to produce any plastic deformation that is required by the matrix deformations associated with cracking.

Since the matrix behavior is a function of strain rate, with greater brittleness at higher rates and greater plasticity at lower strain rates, the limit of crack propagation is greater while it is moving at high speeds than when it is static. When the crack motion arrests, it therefore remains stationary as coupon strain is increased. Additional motion occurs only when the strain has increased enough to reinitiate a stationary crack. This strain is enough to again propagate, and the interface rapidly fails for some distance until the strain is no longer sufficient to advance a moving crack. The difference between the static and dynamic materials properties of the interphase generates this hysteresis which may be quantitated to provide valuable information on the interphase K_{ic} and K_{ac} .

While the crack is paused between jumps, creep occurs at the highly strained crack tip. This plastic deformation leaves behind remanent birefringence patterns that mark the points at which pauses have occurred. These patterns produce the so-called "stick-slip" markings that are commonly observed.

The distance travelled in each crack jump is a function of at least four

variables. These are: 1) The change in interphase fracture behavior with strain rate. 2) The distance from the break in the fiber to the initial crack tip position. 3) Whether the crack was initiated by strain energy released by a fiber failure. 4) The coupon strain at which the jump occurred. Some observations relating to these variables follow.

The distance from the fiber break to the crack tip effects the strain energy available for crack propagation for at least three reasons. The discontinuity at the fiber end may serve as a stress concentrator and locally increase the shear stress. For short fibers that are perfectly bonded, the interface loading goes to zero at the center of the fiber and reaches a maximum at the ends. The frictional tractions across the failed interface/interphase load the fiber in tension to some extent, reducing the stresses at the crack tip. The amount of this shear traction depends on the coefficient of friction across the failed surface, the normal loading across the failed surface resulting from matrix thermal or cure shrinkage and the differences in Poisson's ratio between the fiber and matrix, and the loading of this surface by strain mismatch across it. The friction coefficients only describe the maximum possible traction while the actual traction may be near zero if fiber sliding has accommodated the strains across the failure surface. This may happen since the fiber ends are not always gradually loaded, in particular when the fiber snaps after either fiber failure or interface fracture occur.

2.4.3 RADIAL MATRIX CRACKING

In SFF-ISS samples with strong interfacial adhesion, matrix cracks running radially outward from the fiber axis are often initiated. Drzal [1983] has suggested that these cracks occur near sized fibers because of the formation of a brittle interphase region. This high-modulus, but brittle, region is thought to improve fiber/matrix adhesion but to change the failure mode from interfacial to transverse

matrix cracking, thereby decreasing toughness.

2.4.4 INTERPHASE YIELDING

Plastic deformation of the interphase region sometimes accompanies single fiber fragmentation with high interfacial shear strength. Interfacial shear strengths substantially larger than the bulk matrix shear strength have been reported [Netravali, 1989].

Although it has sometimes been stated that the interfacial shear strength can be no greater than the shear strength of the matrix, because yielding immediately adjacent to the fiber would take place, this is not a limitation for at least four reasons.

1. The matrix is constrained by the presence of the much stiffer, stronger fiber and so has material properties different from the bulk material.
2. The composition of the interphase region may differ from the bulk due to segregation toward the interface or the presence of finishes.
3. The microstructure of the interphase may differ considerably from the bulk material, especially in the case of the transcrystalline interphases sometimes generated in semi-crystalline thermoplastics. These oriented interphases may possess much greater yield strengths in shear than do the spherulitic structures of the bulk material.
4. The extremely small size of the interphase region makes the use of shear strength data obtained from macro-scale specimens questionable. Whether for brittle fracture or plastic yielding, the strengths of very small specimens is almost always greater than for large samples with many more defects to initiate failures present. A change in failure mode from brittle fracture to plastic yielding may also occur with a change in

specimen size. Extensive plastic yielding of material on failure surfaces has been noted for matrices which undergo brittle failure in large specimens [Hibbs, 1987]. Decreasing the thickness of adhesive joints has been found to increase the extent of plastic deformation before failure [Stringer, 1985]

2.5 FIBER STRENGTH DISTRIBUTION EFFECTS

Reinforcing fibers do not have a uniquely defined strength, but a statistical distribution which approximates an exponential function as described in Chapter 3. This distribution may be fairly narrow, with all fragments failing in a closely defined stress interval, as with many glass fibers. Carbon fibers, in contrast, fail over a wide range of stresses. This range is a function of the fiber fragment length, since longer fragments contain greater numbers of all sizes of flaws and have a larger probability of containing a large flaw than short fibers.

This length-strength dependence has been described as a semi-log relationship, with the strength proportional to the logarithm of the fiber length [Phani, 1987]. Other treatments, based upon Poisson-Weibull analyses, have also been proposed [Phani, 1987], [Asloun, 1989].

The strain energy released by fiber failure can exert a considerable influence over both the mode and extent of failure in single fiber composites. This influence is not a simple function of increasing damage with increasing strain energy but may also depend upon the kind of matrix involved. Since fibers fail over a wide range of strains, substantially different failure modes can occur within the same specimen, effecting shear stresses, critical lengths, and measured shear strengths.

Figures 6 and 7 show three breaks in an AS4 fiber in the same coupon at two different coupon strain levels. The two breaks in the top fiber occurred at a low fiber failure strain while the break in the lower fiber was at a significantly higher strain. As can be seen in Figure 6, the high failure strain break has initiated and propagated

a stick-slip type interfacial crack for a considerable distance while the two lower strain breaks have debonded much shorter distances. Figure 7 shows the same three breaks at a higher strain level, approximately 3.0%. The high failure strain break has continued to debond for greater distances than the two low strain breaks. Clearly, the strain energy released as a shock wave from the failing fiber has strongly affected the ability of the interface to transmit stress. This effect is shown in diagrammatic form in Figure 8, which shows a longer stress transfer length associated with the higher failure strain breaks causing extensive debonding, lower, frictional, shear tractions, and a longer final fragment length.

An additional complication arises when different matrices and failure modes are considered. Observations of birefringence patterns in polycarbonate matrix specimens that undergo interphase yielding rather than interfacial cracking show a fiber failure strain energy influence, but of a different sort. At the completion of the test, the lowest failure strain breaks were seen to have more extensive regions of remanent birefringence, an indication of more extensive plastic deformation, than those occurring at higher strains. Birefringent sheaths were approximately twice as long near the low strain breaks than those occurring at medium or high failure strains. Apparently, in the absence of interfacial failure, the greater period of time available for creep causes more extensive plastic yielding of the highly stressed material near the breaks occurring early in the test. This effect is shown in diagrammatic form in Figure 9. The shear stress loading length is greater for breaks occurring at low strains, exactly the opposite of the case for interfacial debonding.

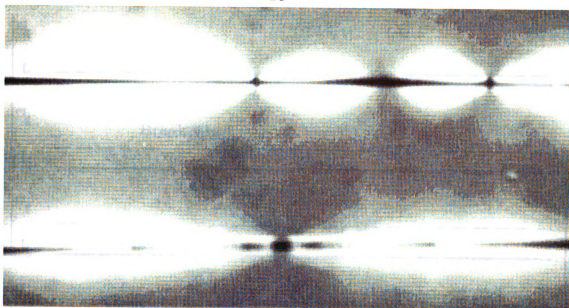


Figure 6. Fiber failure strain energy effects on interfacial failure.

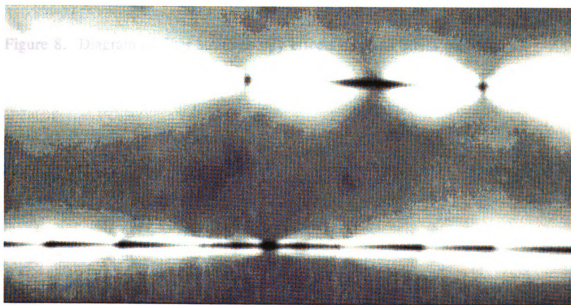


Figure 7. Fiber strain energy effects at higher coupon strain.

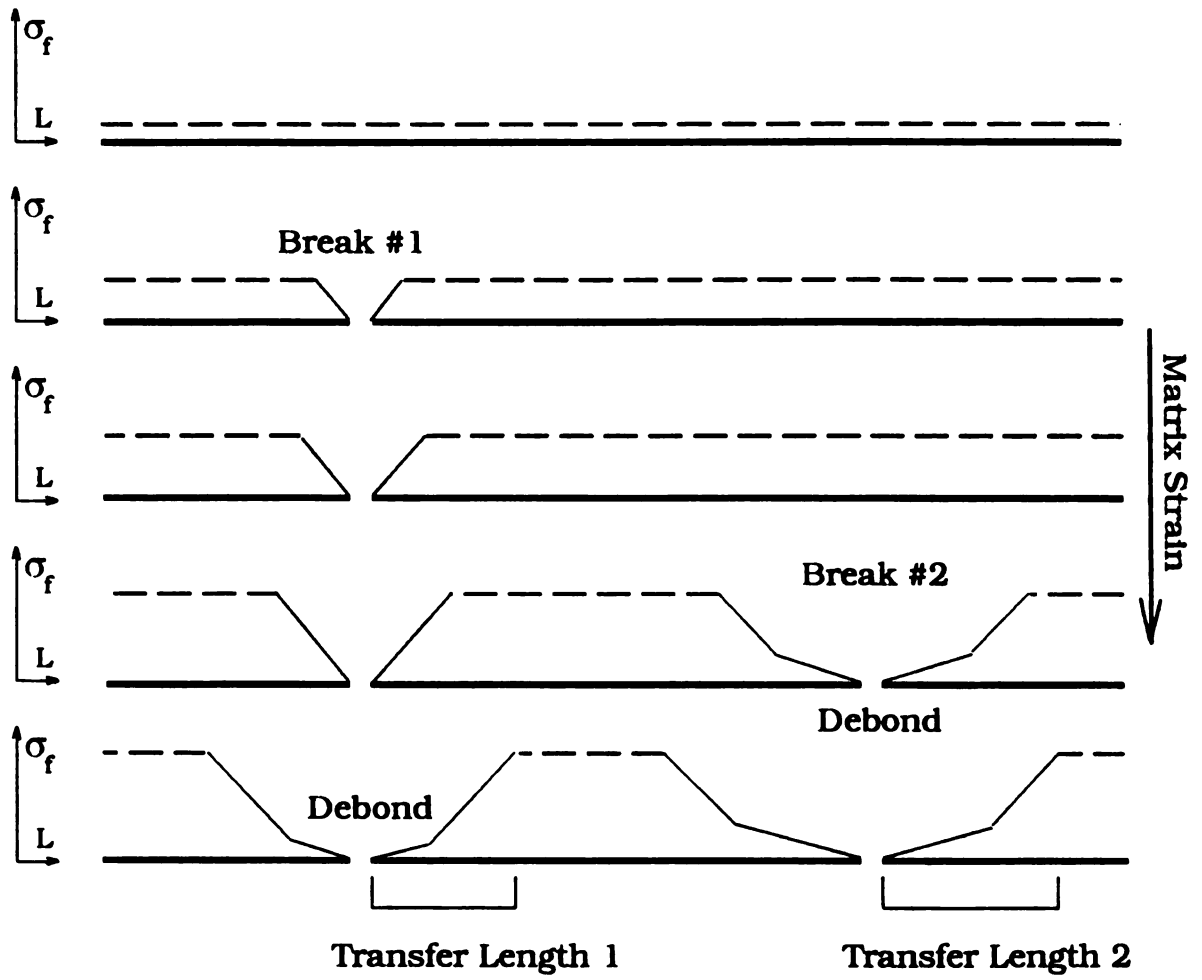


Figure 8. Diagram of fiber strain energy effects on shear stress transfer.

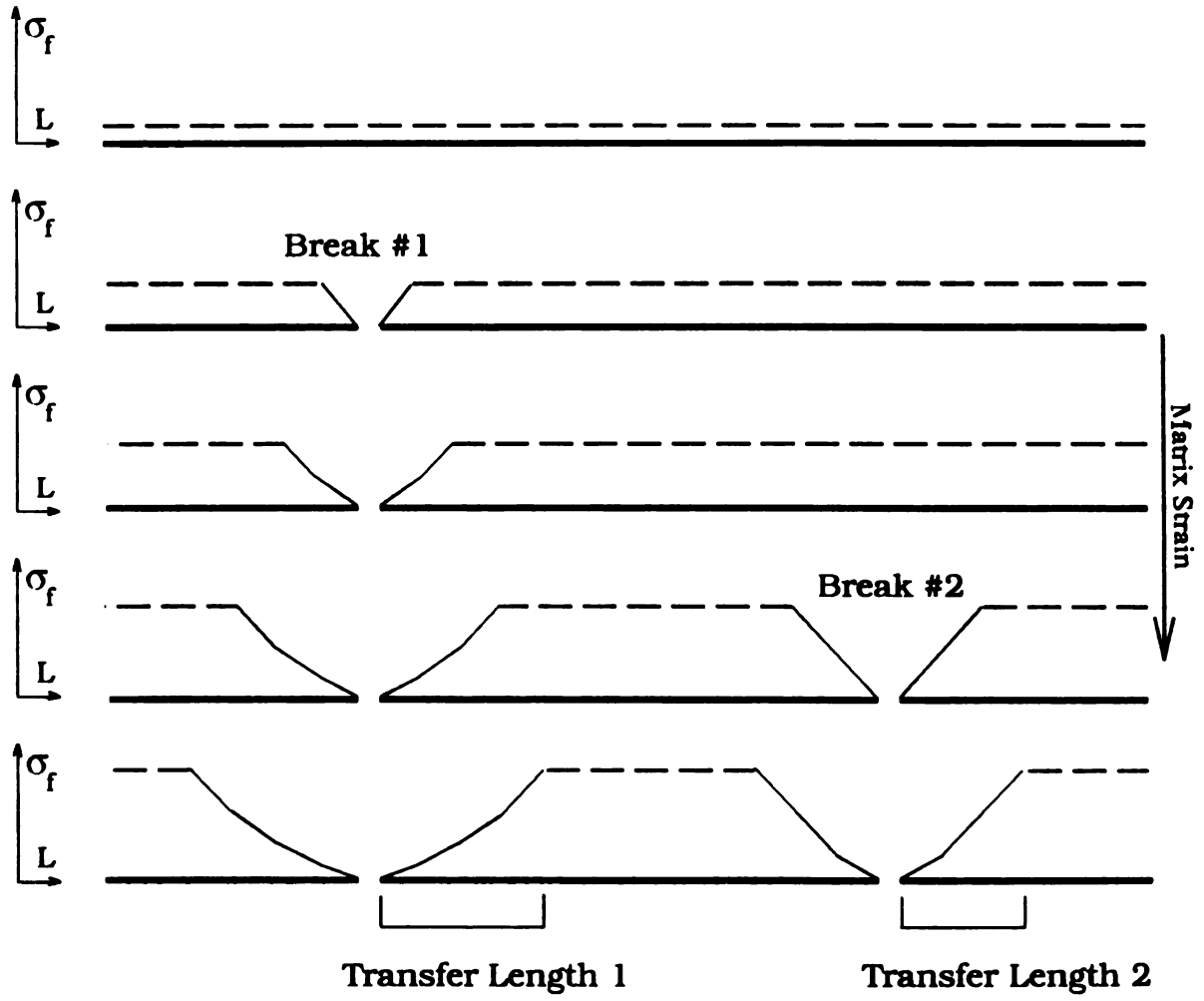


Figure 9. Diagram of fiber failure strain effects on interphase yielding.

The influence of fiber failure strain energy on birefringence patterns and the confusion they can cause is also documented in section 5.4.2.8 with IM6 birefringence images. Uniformly incremented changes in fiber surface treatment in otherwise identical systems gave the appearance of producing completely different failure modes with increasing treatment. By considering the additional variable of fiber failure strain energy release, the failure modes can be seen to change in a consistent, predictable way.

Another influence of fiber strengths on SFF tests arises because fiber failure during the fragmentation test begins at the largest flaws and proceeds to successively smaller sizes, changing the makeup of the flaw distribution throughout the test. The strengths of the fiber fragments are therefore a function of the coupon strain level as well as the fragment length, complicating data analysis. DiBenedetto, et al. have referred to this process as "proof testing" and have altered the strength distributions assumed to compensate for this factor [DiBenedetto, 1985].

2.6 FAILURE MODE INTERACTIONS

The different kinds of failure occurring within single fiber composites are not independent, but may occur in either a competing or cooperative fashion. Strain energy release resulting from radial matrix cracking may act to entirely prevent or reduce interfacial failure which might otherwise occur. Similarly, the initiation of interfacial cracks sometimes prevents the formation of radial matrix cracks by accommodating strains near the fiber ends.

2.7 SFF SPECIMEN FABRICATION EFFECTS

The process of fabricating SFF specimens is largely accomplished manually. It is a tedious and time consuming process which requires appropriate safeguards against fiber-surface contamination and fiber damage. Some considerations and

precautions associated with this process are outlined in this section.

2.7.1 FIBER SURFACE CONTAMINATION

Contamination of the fiber surface is the most serious specimen preparation artifact, and the most difficult to avoid. Even in a clean laboratory environment, fibers may be contaminated from many sources such as skin oils, RTV silicone molds, researcher breath, and other surface active contaminants. Sensitive surface analysis techniques can detect the movement of low molecular weight species over significant distances. Segregation of low molecular weight constituents from the matrix to single fiber surfaces by free energy driving forces may also result in interphase compositions which differ from those in a high V_f composite where an equilibrium state is not attained.

2.7.2 FIBER DAMAGE

Mechanical damage to the fibers during layup does not usually present a problem because the large flaws thus produced do not significantly influence the final fragment length attained. This value is determined instead by the fiber stress at which the final fragments no longer fail. Provided that the fibers are not extensively damaged during handling and layup, the flaws present in these short fragments are not likely to be changed.

A possible exception to this may result from the difficulty in removing single fibers from a sized tow. Although sizing protects fibers from processing induced damage, it makes the separation process substantially more difficult. Thus although finished fibers in an actual, high volume fraction composite may be slightly stronger than their unfinished and unprotected counterparts, finished fibers could be weaker in a single fiber specimen, from the difficulty of separating single fibers.

2.7.3 STRESSES INDUCED BY MATRIX CURING AND COOLING

Dimensional changes occur in the matrix during specimen curing and cooling in thermosets and cooling and crystallization in thermoplastics. These changes can induce normal stresses across the fiber/matrix interface which alter the apparent interfacial shear strength. Normal compressive stresses are also produced by the difference between the Poisson's ratios of the fiber and matrix. These stresses may be different from those present in high volume fraction composites. Residual stresses are also developed from contraction of the matrix during cooling from T_g following consolidation or curing.

2.8 MEASURABLE FRAGMENTATION TEST PARAMETERS

Valuable information about interfacial toughness, strain rate effects, and failure mode modification may be obtainable through additional analysis of SFF tests. The particular parameters which may be measured depend upon the failure mode acting in the SFF specimen. Specimens exhibiting transverse matrix cracking will not have interfacial cracks to measure, for instance. The principal advantage of using the critical fragment length as a summary of SFF behavior derives from its universality. All single fiber specimens which can be strained to completion have a measurable critical length, regardless of failure mode. Specimens with transverse matrix cracks can therefore be directly compared with those undergoing interfacial failures, in spite of some "apples and oranges" ambiguity.

A list of some measurable SFF test parameters follows.

1. Coupon strain at which interfacial cracks are initiated near previously existing low failure strain breaks (without fiber failure strain energy contribution).
2. Coupon strain at which interfacial cracks are initiated, simultaneously with the

fiber break (with fiber failure strain energy assistance).

3. Coupon strain at which interphase yielding occurs near previously existing breaks.
4. Coupon strain increment required to restart an arrested interfacial crack.
5. Distance advanced by a previously existing crack during one "stick-slip" jump.
6. Distance advanced by a newly initiated crack near a previous break, (without fiber failure strain energy).
7. Distance advanced by a newly initiated crack, simultaneously with the fiber break, (with fiber failure strain energy assistance). This occurs at a much lower coupon strain than #6, and with less strain energy available for propagation, the distance traveled is much shorter.
8. L_c/D : The critical length to diameter ratio, the most commonly measured fragmentation test parameter.
9. Failure modes: Observations of the birefringence patterns near fiber breaks provide valuable information on the operative failure modes in fragmentation tests. The ease of these observations is one of the principal advantages of this test over other interfacial testing methods. Birefringence pattern acquisition is described in the following section.

An advantage of recording the strain levels at which particular, well defined failure events occur within the microcomposite is that the experiment is fully

i
c
2
s
Is
un
he
ex

in
re:
the
occ
xatt

controlled. A single failure mode is analyzed by a single algorithm, rather than subjecting an ill-defined and complex mixture to a single treatment. A disadvantage arises from attempts to compare specimens undergoing different failure modes, an arena in which the simple L_c/D approach has advantages.

The consistency of the coupon strains at which interphase yielding takes place near previously existing breaks can be seen in Figures 10-17. These birefringence images show a set of 8 breaks in the same AS4 fiber, each at the same series of coupon strain levels. All breaks occurred at the same, low fiber failure strain energy, which was insufficient to initiate interfacial debonding. As can be seen from the images (and may be more clearly seen in the higher resolution computer screen images) changes in the birefringence patterns for all 8 breaks occur in an almost identical manner. The only differences arise from changes due to randomly occurring, new adjacent breaks.

2.9 STRESS BIREFRINGENCE PATTERN OBSERVATION AND RECORDING

The optical birefringence patterns produced by the local shear stresses surrounding broken single fibers have been used to monitor the progress of the SFF-ISS test and to garner additional information about failure modes. The conditions under which these patterns are recorded have often been incompletely characterized, however, reducing their value and occasionally leading to misleading reporting of experimental data.

As described in the previous section, Figures 10-17 demonstrate that changes in photoelastic patterns are consistent and reproducible, provided that all of the relevant experimental variables are controlled, in particular the fiber failure strain and the coupon strain. As described in section 2.5 and demonstrated in Chapter 5, breaks occurring at different strain levels can completely alter the appearance of birefringence patterns, even when the interfaces are very similar.

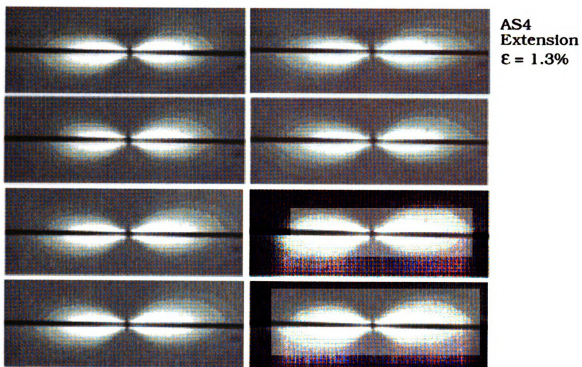


Figure 10. Birefringence patterns for 8 breaks in AS4 fiber, 1.3% coupon strain.

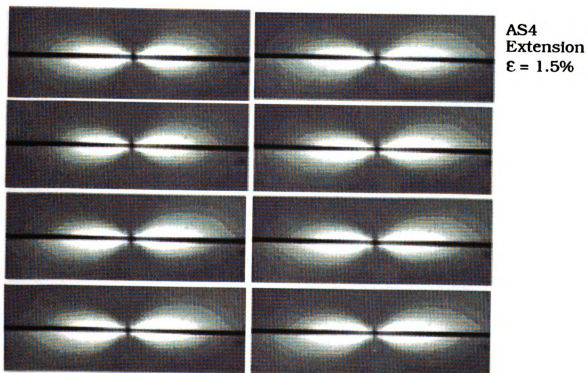


Figure 11. Birefringence patterns for 8 breaks in AS4 fiber, 1.5% coupon strain.

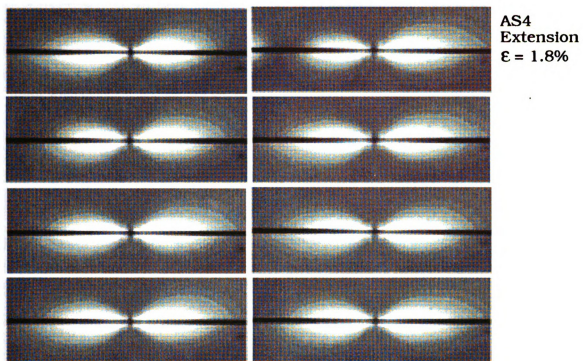


Figure 12. Birefringence patterns for 8 breaks in AS4 fiber, 1.8% coupon strain.

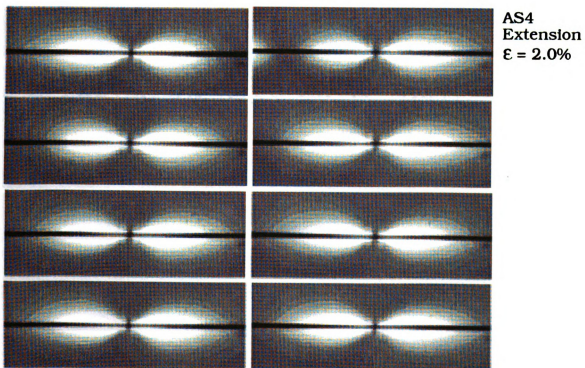


Figure 13. Birefringence patterns for 8 breaks in AS4 fiber, 2.0% coupon strain.

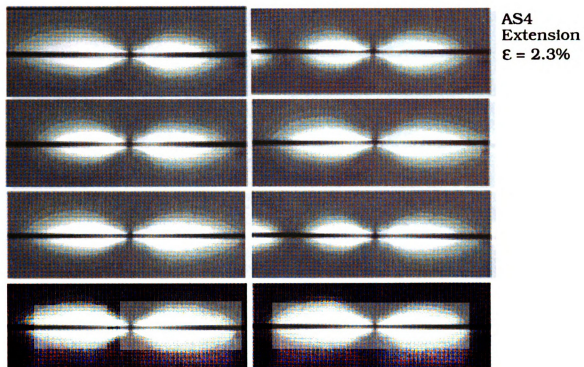


Figure 14. Birefringence patterns for 8 breaks in AS4 fiber, 2.3% coupon strain.

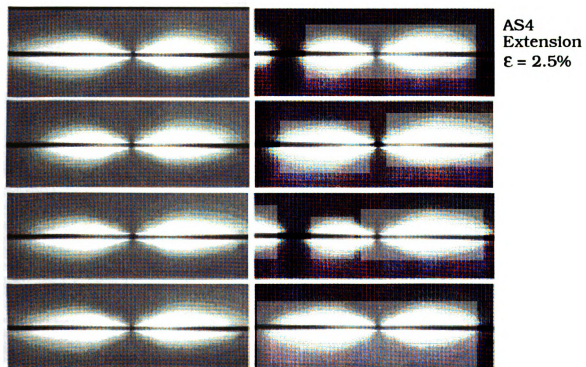


Figure 15. Birefringence patterns for 8 breaks in AS4 fiber, 2.5% coupon strain.

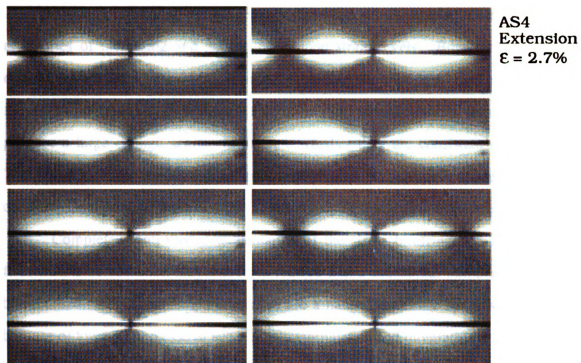


Figure 16. Birefringence patterns for 8 breaks in AS4 fiber, 2.7% coupon strain.

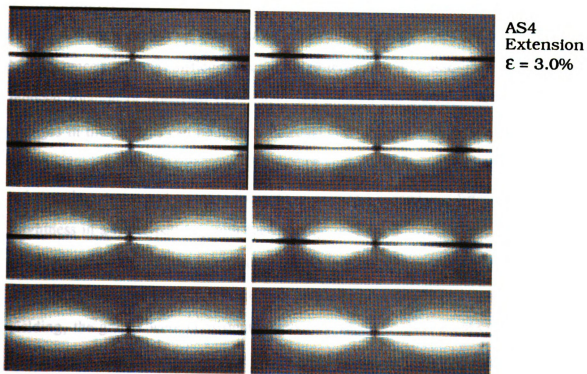
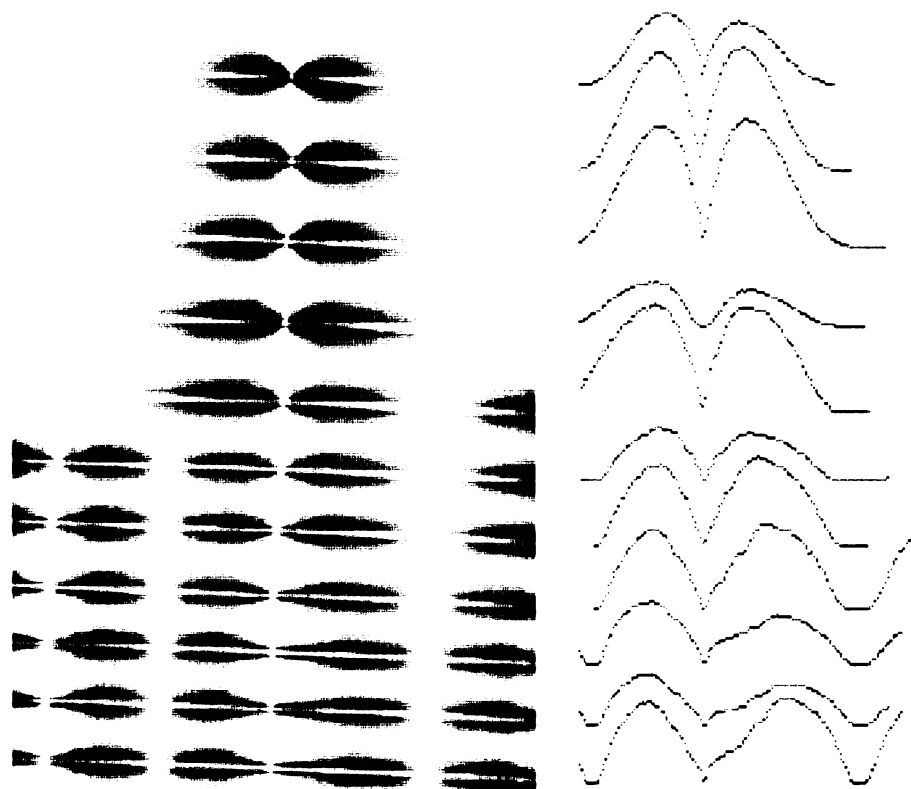


Figure 17. Birefringence patterns for 8 breaks in AS4 fiber, 3.0% coupon strain.

Properly controlled birefringence experiments should consist of sets of images at a series of increasing and decreasing coupon strain levels. Breaks occurring at different strain levels should be recorded, including, at least, low, medium and high failure strain breaks. A few breaks of each type should also be documented, to produce a large enough sample to indicate whether they are consistent or variable. The lengths of the adjacent fragments should also be recorded, since the stress conditions are partly determined by the proximity of the next nearest breaks.

Complete, controlled documentation of the stress birefringence for a single fiber-matrix combination may therefore require that a substantial number of images be recorded. Digitized computer images are a natural candidate for this task, both because of low cost and ease of subsequent manipulation and integration with software analysis. For these reasons most of the images recorded for this work have been acquired by computer. Birefringence sequence acquisition is described in detail in section 5.3.3.9.

Although extracting quantitative information directly from the brightness of birefringence patterns is difficult because the patterns are the consequence of the stress induced rotation of polarized light integrated through the thickness of the sample, changes in the patterns can be readily detected qualitatively, and these changes used to extract quantitative information. Figure 18 shows a series of birefringent images at increasing strains and a plot to the right of each that is produced by integrating the brightness in a raster pattern, with each vertical column of pixels producing a single point on the graph. When interphase yielding begins to occur, in the fourth image from the bottom, the integrated brightness graph shows a discontinuity, where before yielding, the graphs were consistently smoothly varying. This method can be used to determine both the strain level at which yielding begins, with more reliability and consistency than human visual interpretation, and the measure its extent. Quantitative information has been extracted from the birefringence patterns, even though the exact



Birefringence sequence and graph of integrated brightness

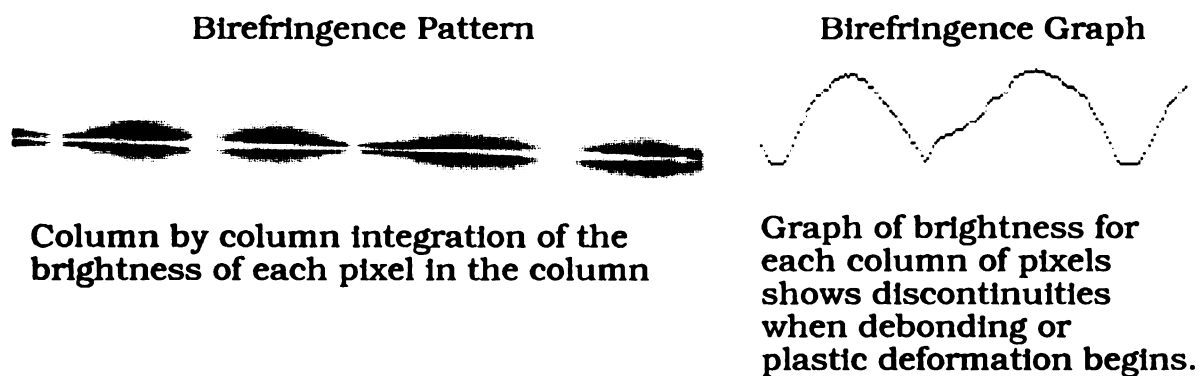


Figure 18. Rasterized integration of birefringence patterns to detect yielding.

nature of the stress distribution and length of the light path has not been addresses.

Another quantitative value which may be acquired involves the measurement of stick-slip advance characteristics. As described in section 2.8, the distances advanced and strain levels and increments required for advance can be a source of interfacial fracture toughness information. Figure 5 shows a birefringence sequence of a stick-slip pattern with the location of each crack arrest denoted by an upside down "T". The consistency of each crack advance distance can be easily seen, with shorter advances at greater distances from the break due to frictional stresses loading the fiber end.

2.10 RAPID SINGLE FIBER FRAGMENTATION TEST DATA ACQUISITION

Fragment measurement has been a tedious and time consuming process. Alternative methods can substantially improve the rate and accuracy of data acquisition, as well as facilitating subsequent computer analysis. As part of this research program, the software and hardware package FiberTrack [Waterbury, 1991], a dedicated single fiber data acquisition and analysis system was developed. This method is described in section 3.3.4. Acquisition rates more than an order of magnitude faster than previous methods may be routinely obtained.

Acoustic emissions from single fiber breaks have been detected and characterized by a number of researchers [Netravelli and Sachse, 1989]. Hamstad and Moore [1986] detected emissions from dry and lubricated tows and were able to distinguish emissions emitted by single fiber breaks and two or more simultaneous breaks.

As part of this research program, a simple apparatus was used to identify emissions from both fiber breaks and subsequent debonding events. These events were recorded at very low frequencies (20 kHz digitization rate) and were similar in form but differed in amplitude, depending on whether they were fiber breaks or

debondings. Apparently, either type of failure excites a similar resonance mode within the specimen.

Acoustic emissions can be readily used to both count fiber breaks and record the coupon strain level at which they occur, an important consideration for in situ fiber strength analysis (Chapter 3). By noting the arrival times of emissions at a pair of transducers, it is also possible to determine the locations of breaks, and so measure the lengths of fiber fragments [Netravali, 1989]. This method may prove somewhat difficult experimentally, however, since the arrival times must be measured with very high precision to accurately measure fragments only fractions of a millimeter in length. The accuracy of these measurements is a function of the velocity of sound within the matrix, itself a function of the modulus and density, the frequency of data digitization, which determines the limiting accuracy of arrival time measurements, and the consistency of the acoustic coupling between the transducers and the specimen.

Interfacial failures can be quantitatively measured in both length and separation by observations of changes in light transmission transverse to the fiber axis. Sargent and Ashbee [Sargent, 1985] were able to measure gaps as small as 5 nanometers, but this method relied upon the transparency of glass fibers and is not applicable to carbon fiber composites.

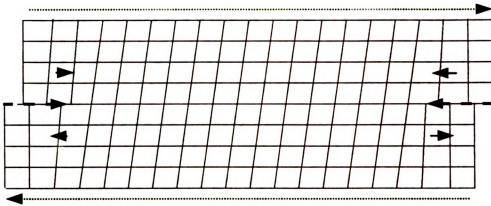
2.11 RELATIONSHIP TO OTHER INTERFACIAL ADHESION TESTS

Fiber-matrix interfacial shear strengths are currently measured by several methods. Agreement between these methods has been very poor, and research is underway to improve the understanding of the relationships between these experimental procedures. Interfacial shear strength tests include the fragmentation test, the pullout test, indentation and push through tests, and droplet pullout or microbonding tests. This section outlines some of the fundamental differences and similarities between these mensuration techniques.

Two factors are often overlooked in comparing fragmentation testing with these methods. Perhaps the most important is the influence of fiber failure strain energy release on interfacial crack initiation, described in section 2.5. Of the above tests, only the fragmentation test inherently includes a contribution from this high frequency loading of the interface. As suggested in sections 2.5 and 5.4.2.8, this energy can completely change the appearance of the failure modes. All other current shear strength measurement techniques derive the energy for interfacial failure without contributions from fiber failure.

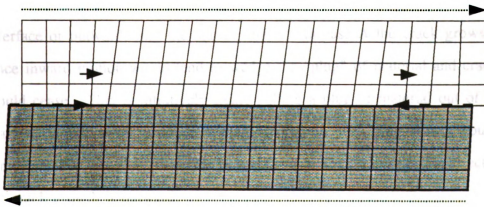
The second fundamental difference among the different shear strength methods involves the symmetry of the advancing mode II crack during debonding. In a homogeneous material, the motion of a mode II crack may be said to be symmetric, as can be seen in Figure 19. As the crack advances in one direction, the material displaces in opposite directions on either side of the crack, each a mirror image of the other. When the crack advances along the interface between dissimilar materials, however, the symmetry is broken. As depicted in Figure 20, the material on one side of the crack displaces in the same direction as the crack advance, while the different material on the other side of the crack moves in the opposite direction from the crack. The crack is asymmetric because the materials moving in the same direction as the crack is different from that moving in the opposite directions.

When there is a significant difference in material properties between the two materials, as with a low modulus and strength matrix surrounding a high modulus and strength fiber, crack asymmetry can effect interfacial debonding characteristics, and measured values of the shear strength. Figure 21 shows four fundamental cases of a cylindrical mode II crack growth through an isotropic plate under different loading and crack initiation conditions. Although this example assumes an isotropic material, the symmetry is still broken by the "inside" and "outside" of the cylindrical crack, which may also be considered to be the same as the fiber and the matrix.



Mode II cracks in a homogeneous material, symmetric case.

Figure 19. Symmetric mode II crack in homogeneous material.



Mode II cracks along a fiber/matrix interface, asymmetric case.

Legend: List of vectors

- - -> Crack propagation direction
- > Matrix displacement direction during cracking
-> Imposed shear stress

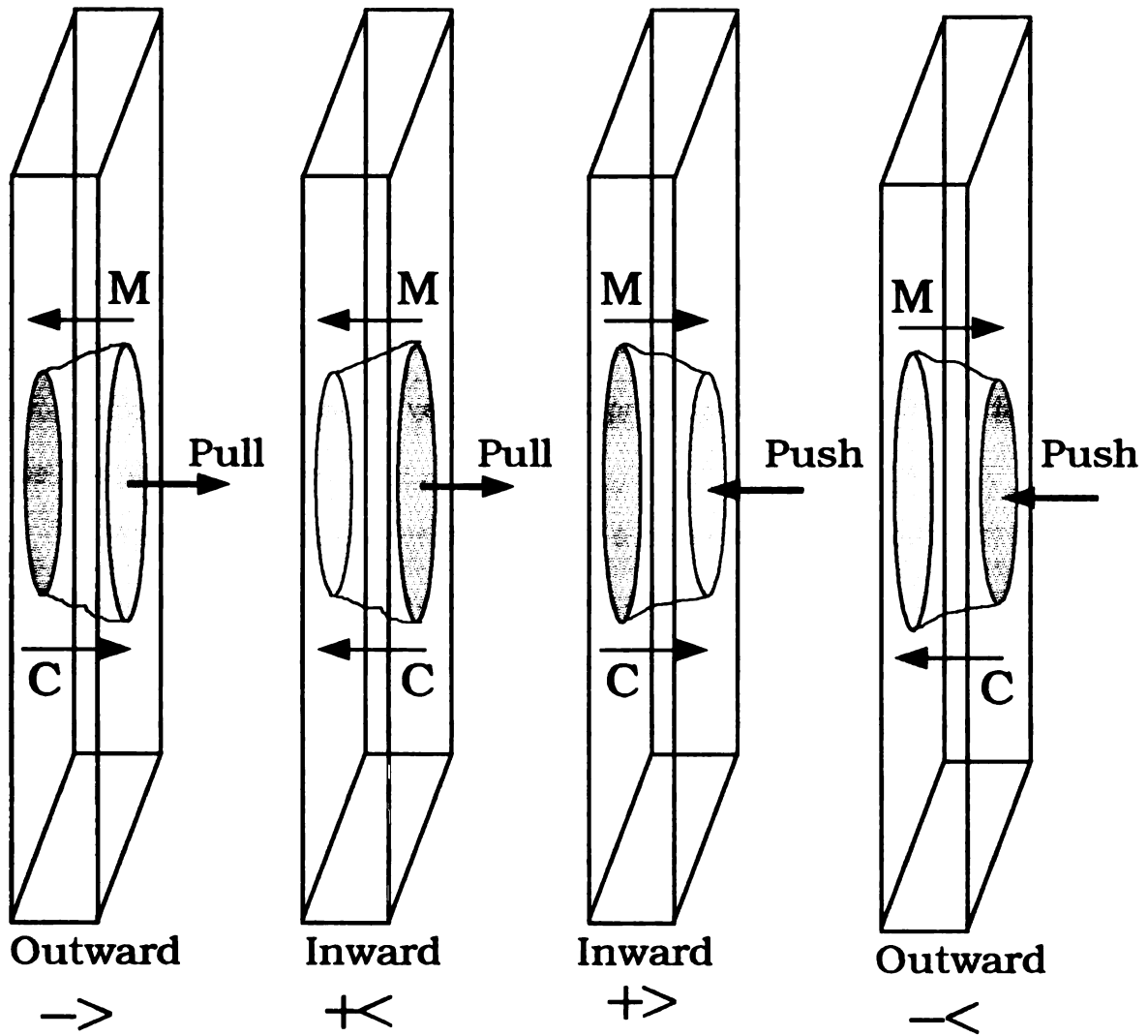
Figure 20. Asymmetry of mode II crack between dissimilar materials.

The four cases are comprised of all combinations of two loading and two crack initiation states. Cases A and B involve loading by exerting a tension traction on a circular region on the right side of the plate. Cases C and D involve loading by exerting a compression traction on circular regions on the right side. The sites of crack initiation complete the symmetry set. In cases A and C crack initiation occurs on the left face with propagation toward the right, while cases B and D initiate on the right face and initiate toward the left. Crack propagation directions are indicated by the "C" vectors. The "M" vector in each diagram indicates the direction that the matrix (outer material) will displace when the crack passes. This is the opposite of the direction that the material is strained by the different loading conditions.

With the four cases so defined, we can now investigate the crack growth properties to evaluate whether they tend to grow inward, toward the fiber-matrix interface or outward, into the matrix region. In case A the crack grows outward, since inward motion would tend to wedge the "plug" of material and crack growth would cease. This is intuitively clear, pulling a plug of material out of a plate of material would never produce a plug tapered in such way that it could not be removed. For this case where the M and C vectors point in opposite directions then, the crack growth is outward.

Case B involves the same loading as case A, but with the opposite crack propagation direction. The plug of material is tapered in the same direction, for the same reason, it could not be removed if it were tapered in the opposite manner. The crack tends to meander inward in this case however, where the M and C vectors are in the same direction.

Case C has loading by a push from the right, with crack initiation from the left propagating toward the right. The M and C vectors are in the same direction, and the growth tendency is inward. Case D has the same loading but opposite crack propagation, the M and C vectors are opposed, and growth tendency is outward.



Legend: "C" advancing crack vector, "M" matrix displacement vector

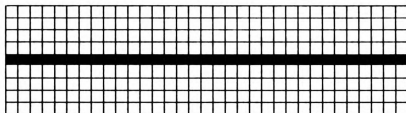
Figure 21. Crack growth habits for 4 crack initiation and loading conditions.

The two cases B and C with aligned M and C vectors both have tendencies to grow inwardly, favoring interfacial failure modes, since the crack will tend to either hug the fiber-matrix interface or meander toward it. Cases A and D have opposed M and C vectors, both have the ability to move outwardly, away from the fiber-matrix interface and into the matrix material. Aligned crack propagation and matrix displacement vectors tend to produce inward growth and interfacial failures, opposed propagation and displacement vectors tend to produce outward growth and failures in the interphase or matrix.

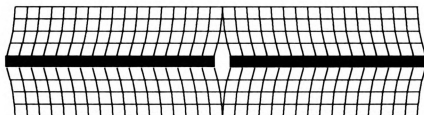
With these tendencies established, we can now analyze the different ISS tests to determine how their symmetries and potential failure characteristics compare. Figure 22 is a diagram of the symmetry factors for matrix shear strains and displacements during interfacial crack propagation in a fragmentation test. In step 1 the entire matrix and fiber region is under tension and the interface is unstressed. Step 2 shows the fiber snapping back after a break, subjecting the interface to shear stress and deforming the matrix. Step 3 shows a crack initiating at the fragment ends and beginning to propagate away from them. The direction of matrix displacement associated with crack propagation is opposite that of the crack propagation direction. Step 4 shows the crack continuing to propagate until arrest.

From the preceding discussion, there is the possibility that this crack can meander outwardly, away from the interface. This motion will leave voids or gaps along the fracture surfaces. Migration toward the interface can also occur, but this motion must compress together the material across the resulting fracture surfaces, requiring considerable energy. The maximum shear stresses, of course, occur nearest the interface and tend to continue to confine it there. This discussion considers the effects of crack symmetry only, and neglects all other mechanics considerations.

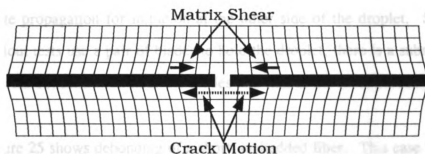
Figure 23 shows a diagram of a pullout test with debonding initiating in two different positions, either at the point where the fiber emerges from the matrix, where



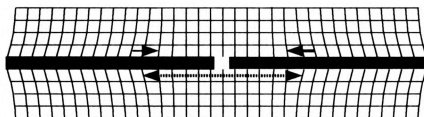
1. Portion of fragmentation test specimen prior to fiber fracture.



2. Fiber snaps back after breaking, briefly displacing matrix.



3. Cracks initiated near fiber ends at shear stress maxima.



4. Interfacial crack propagating toward fragment centers. Matrix shears in opposite direction from crack movement.

Figure 22. Symmetry of interfacial cracking for fragmentation test.

shear stresses might be expected to be maximum, or at the embedded end of the fiber where a local stress concentration may occur. The symmetries of the two cases are different, when the crack initiates at the emergence point the matrix displaces in the same direction as the propagation and growth will tend to be inward, confined strictly to the interface. This behavior has been observed in model gelatine matrix composites as part of this work. When cracking initiates at the embedded end, however, the matrix displaces in the opposite direction from propagation, and outward growth is possible.

Figure 24 shows debonding in a droplet pullout test. This is a similar case to the ordinary pullout test, with two possible initiation cases. The matrix displaces in alignment with the propagation for the case of initiation near the restraining blades, and opposite propagation for initiation at the other side of the droplet. Since most droplet pullout tests use a pair of blades to hold the droplet, there is a substantial and irregular stress concentration near the blades and that is the most probable initiation point.

Figure 25 shows debonding of a short, embedded fiber. This case is identical to the fragmentation case, with the notable exception that there is no contribution from fiber failure strain energy release. The matrix displaces in the opposite direction from the crack propagation, with the possibility of outward growth.

Figure 26 shows debonding for the indentation test. The matrix displaces in the opposite direction from crack propagation, allowing outward crack growth.

These divergent crack growth propensities may also be understood in terms of the climb of an edge dislocation in a crystalline material. Edge dislocations are constrained to motion within a glide plane for conservative motions, i.e. those that do not create or destroy vacancies. Movement out of the glide plane corresponds to a mode II crack growing up or down, it is only possible if vacancies within the crystal, or voids within the matrix are produced or consumed. Whether voids are produced

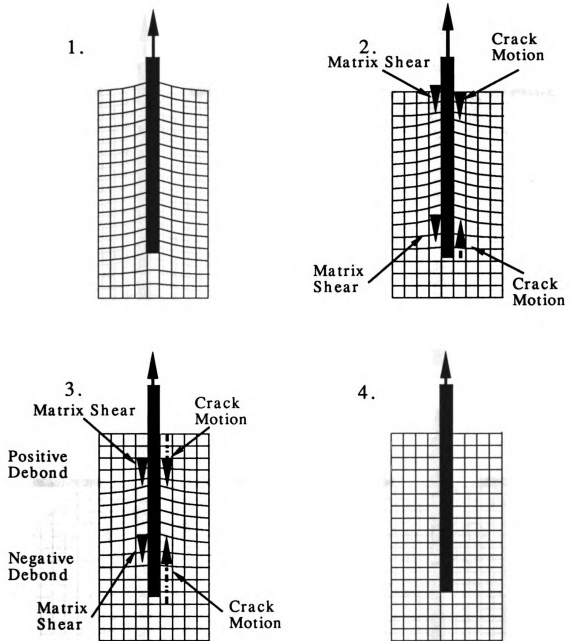


Figure 23. Symmetry of interfacial cracking for pullout test.

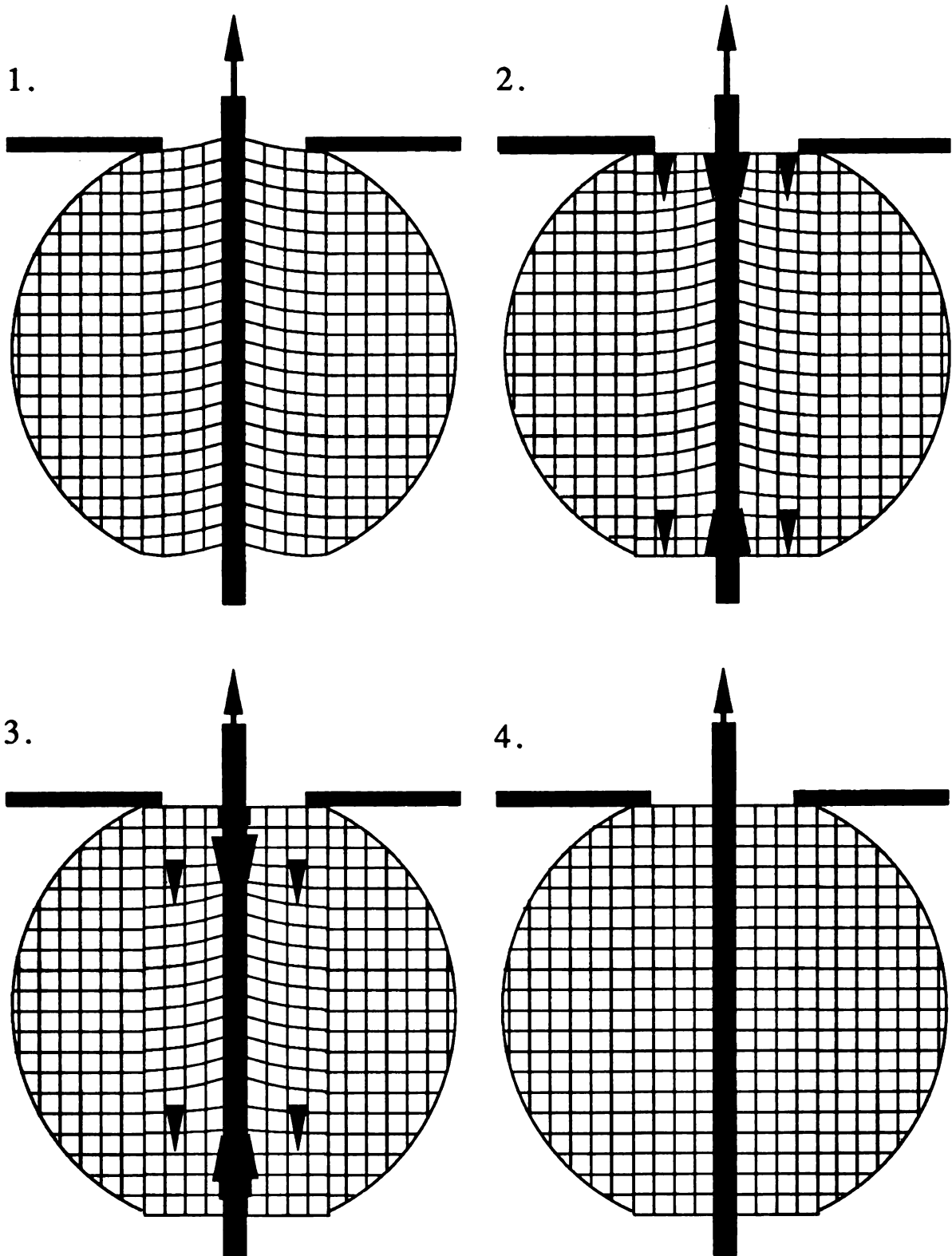


Figure 24. Symmetry of interfacial cracking for droplet pullout test.

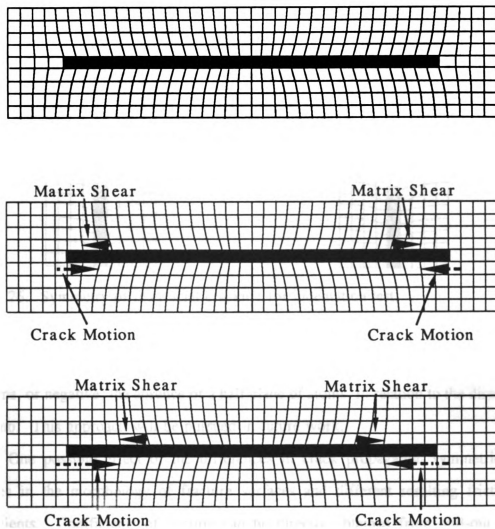


Figure 25. Symmetry of interfacial cracking for short, embedded fiber.

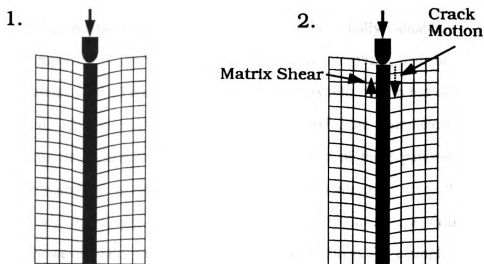


Figure 26. Symmetry of interfacial cracking for indentation test.

or consumed is determined by whether the dislocation is positive, an extra half plane of atoms, or negative, the absence of a half plane of atoms, in relation to the direction of climb. This approach will be pursued in future work.

One possible effect of the differences in crack propagation symmetries is changes in the morphology of fracture surfaces and different resulting frictional coefficients. Coefficients of friction can be directly obtained from pull-out tests [Piggot, 1986, 1988], but these coefficients may differ from those in SFF tests because the initial mode of interfacial failure may not be identical.

The mode II cracks in SFF tests advance in the opposite direction from the matrix displacement, while cracks in pull-out tests advance in the same direction if debonding begins where the fiber enters the matrix, and the opposite direction if debonding begins at the fiber end. These different modes of interfacial failure may produce different failure surfaces, with considerable changes in frictional constants resulting.

5.12 FRAGMENTATION TEST CONCLUSIONS

The fragmentation test contains a wealth of potentially valuable information about the properties of the fiber-matrix interface and interphase, and the interaction of failure modes with all composite constituents. This information has only begun to be exploited, with numerous recordable and reproducible parameters that have received little or no attention in the literature. Some of these parameters extract information with less ambiguity than the critical length approach, since they involve a single mode of failure, analyzed by a single algorithm. The critical length approach, however, also has an advantage in that it allows for a single system for comparing all fragmentation test results.

Fiber failure strain energy release can significantly alter the failure modes and measured critical lengths in fragmentation tests. This effect has been largely ignored in the literature, and has clouded the interpretation of data. Other interfacial shear strength measurement methods do not include a contribution from fiber failure energy and so are fundamentally different measurements. In addition, these methods involve cracking with different symmetries, and therefore different potential crack growth habits and results.

CHAPTER 3

ON THE DETERMINATION OF FIBER STRENGTHS BY IN-SITU FIBER STRENGTH TESTING

Published as:

ON THE DETERMINATION OF FIBER STRENGTHS BY IN-SITU FIBER STRENGTH TESTING, M. C. Waterbury and L. T. Drzal, Journal of Composites Technology and Research, JCTRER, Vol. 13, No. 1, Spring 1991, pp. 22-28.

3.1 IN-SITU FIBER STRENGTH TEST SYNOPSIS

A method is described and experimental results given which demonstrate the feasibility of determining fiber strengths at short gage lengths by monitoring the fiber failure process during the embedded single fiber fragmentation test. A computerized weakest link fiber model was used to perform data analysis, without making assumptions about the statistical nature of the flaw distributions. Fiber strength data at short gage lengths can be directly obtained by this technique without the necessity for extrapolation from longer specimens. A dependence on specimen fabrication technique was found, which demonstrates the necessity of careful control of fiber prestrain. Specially fabricated strain-free specimens tested by this method, the in-situ fiber strength test (ISFS), generated length-strength data that were in close agreement with conventional tension test results.

3.2 ISFS INTRODUCTION

The strength of reinforcing fibers is a function of length, since fiber strength is not uniform, but is determined by a statistical distribution of flaws. In a composite material, stresses are transferred to the fibers from the matrix, limited by the strength of the fiber-matrix interface and adjoining regions, and by the matrix modulus. The

strength of the composite is best related to the strengths of the fiber fragments which can just be fully loaded through this stress transfer process. These fragments may be only a fraction of a millimeter in length, making tension testing difficult.

Fiber strengths can also be a function of specimen strain. The fiber fragments that remain in a strained single fiber fragmentation (SFF) specimen are pieces produced by the failure of the largest flaws in the fiber. With these flaws effectively sorted out by the prior failure process, the final fragments are comprised of a nonrandom sample of material. In contrast, the gage sections of the fibers in tension tests consist of randomly selected segments, containing flaws of all sizes. Tension testing of randomly selected fibers will therefore underpredict the strengths of fiber fragments in the SFF composite.

A number of researchers [Henstenburg, 1989], [Wagner, 1990], including one of the authors of the current publication (M.C.W.), have independently proposed an alternative to single fiber tension testing, the in-situ fiber strength test. This method may surmount these problems by testing fibers that are embedded in a tensile coupon of a model matrix material. This technique can virtually eliminate gripping and alignment problems since the fiber is uniformly supported by the matrix material. Because of this, measurements at short gage lengths can be obtained without the necessity for extrapolation from longer specimens. While methods are available for making this extrapolation [Asloun, 1989], direct confirmation by experiment would place these techniques on a more secure footing. The test also generates flaw population data in a form that can provide more complete and relevant information about defects than does the simple tension test, allowing improvements in process design and quality control. Since many breaks occur in a single ISFS test coupon, data acquisition can be orders of magnitude faster than for the simple tension test, increasing the sample size and thereby enhancing the resolution.

This paper describes the ISFS testing technique and demonstrates that,

provided certain essential requirements are met, the results so obtained are reproducible, consistent, and in agreement with standard tension tests.

3.3 ISFS EXPERIMENTAL PROCEDURE

3.3.1 SINGLE-FIBER FRAGMENTATION TEST

Since the single fiber fragmentation (SFF) test has been extensively described elsewhere [Drzal, 1980], it will only be briefly reviewed here.

A representation of the approximate fiber stress distribution throughout the test is shown in Figure 27, which represents the approximate fiber tensile stress distribution during the course of the single fiber fragmentation test, assuming a constant shear traction without debonding.

One or more isolated fibers are centrally embedded in a small tensile coupon of epoxy or other, usually transparent matrix, parallel to the gage section. As the coupon is raised to a strain level approximately three times greater than the failure strain of the fiber, the fiber repeatedly fails. This process is limited when the length of the remaining fragments reaches a critical value, often called the critical length, L_c . This limiting value, along with the strengths of the fiber fragments, forms the basis of the single fiber fragmentation interfacial shear strength test.

Fiber failure during the single fiber fragmentation test begins at the largest flaws and proceeds to successively smaller sizes, changing the makeup of the flaw distribution throughout the test. The strengths of the fiber fragments are therefore a function of the coupon strain level as well as the fragment length, complicating data analysis.

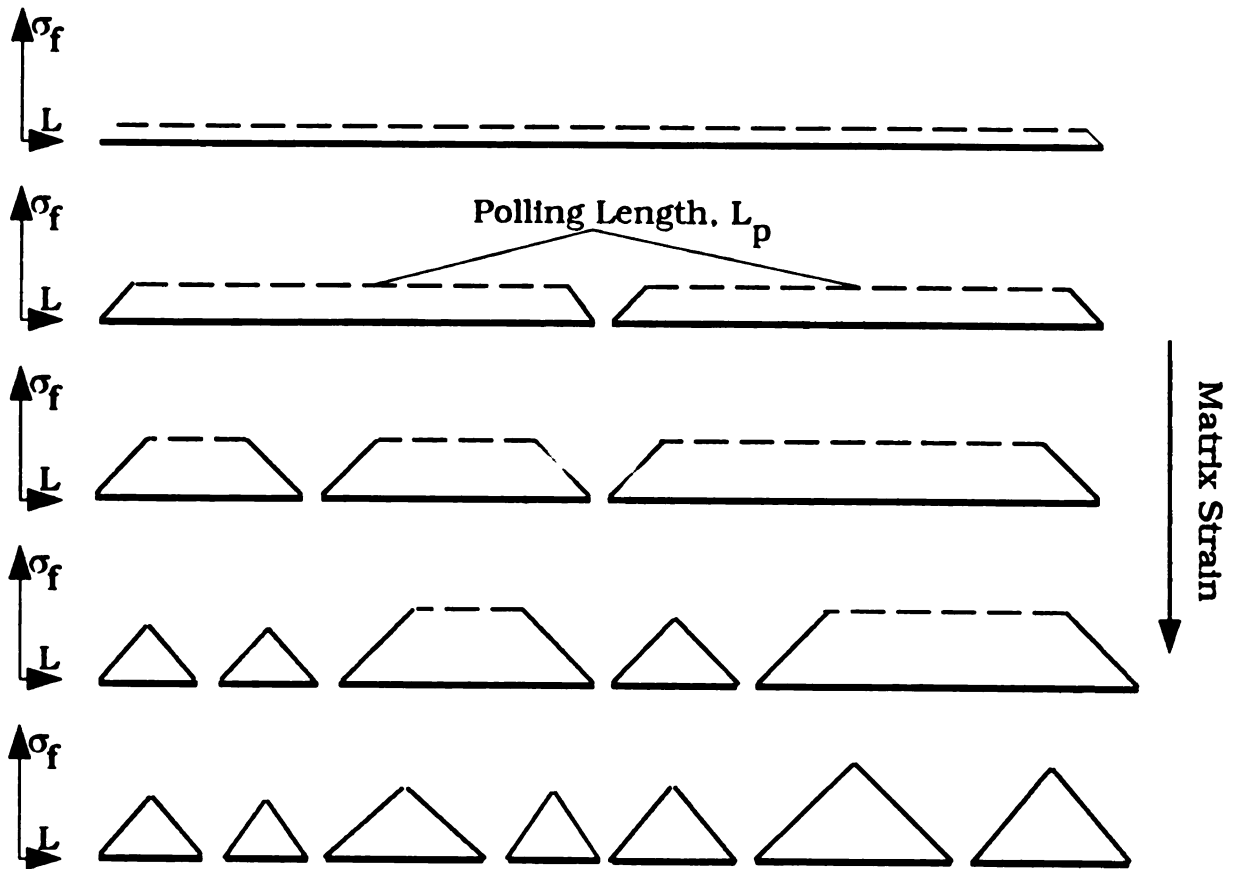


Figure 27. Fragmentation stresses and polling lengths.

3.3.2 IN-SITU FIBER STRENGTH TEST

During the early stages of the single fiber fragmentation test, the fiber failure process is well defined. The locations of all new breaks observed in this study were found to be well away from the ends of fiber fragments, where the fiber strain cannot be uniquely determined, since it may be significantly less than that of the matrix. The strains at failure within the central region of each fiber fragment, however, can be accurately monitored, forming the basis for the in-situ fiber strength test.

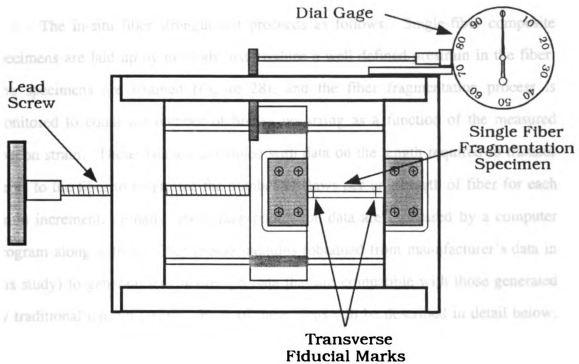


Figure 28. Straining stage for single fiber fragmentation test.

In general, this value is not exactly equal to the matrix strain, since some stress is likely to exist in the fiber at zero coupon strain. Fibers that are misaligned or curved may also undergo rotations rather than axial extensions as coupon strain is increased. Although these effects have a minimal influence on single fiber fragmentation interfacial shear strength tests since the specimens are strained well past the completion of fiber fragmentation, they can strongly skew ISFS results.

The requirement of a well defined fiber prestrain precludes the use of the same specimens for both interfacial shear strength and ISFS measurements, since the particular cure histories of interfacial shear strength specimens will usually leave some unknown value of fiber strain. An additional reason for this prohibition is the possibility that the highly stressed interfacial region may be subject to creep when strained to the limiting fragment length in a series of steps rather than monotonically. Final fragment lengths of incrementally strained specimens tend to be longer than

those that are smoothly strained.

The in-situ fiber strength test proceeds as follows. Single-fiber composite specimens are laid up by methods that produce a well-defined prestrain in the fiber. The specimens are strained (Figure 28), and the fiber fragmentation process is monitored to count the number of breaks occurring as a function of the measured coupon strain. These data are combined with data on the length required to transfer stress to the fiber to determine the number of flaws per unit length of fiber for each strain increment. Finally, these flaw population data are processed by a computer program along with the fiber tensile modulus (obtained from manufacturer's data in this study) to generate length-strength data that are compatible with those generated by traditional tension testing. Each of these steps will be described in detail below.

3.3.3 ISFS SPECIMEN FABRICATION

One set of single fiber specimens was laid up in an epoxy matrix, DER 331/MPDA, cured 2 hours at 75 °C followed by 2 hours at 125 °C. The fibers were affixed to room temperature vulcanizing silicone specimen molds with a hot-melt thermoplastic glue which flows viscoelastically during solidification, allowing the fibers to be drawn through the glue and accurately straightened. An additional attachment with rubber cement maintained this alignment as curing proceeded.

A second set of specimens was produced with a solvent deposition technique intended to eliminate, or at least minimize, fiber prestrain. Fibers were laid onto precut, 0.8 mm thick polycarbonate coupons and secured in place away from the gage length with hot melt glue. Four layers of a 5% solution of polycarbonate in methylene chloride were spin coated over the fibers at 5 minute intervals. Specimens were then held at 75 degrees °C for 24 hours before testing.

Fiber-matrix adhesion for solvent deposition specimens is poor [Bascom, 1987], [Waterbury,1990], imposing a severe limitation on the equivalent fiber gage

length which may be tested. The feature of interest for the purposes of this study was the absence of fiber prestrain.

3.3.4 Data Acquisition

Data acquisition was performed with FiberTrack [Waterbury, 1990], a software and hardware system specifically developed to perform both interfacial shear strength and ISFS fiber fragment length measurements at high speeds. Hardware consisted of a microstraining stage mounted on a Newport® translation stage with a digital position readout, both mounted on a transmitted, polarized light microscope. A custom interface provided both control signals to activate the translation stage, and concurrent timing signals to the FiberTrack software running on a Amiga® computer (Figure 29).

Measurements proceeded as follows. The initial length between transverse fiducial marks (Figure 28) on the specimen gage section was measured with the translation stage. The specimen was then strained in approximate 0.25% strain increments, determined with a dial gage and calibration curve. The break positions were measured after each strain increment. This was accomplished by positioning the specimen at the first fiducial mark, translating the stage at a constant rate, and clicking the "mouse" button as each break passed a crosshair in the microscope, sending a timing signal to the computer. The translation was halted at the second fiducial mark and the distance traversed was noted from the translation stage readout.

The FiberTrack software then calculated the break positions by interpolating between the time elapsed for the entire motion and the times of each break passage. These positions were saved to a diskette and the strain was accurately calculated by comparing the current and initial gage lengths. In this manner, break positions can be measured without having to stop the stage motion at each break, providing an order of magnitude speed improvement over less automated procedures.

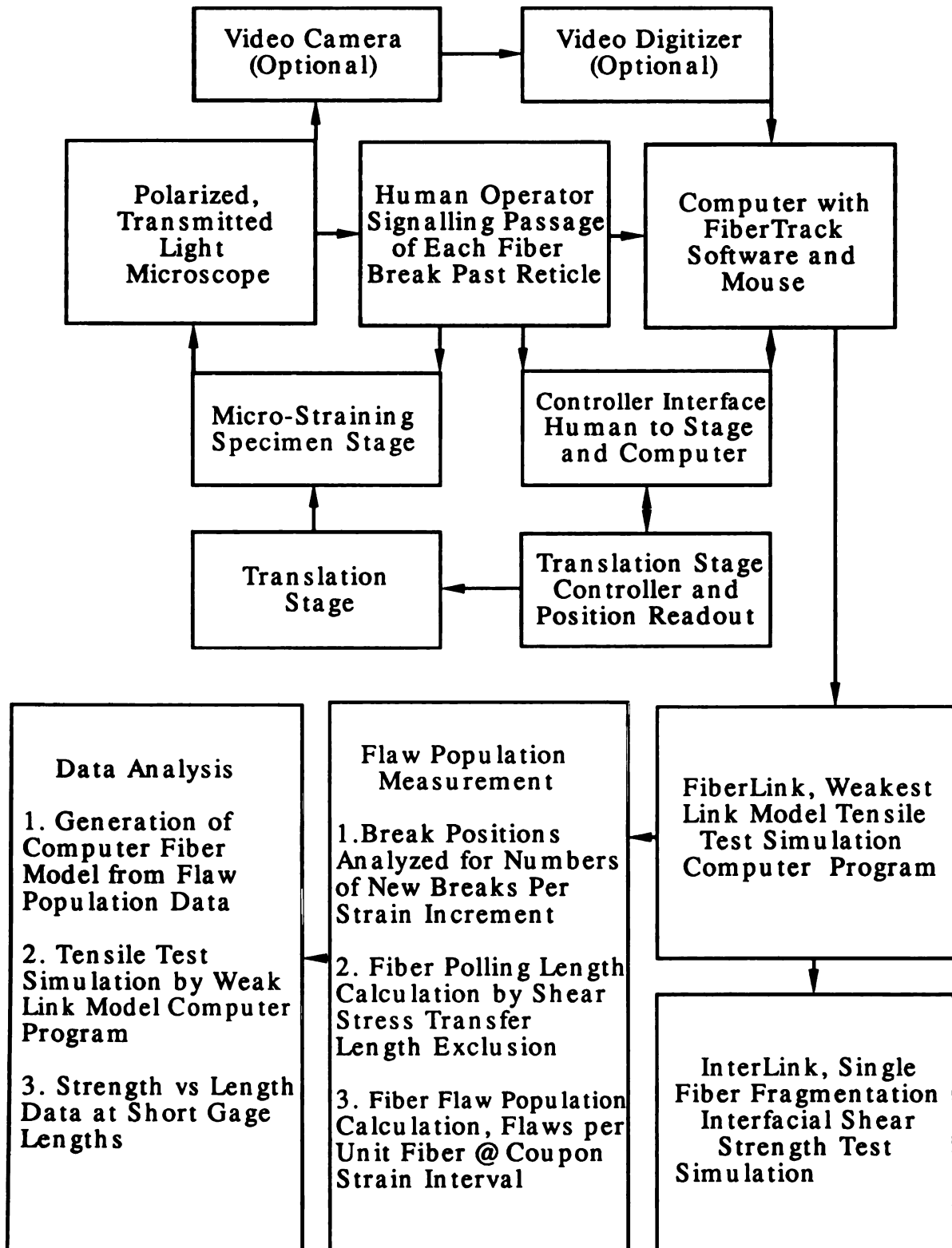


Figure 29. Block diagram of FiberTrack/FiberLink

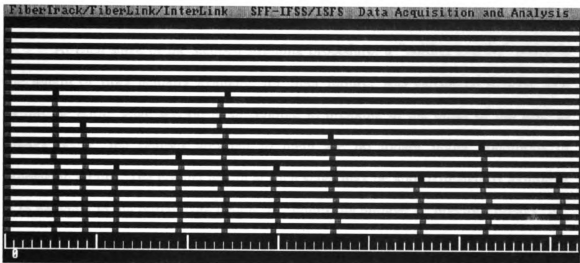


Figure 30. Fiber break positions recorded by FiberTrack.

For interfacial shear strength testing, the data were automatically subjected to a Weibull/Poisson analysis to determine interfacial shear strengths.

3.3.5 ISFS CALCULATIONS

After the positions of all breaks in each strain increment were recorded, the complete set of "tracks" of break positions was displayed, and the new breaks appearing in each track located (Figure 30). These breaks were always found to lie somewhere within the central portions of the fiber fragments, rather than adjacent to previous breaks where strain is poorly defined.

The new breaks occurring at each strain level were then apportioned among strain increments of 0.25% by linear interpolation to compensate for the small deviations between these uniform increments and the actual, slightly non-uniform steps. Each new break occurring between measured strains of 1.27 and 1.52% strain, for instance, was allocated as adding 0.92 breaks to the 1.25 to 1.5% group and 0.08 breaks to the 1.5 to 2.0% group. This introduces an error which is small provided that the initial sampling increments are close to the desired 0.25% steps. Continuous

recording of breaks by acoustic emission will eliminate this approximation.

At each stage of the stepped straining procedure, a "polling length," which is the length of fiber actually available for fiber failure, was calculated (Figure 27). While the entire gage section is susceptible to breaking at the onset of the test, as breaks occur, the regions adjacent to them are no longer under conditions of increasing strain. The polling length at each stage may be approximated by assuming it to be equal to the initial gage length, L_0 , minus the number of previous breaks, N_b , times the critical length, L_c .

$$\text{Polling Length, } L_p = L_0 - (N_b * L_c)$$

This formula may be used with simple acoustic emission data acquisition, since only the number of breaks and the final critical length are required. A refinement of this calculation to consider strain level may be desirable, since the transfer length at lower strains is actually less than the the final critical length. A transfer length which is proportional to coupon strain could be used as a first order improvement.

The number of flaws per 25 mm in each 0.25% strain increment was then calculated from the number of new breaks, B , and the polling length, L_p , in millimeters by:

$$\text{Flaws per 25 mm, } F_{25} = B * 25/L_p$$

These flaws were then averaged for all specimens in each set and plotted at the end of each strain increment to produce the graphs of flaws/25 mm versus strain increment.

The fiber tensile modulus was obtained from manufacturer's data sheets for the purpose of this feasibility demonstration.

3.3.6 COMPUTER TENSION TEST SIMULATION

A computer link-model fiber was then generated and tested in the following manner. A 10,000 element link strength array was set up to represent the strength of

the weakest part of each 100 micron link. Each link was initialized with a strength of 2,000 ksi as a limiting case. The experimentally determined flaw population data was then used as a guide to populate the links in this array with the correct numbers of flaws. This process was performed in the order of strongest to weakest flaws, since many links have more than one flaw and the link strength is determined by the weakest flaw present. In the case of fractional numbers of flaws, a flaw was either assigned, or not assigned, based on the probability of one occurring. Beyond the gage length range in which test results were valid, the flaw distribution was assumed to follow the experimentally determined exponential distribution. This is equivalent to extrapolating to shorter gage lengths for this pilot study. Matrices with sufficiently high interfacial shear strength are available to make this unnecessary in future work.

One meter long fibers, each simulated by 10,000 one hundred micron links were produced in this manner and tested as follows.

Testing proceeded by starting at many randomly selected locations and checking for the weakest link occurring within the selected gage length. This link was taken as the strength of that fiber segment and these values were stored, averaged, and a standard deviation calculated. In this manner, six, one meter simulated fibers were produced and tested at various gage lengths to produce the final length-strength data. This represents a statistical oversampling of the original data since the flaw population data were obtained by testing about 200 mm of real fiber.

3.3.7 ACOUSTIC EMISSION DETECTION

To explore the possibility of acquiring ISFS data by acoustic emissions, a simple detection and recording system was developed. A miniature condenser microphone element was modified by removing the protective, external membrane and exposing the condenser diaphragm. A drop of gel-type quick-setting epoxy was applied to the center of this diaphragm and allowed to protrude slightly from the

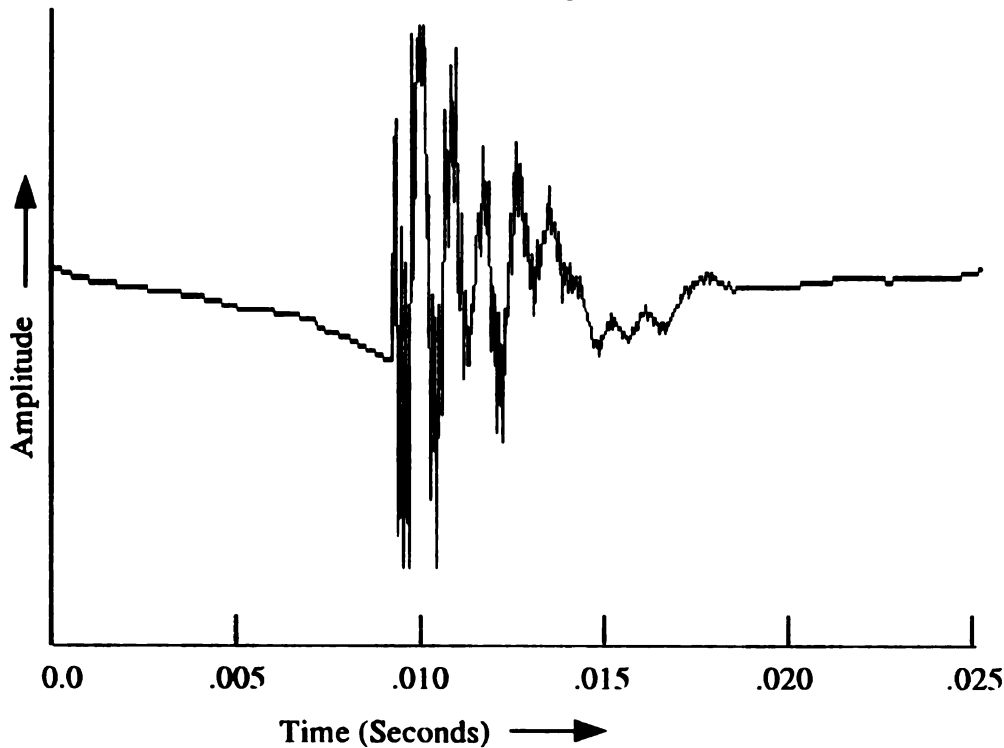


Figure 31. Acoustic emission from carbon fiber failure.

element to provide an acoustic link to the specimen. The element was then strapped to the gage section of a specimen with a rubber band.

After preamplification and passage through a band pass filter to eliminate low frequency components, the output of this element was applied to an audio frequency digitizer and sent to an Amiga computer equipped with 2.5 megabytes of RAM. In this manner, a complete acoustic waveform up to 100 seconds in duration, sampled with eight bits precision at a 20 KHz sampling rate, could be acquired.

An example of a typical fiber break acoustic emission trace appears in Figure 31. The horizontal axis is time while the vertical axis represents sound amplitude sampled at $1/20000$ second intervals. The trace is characterized by a rapid rise time and a slow decay with a predominant frequency in the range of a few kilohertz. The initial, much higher frequency shock wave produced by the failing fiber apparently

excites this low frequency resonance within the stretched specimen. When replayed as a sound through an amplifier and speaker at a reduced frequency, the trace resembles that produced by a plucked string.

3.4 ISFS RESULTS AND DISCUSSION

Two sets of in-situ fiber strength tests were performed as described above, using six 25 mm fibers in an epoxy matrix and nine 25 mm fibers in solvent deposited polycarbonate (PC).

The number of flaws per 25 mm, per strain increment for each of the nine specimens in the PC tests appear in Figure 32. As can be seen, the scatter in this raw data was substantial, resulting from the small number of breaks in each specimen. Figure 33 and Table 1 depict the average number of flaws for the epoxy and PC matrix specimens. A smooth increase is seen up to about 2.25% coupon strain for the PC specimens and 2.75% for the epoxy matrix, followed by a drop off as a result of the limitations imposed by the interfacial shear strength. This drop off occurs later for the epoxy matrix case with its stronger interface, allowing much shorter gage lengths to be measured.

Table 1. Flaws per 25 mm @ strain increment for AS4 fibers.

Coupon Strain (%)	Fiber Stress (MPa)	Epoxy Matrix Fiber Flaws per 25 mm	PC Matrix Fiber Flaws per 25 mm
1.00	2346	1.0	0.40
1.25	2932	0.5	0.13
1.50	3519	2.2	0.99
1.75	4105	6.7	3.33
2.00	4692	19.8	6.70
2.25	5278	28.4	12.16
2.50	5865	64.5	12.93
2.75	6451	82.3	13.31

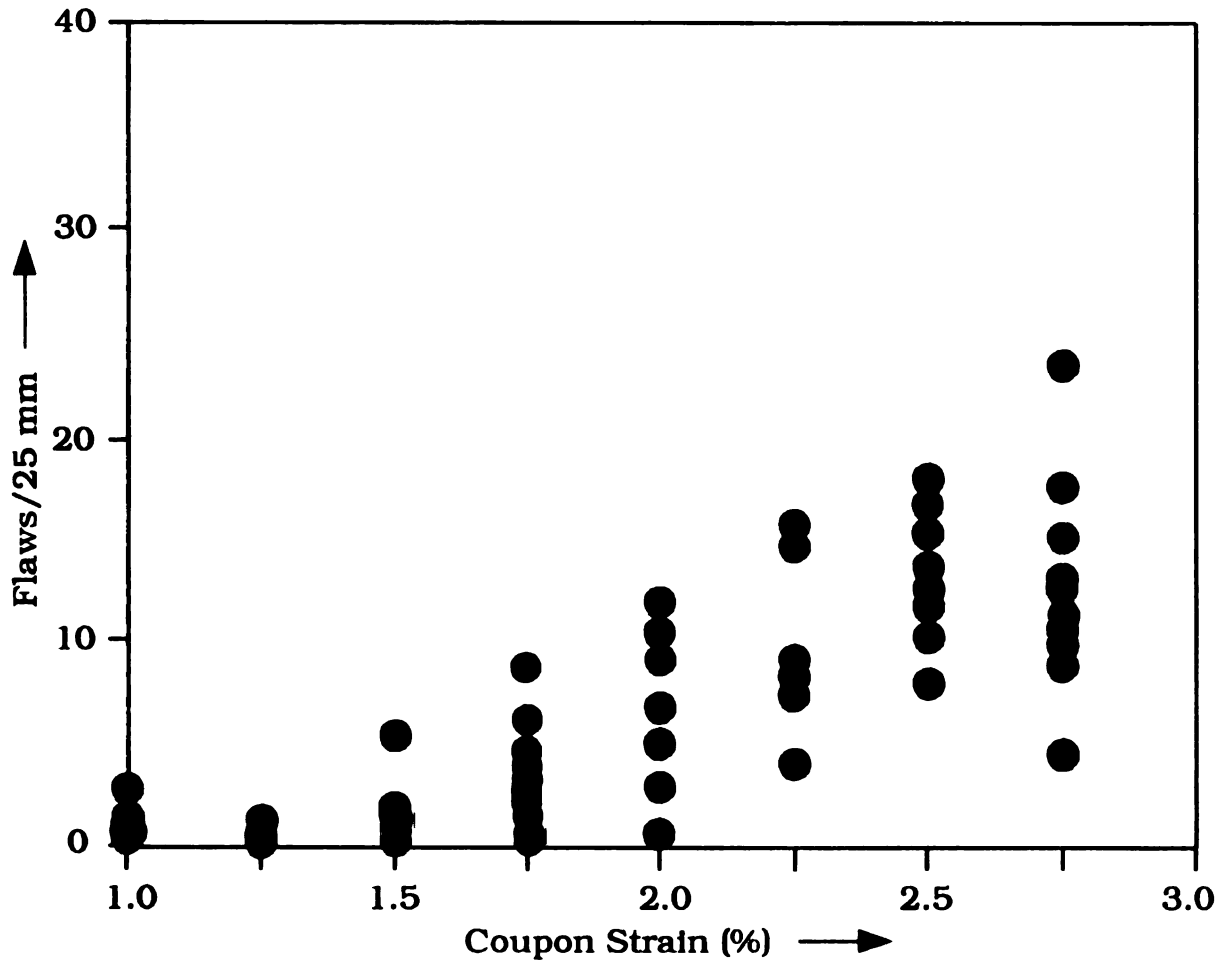


Figure 32. Flaws versus strain increment by specimen in PC.

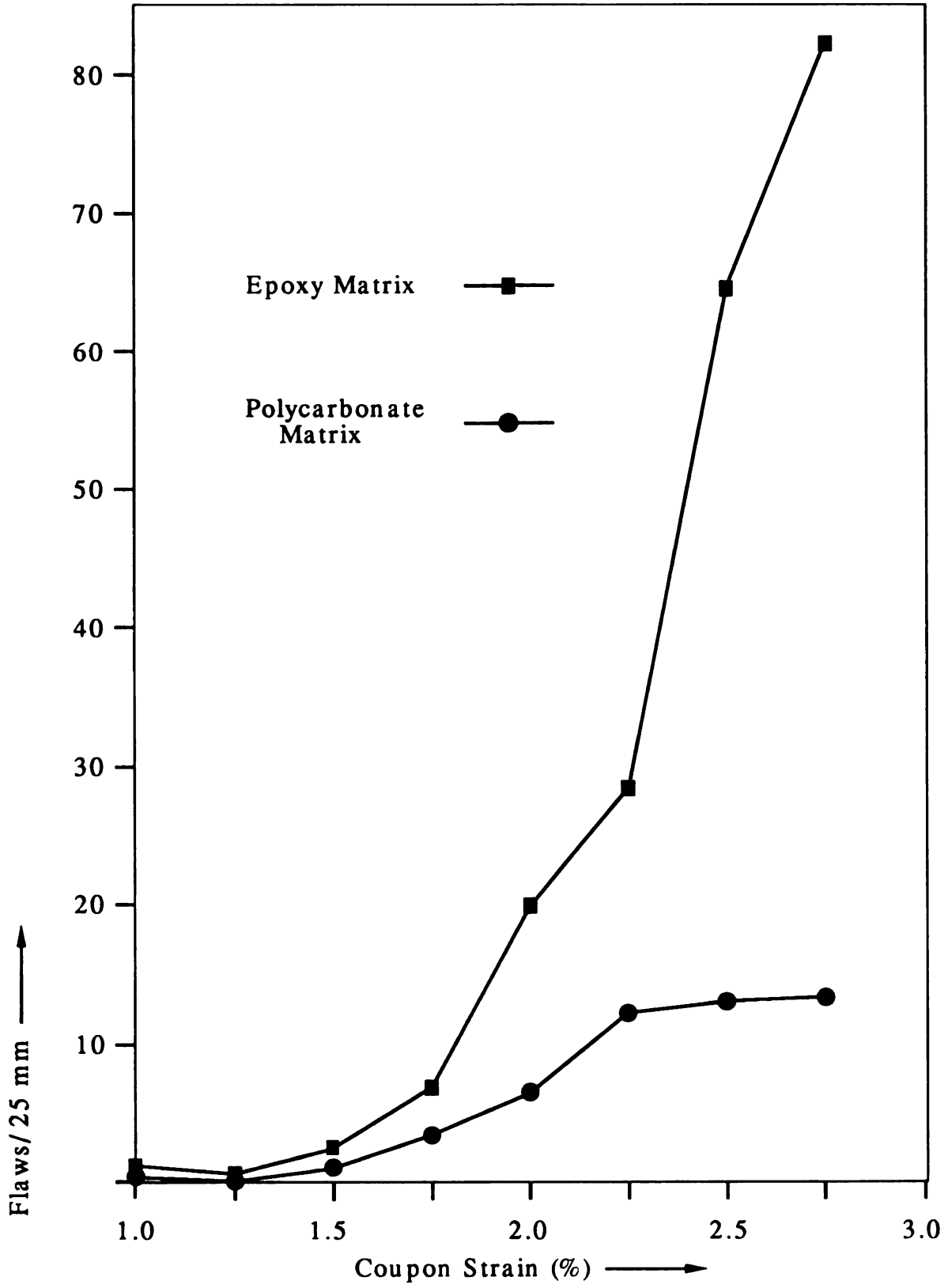


Figure 33. Flaws versus strain for AS4 fibers in PC and epoxy.

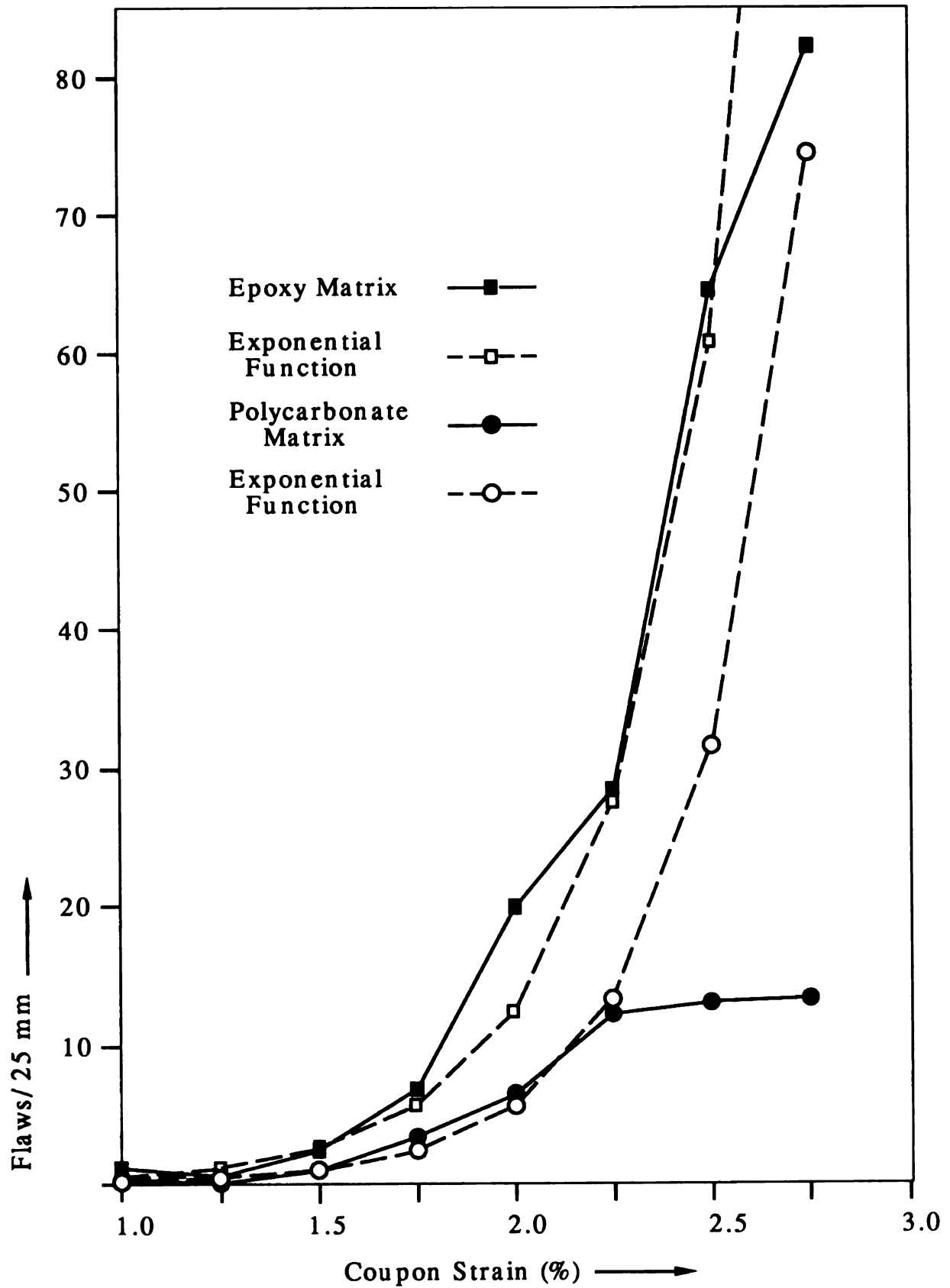


Figure 33. Flaws versus strain and exponential curves.

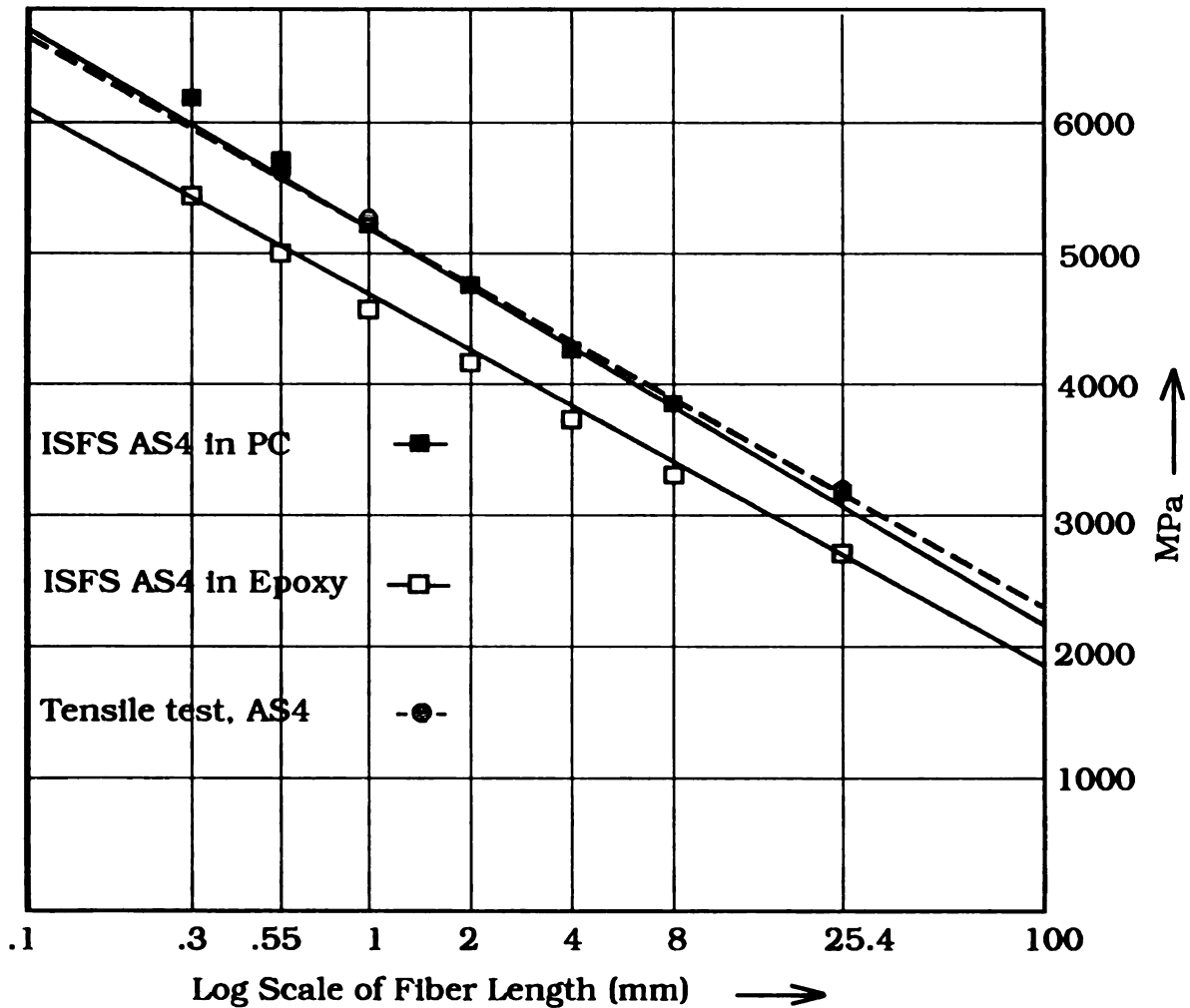


Figure 34. In-situ and ex-situ fiber strengths.

Table 2. In situ and ex situ AS4 fiber strengths.

Gage Length (mm)	Conventional Tension Test (MPa)	In-Situ Fiber Strength	
		Epoxy (MPa)	Polycarbonate (MPa)
25.4	3215 ± 966	3188 ± 704	2698 ± 518
8.0		3850 ± 738	3347 ± 725
4.0		4264 ± 787	3733 ± 752
2.0		4720 ± 856	4175 ± 773
1.0	5285 ± 1731	5223 ± 911	4582 ± 814
0.55	5644 ± 994	5693 ± 945	4996 ± 869
0.3		6189 ± 973	5437 ± 883

Figure 34 plots the epoxy and PC specimen data along with exponential functions which differ only by a constant multiple, or, equivalently for this type of function, by a constant strain offset. The curves correspond closely, showing that the test yields an approximate exponential dependence of new breaks per unit length on coupon strain within the early part of the graph, falling off when the shear traction imposed limit is reached.

The difference between the epoxy and PC results shows a dependence on specimen preparation technique, probably as a result of fiber strain produced by dimensional changes in the matrix. This indicates that specimens for this test must be produced by a technique that either leaves a negligible or well defined initial strain in the fiber allowing accurate determination of the strains at failure throughout the test.

The flaw population data obtained by the ISFS test and processed with the FiberLink computer model to convert it to the form of strength versus fiber gage length appear in Figure 35 and Table 2 along with data obtained by conventional fiber tension testing [Drzal, 1982]. The prestrain free PC matrix ISFS data show a very close correspondence with the tension test results in both the value of fiber strength and the slope of strength versus $\log(\text{gage length})$.

A least squares fit of the strength versus the base ten logarithm of the gage length (Figure 35), shows an intercept of 5273 MPa at 1 mm gage length for the conventional tension test results and 5272 MPa for the PC ISFS results. This virtually identical result is somewhat coincidental since it is less than the natural scatter in the data. The slopes were also in agreement, -1464 MPa per unit $\log(\text{gage length})$ for the tension test and -1555 MPa for the PC ISFS test, a difference of about 5%.

The epoxy matrix ISFS data is in agreement in slope but shows an offset corresponding to a pretension of 0.25% fiber strain at zero coupon strain. The least squares fit for this data gave an intercept of 4628 MPa at 1 mm length and a slope of

-1413 MPa per log (gage length).

This value is in agreement with experimental results and theoretical predictions made by others in this laboratory,^a which suggests that the strain on the fibers in epoxy-matrix single-fiber fragmentation specimens prepared with this cure schedule will be approximately 0.2% in tension. This prediction was made based on the changes in thermal expansivity of the matrix during the cure cycle in relation to when gelation occurs.

Small tensile strains in single-fiber composites have also been detected by Raman spectroscopy [Galiotis, 1988, 1990]. Pretension may be an artifact of the specimen preparation process, which involves aligning the fibers in a silicone mold and securing them with adhesives. These results contradict the notion that a net compression is exerted and are under further investigation.

3.5 COMPARISON OF IN-SITU FIBER STRENGTH AND CONVENTIONAL FIBER TENSION TESTS

In-situ fiber strength testing offers the potential for significantly enhancing the rate of tensile strength data acquisition. Each 25 mm of fiber in a strong interface specimen fails approximately 50 times within the well defined failure portion of the single fiber fragmentation test, providing the equivalent to 50 fiber tension tests with a single-fiber specimen. Longer gage length, multiple fiber specimens can produce hundreds of tensile data points in a single, semiautomated test. This may represent two orders of magnitude improvement over previous methods. High resolution fiber tension tests require large numbers of data points since the resolution increases by only the square root of the number of samples.

Strength data at short gage lengths are required for the analysis of composite properties and single fiber fragmentation interfacial shear strength tests. A suitable
a. Kalantar, J.K., Drzal, L.T., to be published.

matrix for ISFS specimens should have high interfacial shear strength and a high modulus to facilitate this process. The fiber prestrain must be consistent and must be calibrated against conventional tension tests or against strain-free specimens prepared by solvent deposition.

3.6 ISFS CONCLUSIONS

The feasibility of determining fiber strengths at short gage lengths by in-situ fiber strength testing has been demonstrated. Results obtained from single-fiber fragmentation, in-situ fiber strength testing are in close agreement with those from short gage length fiber tension tests. The number of fiber flaws per unit length was found to increase exponentially with increasing strain increment.

The necessity of determining fiber prestrain produced during specimen fabrication was shown. A computerized weakest link model has been developed to analyze the experimentally determined fiber flaw distributions and to simulate the single-fiber fragmentation process.

CHAPTER 4

DETERMINATION OF FIBER VOLUME FRACTIONS BY OPTICAL NUMERIC VOLUME FRACTION ANALYSIS

Published as: Determination of Fiber Volume Fractions by Optical Numeric Volume Fraction Analysis, Waterbury, M.C., Drzal, L.T., Journal of Reinforced Plastics and Composites, JRPC, Vol. 8, Nov. 1989, pp. 627-636.

4.1 ONVFA SYNOPSIS

A method for determining the fiber volume fraction in continuous fiber composites by automatically counting the fiber ends per unit area in digitized microscope images of representative cross sections has been developed. Since fiber counts are digital variables, the accuracy of the method is essentially independent of small variations in microscope focus and specimen surface preparation. In addition to producing averaged data, the method enables the construction of volume fraction variation profiles ranging from the finest possible scales up to full size components. Results are in agreement with values obtained by acid digestion tests.

4.2 ONVFA INTRODUCTION

Composite volume fraction determinations based on image analysis techniques have been pursued with the intention of supplanting methods employing matrix removal by combustion, solvent, or acid digestion [Cilley, 1974] with a cleaner, more accurate technique which can provide distribution profiles along with averaged data

[ASTM]

fiber n

the ma

matric

analysis

1987 A

metallo

from t

inheren

light di

Variatio

differen

in illum

I

factors c

sections

change v

fractions

fiber dia

sample o

fiber area

the reaso

[ASTM, 1987 A], [ASTM, 1987 B]. An alternative approach is also essential for fiber/matrix combinations for which no suitable solvent is available which can remove the matrix without attacking the fibers, as with high performance thermoplastic matrices.

Composite volume fractions determined by conventional areal and lineal image analysis techniques have been shown to be in error by as much as 10-15% [ASTM, 1987 A]. Highly variable results are also commonly produced by the parent metallographic methods [Jock, 1986]. These errors are unavoidable since they result from the small size of modern reinforcing fibers (e.g. 5 microns) in relation to the inherent resolution limitations of light microscopes, one half of the wavelength of the light divided by the numerical aperture of the lens, approximately .25 microns. Variations in fiber images also result from rounding of fiber ends during polishing, differences in polishing action in fiber and matrix rich regions, surface residue, drift in illumination sources, and focal differences across the image plane.

It was recognized that more accurate values with less susceptibility to these factors could be obtained by counting large samples of fiber ends emerging from cross sections of the composite since the number of fibers is a digital value and does not change with the brightness or apparent area of the fiber images. Absolute volume fractions may be obtained from these fiber counts without knowledge of individual fiber diameters because the average cross sectional area of any sufficiently large sample of fibers rapidly approaches the average for all of the fibers. Although the fiber areas cannot be measured with sufficient precision by purely optical means for the reasons previously outlined, approximate values may be obtained from product

specifi

the tow

digitiz

since it

clearly

fiber-f

contain

screen

and ma

determ

boxes a

may be

visualiza

number

informat

made mo

same dig

the void

Void voi

small fra

fiber we

specification sheets, and more precise values may be determined from the weight of the tow and the fiber density [ASTM 1987 B] measured with the same batch of fibers.

An image analysis program to perform this task can be optimized to process digitized microscope images (Figure 36) containing very large numbers of fibers, since it only requires enough information to identify the fibers, without attempting to clearly resolve their sizes. Accurate fiber counts are produced in spite of apparent fiber-fiber contact and damaged fiber ends (Figure 37). This program produces a file containing not only the total number of fibers in the image but also their individual screen coordinates, which may be analyzed for detailed information about the fiber and matrix volume fraction distributions, or subjected to a Fourier-type analysis to determine the average spacings between matrix rich regions.

Simple distribution statistics may be obtained by dividing each image into small boxes and finding the number of fibers in each (Figure 38). Fiber maps (Figure 39) may be constructed by plotting each fiber with a single white pixel to allow for the visualization of large regions of composite cross sections. Statistical profiles of the number of boxes containing a given number of fibers can provide quantitative information about the incidence of matrix rich regions, allowing comparisons to be made more reliably (Figure 40). Void volume fractions may be obtained from the same digitized images by conventional areal analysis with reasonable accuracy since the void dimensions are generally large with respect to the optical system limitations. Void volume fractions determined by acid digestion have limited accuracy due to the small fractions being measured and the strong influence that the matrix density and fiber weight measurements have on this value.

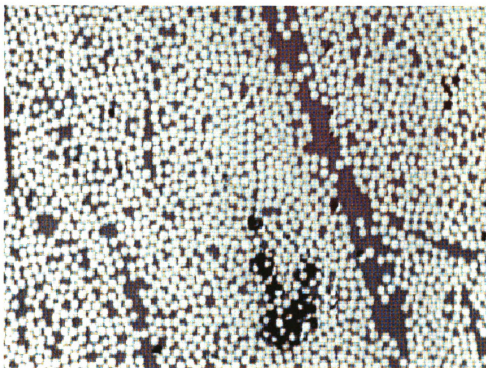


Figure 36. Digitized image of graphite/epoxy composite.

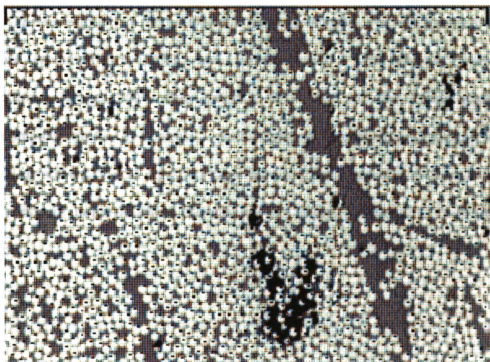


Figure 37. Same image with fibers counted and tagged.

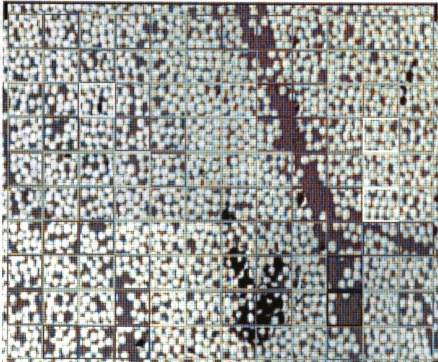


Figure 38. Boxes shaded to indicate number of fibers.

The time required for an ONVfA analysis includes that for standard micro-structure specimen preparation, and approximately 4 minutes per image for digitization, storage, and image analysis, with most of this being unattended microcomputer time. In contrast, volume fraction determinations through matrix removal by solvent or acid digestion involve boiling the composite in toxic chemicals for a period of hours followed by washing and drying of the fiber mass prior to weighing.

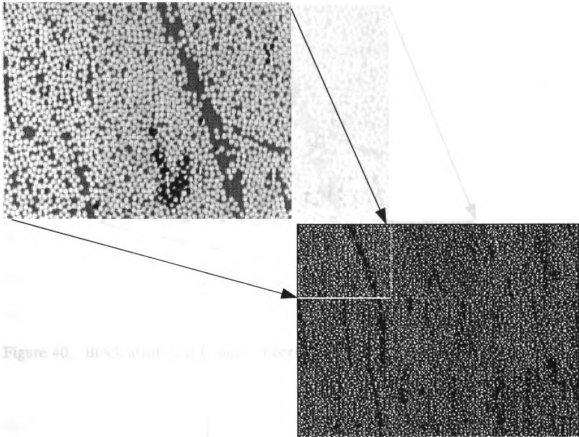


Figure 40. Black and white fiber map.

Figure 39. Fiber map, one white pixel per fiber.

The spatial resolution of this method is extremely fine, an accurate volume fraction may be determined by a single digitized image with an effective sampling volume of only about 50 micrograms of material, selected from any point in a composite cross section. Fiber distribution determinations within the image give quantitative information on an even finer scale, limited only by the size of the fibers themselves.

This report describes ONVfA in its current state of development and presents experimental data which demonstrate the accuracy and resolution of the method.

Figure

Figure 4

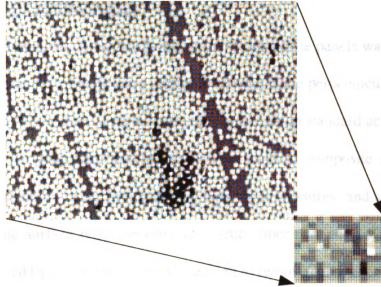


Figure 40. Block areal density map, (fibers/box).

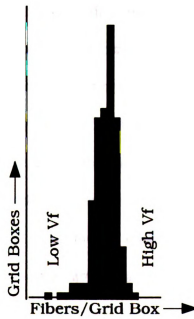


Figure 41. Fiber areal density distribution function.

4.3 ONVFA EXPERIMENTAL

ONVfA analysis of unidirectional graphite composite panels was conducted in the following manner. Panels were sectioned along a plane perpendicular to the fiber orientation and two or three samples from each were cast in standard acrylic specimen mounts. The surfaces were then polished with standard composite microstructure preparation techniques using firm polishing laps, light pressures, and sharp abrasives to minimize the surface relief between the harder fiber-rich and softer matrix-rich regions, followed by thorough ultrasonic cleaning to remove particulate residue. Care was also taken to ensure that the polished surfaces were flat and parallel with the bottoms of the specimen mounts in order to minimize focusing errors.

Microscope images of the prepared microstructures were then converted to digital form by a computer with a video digitizer an analog to digital converter which transforms the composite video signal from a video camera into a 320 X 200 pixel or 640 X 400 pixel image with 16 levels of brightness. Typical low resolution images cover an area of approximately .35 X .25 millimeters and contain from 1500 to 2000 fibers in a screen. The coverage area was determined by digitizing images of a 100 line/mm reticle along with each set of images.

Fiber volume fractions were directly obtained by multiplying the number of fibers in each image by the average area of a fiber and dividing by the area of the counting field without additional calibration factors.

The average cross sectional area of a fiber can be calculated from information from product data sheets, and can be more precisely determined by weighing sections of dried tow from the same lot or spool and dividing by the density, the number of

fibers in the tow and the length weighed. The fiber area used in this study was calculated from the tow weight and density data supplied by the fiber manufacturer for the same lot of fibers used to make the composite plates in the AC series of specimens.

Void volume fractions were determined by performing conventional areal image analysis on images for which optical contrast was maintained between the dark matrix and the darker void regions. The void fraction was taken as the simple ratio of these darker pixels to those associated with the fiber and matrix. The accuracy of this method depends upon the size of the voids being large in comparison with the resolution of the imaging system.

4.4 ONVfA EQUIPMENT

The equipment employed in this experiment was as follows:

Amiga 500 Computer

Digi-view video digitizer

Panasonic WV 1410 B/W video camera

Olympus BHT Microscope with reflected light, IC20 20X objective lens, MTV video camera adapter, 2.5 X photo projection lens

Microstructure specimen mounting and polishing equipment

4.5 ONVFA SAMPLE CALCULATIONS

The area within the counting region was measured as follows. Images of an Olympus 100 line/mm calibration slide were digitized during the data acquisition session. At least three measurements of the horizontal and vertical spacings on the image of this slide were made to determine that 292 pixels = .35 millimeter horizontally, and 116 pixels = .15 millimeter vertically. The effective region scanned by the counting software measures 316 X 202 pixels.

$$.35 \text{ mm}/292 \text{ pixels} = 1.199 \text{ microns/pixel horizontally}$$

$$.15 \text{ mm}/116 \text{ pixels} = 1.293 \text{ microns/pixel vertically}$$

$$(1.199 \text{ microns/pixel}) \times 316 \text{ pixels} = .3787 \text{ mm/horiz.}$$

$$(1.293 \text{ microns/pixel}) \times 202 \text{ pixels} = .2612 \text{ mm/vert.}$$

$$.3787 \text{ mm} \times .2612 \text{ mm} = .0989 \text{ mm}^2/\text{image}$$

The average fiber cross sectional areas were calculated as follows. From the Hercules data sheet for lot 708 - 4C:

$$\text{Density } .0636 \text{ lb/in}^3 = 1.7605 \text{ g/cm}^3 = .0017605 \text{ g/mm}^3$$

$$\text{Weight } 47.94 \times 10^{-6} \text{ lb/in } 12\text{K tow} = 8.561 \times 10^{-4} \text{ g/mm}$$

$$\text{Fiber Weight } (8.561 \times 10^{-4} \text{ g/mm tow})/12,000 = 7.134 \times 10^{-8} \text{ g/mm}$$

$$\text{Area per fiber } 7.134 \times 10^{-8} \text{ g/mm} / .0017605 \text{ g/mm}^3 = 4.052 \times 10^{-5} \text{ mm}^2$$

The volume fraction may then be determined from the average number of fibers counted per image by:

$$V_f = \text{Fibers per image} * \text{Area per fiber}/\text{Area per image}$$

For the example specimen fibers in 6 images from each of 3 samples from the same composite plate were counted and averaged. Acid digestion tests were

performed on 3 other samples from the same plate.

$$V_n = 1807 * 4.052 \times 10^{-5} \text{ mm}^2 / .0989 \text{ mm}^2 = 74.0\%$$

$$V_o = 1755 * 4.052 \times 10^{-5} \text{ mm}^2 / .0989 \text{ mm}^2 = 71.9\%$$

$$V_b = 1763 * 4.052 \times 10^{-5} \text{ mm}^2 / .0989 \text{ mm}^2 = 72.2\%$$

$$\text{Average fiber volume fraction by ONVfA} = 72.7\%$$

The acid digestion fiber volume fractions for three samples from the same plate measured according to ASTM procedure D3171-76 were:

$$V_f \text{ by acid digestion} = 73.0\%, 70.4\%, 71.8\%$$

$$\text{Average} = 71.7\%$$

4.6 ONVFA RESULTS AND DISCUSSION

A set of three unidirectional composite plates was fabricated by autoclave curing from Hercules AS4 fibers in untreated, treated, and treated and sized condition. Optically determined fiber volumes reported for these specimens, designated AC-1, AC-2, and AC-3, are averages of six images per specimen with three specimens from each composite plate for a total of 18 images per plate. Three additional sets of 8 images each were made of the AC-3 plate as a check on repeatability. A second group of three plates fabricated by hot pressing and designated HP-1, HP-2, and HP-3 was also analyzed by both methods, with two acid digestion tests performed per plate and two sets of 12 images each utilized for ONVfA data. The fiber volume fractions determined by ONVfA and acid digestion appear in Table 3 and are plotted in Figure 44.

Table 3. Volume fractions by ONVfA and Acid Digestion.

Sample	HP-1	HP-2	HP-3	AC-1	AC-2	AC-3
Vf Fibers	%	%	%	%	%	%
ONVfA #1	65.9	66.3	66.6	74.0	69.6	69.2
ONVfA #2	64.4	65.9	67.3	71.9	68.2	69.1
ONVfA #3				72.2	66.1	68.5
ONVfA #4						67.9
ONVfA #5						67.0
ONVfA #6						67.0
ONVfA Average	65.0	66.1	67.0	72.7	68.0	67.7
Acid D. #1	67.4	65.5	64.4	73.0	68.4	70.3
Acid D. #2	65.1	64.2	65.1	70.4	67.8	68.7
Acid D. #3				71.8	68.1	69.7
AD Average	66.2	64.8	64.7	71.7	68.1	69.6
Difference (ONVfA-AD)	-1.2	-1.3	2.2	1.0	0.1	-1.9
Low Vf Regions (< 75% Ave.)	10.5	5.6	6.9	5.6	4.2	1.8

The results are in agreement to within better than 2.5%, with a standard deviation of 1.4% between the two methods. The ONVfA results are randomly higher or lower than the acid digestion values, with a negligible systematic error.

Fiber "maps" which represent each fiber in a composite cross-section with a single white pixel were constructed by combining 9 images from each of the composite specimens and appear in Figures 42 and 43. Fiber distribution functions for these same images were obtained by dividing the screen into 25 X 30 micron boxes and determining the number of fibers in each. The results plotted in the graphs in Figures 42 and 43 quantitatively describe the visually evident matrix-rich regions of

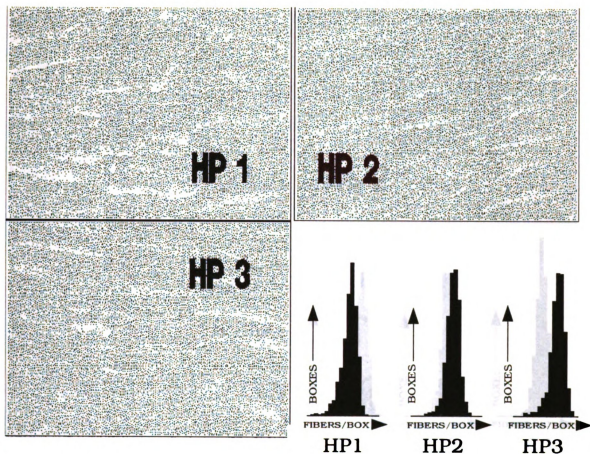


Figure 42. Fiber maps and distributions for HP1, 2, and 3.

these composite specimens. The percentages of boxes which contain fewer than 75% of the average number for the composite are listed in Table 3. The largest matrix-rich regions appear in specimen HP-1 which shows a broad distribution function and low fiber counts in 10.5% of the boxes while the most uniform appearing composite is specimen AC-3, which shows a narrow distribution function and low fiber counts in only 1.8% of the boxes. The average volume fractions for these same composites differ by only 3%.

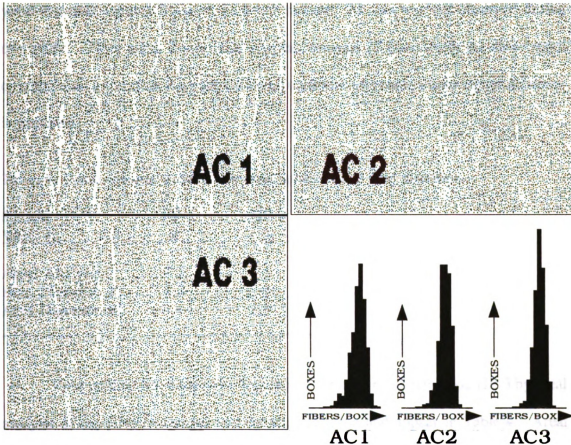


Figure 43. Fiber maps and distributions for AC1, 2, and 3.

The principal source of errors in the ONVfA data was probably changes in image size due to drift in the non-solid state video camera employed for digitizing. The standard deviation among the calibration image areas was 1.4%, coincidentally the same as that of the differences between the acid digestion and ONVfA results. These size errors can be substantially reduced either by using a dimensionally-stable CCD video camera or by including calibration marks in each image.

Another potential source of error is from systematic variations in the average fiber areas. Regions with consistently smaller or larger-than-average fibers would

yield incorrect volume fractions with this method, but this was not observed during this study. Fiber areas determined by measurements of fibers from the same spool or batch used to produce the composite can minimize this error where higher accuracy is required.

Table 4. Void volume fractions by areal analysis and acid digestion.

Sample Void Vf	HP-2 %	HP-3 %
Areal Analysis	4.2	3.5
Acid Digestion #1	4.8	2.8
Acid Digestion #2	5.1	1.8

Void volume fractions were determined for specimens HP-2 and HP-3 by areal analysis of the ONVfA images and by acid digestion and appear in Table 4. Areal analysis yielded a void volume fraction of 4.2% for HP-2 compared with 4.8 and 5.1% by acid digestion (ave. = 4.9%) and 3.5% for HP-3 compared with 2.8 and 1.8% (ave. = 2.3%) by acid digestion. These results show general agreement but more data and more precise acid digestion tests are required to document the accuracy of this method.

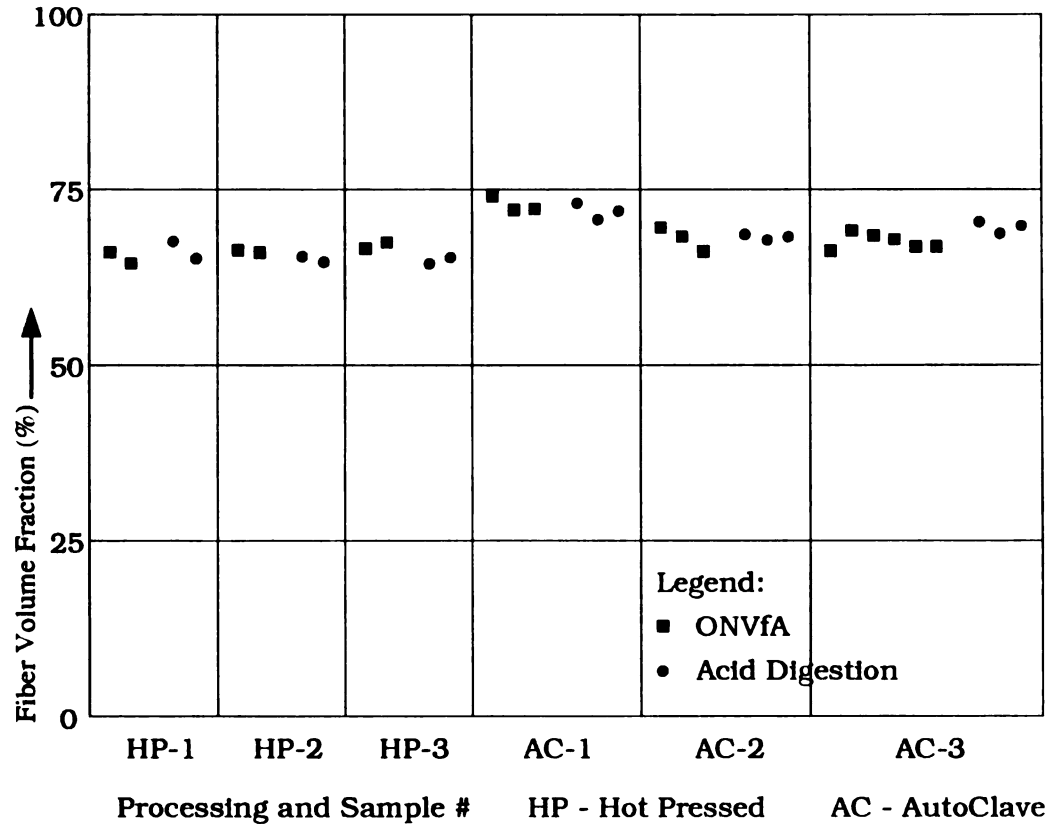


Figure 44. Fiber fractions by ONVfA and acid digestion.

4.7 FUTURE ONVFA WORK

ONVfA will be extended to apply it to a variety of fiber/matrix combinations, and to off-axis and non-unidirectional composites. Fiber maps produced by the method will also be integrated with void fraction information obtained by areal analysis to produce integrated representations of the distributions of fibers, matrix, and voids.

4.8 ONVFA CONCLUSIONS

An optical method for the determination of composite volume fractions has been developed. The accuracy of the method is not influenced by small image variations because the data is extracted as a digital parameter, the number of fibers. The method is an absolute technique, which does not require calibration by any other test, and which provides fiber volume distribution information with unequalled spacial resolution.

CHAPTER 5

EFFECTS OF OXIDATIVE SURFACE TREATMENTS ON FIBER SURFACE CHEMISTRY, FIBER-MATRIX ADHESION AND COMPOSITE MECHANICAL PROPERTIES OF INTERMEDIATE MODULUS CARBON FIBERS IN DGEBA/MPDA EPOXY

5.1 IM6 SYNOPSIS

Intermediate modulus Hercules IM6 carbon fibers with different amounts of electrochemical oxidative surface treatments, and with an epoxy-compatible size were subjected to an integrated set of surface analysis and mechanical tests to develop relationships between processing, chemistry, and properties. Surface analyses included XPS determination of surface oxygen and nitrogen, micro-Wilhelmy measurements of polar, dispersive, and total surface free energy, and SEM observation of surface morphology. Mechanical tests included single fiber tension tests, single fiber fragmentation interfacial shear strength tests, and mode II fracture toughness, short beam shear strength, and transverse flexural strength tests on unidirection composites fabricated with a DGEBA/MPDA epoxy.

The first increment of surface treatment was found to produce a rapid increase in surface oxygen, polar surface free energy, interfacial shear strength (ISS), interlaminar shear strength, mode II fracture toughness, and transverse flexural strength. Additional surface treatment caused surface oxygen, polar surface free energy and ISS to increase at a lower, linear rate. Interlaminar shear strengths were found to increase with the first increment of surface treatment, and to remain approximately constant with additional surface treatment, indicating a transition to a matrix-dominated failure mode. Mode II fracture toughness increased approximately linearly with ISS, except for the sized fiber, which showed significantly greater

toughness. Transverse flexural strength results were somewhat variable, and may have been influenced by artifacts from fiber bridging or volume fraction differences.

5.2 IM6 INTRODUCTION

A coordinated set of experiments was performed to attempt to gain an understanding of the nature of the changes in fiber/matrix adhesion that occur with increasing surface treatment and with sizing of PAN-based carbon fibers in an epoxy matrix. These experiments were directed at measuring changes in fiber surface composition and energetics, determining the influence these changes make in the behavior of single fiber composites, and investigating the changes in the properties of actual composite specimens. The tests were performed using Hercules Magnamite® IM6 fibers and are hereafter referred to as the "IM6" program.

Fiber/matrix adhesion for carbon fibers in thermoset epoxy matrices has been the object of numerous research efforts in recent years, since adequate adhesion is understood to be a necessary condition for good composite performance. Some of these programs have investigated the basic physical and chemical mechanisms of adhesion, some have explored the influence of specific fiber surface treatments on adhesion, while others have attempted to develop relationships between different adhesion levels and composite properties.

One approach to the study of chemical aspects of fiber/matrix adhesion has been in terms of acid/base interactions. Schultz, et al, investigated the adhesion of an epoxy matrix to untreated, treated, and treated and sized fibers by comparing an acid/base interaction parameter and surface free energy measurements, with fragmentation test measurements [Schultz, 1987]. It was claimed that adhesion correlated well with this specific interaction parameter, as measured by inverse gas chromatography with acidic and basic probes, but very poorly with the total surface free energy. These results must be considered in terms of the three types of fibers

studied, however. The surface free energy of a sized fiber is that of the sizing, not of the fiber itself. The formation of an interpenetrating polymer network and of crosslinks between the size and the matrix make simple surface energy interactions a questionable physical model. A series of more than two treated but unsized fibers are also needed to draw valid conclusions on this matter.

Recently, XPS was combined with adsorption studies to quantify the amount of chemisorption between a similar AS4 fiber and both epoxy and amine functional groups. Results indicated that the amount of either amine or epoxy chemisorbed was less than 3% of the surface coverage [Hook, 1990].

A correlation between acid/base character and fiber/matrix adhesion has also been demonstrated by Farinato [1990], using continuous flow microcalorimetry. Of particular interest was the finding that although most probes used were reversibly, physically adsorbed, primary and secondary amines were found to be irreversibly, chemically adsorbed. Since amines are present in the MPDA curing agent used in this study, this suggests a possibility for primary chemical bond formation.

Crosslinking of epoxy resins in the presence of surface oxidized carbon has been studied by FTIR [Garton, 1988]. Working with carbon black with an extremely high surface area/weight ratio to maximize the spectra of species near the surface, increasing oxidative surface treatment was found to increase crosslinking interactions by the adsorption of the tertiary amines in the catalyst.

Numerous experimental surface coatings and treatments have been tested in efforts to improve fiber/matrix interphase characteristics. Electrocopolymerization of various polymers directly onto fiber surfaces has been shown to produce small increases in adhesion [Wimolkiatisak, 1989]. While the mechanism of action of epoxy compatible finishes is usually described as promoting wetting and protecting the fibers during handling, Drzal, et al, have proposed that it forms a higher modulus, but brittle interphase that promotes adhesion while reducing toughness [Drzal, 1983].

The carbon fiber epoxy matrix interface has recently been reviewed by two researchers [Wright, 1990], [Hughes, 1991]. Wright summarized results of studies of alternative polymer fiber coatings, electrodeposition and electropolymerisation techniques, theoretical analyses, and surface analytical methods. Wright concludes that the bulk of current evidence suggests that primary covalent bond formation is not a significant contributor to interfacial adhesion, that fiber surface area is a negligible factor, and that the removal of a weak fiber surface layer and an increase in polar surface interactions are the primary adhesion factors.

Hughes critically reviews carbon fiber/epoxy matrix interface research and composite property influences [Hughes, 1991]. Possible sites of failure within the fiber, interphase, and matrix are addressed, and the effects of Poisson's ratio differences addressed. Work on the internal and surface structure of carbon fibers and their influence on failure are cited. Hughes concludes that simple conclusions about optimal fiber surfaces are difficult to draw, due to the numerous relevant factors and contradictory literature. He does state that adhesion is increased by some degree of disorder in the fiber surface, by surface oxidation, and by mechanical interlocking, particularly for high modulus fibers. The effects of sizing are considered highly variable, probably depending on the fiber and size.

This portion of the current research effort was directed toward an investigation of the effects of electrochemical surface treatment on the adhesion of intermediate modulus PAN based carbon fibers to an epoxy matrix, and the resultant influence on composite properties. The experimental program, results, and interpretation are described in the following sections. Finally, chapters 6 and 7 investigate adhesion to amorphous and semicrystalline thermoplastics with linear polymer structures for comparison with this work on crosslinked, thermoset epoxy. The conclusions section (chapter 8), will attempt to form an understanding of how the differences in chemistry and structure influence fiber/matrix adhesion.

5.3 IM6 EXPERIMENTAL PROGRAM

The IM6 experimental program involved specially treated carbon fibers obtained through the TTCP-TP3 program (The Technical Cooperation Panel, Technical Panel 3), an international research effort involving teams working in the United States, United Kingdom, Canada, Australia, and New Zealand. A standard, DGEBA/MPDA epoxy matrix material was used to allow results to be compared with other sets of tests performed in this and other laboratories. The fibers were characterised by several methods and were fabricated into single fiber fragmentation specimens and high volume fraction unidirectional composite panels which were subjected to mechanical testing. These materials, their characterization, and the subsequent experimental program are described in this section.

5.3.1 IM6 EXPERIMENTAL MATERIALS

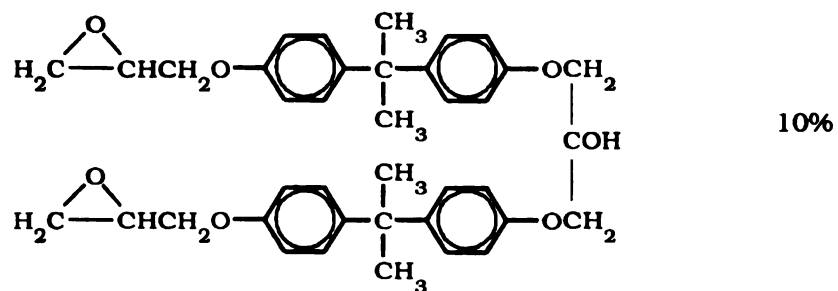
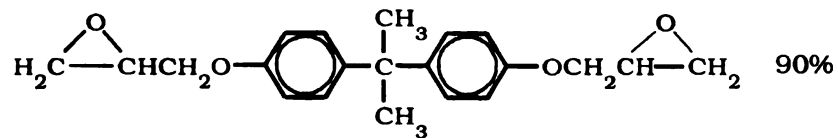
Hercules Magnamite[®], IM6 intermediate modulus polyacrylonitrile based carbon fibers were produced in a large, single batch, divided into sub-batches and surface treated to different extents by a proprietary electrochemical oxidation process. These treatments were defined as ratios of the standard surface treatment, considered to be 100%, and were 0% (untreated), 20%, 100%, 200%, and 600%. These ratios were determined by the number of coulombs of charge passed per unit fiber surface area in the course of the surface treatment compared with that passed for the nominal 100% treatment. An additional batch was given 100% treatment and coated with a proprietary epoxy-compatible "G" finish. The designations of the six fiber surface conditions are: Untreated - 0ST, 20% treated - 20ST, 100% treated - 100ST, 200% treated - 200ST, 600% treated - 600ST, and 100% treated and coated - 100GST.

Table 5. Properties of IM6 fibers summarized from Hercules data sheet

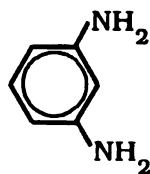
<u>Property</u>	<u>U.S. Units</u>	<u>SI Units</u>
Tensile Strength	635,00 psi	4,378 MPa
Tensile Modulus	40.4 mpsi	278 GPa
Ultimate Elongation	1.50%	1.50%
Carbon Content	94.0%	94.0%
Density	.0627 lb/in. ³	1.73 g/cm ³
Filament Shape	round	round
Tow Twist	none	none
Tow Cross Sectional Area	4.17 X10 ⁻⁴ in. ²	0.27 mm ²
Fiber Cross Sectional Area	3.475X10 ⁻⁸ in. ²	2.247 X 10 ⁻⁵ mm ²
Fiber Diameter	1.05X10 ⁻⁴ in.	5.343 microns

The properties of IM6 fibers are summarized in Table 5. The tensile modulus of 278 GPa (40.4 mpsi) is greater than that of lower modulus fibers such as Hercules® AS4, used as a standard in other programs in this laboratory due to pyrolysis of the PAN precursor at higher temperatures and with greater draw ratios. This difference in processing may be expected to produce a more highly oriented and more graphitized structure with a greater number of graphitic basal plane sites exposed on the surface and fewer edge, corner, or disordered non-graphitic carbon sites.

The epoxy matrix material used for all IM6 series tests was Dow Chemical Corporation, DER 331 resin, the diglycidyl ether of bisphenol-A, (DBGEBA) cured with a stoichiometric ratio (14.5 phr) of metaphenylene diamine (MPDA). The chemical structures of these epoxy constituents are shown in Figure 45.



DER 331, diglycidyl ether of bisphenol -A



meta-phenylene diamine (MPDA)

Figure 45. Chemical structures of epoxy precursors.

The cure cycle used for all specimens in the IM6 program, both fragmentation and full scale composite, was 2 hours at 75 °C followed by 2 hours at 125 °C and slow cooling to room temperature in the oven or autoclave. Additional details on processing appear in the sections on specimen fabrication. This cure cycle was chosen to produce a matrix with identical properties to those of other research programs for purposes of comparison. The initial tensile modulus of this matrix is 3.6 GPa (525 ksi) and the tensile strength of bulk specimens is 89.6 MPa (13 ksi).

5.3.2 CHARACTERIZATION OF FIBER SURFACE PROPERTIES

Surface properties of the treated IM6 fibers were characterized by X-ray photoelectron spectroscopy for chemical composition, by micro-Wilhelmy wetting studies to determine surface energetics, and by scanning electron microscopy to determine surface morphological characteristics. The details of each of these sets of experiments are described in the following sections.

5.3.2.1 XPS Surface Composition Analysis

The surface chemical compositions of the five treated, but unsized fibers were determined by x-ray photoelectron spectroscopy. Analyses were performed for surface oxygen, nitrogen, and, by difference, carbon concentrations. Complete sets of measurements were performed by two different XPS operators, Tad Devilbiss, and Kevin Hook, using magnesium and aluminum anodes respectively.

X-ray photoelectron spectroscopy exposes a surface to a beam of approximately monochromatic x-rays in an ultra-high vacuum chamber. Under this well-defined excitation energy, surface species are ionized, resulting in the emission of outer shell electrons. The kinetic energy of the emitted electrons is equal to the difference in energy between the X-ray photons and the binding energy of these outer electron orbitals. This kinetic energy is measured by noting their deflection under a magnetic

field in a hemispheric energy analyzer. The binding energy is calculated and compared with those of known species to identify and quantify the composition of surface species. This information can also be used to deconvolute the bonding state of the species, since this influences the binding energy.

XPS measurements were performed with a Perkin-Elmer PHI 5400 X-ray photoelectron spectrometer with two different target anodes used. An Mg K-alpha standard source was used for the first set of measurements while the second was performed with a toroidal Al K-alpha monochromatic source.

5.3.2.1.1 Chemical Composition

The chemical composition of the fiber surfaces were determined by comparing peak areas for emissions from the C_{1s} , O_{1s} , and N_{1s} electron orbitals.

5.3.2.1.2 Chemical Group Deconvolution

Changes in bonding state exert an influence in the binding energy of all electrons in a species, allowing information on the molecular state to be extracted from XPS data. These data were obtained by deconvolution of the C_{1s} peaks. The C_{1s} peaks allowed the separation of the carbon atom bonding states into graphitic, phenolic (C-O-H), ketonic (C=O), and carboxylic (O-C=O).

5.3.2.2 Micro-Wilhelmy Surface Energy Measurements

Fabrication of composite materials without voids and with adequate fiber/matrix adhesion is only possible if the matrix material properly "wets" the fibers, that is, the surface tension of the fibers must be less than that of the liquid phase.

$$\gamma_{SV} - \gamma_{SL} = \gamma_{LV} (\cos \theta)$$

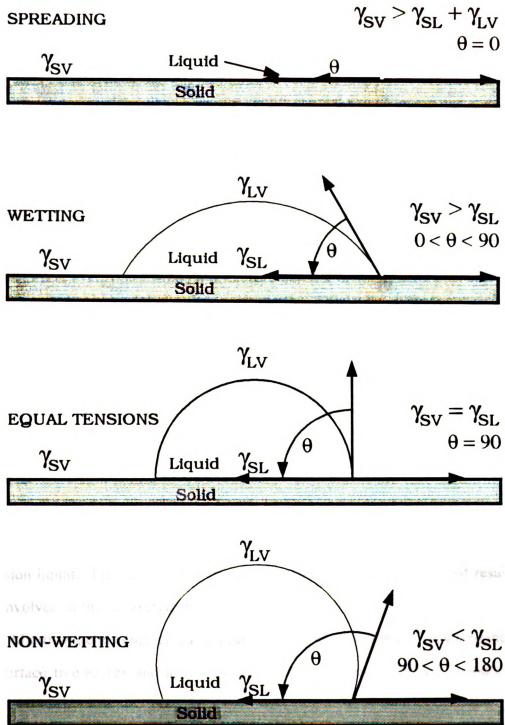


Figure 46. Surface tension influence on contact angles.

The micro-Wilhelmy balance [Li, 1984], [Hammer, 1980], is designed to measure the work of adhesion of liquids with different degrees of polarity to solid fiber surfaces. This work is defined as the energy required per unit area to displace a liquid from the surface of a solid, substituting a solid-vapor interface for the previously existing solid-liquid interface.

$$W_A = \gamma_{LV} + \gamma_{SV} - \gamma_{LS}$$

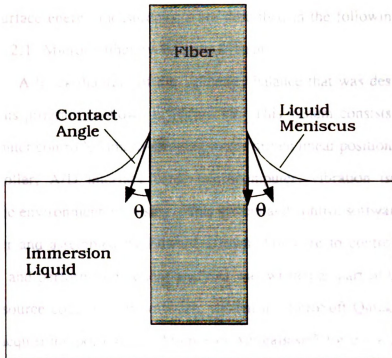
where W_A is the work of adhesion, γ_{LV} is the Liquid-Vapor surface tension, γ_{SV} is the Solid-Vapor surface tension, and γ_{LS} is the Liquid-Solid surface tension.

The value of the contact angle of a liquid on a solid surface, at equilibrium, is determined by the surface energies of the solid-vapor and liquid-vapor interfaces. Contact angles of 0 degrees (Figure 46) exist when the liquid spreads over the solid without limit. Contact angles between 0 and 90 degrees are considered to represent wetting, while angles from 90 to 180 degrees occur when the liquid does not wet the solid. At exactly 90 degrees the surface tensions of the liquid-vapor and solid-vapor interfaces are equal. These relationships for the equilibrium condition are represented by the Young equation:

$$\gamma_{LV} = \gamma_{LS} + \gamma_{LV} * \text{COS}(\theta) \text{ where } \theta \text{ is the contact angle.}$$

The Wilhelmy balance determines liquid-solid contact angles by measuring the force exerted on a solid object with a known perimeter when it is wetted by an immersion liquid. Figure 47 shows the surface tension, contact angle, and resultant force involved in this measurement.

Micro-wilhelmy contact angle measurements were performed to determine the fiber surface free energy and to resolve it into the polar and dispersive components [Kaelble, 1974].



$$\text{Downward force } P = \gamma_{LV} \cos(\theta)$$

Figure 47. Fiber wetting force and contact angle measurement.

This resolution is made possible by assuming that the total free energies of the solid and liquid phases are equal to the sum of their polar and dispersive components.

$$\gamma_L^T = \gamma_L^P + \gamma_L^D$$

$$\gamma_s^T = \gamma_s^P + \gamma_s^D$$

With suitable rearrangements and substitutions [Kaelble,1974], [Hammer, 1980] the following expression may be obtained:

$$[\gamma_L(1 + \cos(\theta))/2\gamma_L^D]^{1/2} = \gamma_s^D]^{1/2} + \gamma_s^P]^{1/2} (\gamma_L^P/\gamma_L^D)^{1/2}$$

A plot of $\gamma_L(1 + \cos(\theta))/\gamma_L^D]^{1/2}$ against $(\gamma_s^P/\gamma_s^D)^{1/2}$ for immersion in two or more liquids with different polarities should yield a straight line with a slope and intercept equal to γ_s^P and γ_s^D .

The micro-Wilhelmy balance system that was designed for this program and

the surface energy measurements are described in the following section.

5.3.2.2.1 Micro-Wilhelmy Balance System

A block diagram of the Wilhelmy balance that was designed and constructed for this program is shown in Figure 48. This system consists of an electrobalance, computer controlled micro-stepping motor driven linear positioning stage, temperature controller, A/D interface card, microcomputer, vibration isolation table, and an acrylic environmental housing. This system and control software was designed by the author and assembled by Edward Drown. Software to control the balance, acquire data, and perform subsequent analyses was written as part of this research program. The source code for this software, written in MicroSoft QuickBasic® for the control and acquisition portion, and MicroSoft AmigaBasic® for the analysis portion, appears in Appendix D. The balance control and data acquisition software uses the microcomputer to integrate the operations of the positioning stage, electrobalance, A/D converter, and temperature controller to provide a flexible, programmable operating environment for contact angle measurements.

The data acquisition sequence was as follows. The electrobalance output was first calibrated in the following manner. With the electrobalance, computer, A/D converter and software operating, the system electronics were allowed to stabilize for several minutes. With nothing on the electro-balance the A/D output was measured and set as the zero baseline. A 20 milligram weight was then placed on the balance at the reference weight position, 1/5 of the distance from the fulcrum as the sample point, and therefore 1/5 as sensitive. This reference provided a calibration for the balance electronics and A/D convertor, and set up the software to provide an output calibrated in micrograms. Following calibration the weight was removed.

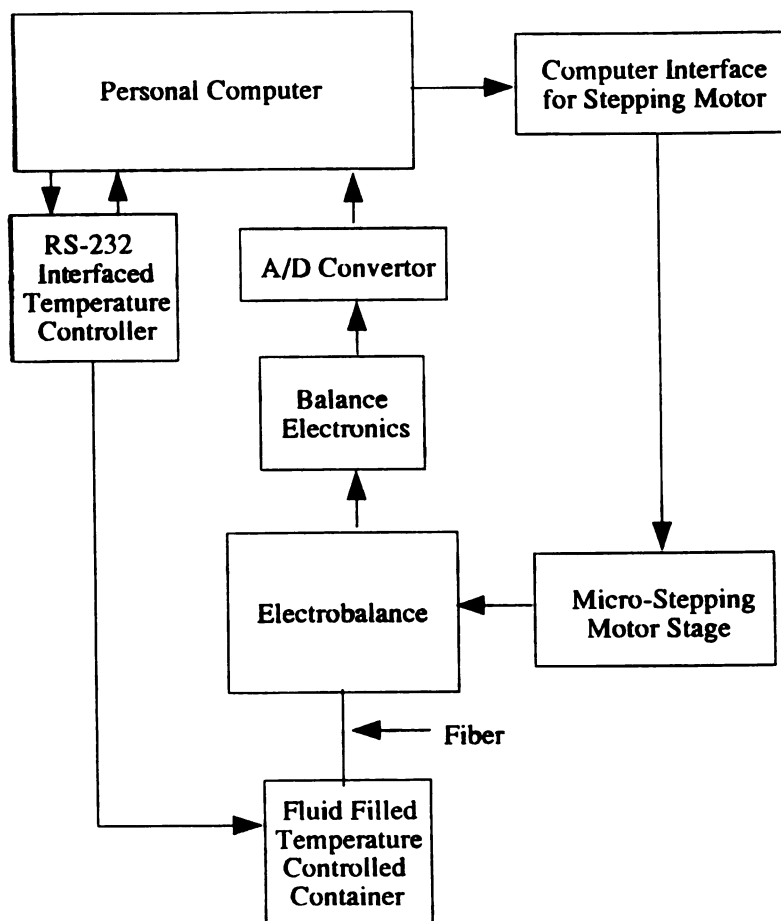


Figure 48. Block diagram of micro-Wilhelmy wetting balance.

A set of fibers was mounted on nichrome or nickel mounting hooks with cyanoacrylate adhesive, taking care not to contaminate the fiber surface away from the hook and to align the fiber axis accurately with the hook wire. The mounted fibers were allowed to dry at least 24 hours in a dessicator before measurement.

A mounted fiber was suspended from the loading hook of the electrobalance and the balance output was set as the zero by the software, prior to immersion in the liquid. The stage and electrobalance were then lowered by a manual command through the computer until the fiber end was immersed in the liquid. The fiber was carefully inspected to insure that it was immersed at a 90 degree angle to the liquid surface and was not bent, or held out of the liquid by surface tension. This was a particular problem with the untreated, low polar surface free energy fibers in a polar liquid with high surface tension (water).

Ensuring that the fibers were accurately orthogonal to the liquid surface was the most difficult part of the data acquisition sequence, and resulted in the principal source of error. This is mainly due to the extremely small diameter of the fibers under investigation, 5.35 microns, and the dependence of bending stiffness on the fourth power of the radius. For comparison, AS4 fibers with a diameter of approximately 7 microns and a modulus 25% lower have a bending stiffness about 2.25 times greater, making measurements much easier.

Following immersion and inspection the computer was instructed to perform the following data acquisition sequence. The fiber was advanced 1.25 mm into the immersion liquid and 30 seconds were allowed to elapse to stabilize the wetting force. The load was then measured repeatedly and averaged by the software. After 5 immersion, pause, and load measurement cycles the the contact angles were calculated from the measured load and the user inputted fiber diameter (perimeter) and the liquid surface tension. Sets of 5 measurements were repeated until consistent values were obtained as a further check on fiber/liquid alignment.

5.3.2.2.2 Micro-Wilhelmy Experimental Program

Contact angles were measured for sets of fibers with each extent of surface treatment in distilled water and ethylene glycol. At least six separate fibers were tested for each contact angle measurement, with multiple immersions and angle measurements as described above until consistent values were recorded.

Average fiber diameters were used for perimeter calculations rather than measuring each fiber individually because the small variance in diameter made this unnecessary while the small diameter of the fibers makes direct optical measurements inaccurate. Diameter measurements made with a light microscope and Filar eyepiece produced identical coefficients of variation between measurements on the same or different fibers. This indicated that the actual variation in fiber diameter was not measurable by this technique.

5.3.2.3 Fiber Surface and Cross Section Examination

Fiber surfaces were examined by scanning electron microscopy (SEM) on a JEOL JSM T330 SEM. Fibers were mounted on aluminum stubs with conductive adhesive and gold sputter coated to a thickness of approximately 100 nm. To improve contrast for surface morphology observations, fibers were tilted at 60 degrees to the horizontal plane, (30 degrees to the incident electron beam). Without this tilt angle the fibers appeared as perfectly smooth cylinders, with no resolvable surface detail.

A minor artifact resulting from electron beam damage to the gold sputter coating layer during focusing and contrast adjustment was unavoidable. This damage appears as a faint rectangular region in each image, and does not interfere with the interpretation of surface morphological characteristics.

Fibers were prepared for cross sectional SEM observation by mounting on diagonal mounting tabs on aluminum stubs with conductive paint, cutting the fiber ends with sharp, surgical scissors, and sputter coating with approximately 100 nm of

gold. An attempt was made to prepare the fiber ends by breaking the fibers in tension but the strength of the conductive mounting medium was insufficient. Attaching the fibers with epoxy, breaking the fibers, and then grounding them with conductive paint would allow these observations to be made.

5.3.3 IM6 MECHANICAL TESTING

Mechanical testing of IM6 composites consisted of single fiber tension tests, fragmentation tests, and three sets of macro-scale mechanical tests on fibers with each of the six surface treatments. The macro-scale composite tests were performed by Dr. Madhu Madhucar and were chosen for their sensitivity to interfacial effects and were: mode II fracture toughness (end-notched flexural specimens), short beam shear strength, and transverse flexural strength. Mechanical tests that show only a weak dependence on interfacial strength and toughness, such as axial tensile strength, were not a part of this study. The experimental procedures for the mechanical testing program are described in the following sections.

5.3.3.1 Fiber Tensile Strength Tests

Tensile strength data for the series of IM6 fibers was available from other TTCP participants only for 23 mm gage length fibers. Interpretation of fragmentation test results requires a knowledge of the fiber strength at much shorter lengths, comparable to the critical length attained during this test. To allow a meaningful extrapolation to these lengths, tension tests at 2 mm gage lengths were performed for two of the fiber types.

At 23 mm gage length, the highest and lowest strength fiber types were the 200ST and untreated fibers, respectively. These two types were chosen to test at 2 mm gage length with the expectation that this would bracket the range of fiber types at this shorter length.

Testing was performed by A. Ozzelo with an apparatus developed in this laboratory for short gage length testing of reinforcing fibers, consisting of a fiber mounting system, a translation stage, a 250 gram micro-load cell, and a chart recorder for data acquisition.

Fifteen fibers each of the 200ST and untreated fiber types were subjected to monotonic tension testing. Loads at failure were determined by measuring the maximum deflection on the chart recorder, converting to millivolts and to grams at maximum load. Fiber areas were determined by assuming a 5.35 micron diameter and a circular cross section. Stresses were calculated as engineering stress, (load/initial area), since the strain was small. The results of testing and details of the extrapolation method used to approximate tensile strengths at the critical lengths appear in section 5.4.2.1.

5.3.3.2 Interfacial Shear Strength Tests

Single fiber fragmentation tests, (SFF) were performed to measure the interfacial shear strengths for each of the fiber treatments. A diagram of a typical fragmentation test coupon is shown in Figure 49. This technique is described and analyzed in detail in Chapter 2 and will not be repeated here. Fiber strengths at critical lengths were determined by short gage length tensile tests and extrapolation in a manner described in section 2.4.2.1. Fiber diameters were initially measured by Filar eyepiece, but this method was found to be inaccurate for small diameter fibers with only a small variation in diameter. For this reason, the average fiber diameter from the Hercules product data sheet was assumed.

Fragment lengths were measured by two different techniques. Initial measurements were performed with a Filar eyepiece, calibrated against an Olympus calibration slide. Following the development of the FiberTrack, fragmentation data acquisition and analysis system described in section 3.4.4, subsequent tests were

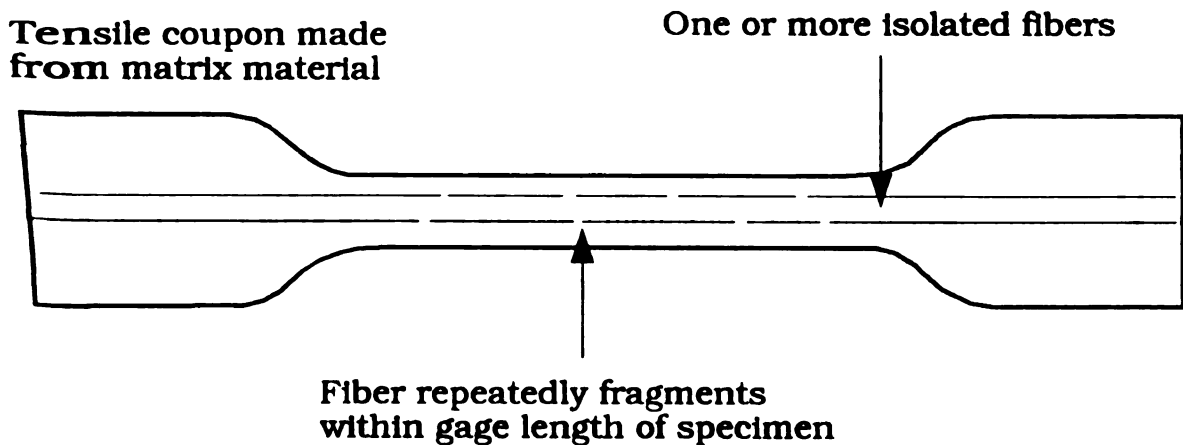


Figure 49. Single fiber fragmentation test specimen.

performed with this system. Fragmentation test data have been reported in several forms in the literature, including mean fragment lengths, L_c/D aspect ratios, and as interfacial shear strengths calculated by either a simple shear lag analysis or, with the additional consideration of the statistical nature of fiber failure, a Poisson-Weibull type analysis. The relative merits of these approaches are discussed in Chapter 2.

In this investigation, fragment length data were reduced by performing a Poisson-Weibull analysis to determine the Weibull scale and shape parameters, and from these an indication of the approximate interfacial shear strength. This method has the advantage of simplicity, and ease of comparison with other work using an identical approach. All Weibull and Gamma function calculations were performed with the FiberTrack system.

5.3.3.2.1 Fragmentation Specimen Fabrication

Fragmentation specimens were fabricated by the following technique. The outermost layer of each spool of fibers was unwound and discarded, exposing inner fibers less likely to have been damaged or contaminated during handling and shipping.

Segments of tow approximately 25 cm. (10 inches) in length were cut off and stored in aluminum foil packets, taking care to handle the segments only at the ends. The spools of fibers were then repackaged in aluminum foil and stored for later use in the macro-scale composite specimens.

In a clean work area with intense illumination and minimal air currents, a foil packet was opened and single fibers withdrawn while taking care prevent contamination and minimize fiber damage. One end of the tow was teased and spread until single fibers were accessible and one fiber was seized between the right thumb and forefinger. This fiber was then pulled out from the tow along the tow axis to minimize snagging due to lateral forces. When the fiber was pulled nearly free but still attached to the tow it was grasped at the left end by the left hand and removed from the tow.

The single fiber was then laid across the end sprues and gage section of a room temperature vulcanizing silicone mold and released with the right hand. The right side was secured at the outer edge of the sprue with a drop of hot-melt adhesive which was then allowed to solidify. The fiber was then drawn straight by a light tension from the left side and secured at the outer edge of the left spue by a second drop of hot-melt adhesive. Light tension was maintained as the adhesive solidified, leaving the fiber straight and accurately aligned with the gage section. This method provides an advantage over attachment with rubber cement because the hot-melt adhesive flows viscously until solidified, allowing better fiber positioning. The fiber was further anchored in place with drops of rubber cement applied at the inner edges of the end spues to maintain attachment during the rising temperature portion of the cure cycle, when the hot-melt adhesive melts.

After fibers were mounted in all eight cavities in the mold, the dangling fiber ends were trimmed off and the mold assembly stored in a dessicator overnight to allow the rubber cement solvent and surface moisture to evaporate.

Resin was prepared in the following manner. A sufficient amount of a stoichiometric ratio of DGEBA and MPDA (14.5 phr of metaphenylene diamine in the diglycidyl ether of bisphenol-A) were weighed in disposable laboratory beakers and placed in a vacuum oven at 75 °C and under a very slight vacuum to initiate outgassing while avoiding boiling the MPDA. The MPDA was stored in a dark refrigerator prior to use to minimize degradation. When the MPDA was fully melted the beakers were removed, thoroughly mixed, and returned to the vacuum oven. Outgassing then proceeded at low vacuum until the resin mixture stopped bubbling, approximately five minutes.

The mold assemblies were withdrawn from the dessicator and briefly outgassed in the vacuum chamber to completely dry the surface. The molds were then removed and placed on a surface tilted approximately 20 degrees to the horizontal. The resin/hardener mixture was introduced to the mold cavities by pouring from the elevated ends. This causes the resin to sweep along the fiber and avoids entrapment of air bubbles. The filled molds were lowered to horizontal and excess resin was removed with a dropper from the ends, taking care not to disturb the fibers.

The filled mold assemblies were then placed in the curing oven which had been previously raised to the initial cure temperature of 75 °C. Following the complete cure cycle of 2 hours at 75 °C and 2 hours at 125 °C the oven was allowed to slowly cool overnight and the specimens removed at room temperature.

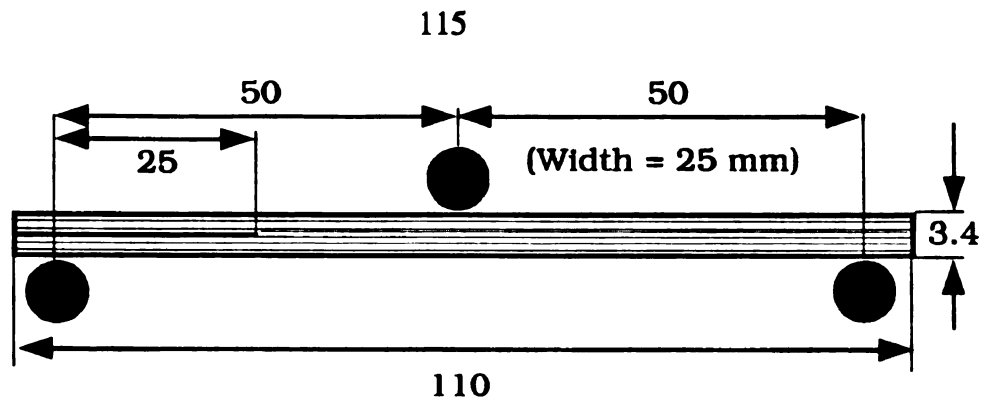
5.3.3.3 Fabrication of Composite Specimens

High volume fraction unidirectional composite panels were fabricated for mechanical testing by the following means. Unidirectional prepreg tape was first fabricated by hot melt prepregging, and then cut, laid up into composite panels, and consolidated and cured in an autoclave. Tape was produced by passing the fiber tow through a batch of DGEBA/MPDA held at 52 °C (125 °F) and removing excess resin

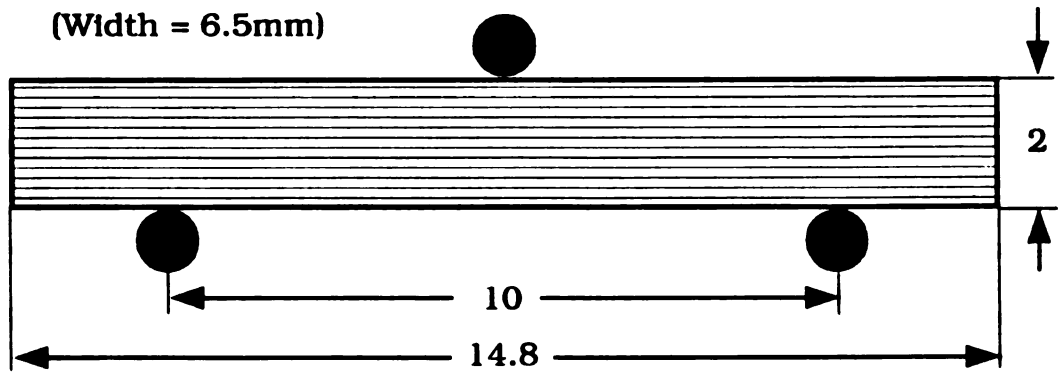
by passage through a slit die. The impregnated tow was wound onto a mylar film covered drum at a tension of about one kilogram and a speed of approximately 3 meters per minute. When a single layer tape was complete the mylar film was cut, removed from the drum and manually laid up to form the unidirectional composites. A teflon release layer was incorporated at the central plane of the 24 ply laminate panels for the mode II fracture toughness specimens.

Specimens were cured in an autoclave for 2 hours at 75 °C (167 °F) and 2 hours at 125 °C (257 °F) and 0.69 MPa pressure (100 psi). The vacuum bags were evacuated for 15 minutes at the beginning of the cycle to remove air and dissolved gasses and then the vacuum was released. Specimens were slowly cooled to room temperature before removal from the autoclave.

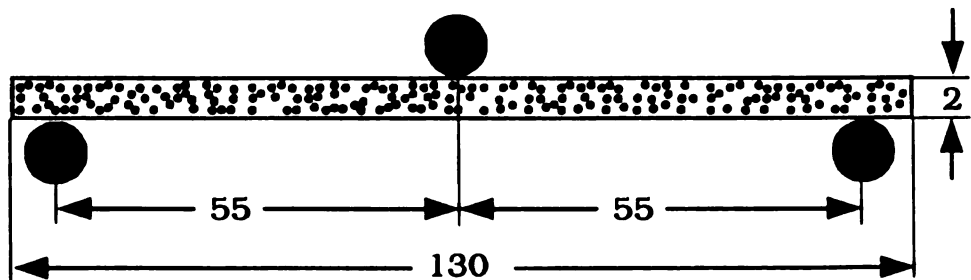
Test specimens in the geometries shown in Figure 50 were cut from the composite panels by a high-speed diamond impregnated saw with a water cutting fluid.



End Notched Flexure Specimen (Mode II Fracture Toughness)



Short Beam Shear Strength Specimen



Transverse Flexural Strength Specimen

Figure 50. Mechanical test specimen diagrams.

5.3.3.4 Volume Fraction Analysis by ONVfA

The composite plates produced for mechanical properties evaluation were characterized by three different means. Fiber volume fractions were determined by Optical Numeric Volume Fraction Analysis, (ONVfA), which was developed as part of this research effort and is described in detail in chapter 3 was performed by Brian Rook. The statistical distribution of fibers was determined by the same means to find the amount of fiber poor regions. Void contents were measured by areal image analysis.

5.3.3.5 Mode II Fracture Toughness Tests

End-notched flexural specimens were produced from the 24 ply, unidirectional panels with the previously incorporated teflon release strip serving as the crack starter. These specimens were subjected to three point bending on a closed-loop servohydraulic actuated MTS mechanical testing machine by Dr. Madhu Madhukar. Strains were monitored by adhered strain gages and extensometers and recorded with an IBM PS2/30[®] microcomputer data acquisition system. Maximum specimen deflections were obtained from the machine crosshead displacement.

5.3.3.5 Transverse Flexural Tests

Three point transverse flexural data were obtained in accordance with ASTM D-790 specifications. Testing and data acquisition was performed on the MTS testing machine described in section 5.3.3.4 by Dr. Madhu Madhukar. The specimen deflection at the midpoint was taken to be equal to the crosshead displacement.

5.3.3.6 Short Beam Shear Tests

Short beam shear strength tests were performed in accordance with ASTM D-2344 specifications. Testing and data acquisition was performed on the MTS testing

machine described in section 5.3.3.4 by Dr. Madhu Madhukar. These specimens are designed to fail in shear along the central plane rather than by microbuckling or tensile failure at the top or bottom. This is accomplished by making the specimens relatively short, since the midplane shear is proportional only to the shear traction, and is not a function of length while the tension and compression stresses increase with increasing specimen length.

5.3.3.7 SEM Fractography of mode II and Transverse Flexure Surfaces

Failure surfaces of end-notched flexural specimens (mode II) and transverse flexural specimens were examined by scanning electron microscopy. Documentation was performed by producing raster-scan photographs at specific distances from the crack-initiation notch with the built in Polaroid camera and by videotaping the SEM's composite video output while traversing stepwise across large regions of the failure surface. In this manner high resolution photographic images of representative sites were recorded for publication and interpretation. While large areas of the failure surfaces were stored on videotape at lower resolution for later observation and verification of the representative character of the photomicrographs.

5.3.3.8 Birefringence Evolution Sequence Acquisition

Birefringence evolution sequences and animations (BES and BEA) were produced for each of the IM6 surface treatment and sizing conditions in DER 331 with 14.5 phr MPDA cured under the standard conditions (2 hr at 75 °C and 2 hr. at 125 °C). These sequences consist of sequences of microscope images of the regions surrounding fiber breaks, viewed under crossed polarizers, and recorded at incremented coupon strains.

By assembling entire sequences of images for subsequent analysis, this method provides a more complete picture of the nature of interfacial shear stresses, and of the

interfacial failure modes, than do images obtained at a single strain level.

For complete documentation of birefringence patterns, all of the relevant experimental variables must be recorded or controlled. In addition to the fiber type, surface treatment, matrix type and cure conditions, other factors may exert both a quantitative influence on the extent of interfacial failure, and a qualitative influence on the failure mode. The coupon strain at which the images are obtained is the most obvious of these factors, and has been reported by some, but not all researchers. The strain-at-failure of the fiber break at the center of the birefringence pattern also strongly effects their characteristics, and appears to have been neglected. The lengths of the fiber fragments adjacent to each break may also play a role in determining the mode of failure.

In this investigation, the first image in each birefringence sequence was recorded at approximately the strain-at-failure of the break. This was accomplished by viewing a large region of the specimen at low magnification while slowly increasing the coupon strain. When a new break occurred, straining was immediately halted, the strain recorded, and the sequence acquisition begun.

Acquisition was performed by digitizing the composite video output of a Panasonic® CCD video camera attached to an Olympus® microscope with crossed polarizers. Digitization was accomplished with a DigiView® video A/D convertor interfaced with an Amiga 500® microcomputer. Images were acquired in a low resolution mode, 320 X 200 pixels at 16 shades of gray (4 bit gray scale resolution). While beneath the maximum available resolution of 768 X 480 pixels with 16 shades of gray, this precision was sufficient to resolve most of the important image details.

Sequences of images at successive strain increments were acquired in the following manner. The length at zero strain between transverse fiducial marks on the specimen gage section was determined by noting the distance translated by the Newport® stage while moving between the marks as compared against an eyepiece

reticle. This length was taken as the reference L_0 and used to measure the coupon strain. The coupon strain was incremented by increasing the displacement of the straining stage (described in section 3.3.2). This increase was determined by advancing a predetermined displacement as measured with a machinists' dial gage. The actual coupon strain was then determined by measuring the change in the distance between the transverse fiducial marks.

Each image was centered on a fiber break which occurred at a well defined fiber failure strain as described previously. The distance from this break to a fiducial mark was noted to allow subsequent identification. After incrementing and measuring the coupon strain, the stage was advanced until the break of interest was located, and the break was accurately centered against a crosshair drawn on the video monitor to minimize rigid body displacements. The image was then digitized and saved to diskette.

A series of birefringence images was defined prior to acquisition, including the measured strain at fiber failure, the intended strain increments during extension and retraction of the coupon, the strain at maximum extension, and from these values, the number of images. This series of strain levels was approximated by use of the dial gage and a previously made calibration graph, and measured more precisely during acquisition as described previously.

A sequence of digitized birefringence images saved on a diskette was then loaded as frames in a computer animation and graphics program for subsequent processing. Each image was then precisely positioned to cancel all remaining rigid body motion and make the fiber break appear in the same screen location in subsequent frames. The entire sequence of images was then framed and "grabbed" as an "animation brush". This brush was saved to disk and used to produce birefringence evolution animations and the birefringence sequences that appear in section 5.4.2.8. These sequences were printed out with a laser printer controlled by

a desktop publishing program.

During the course of these investigations it has become increasingly clear that meaningful, representative fragmentation test birefringence patterns can only be acquired when all of the relevant experimental variables have been controlled or recorded. More than one break at each of a range of fiber failure strains and coupon strains may be required to present a complete, representative set of birefringence patterns. Additional discussion of these variables appears in sections 2.5 and 5.4.2.8.

5.4 IM6 RESULTS AND INTERPRETATION

The results and interpretation for the IM6 experimental program appear in this section. Where appropriate, comparable data for Hercules AS4 fibers, obtained from other researchers in this laboratory, are included to indicate trends.

5.4.1 FIBER SURFACE ANALYSIS RESULTS

The results of the fiber surface analyses by XPS and surface morphological examination by SEM appear in the following sections.

5.4.1.1 Surface Chemical Composition Results

The XPS surface composition analysis results for IM6 fibers with increasing oxidative surface treatment appear in Table 6 and are plotted in Figure 51 (surface oxygen percentage) and Figure 52 (surface nitrogen percentage).

The untreated fibers were found to have a very low surface oxygen percentage, 2.21%. Surface treatment to 20% of the nominal value resulted in significantly greater surface oxygen, 5.59%, a threefold increase. Surface treatments to 100%, 200%, and 600% of the nominal value further raised oxygen content at a rate that was closely linear to treatment percentage over the range from 20% to 600%, as can be seen in Figure 51. This rate of increase was much lower than for the step from

untreated to 20%. resulted in 8.26% oxygen. These results were consistent for all samples, and in good agreement with results from a previous analysis, except for a small, consistent, shift of approximately 2.25% which may be attributed to calibration differences.

Table 6. Surface oxygen, nitrogen, and functional groups on IM6 fibers.

Treatment	0%	20%	100%	200%	600%
Oxygen (%)	2.21	5.59	6.85	8.26	15.62
Std. Dev. (%)	0.51	0.72	0.36	0.39	1.34
Nitrogen (%)	1.68	1.85	1.86	1.88	4.77
Std. Dev.(%)	0.44	0.36	0.25	0.26	0.41
Phenolic (%)	1.2	4.4	4.7	4.9	6.5
Ketonic (%)	1.9	2.8	3.1	4.3	8.6
Carboxylic (%)	2.3	2.5	2.5	2.3	3.0

Surface nitrogen percentages measured by XPS appear in Table 6 and Figure 52. Nitrogen remained nearly constant at about 1.8% for surface treatments ranging from 0% to 200% surface treatment, but increased significantly with 600% surface treatment to 4.77%. These results are also in agreement with those from the previous analysis, except that an increase was also found to occur between 100% and 200% surface treatment in that set of tests.

The large increase in oxygen content resulting from 20% surface treatment in comparison with the smaller rate of increase from 20% to 600% treatment may result from either or both of a pair of mechanisms. One possible source of this change in reactivity is the availability of edge and corner sites on the graphitic lattice of the untreated fibers, as well as bonding sites on more disordered, non-graphitic carbon.

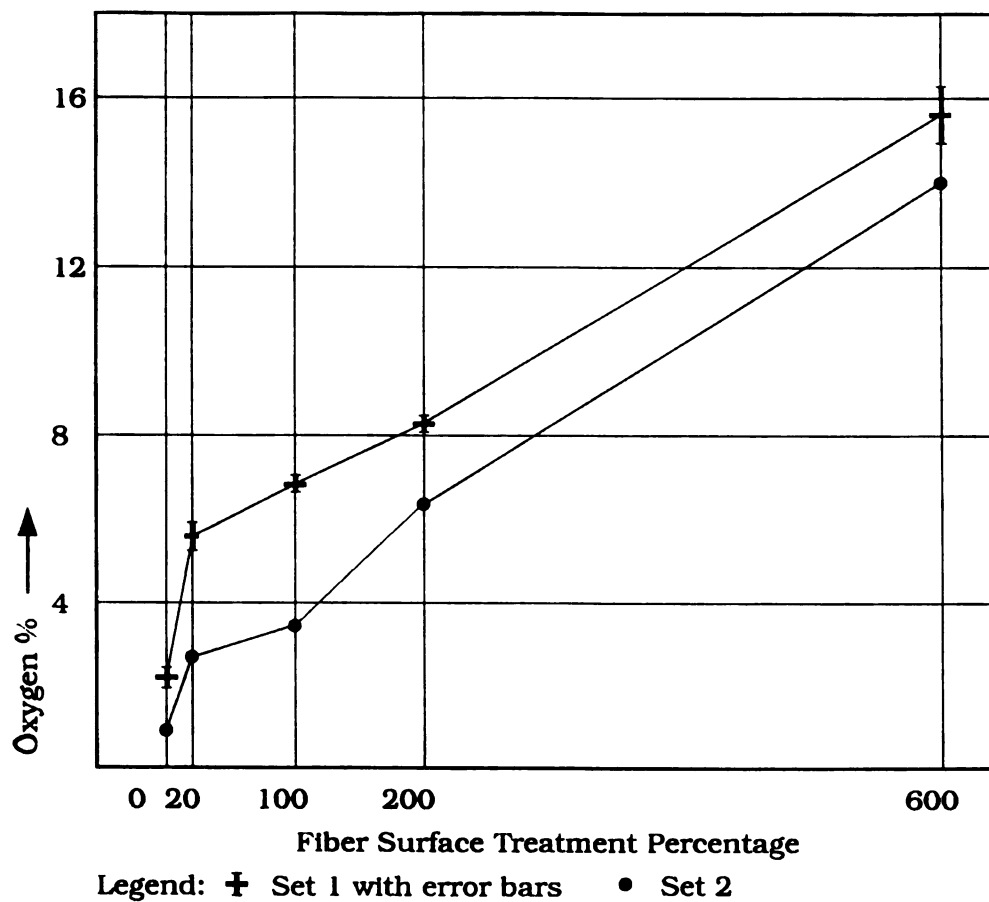


Figure 51. Surface oxygen percentage by XPS.

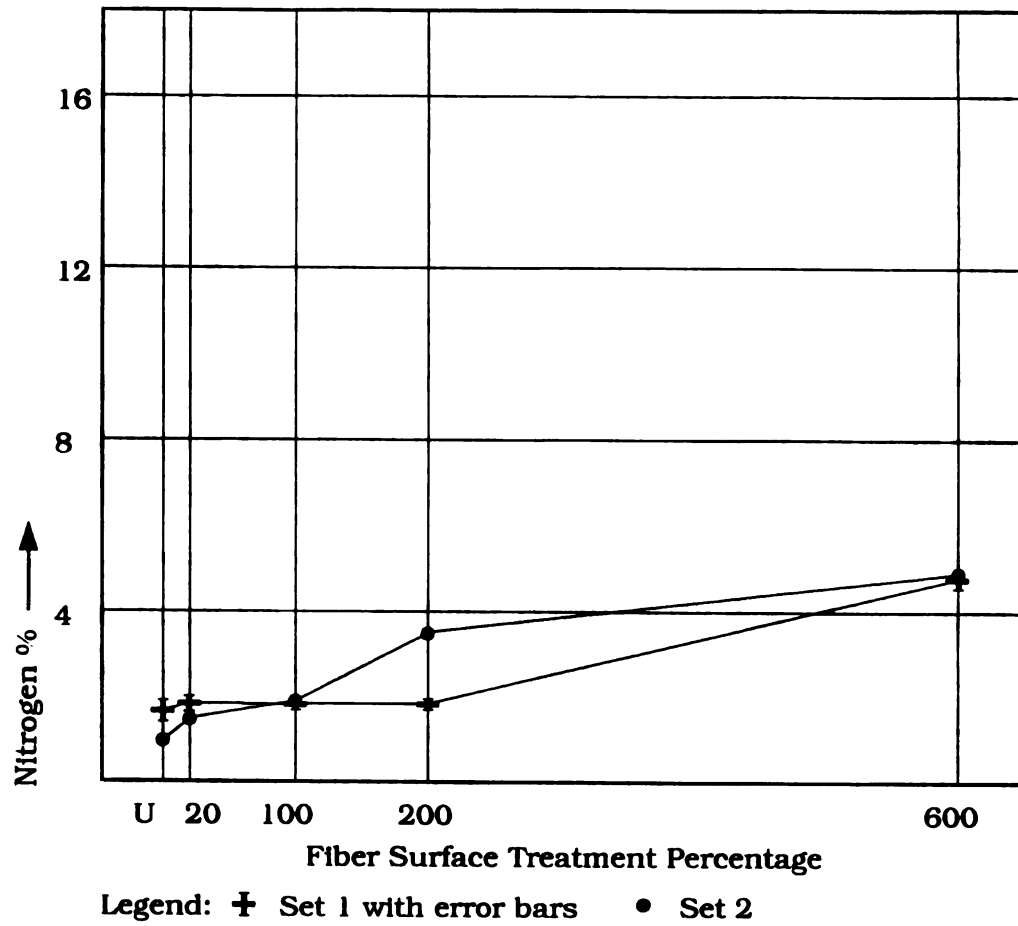


Figure 52. Surface nitrogen percentage by XPS.

Carbon atoms in these configurations are much more susceptible to attack by reactive species than are the extremely stable graphitic basal plane atoms. The availability of a greater number of these sites would result in an initial, rapid uptake of oxygen by the untreated fiber, followed by a slower reaction rate when the most active sites are filled and the basal plane atoms are all that remains.

A second possible mechanism is the removal of an exterior "skin" during the early stages of electrochemical oxidation. A "skin-core" morphology for PAN based fibers has been reported in the literature [Lee, 1991]. The removal of carbon material from fibers during the surface treatment process has also been noted [Drzal, 1987].

Since this analysis would require access to information that is proprietary to Hercules Corporation it was not further addressed in this work. However, based on the available data, the relatively small amount of treatment required to effect the change, only 20% of the nominal value, or less, since the slope appears to have already changed when this lowest treatment level is attained, appears to favor the depletion of reactive sites model over the skin removal model.

5.4.1.2 Chemical Group Deconvolution Results

Deconvolution of the XPS spectra was performed by Kevin Hook and Javad Kalantar and the results appear in Table 6 and are plotted in Figure 53. The groups were designated in three types; phenolic carbon within an aromatic ring structure and singly bonded to oxygen, ketonic carbon doubly bonded to oxygen, and carboxylic carbons bonded to two oxygen atoms, one singly and one doubly. The carboxylic carbon concentration remained approximately constant for all surface treatments at 2.5%, increasing slightly with 600% surface treatment to 3.0%. In contrast, both the phenolic and ketonic carbon atom concentrations increased with increasing surface treatment, following the same pattern as the surface oxygen percentage.

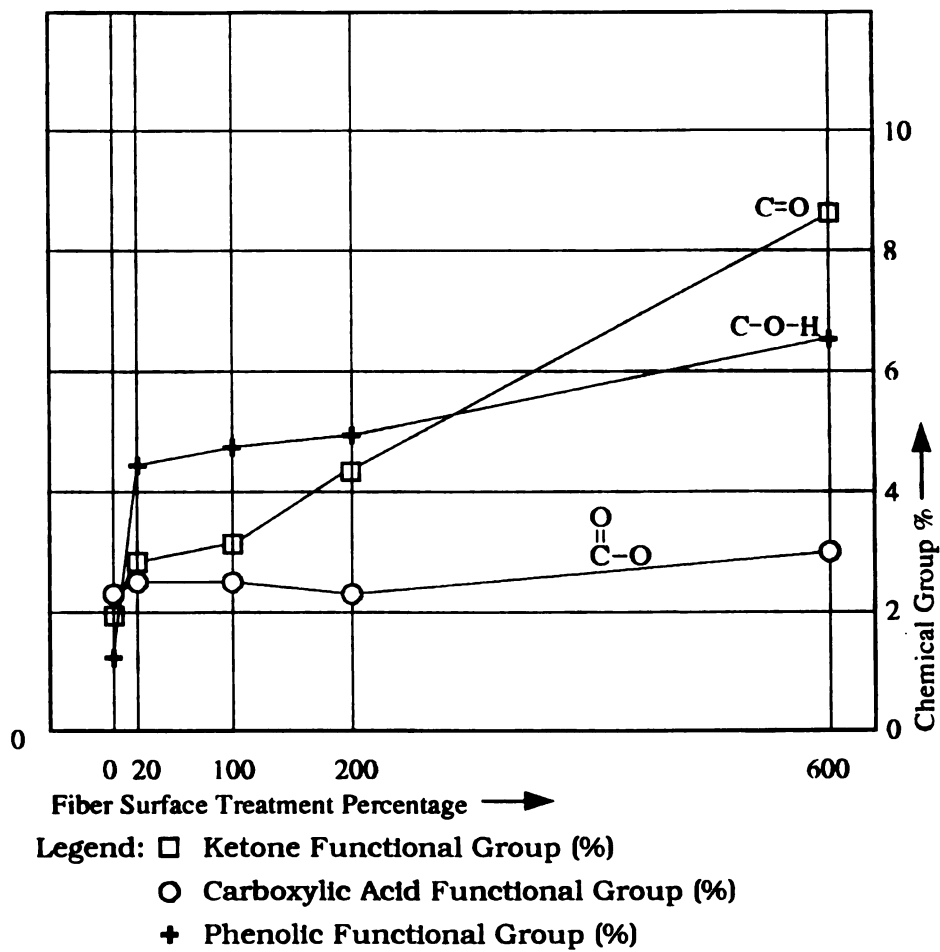


Figure 53. Surface functional groups versus surface treatment.

The untreated fibers were found to contain very low concentrations of phenolic and ketonic carbon while surface treatment to 20% substantially increased both group concentrations. Additional treatment between 20% and 600% increased concentrations at rates that were very nearly linear with respect to the surface treatment. The rate of increase of ketonic carbon was approximately 2.8 times faster than that of phenolic groups. Both increases matched a linear least squares fit with correlation coefficients greater than .996 over the interval from 20% to 600% surface treatment.

While the increase in functional group percentage was highly linear over the range from 20% to 600%, this rate was about a factor of 40 lower than that between 0% and 20% surface treatment for the phenolic carbons and a factor of 4 lower for ketonic carbons. Clearly, the carbon on the virgin fiber surface is much more susceptible to electrochemical oxidation than that on treated fibers.

5.4.1.3 Micro-Wilhelmy Surface Energy Results

The results of the micro-Wilhelmy surface free energy measurements appear in Table 7 and are plotted in Figure 54. Results are reported as the total surface free energy and decomposed into polar and dispersive components.

The polar component of the surface free energy increases significantly with increasing surface treatment in the increments from 0% to 20% surface treatment and from 200% to 600%. Negligible change occurred between 20% and 200% surface treatment. This closely follows the pattern of surface oxygen percentage, as indicated in Figure 55, which plots polar surface free energy against surface oxygen percentage.

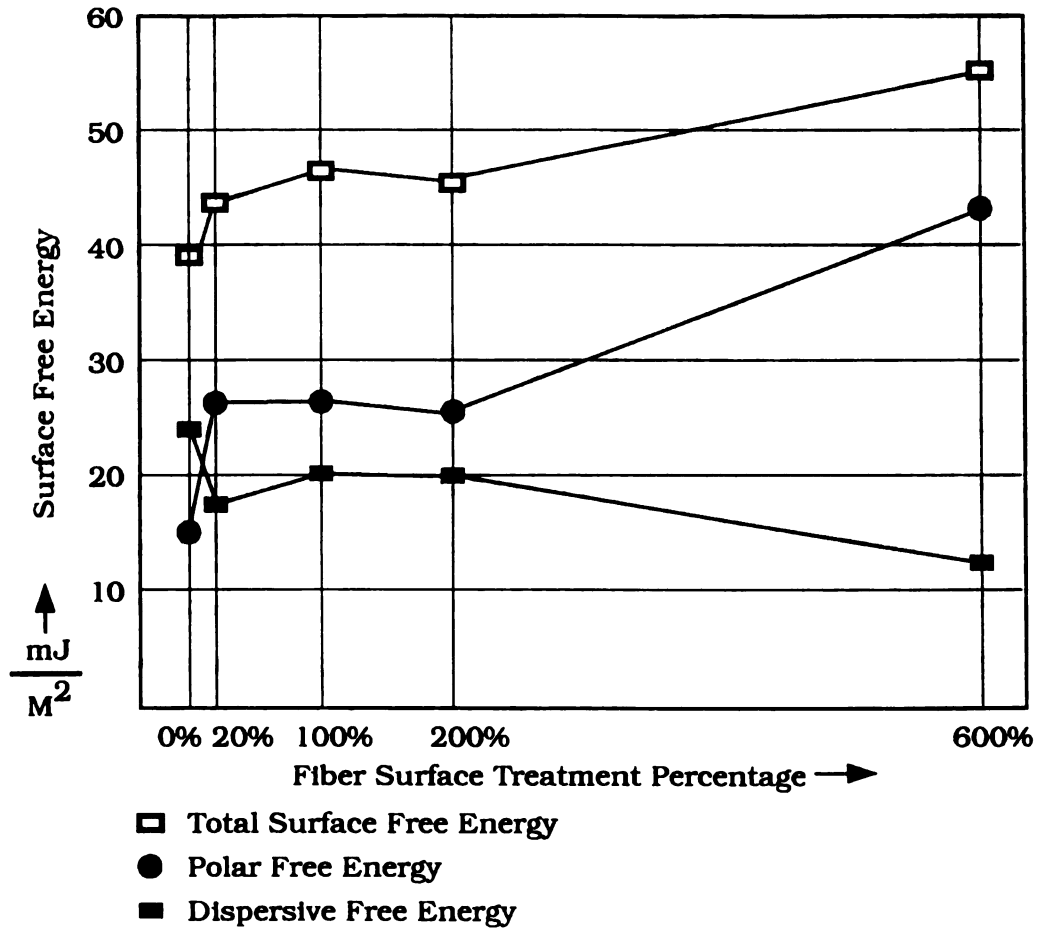


Figure 54. Fiber surface free energy versus surface treatment.

Table 7. Polar, dispersive, and total free energies on IM6 fibers.

Surface Treatment	0%	20%	100%	200%	600%
Dispersive Surface Free Energy (mJ/M ²)	24.0	17.4	20.0	19.1	12.1
Polar Surface Free Energy (mJ/M ²)	14.8	26.1	26.3	25.4	43.0
Total Surface Free Energy (mJ/M ²)	38.8	43.5	46.3	45.3	55.1

Since oxygen is a strongly electronegative species, it tends to withdraw electrons from carbon when chemical bonds exist between the two, producing a net electrical dipole. An increase surface oxygen chemisorbed on a carbon substrate should therefore increase the polar component of the surface free energy, as observed. The close correlation between surface oxygen and polar free energy plotted in Figure 55 provides support for both experimental results and for the conclusion that the oxygen is present in chemisorbed, rather than physisorbed form.

The dispersive free energy undergoes little change with increasing surface treatment, aside from small decreases between 0 and 20% and between 200% and 600%, the same increments that produce large increases in the polar component. This reduction probably results from the lower lability of electrons in the electronegative species, oxygen and nitrogen, which are increased substantially in these treatment intervals, as compared with the more mobile electrons present in graphitic carbon.

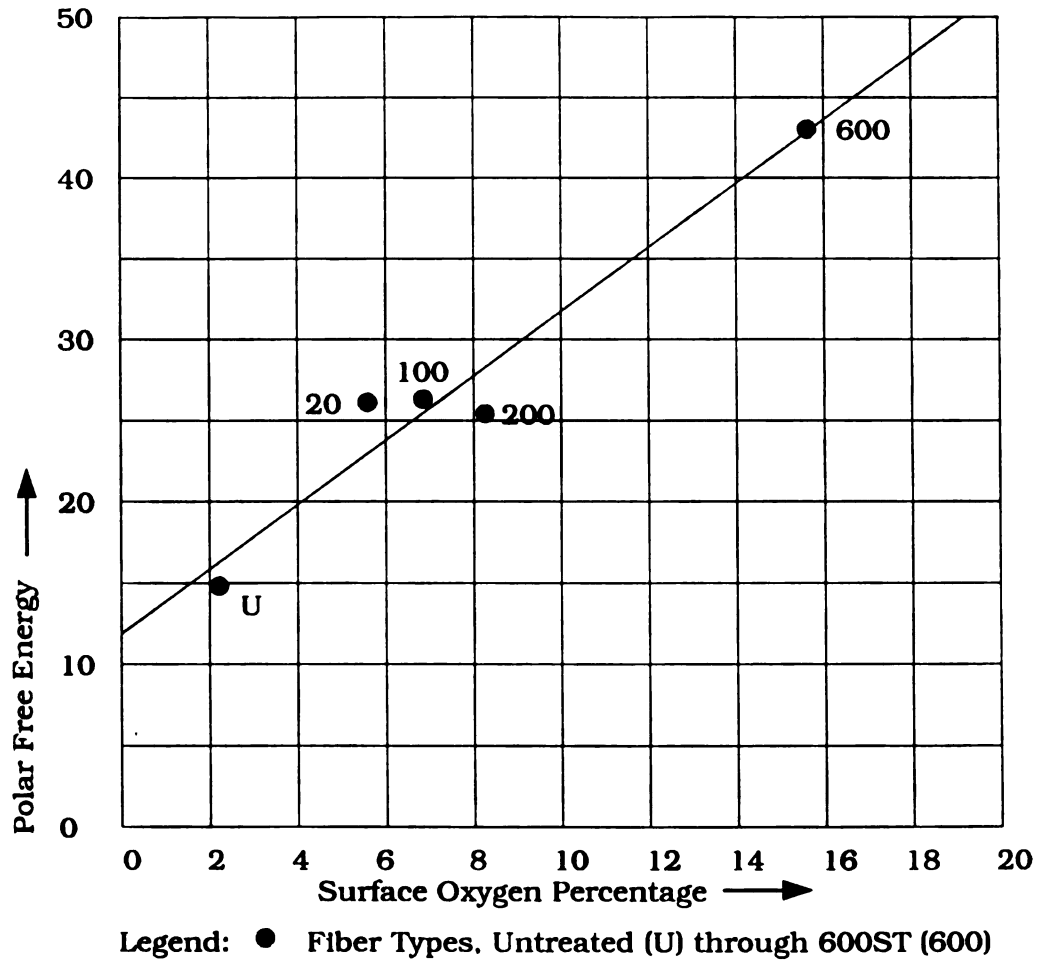


Figure 55. Polar free energy versus surface oxygen percentage.

5.4.1.4 Fiber Surface and Cross Section Examination Results

Fiber surface morphology was observed by scanning electron microscopy. No significant changes in morphology were detectable by this method for the range of surface treatments investigated. Faint axial striations were observed for all surface treatments (Figures 56 and 57). The relief of these striations was much shallower than that of AS4 fibers, as indicated by the much greater difficulty in producing an image with noticable contrast.

The finish on the 100GST fibers was observed to be somewhat irregular, varying in thickness along the length of the fiber. This irregularity was small enough, and the change occurred over a length of fiber long enough, that it could not be readily recorded photographically. Magnifications that were low enough to include a length of fiber with irregularities were too low for the changes to be visible. Higher magnifications which could resolve the surface properly did not include enough of the fiber to show any changes. By using high magnifications and translating the stage parallel to the fiber axis, however, changes in the thickness of the finish were apparent. Striations were faintly visible on these fibers in regions where the finish was very thin.

An SEM of the cross section of an IM6 fiber appears in Figures 58 and 59. A folding pattern that results from the pyrolysis and extension of the PAN precursor material can be seen. The fact that the fibers are not homogeneous, defect free structures is also evident. The fiber interior is complex and convoluted, with many levels of structure from the graphitic mosaic at a scale of tens of Angstroms, through these folds, a micron or more in extent.

This intrinsic defect structure influences the failure behavior of carbon fibers and impacts both the fragmentation tests and the performance of macroscale composites.

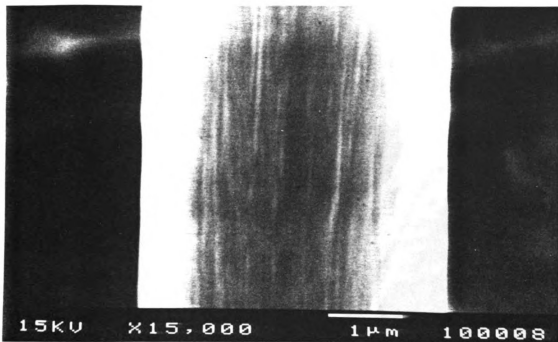


Figure 56. SEM of fiber surface morphology #1.

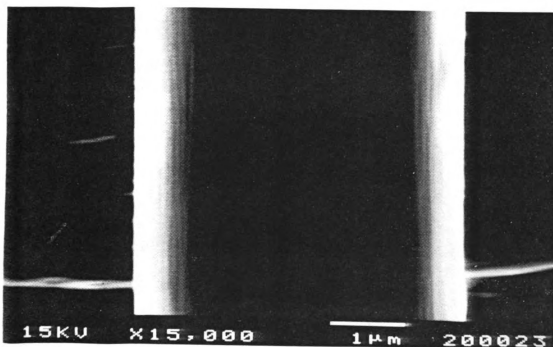


Figure 57. SEM of fiber surface morphology #2.



Figure 58. SEM of fiber cross section #1.



Figure 59. SEM of fiber cross section #2.

5.4.2 MECHANICAL TEST RESULTS

The results of the mechanical testing program appear in this section.

5.4.2.1 Fiber Tensile Strength Results

The results of the fiber tensile tests appear in Figure 60, plotted along with those measured at 23 mm gage lengths by other TTCP participants.

Although the untreated and 200% surface treated fibers were chosen for short gage length testing because they were expected to represent the weakest and strongest, respectively, values for the complete set of fiber conditions, the measured strengths were reversed in order. The untreated fibers were found to be slightly, but consistently, stronger than those with 200% surface treatment at 2 mm gage length, in contrast to their order at 23 mm. This result also runs counter to the usual experience that untreated fibers are weaker than those with some degree of surface treatment, a finding that has been attributed to the removal of a surface layer containing flaws that initiate failures.

Since the surfaces of the IM6 fibers were found to be considerably smoother than Hercules AS4 fibers when examined with scanning electron microscopy, the strength difference may result from the lack of critical sized flaws at sufficiently short gage lengths. These small differences may also result from spool-to-spool strength variations, and may have no real significance. Additional data was not available and attempts to draw any conclusions on this matter were not pursued.

The requirement for a knowledge of the fiber strengths at short gage lengths was met with these data by making the following assumptions and extrapolations. Since the strength was found to be a weak function of surface treatment, and since this function reversed when moving from long to short gage lengths, this factor was assumed to be negligible when making the extrapolation to critical length. Instead, an average value for the strength at both 23 mm and 2 mm gage lengths was

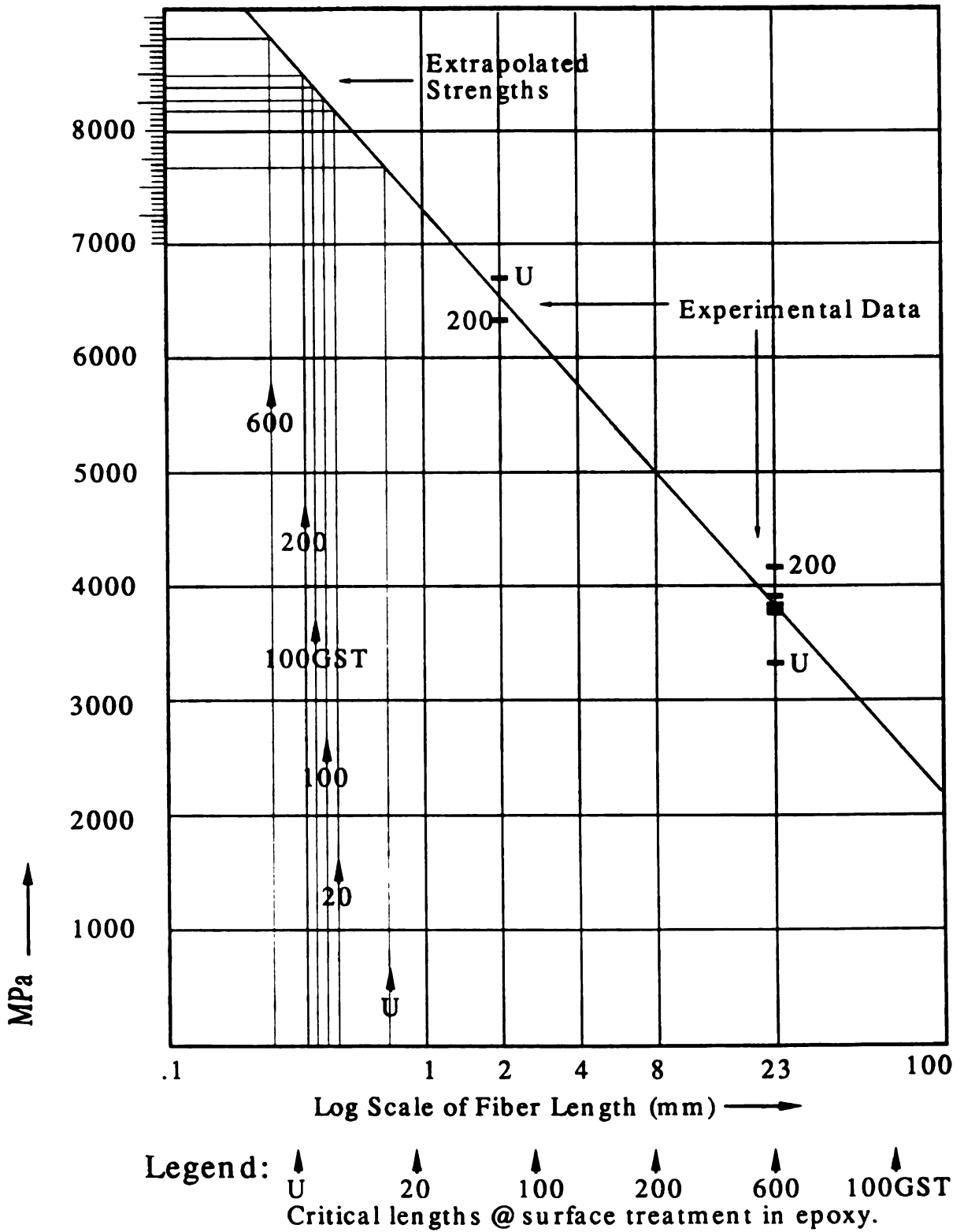


Figure 60. Extrapolation of fiber tensile strengths to critical lengths.

determined for all the fiber types measured (all types at 23 mm, untreated and 200%ST at 2 mm). These two average values were plotted on a semi-log graph of the strength versus the log of the gage length (Figure 60). A line between the two points was extended to the range of the critical lengths and the strength at the measured critical length for each surface treatment read from the graph. These strengths are reported in Table 8.

Table 8. Critical lengths, L_c/D 's, tensile strengths, and ISS for IM6 fibers.

Fiber Surface Type	Critical Length (microns)	L_c/D ($D = 5.35$)	Weibull Shape Parameter	Strength @ L_c (MPa)	ISS (MPa)
0%	708	132	3.6	7700	37
20%	466	87	2.8	8200	66
100%	413	77	3.3	8300	70
200%	349	65	3.1	8400	86
600%	267	50	3.3	8800	115
100GST	348	65	2.9	8500	90

5.4.2.2 Fiber Volume Fractions and Distributions

The fiber volume fractions, void volume fractions, and percentages of fiber-poor regions for the 24 ply, and 12 ply composite panels appear in Table 9 and appear in Figures 61 and 62. The fiber volume fractions for most panels were found to be approximately constant, with only minor variations, except for lower fiber fractions found in the 24 ply 100GST panel, at 59.3% and the 12 ply 600%ST panel, at 62.6%.

The average volume fractions and standard deviations for the two types of composite panels for all six fiber types were found to be:

$$12 \text{ ply average} = 68.7\%, \text{ deviation} = 3.3\%$$

$$24 \text{ ply average} = 68.7\%, \text{ deviation} = 4.7\%$$

The fiber-poor regions, defined as the percentage of 25 micron square regions containing less than 75% of the average number of fibers, were also very consistent, with slightly higher than usual numbers for the 24 ply 600%ST and 12 ply 100%ST

panels. These values are still low enough to indicate good quality composites with uniformly distributed fibers and minimal impact on material properties.

The void volume fractions for all panels were found to be well under 1% for all cases except the 12 ply 600%ST and 100GST panels, which were found to have 1.4% and 1.5% void contents respectively.

In summary, ONVfA and areal void analysis suggests that all panels were well fabricated, with minor defects present in the 12 ply 600%ST and 100GST panels from voids, and lower than average fiber volume fractions present in the 24 ply 100GST and 12 ply 600%ST panels.

Table 9. Fiber and void volume fractions by ONVfA.

<u>Panel Type</u>	<u>0%</u>	<u>20%</u>	<u>100%</u>	<u>200%</u>	<u>600%</u>	<u>100GST</u>
12 Ply						
Fiber V_f %	72.1	68.7	72.7	68.0	62.6	68.0
Void V_v %	0.3	0.8	0.4	0.4	1.4	1.5
24 Ply						
Fiber V_f %	72.5	71.9	71.6	70.7	66.2	59.3
Void V_v %	0.6	0.4	0.3	0.3	0.1	0.0

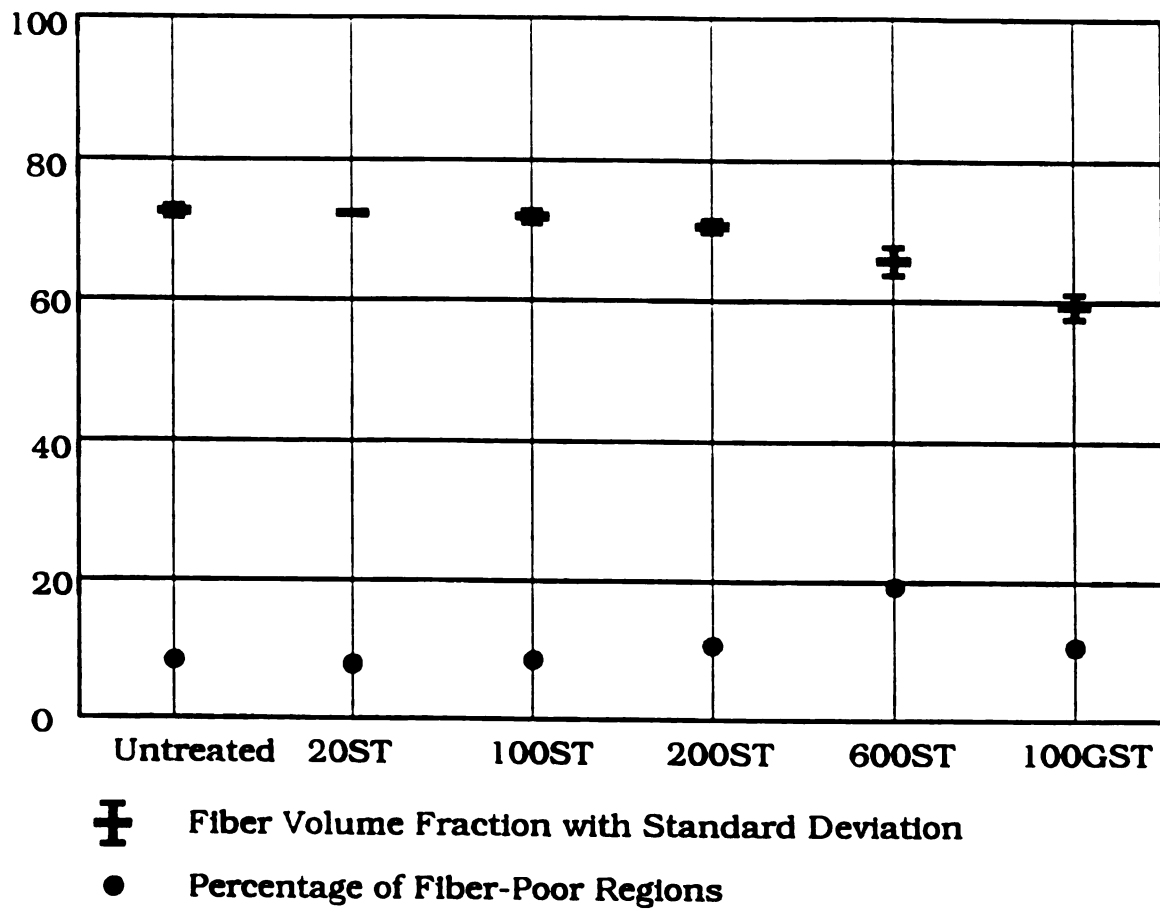


Figure 61. Fiber volume fractions and distributions for 24 ply laminates.

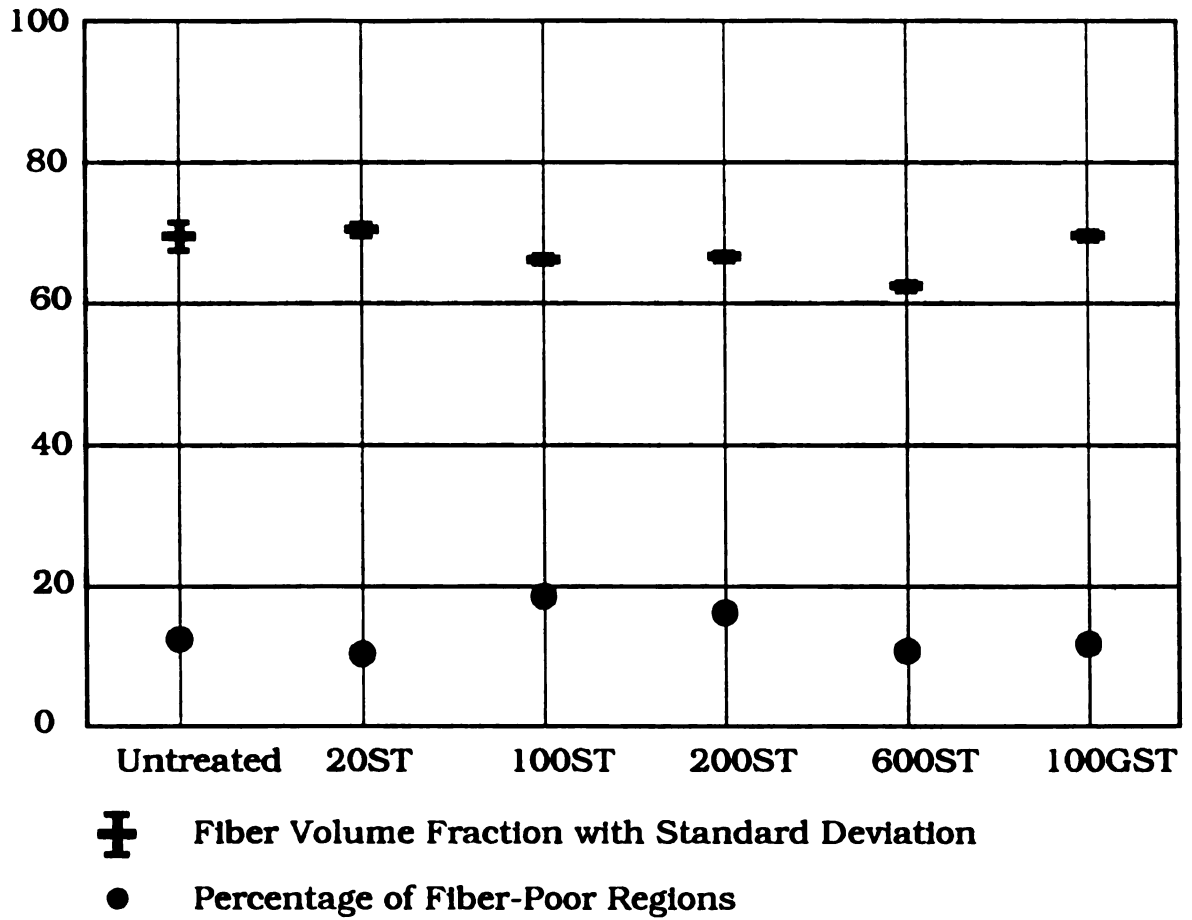


Figure 62. Fiber volume fractions and distributions for 12 ply laminates.

5.4.2.3 Interfacial Shear Strength Results

The results of the single fiber fragmentation interfacial shear strength tests appear in Table 8 and are plotted in Figures 63 and 64. The untreated fibers showed very poor adhesion, with an L_c/D of 132 and an ISS of 37 MPa. Adhesion improved substantially with 20% surface treatment. The L_c/D ratio decreased to 87, the ISS increased to 66 MPa.

Surface treatment to 100% of the nominal value further improved adhesion, but by a smaller amount than for the step from 0% to 20%. The L_c/D ratio decreased to 77 and the ISS increased to 70 MPa. Treatment to 200% again increased adhesion, with L_c/D equal to 65 and ISS of 86 MPa.

Surface treatment to 600% of the nominal value significantly increased adhesion to 115 MPa. A nearly linear increase in ISS was observed over this large increment in surface treatment as shown in Figure 63.

The sized fibers, 100GST, showed an increase in ISS over the 100%ST equally treated but unsized fibers, giving an ISS approximately equal to that of the 200% surface treatment.

Figure 64 shows the ISS values of surface treated IM6 fibers along with those for untreated (AU4), surface treated (AS4) and treated and sized (AS4C) carbon fibers. Although the moduli of the IM6 fibers is about 25% higher than the AS4 fibers, corresponding to greater orientation achieved during fabrication, the ISS values for the corresponding types are virtually identical. Surface treatment results in significant increase for both types, and sizing adds another smaller, but still significant increase.

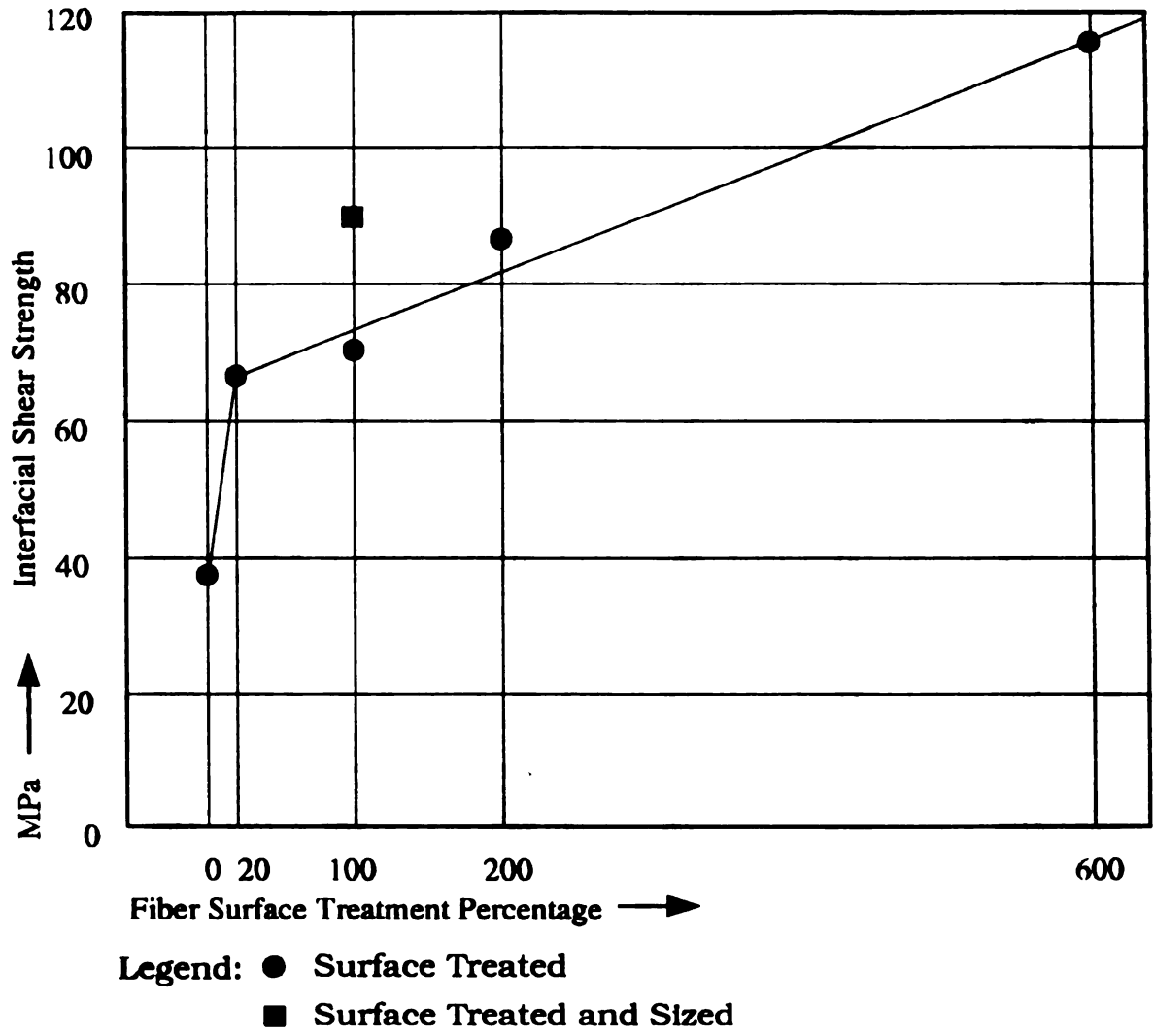


Figure 63. Interfacial shear strengths for IM6 fibers.

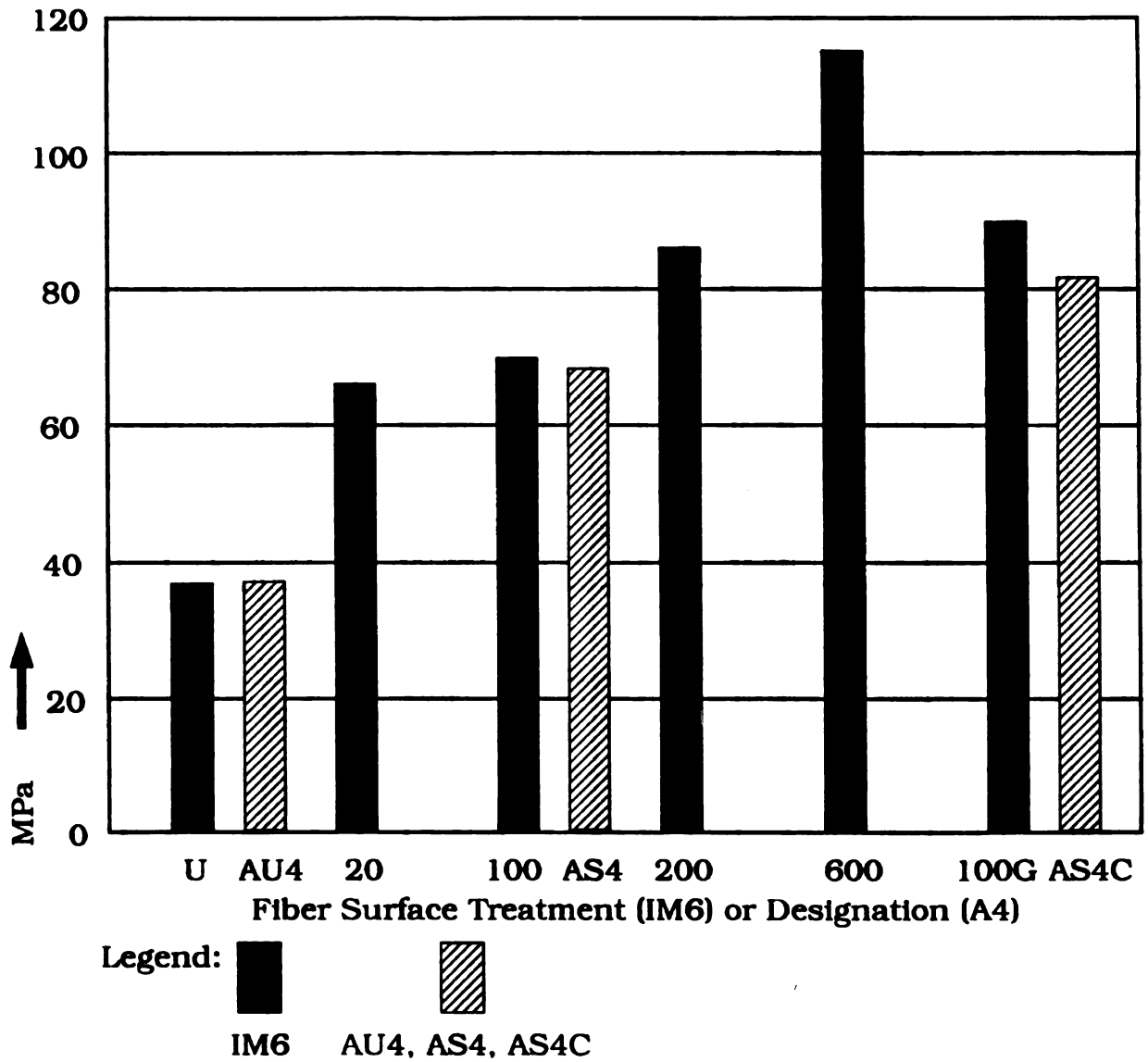
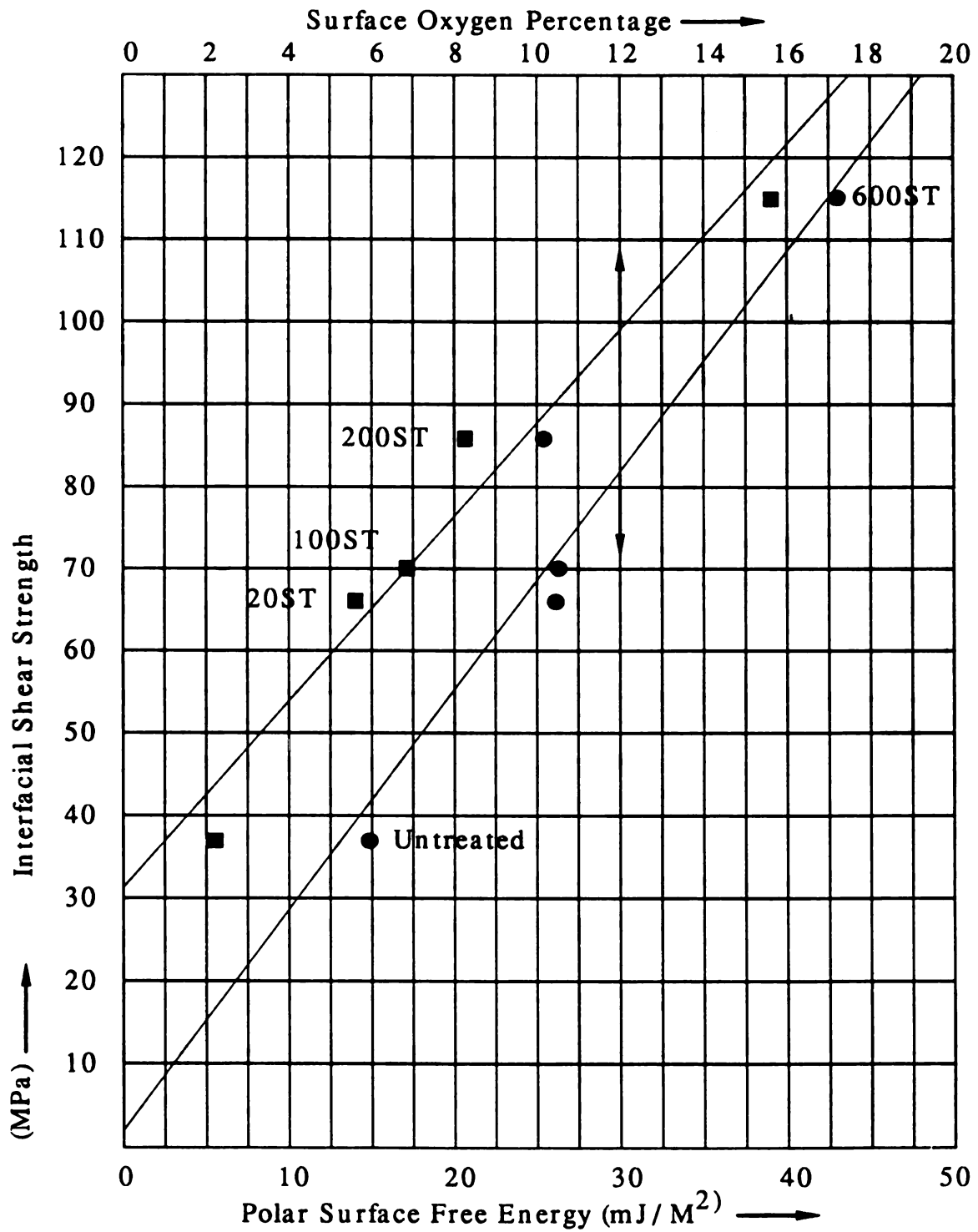


Figure 64. Interfacial shear strengths for IM6 and A4.



Legend:

- Interfacial Shear Strength versus Polar Surface Free Energy
- Interfacial Shear Strength versus Surface Oxygen Percentage

Figure 65. ISS versus surface oxygen and polar surface free energy.

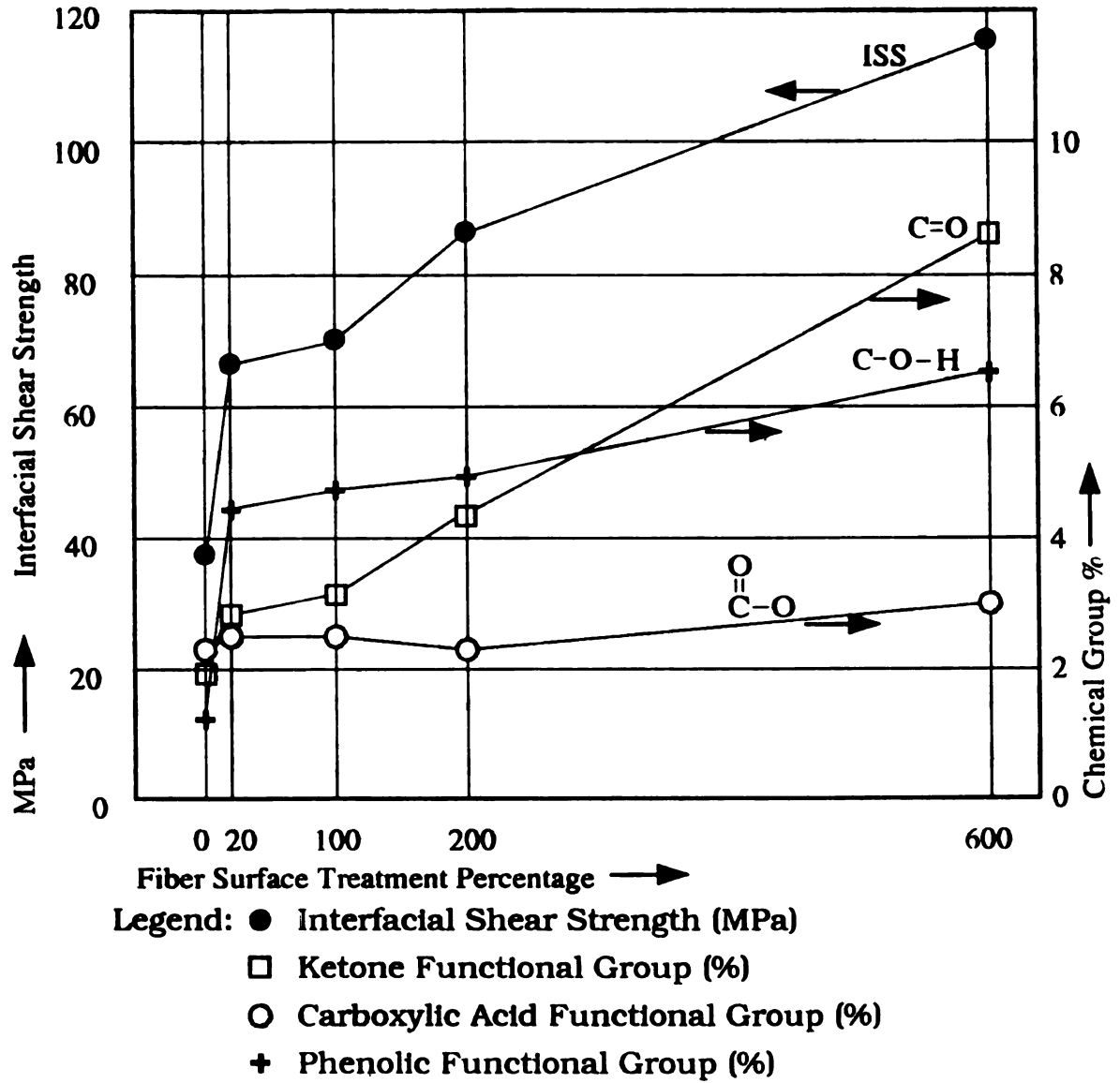


Figure 66. ISS and functional groups versus surface treatment.

Figure 65 plots the interfacial shear strength for IM6 fibers against the surface oxygen percentage and polar surface free energy. Both plots are approximately linear, indicating a close correspondence between the surface treatment, surface oxygen, surface free energy, and ISS.

Figure 66 shows both the interfacial shear strength and the surface functional groups plotted against the surface treatment percentage. The similarity in the pattern of rapid increase in property, or composition, with initial surface treatment increment followed by a slower rate of increase with additional surface treatment can be clearly seen.

5.4.2.3.1 Birefringence Evolution Sequence Interpretations

Birefringence sequences for each fiber surface treatment condition appear in Figures 67 - 72. The coupon strain is listed at the right of each image, and the first image in each sequence was taken at the approximate failure strain of the break. As described in Chapter 2, the strain-at-failure of fiber breaks can have a significant impact on failure modes. These images of only one break per fiber surface treatment can only represent the behavior of the system at that break's failure strain and may not be the same as the behavior at lower or higher strains.

The untreated fiber (Figure 67) gave extremely weak birefringence patterns, indicative of an interfacial failure mode and weak frictional tractions after debonding. This fiber break occurred at 1.6% coupon strain, which was sufficiently high for the fiber to undergo interfacial debonding immediately upon failure. These patterns were significantly less intense than those for AU4, untreated A4 carbon fibers. Debonding occurs by a stick-slip crack advance, but the distance the crack propagates is very large compared with the fragment lengths and so this is not always evident.

Surface treatment to 20% (Figure 68) resulted in substantially stronger birefringence patterns, with interfacial debonding by a stick-slip crack advance.

Although it is difficult to see in the printed image, the break was accompanied by the initiation of a short interfacial crack. This crack advances in increments with increasing strain, leaving behind very strong stick-slip markings where plastic deformation occurs at crack arrest points.

The 100%ST fiber break (Figure 69) occurred at only 1.1% coupon strain. Strain energy was low enough that no interfacial failure occurred at the strain level of fiber failure for this strongly adhered fiber, with the fiber end displacement accommodated only by elastic and plastic matrix deformation. Without the fiber failure strain energy to initiate debonding, increasing coupon strain was not accompanied by interfacial crack advance, but by further plastic deformation of the matrix. Between 2.3% and 2.34% coupon strain an interfacial, or close to interfacial crack is finally initiated. This crack propagates a substantial distance in its first (and only) jump since there is considerable strain energy available at this high coupon strain. The resultant birefringence patterns appear to be completely different from those for 20%ST and 200%ST specimens, but this difference results from the fiber failure strain difference, not from a change in fiber surface properties.

The 200%ST sequence (Figure 70) shows a break that happened to occur at a somewhat higher strain, 2.2% coupon strain, with approximately 4 times the fiber failure strain energy of the 1.1% break in the 100%ST fiber. Although it is difficult to see in the printed images, the computer image clearly shows that an interfacial crack was initiated simultaneously with fiber failure. This crack propagates in jumps with small increments in strain, again leaving the characteristic stick-slip patterns behind.

The 600%ST break occurred at 1.5% coupon strain (Figure 71), insufficient to initiate a crack in this very strongly adhered fiber. Interfacial, or near interfacial failure eventually occurs at about 3.3% coupon strain, significantly higher than the 2.34% required to statically (without fiber failure strain energy) initiate a debond in

the less strongly bonded 100%ST fiber. The use of coupon strain required to initiate debonding as a means of characterizing interfacial adhesion is discussed in detail in Chapter 2. When debonding is initiated, the propagation distance is substantial, as with the case of the low fiber failure strain 100%ST fiber, because a large amount of strain energy is available for its advance. Also as with the 100%ST sequence, the stick-slip patterns are not closely spaced, because of the fiber failure strain energy, not the fiber surface adhesion level.

The 100GST birefringence sequence (Figure 72) documents a 1.6% coupon strain fiber break, a level low enough not to initiate an interfacial crack. What appears to be a gradual, interphase yielding occurs between 2.3% and 2.4% coupon strain. This corresponds well to the 2.34% strain required to statically initiate an interfacial failure in the unsized, 100%ST fiber. Further yielding or possible interfacial cracking occurs at the 2.6% strain level. Upon release of the coupon strain the region that appeared to yield at 2.4% is left with a stronger, small diameter sheath of birefringence than the segment of fiber that appeared to fail interfacially between 2.5% and 2.6% coupon strain, where there is almost no visible remanent birefringence. This may indicate a change in failure mode along the fragment from local plastic yielding of the sizing material between 2.3% and 2.5% coupon strain to interfacial failure between 2.5% and 2.6% coupon strain. This sizing is a Heculestm "G" type size, described by the manufacturer as a toughened epoxy-compatible size. Interphase yielding may therefore be more likely in these specimens than in the ones with unsized fibers.

In summary, the predominant failure mode for the untreated and treated but unsized fibers was by interfacial cracking, with the initiation and propagation characteristics heavily influenced by the fiber failure strain energy. The sized, 100GST fiber also appeared to include some plastic deformation of the interphase region, along with eventual interfacial failure.

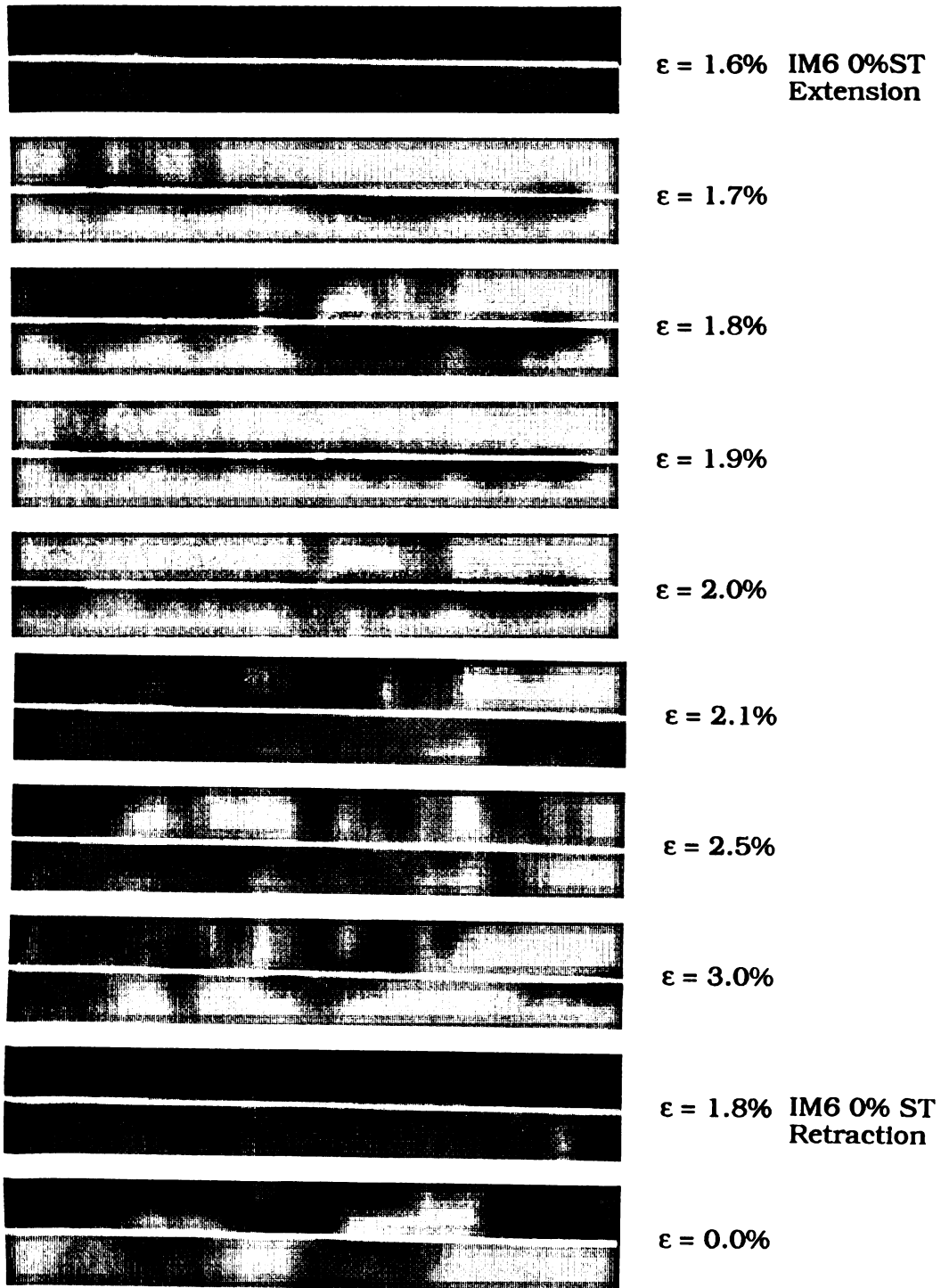


Figure 67. Birefringence sequence for untreated IM6 fiber.

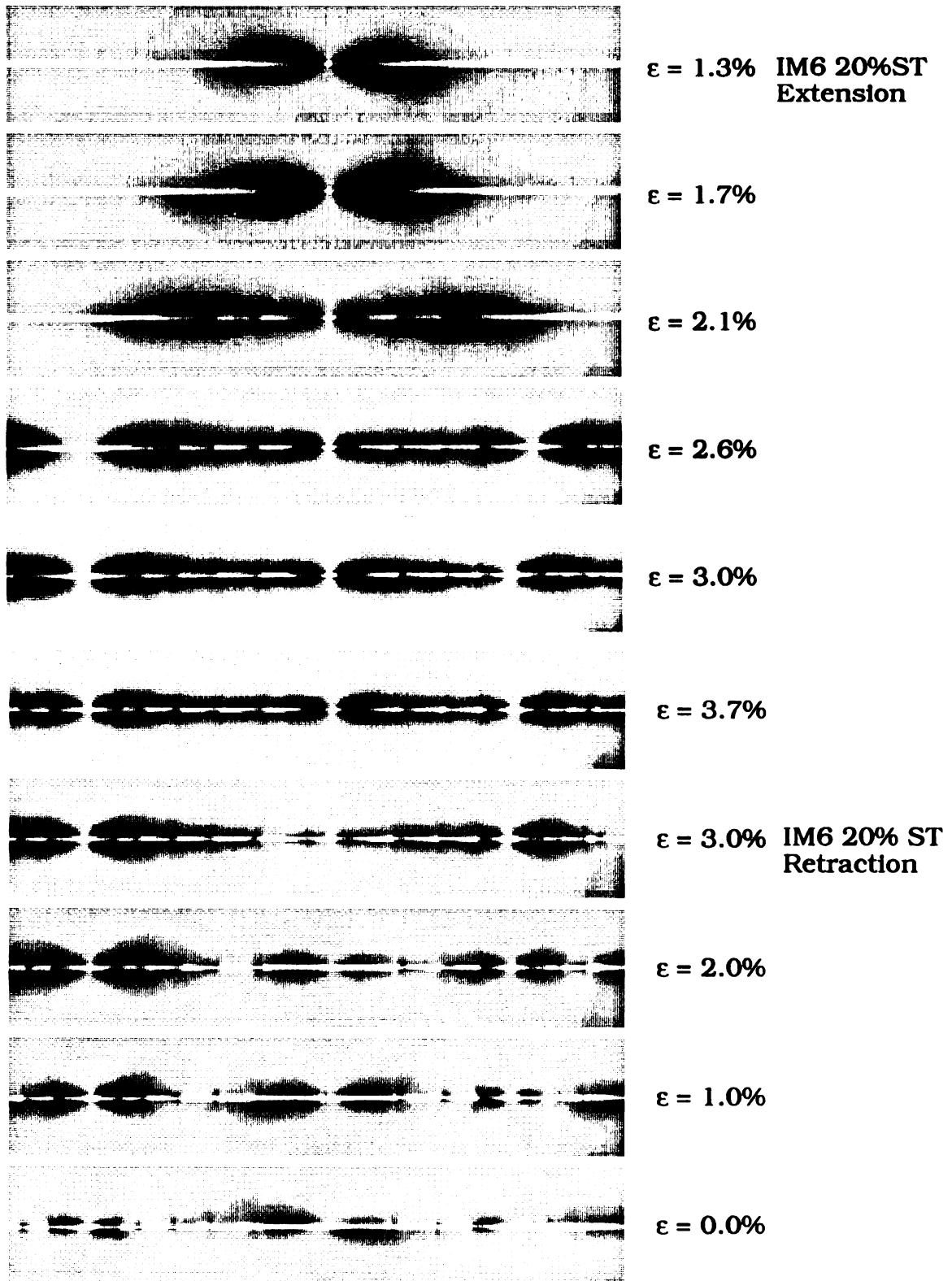


Figure 68. Birefringence sequence for 20%ST IM6 fiber.

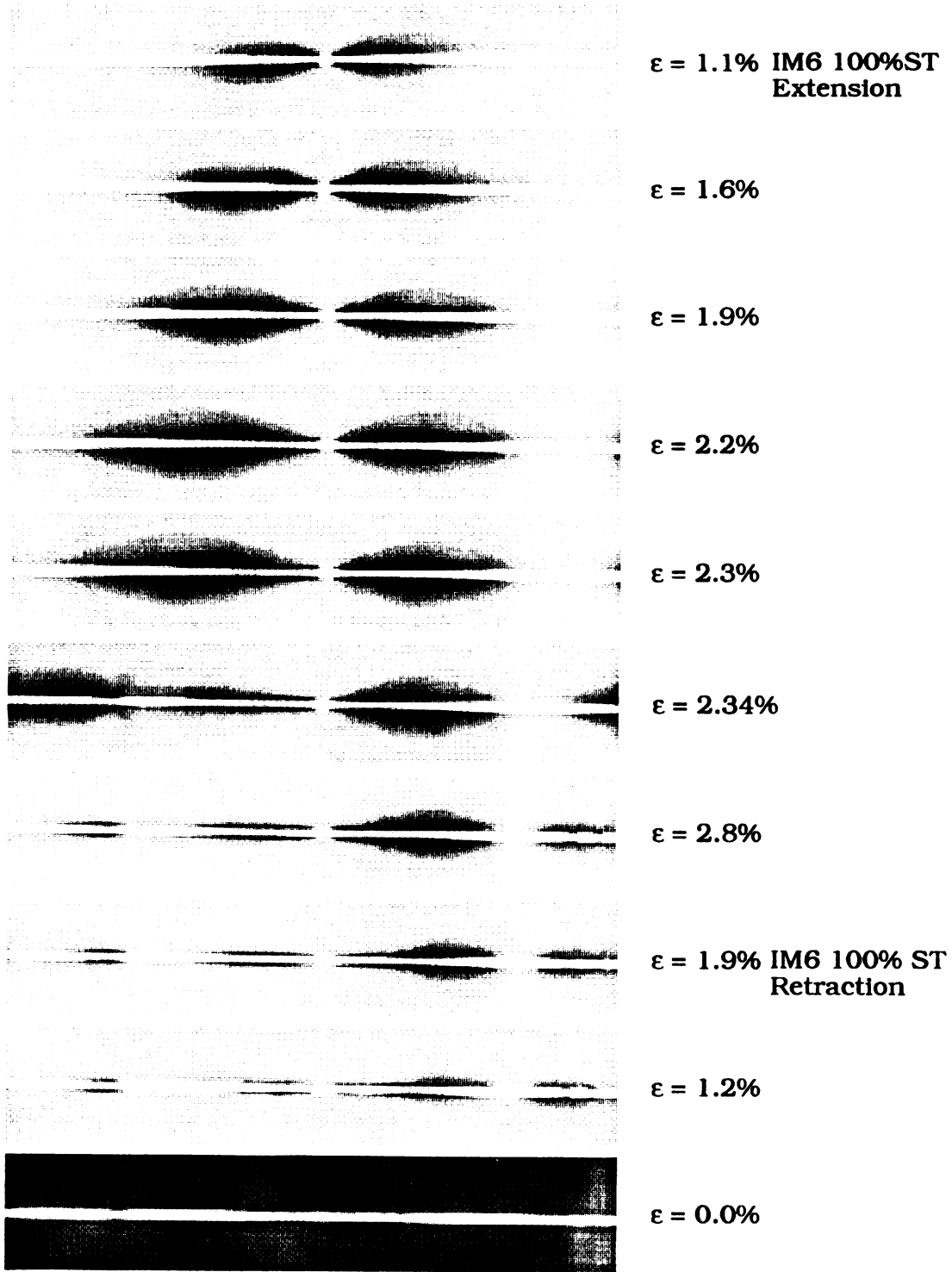


Figure 69. Birefringence sequence for 100%ST IM6 fiber.

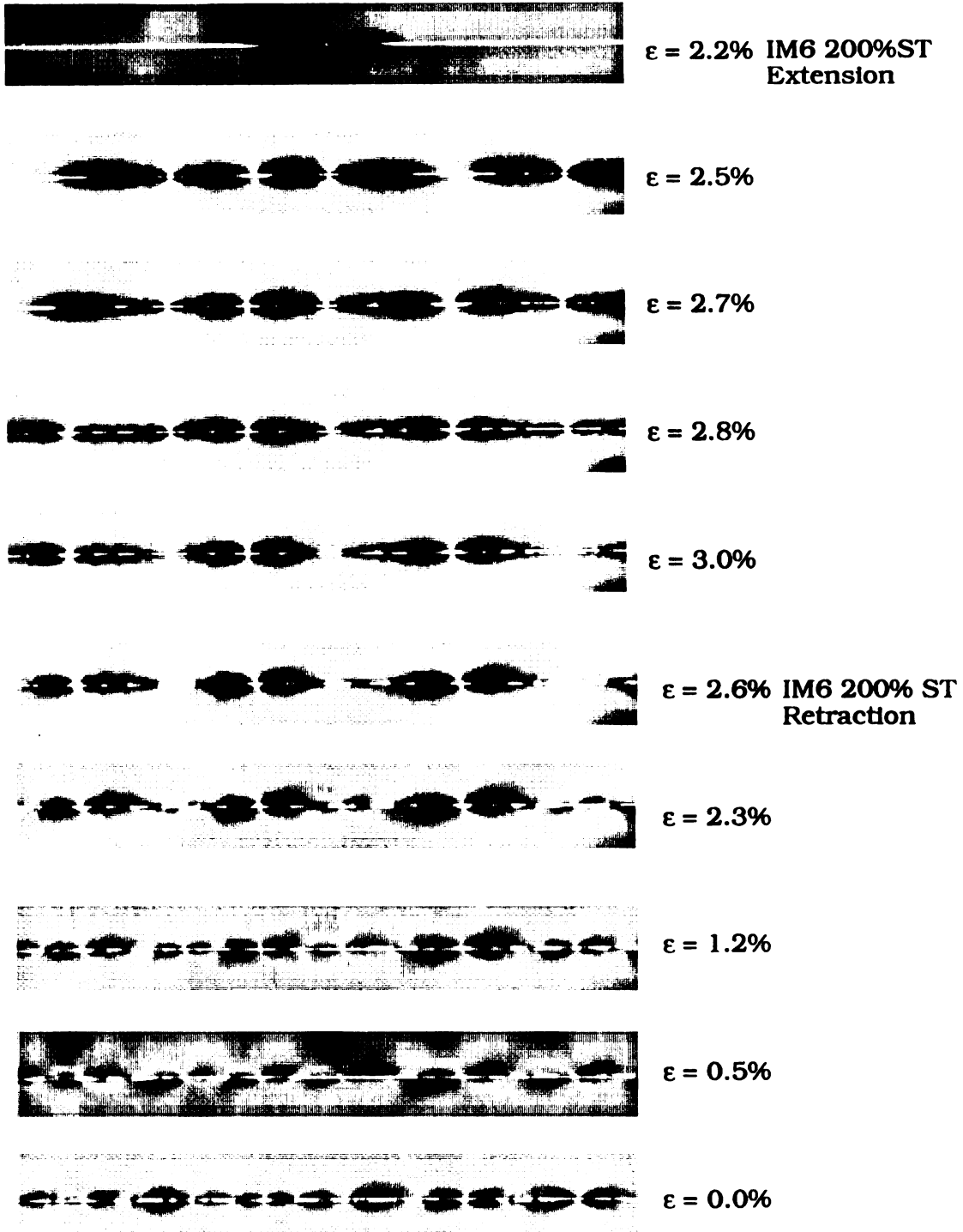


Figure 70. Birefringence sequence for 200%ST IM6 fiber.

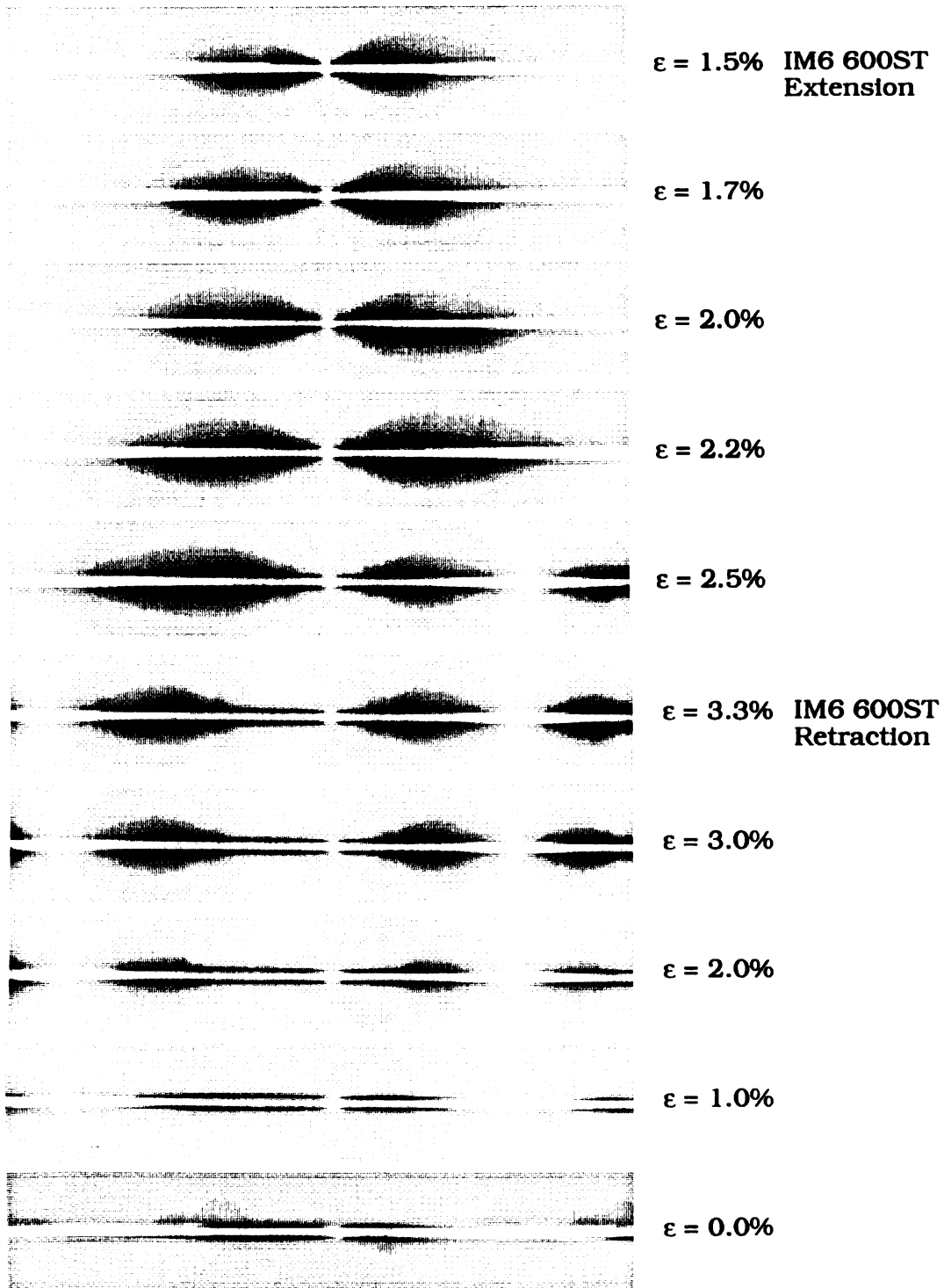


Figure 71. Birefringence sequence for 600%ST IM6 fiber.

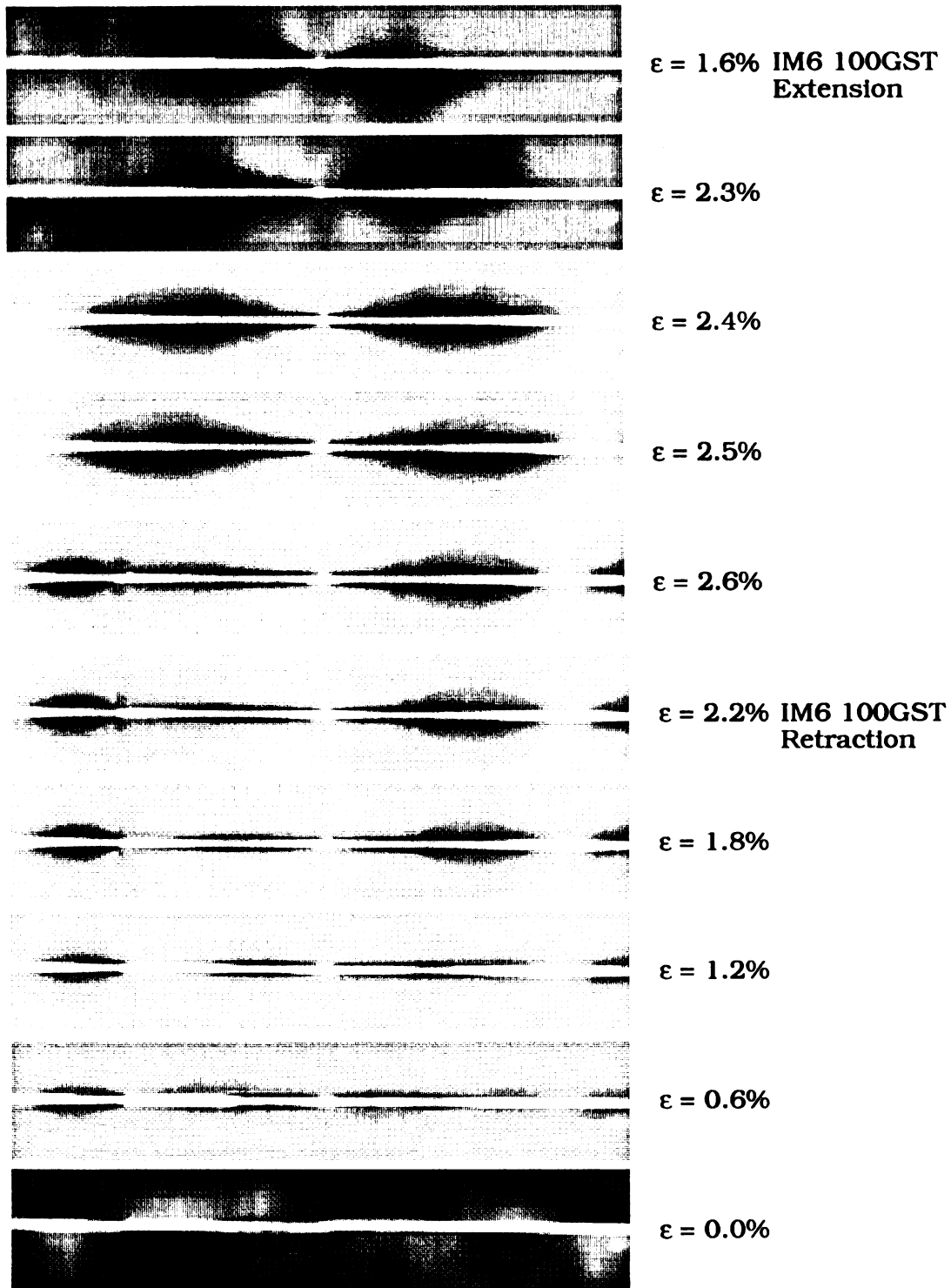


Figure 72. Birefringence sequence for 100GST IM6 fiber.

5.4.2.4 Mode II Fracture Toughness Results

The results of the mode II fracture toughness tests appear in Table 10 and are plotted in Figure 73. The fracture toughness for all fiber types increases consistently with increasing surface treatment, and also increases substantially with the addition of the size in the 100GST fiber composites. The largest increase is seen between the poorly bonded, untreated fiber and 20% surface treatment, as with the surface oxygen and interfacial shear strength, with smaller but still substantial increases seen for the other surface treatment increments. The influence of improved fiber-matrix adhesion on mode II fracture toughness appears to reach a limiting value between 200%ST and 600%ST with only a small toughness increase in spite a substantial ISS increase. This may be attributed to the failure mode moving away from the interface and into the matrix, at which point the improved interface properties would have no effect.

Also of considerable interest is the significant increase in toughness for the 100GST fiber when compared with either the 100%ST unsized fiber or the 600%ST unsized fiber. The ISS of the 100GST fibers was lower than that of the 600%ST, but the birefringence sequence showed interphase yielding that was not operative in the other surface treatment conditions. Since even a small amount of plastic deformation consumes far more energy than any interfacial fracture, the birefringence sequence and mode II fracture toughness data give a strong indication that this failure mode makes a contribution to the performance of the 100GST composite.

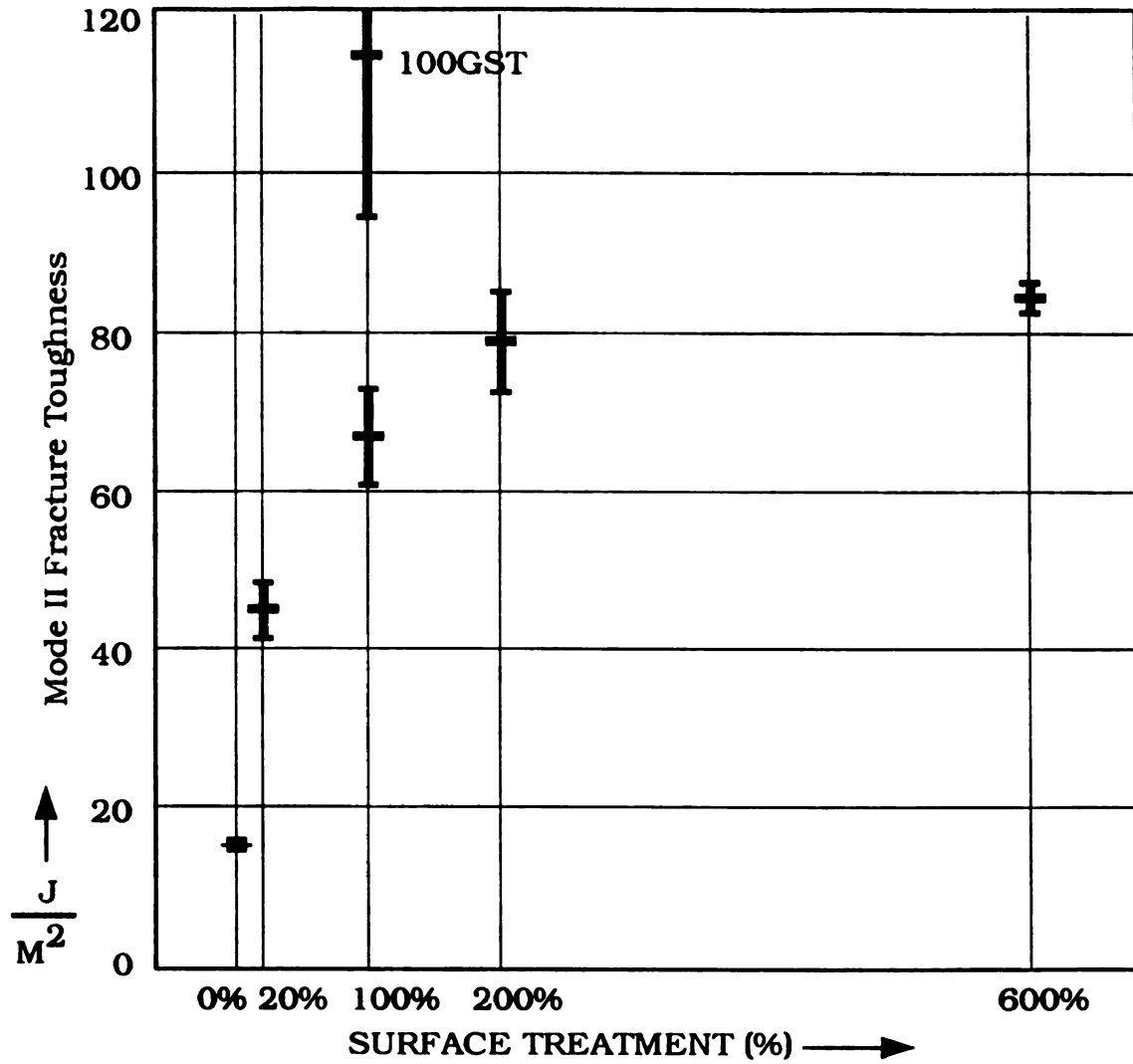


Figure 73. Mode II fracture toughness for IM6 composites.

Table 10. Mode II fracture toughness for IM6/epoxy composites.

Fiber Type	0%	20%	100%	200%	600%	100GST
Mode II Fracture Toughness (J/m ²)	15.3	45.7	67.0	78.6	84.6	118.0
Std. Dev. (J/m ²)	1.3	7.0	12.2	12.4	4.0	47.4

fractu

were

100G

failure

gener

also fa

time f

comp

in the

betwe

of whi

5.4.2.5

in Figu

predict

possibl

low tra

The 20

identica

a matri

fibers.

600% S

measure

constant

large d

The differences in standard deviation between the different surface treatments' fracture toughnesses is also an interesting result. The untreated and 600%ST values were very consistent, the 20%ST, 100%ST, and 200%ST less consistent, and the 100GST was highly variable. The untreated fibers underwent consistent interfacial failure at very low stresses, absorbing little strain energy in the process, and generating consistent values for mode II toughness. The 600%ST fiber composites also failed in a consistent manner, since fiber-matrix adhesion was very high, but this time failure strain energy was determined by the matrix properties. The 100GST composites were seen to undergo combined interphase yielding and interfacial failure in the birefringence sequence. The large difference in strain energy absorption between these failure modes, and the variation, even within the same fiber fragment, of which mode was active, may account for this variability.

5.4.2.5 Transverse Flexural Results

The results of the transverse flexural tests appear in Table 11 and are plotted in Figure 74. Although the mode II fracture toughness results followed clear and predictable patterns, the transverse flexural results are somewhat enigmatic, and were possibly dominated by an experimental artifact. The untreated fibers displayed a very low transverse strength, as might be expected from the poor fiber-matrix adhesion. The 20%ST, 100%ST, and 200%ST fiber composites all showed approximately identical, higher levels of transverse flexural strength. This indicates a transition to a matrix-dominated failure mode from the interfacial mode active in the untreated fibers. A dropoff in both transverse flexural strength and modulus occurred at 600%ST which may be attributed to the lower volume fraction of fibers present, as measured by ONVfA. With a lower V_f , and the resultant lower flexural modulus, a constant strain to failure would produce the lower measured strength value. A much large dropoff occurs for the 100GST fiber composite, with less than half the

transverse flexural strength of any of the treated but unsized fiber composites.

A possible complication in the interpretation of the results of this test may be seen in the SEM fractographs of the transverse flexural specimens, and in the process of preparing these specimens for observations. The two pieces of the broken flexural specimens were usually still attached by bridging fibers, which had to be pulled free to separate and expose the fracture surfaces. The fibers were also seen to be somewhat imperfectly aligned, as a result of the manual layup process. Although this would have little influence on mode II toughness tests, where failure propagates along the fibers, any bridging fibers could significantly influence transverse flexural strengths, since the fibers are very much stronger than the matrix material. The extent of the impact of this factor may not be fully resolvable, since quantification of fiber misalignment would be a difficult process and was not undertaken.

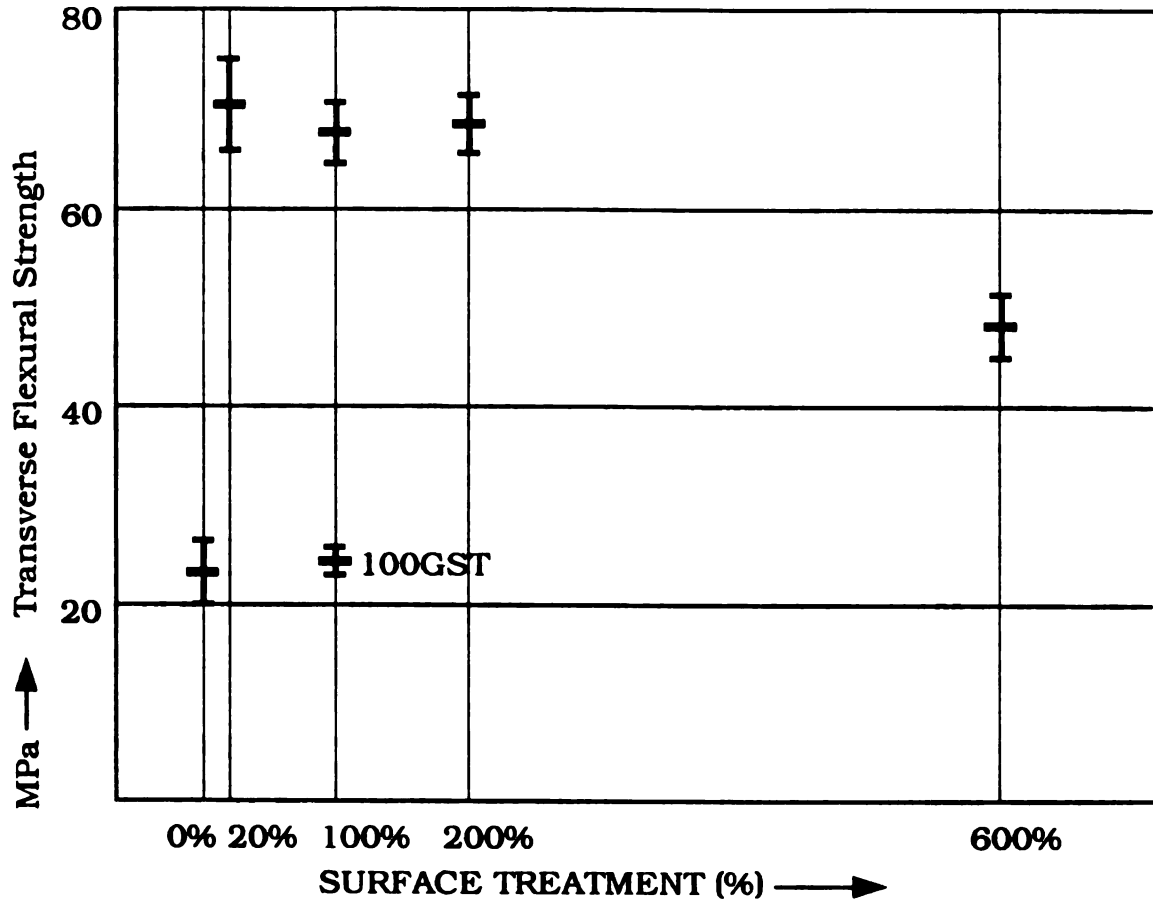


Figure 74. Transverse flexural strengths for IM6 composites.

Table 11. Transverse flexural strengths and moduli for IM6 composites.

Fiber Type	0%	20%	100%	200%	600%	100GST
Transverse Flexural Strength (MPa)	23.2	70.7	67.8	68.5	48.8	34.5
Std. Dev.	6.4	9.2	6.2	5.8	6.4	2.8
Transverse Flexural Modulus (GPa)	8.8	11.3	12.3	12.1	9.4	9.6
Std. Dev.	1.9	0.9	0.6	1.5	1.0	0.5

5.4.2

in Ta

low l

fiber-

fiber

slight

is slig

indica

interfa

theref

failure

failure

condi

confir

at ma

surpri

short

interf

5.4.2.6 Interlaminar Shear Strength Results

The results of the short beam shear, interlaminar shear strength tests appear in Table 12 and are plotted in Figure 75. The untreated fiber composites showed very low levels of interlaminar shear strength (ILSS), as expected due to the very weak fiber-matrix adhesion. The surface treated but unsized and surface treated and sized fiber composites all showed higher, approximately identical ILSS, with the 600%ST slightly higher than the others. Compared to the large change in ISS, this constancy is slightly surprising. Upon analysis, however, the consistent ILSS values are an indication that the failure mode for all of these composites has moved away from the interface, and is dominated by failure within the matrix material. The ISS values, therefore, have no impact once the surface treatment is sufficient to achieve this failure mode change.

Although the fragmentation test specimens commonly underwent interfacial failures for all fiber types studied, except for the 100GST fibers, the loading conditions are somewhat different in the short beam shear test. Rather than being confined to a cylinder around the perimeter of the fiber, the shear stresses are applied, at maximum, along a plane passing through the composite midsection. It is not surprising that failure can be successfully transferred to a plane in the matrix for the short beam shear specimens, while the locus of failure tends to be confined to the interfacial region in the fragmentation test specimens.

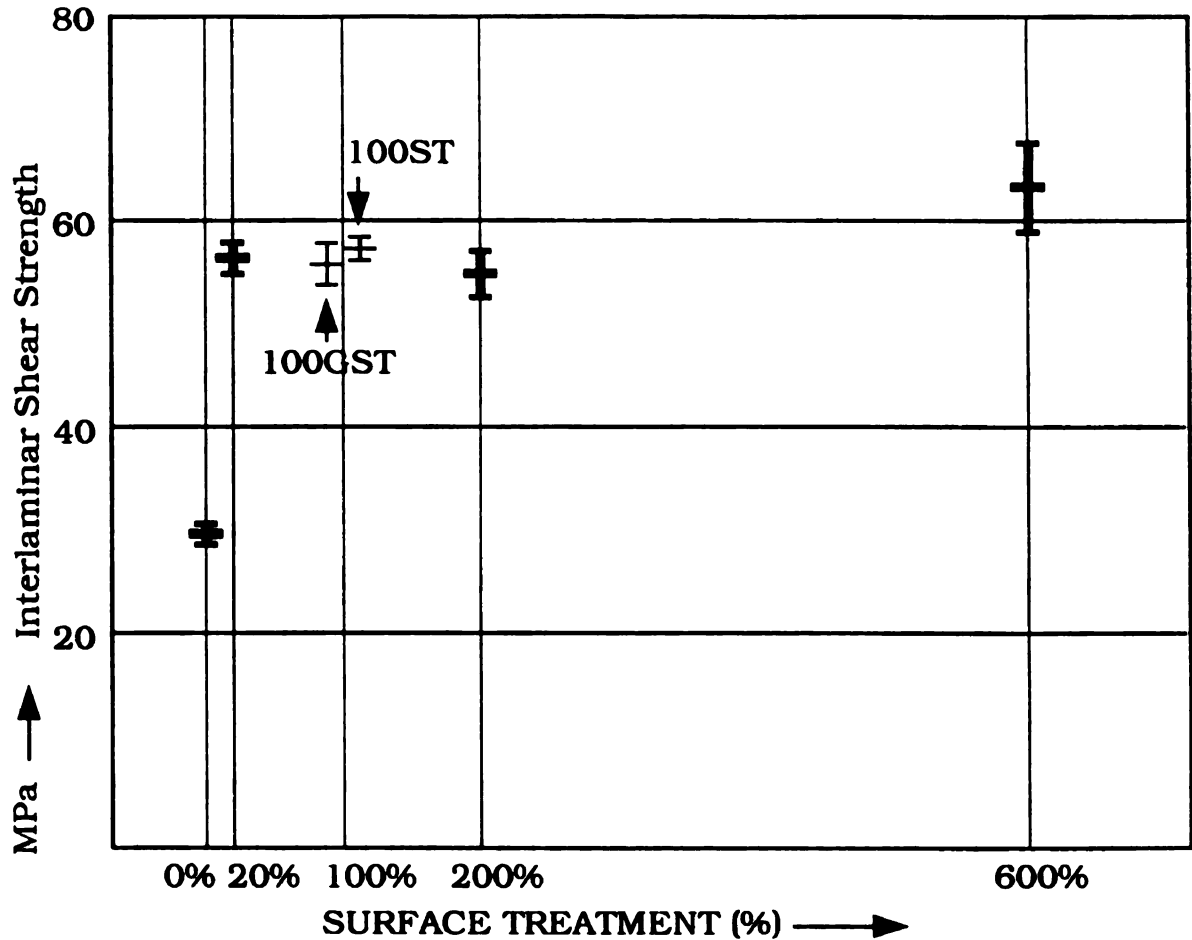


Figure 75. Interlaminar shear strengths for IM6 composites.

Table 12. Interlaminar shear strengths for IM6/epoxy composites.

Fiber Type	0%	20%	100%	200%	600%	100GST
Interlaminar Shear Strength (MPa)	29.5	56.3	57.3	54.7	63.1	55.8
Std. Dev.	1.7	3.0	2.6	4.7	8.4	4.0

5.4

tran

76-8

87)

II fa

failu

fabri

comp

benea

the m

slight

portio

the fra

with

of the

and 8^e

to show

87). A

a decre

these s

matrix

conspic

5.4.2.7 SEM Fractographic Analysis

Scanning electron micrographs of end-notched flexural (mode II fracture) and transverse flexural specimens for each surface treatment condition appear in Figures 76-87. Mode II fractures are shown at 200X (Figures 76-81) and 1000X (Figures 82-87) while transverse flexural fractures are shown at 500X (Figures 88-93). The mode II failures occurred in the same direction as the fiber orientation, while the flexural failures were transverse to the fiber axis.

As can be seen in Figures 76 and 82, axial mode II failure of composites fabricated from untreated fibers yielded fracture surfaces with the fibers almost completely stripped clean. Almost the only visible matrix material is that constrained beneath the fibers. Very small regions of "hackles" can also be seen, usually where the matrix is constrained behind pairs of fibers.

Surface treatment to 20% of the nominal value (Figures 77 and 83) results in slightly increased matrix retention, some regions of exposed matrix occur while most portions are bare fiber. Further treatment to 100% results in significant changes in the fracture surface morphology (Figures 78 and 84). Most of the surface is covered with hackles and adjacent regions of matrix material, with only the topmost portions of the fibers exposed. This same morphology was exhibited by the 200% (Figures 79 and 85) and 600% (Figures 80 and 86) surface treated composites.

Composites fabricated with the epoxy-compatible finished fibers, 100GST seem to show lower amounts of retained matrix on mode II failure surfaces (Figures 81 and 87). A reduced incidence of hackle formation was also evident. The appearance of a decrease in matrix retention may result from the decrease in hackle numbers, since these structures are the most visible components of the exposed matrix. Smooth matrix regions are much more difficult to identify and quantify than structures which conspicuously differ from the fiber surfaces.

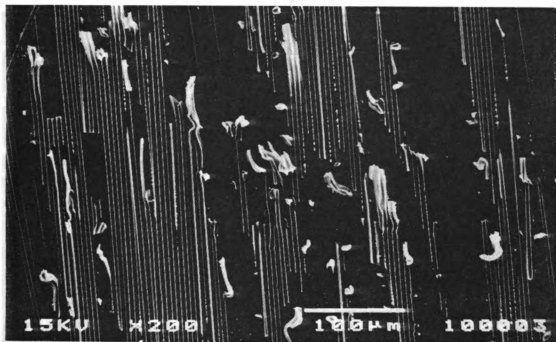


Figure 76. 200X SEM, untreated mode II fracture.

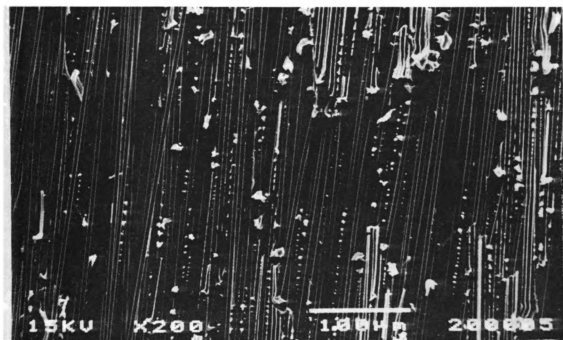


Figure 77. 200X SEM, 20% treated mode II fracture.

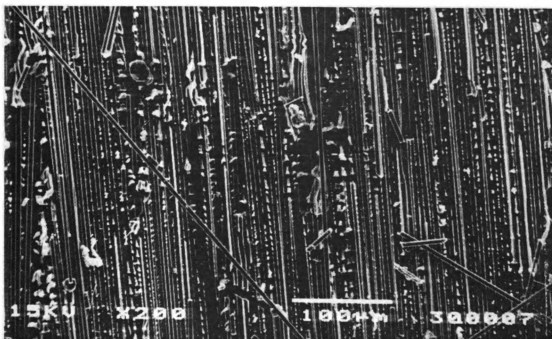


Figure 78. 200X SEM, 100% treated mode II fracture.

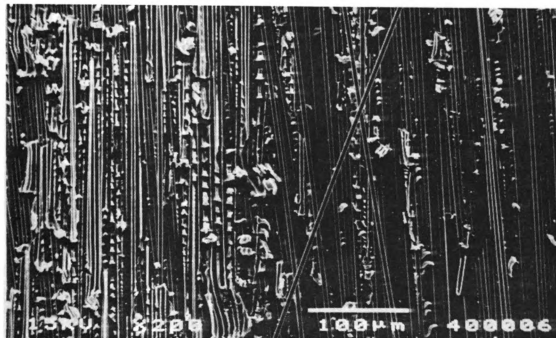


Figure 79. 200X SEM, 200% treated mode II fracture.

F

Fi

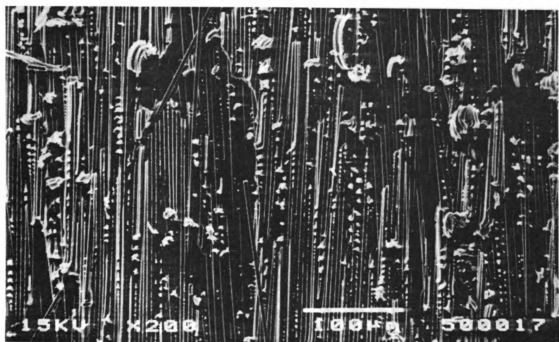


Figure 80. 200X SEM, 600% treated mode II fracture.

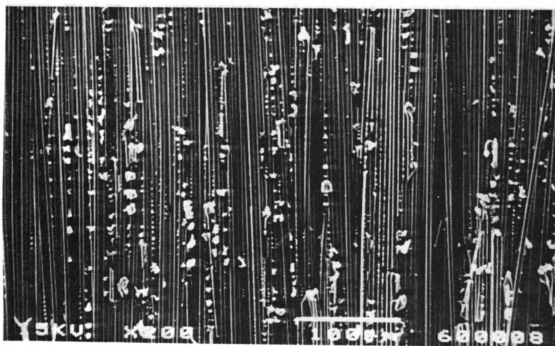


Figure 81. 200X SEM, 100% GST sized mode II fracture.

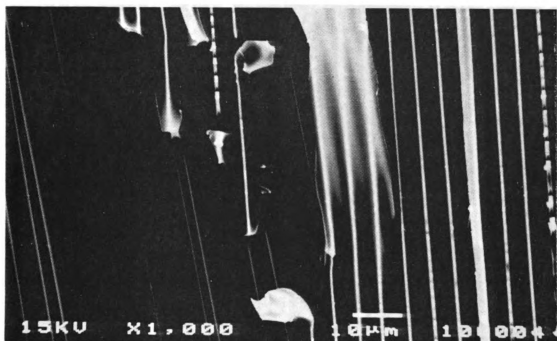


Figure 82. 1000X SEM, untreated mode II fracture.

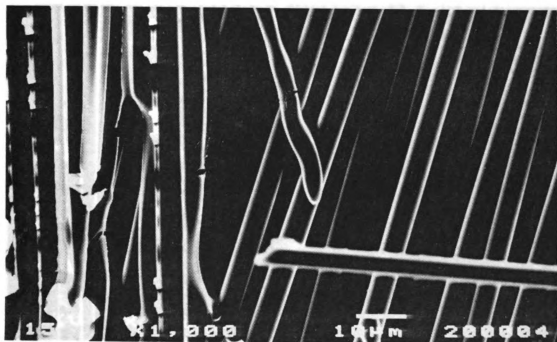


Figure 83. 1000X SEM, 20% treated mode II fracture.

Fig

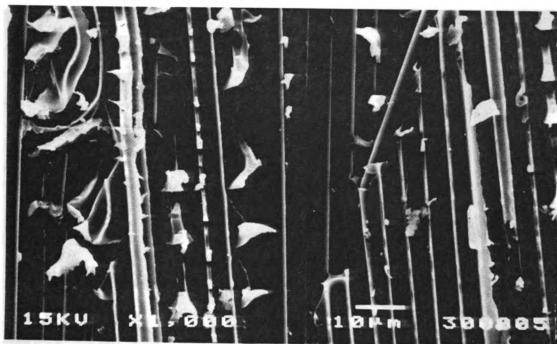


Figure 84. 1000X SEM, 100% treated mode II fracture.

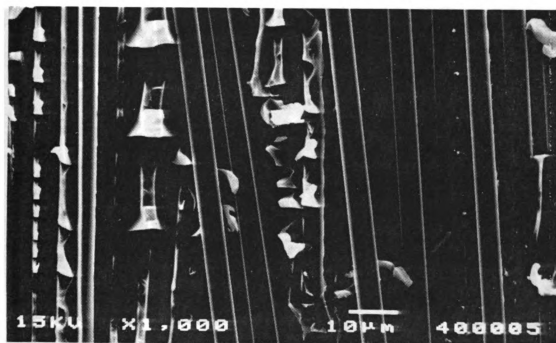


Figure 85. 1000X SEM, 200% treated mode II fracture.

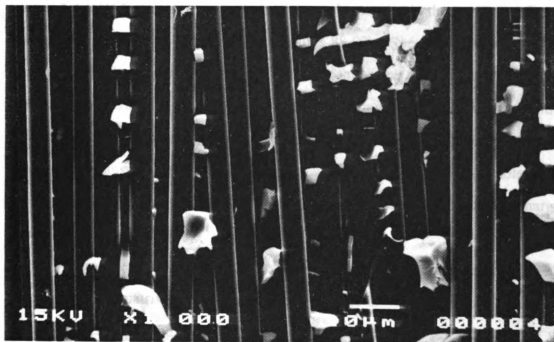


Figure 86. 1000X SEM, 600% treated mode II fracture.



Figure 87. 1000X SEM, 100% GST sized mode II fracture.

fra

bro

pie

litt

exp

pee

phe

strip

struc

Artifacts from specimen preparation may be present in the transverse flexural fractographs because of fiber bridging (Figures 88-93). Specimens were not cleanly broken into two pieces but remained joined after failure by misaligned fibers. These pieces were separated by hand, and most of the bridging fibers were removed with as little disruption of the fracture surface as possible. Final surfaces were mainly exposed by transverse flexural failure, but with small regions attributable to this peeling of bridging fibers. Some loosely attached fibers remained, producing charging phenomena in the SEM.

All transverse flexural specimens appeared to present fiber surfaces completely stripped free of matrix material, regardless of fiber surface treatment. No hackle structures were observed anywhere on any transverse flexural surfaces.

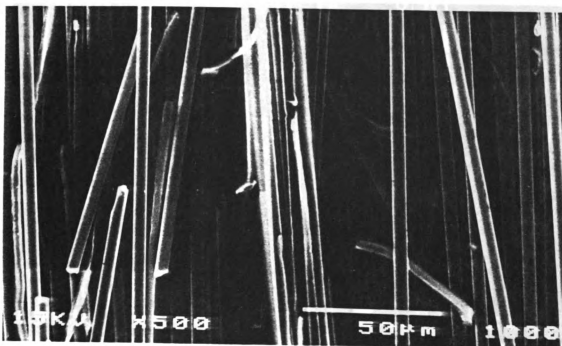


Figure 88. 500X SEM, untreated transverse flexural fracture.

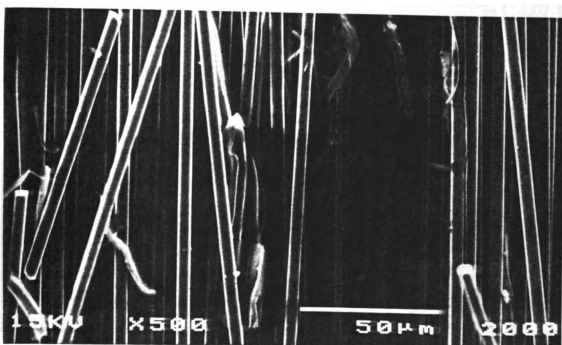


Figure 89. 500X SEM, 20%ST transverse flexural fracture.

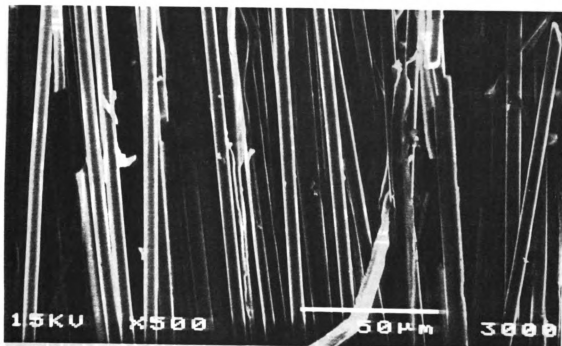


Figure 90. 500X SEM, 100%ST transverse flexural fracture.

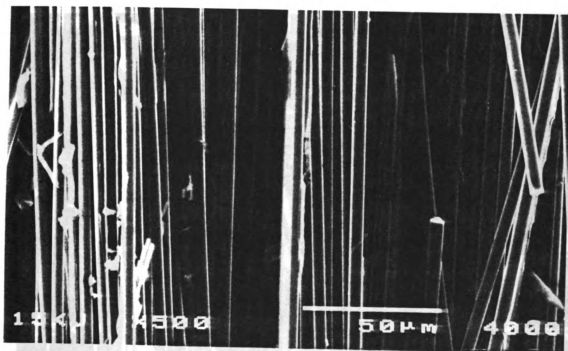


Figure 91. 500X SEM, 200%ST transverse flexural fracture.

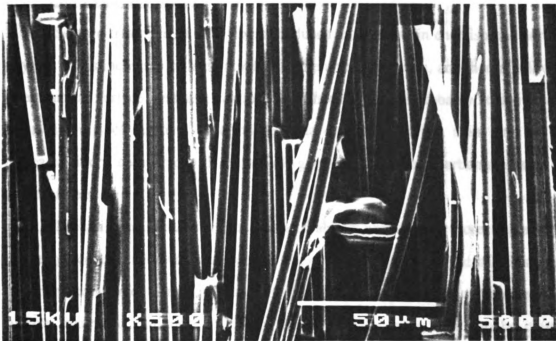


Figure 92. 500X SEM, 600%ST transverse flexural fracture.

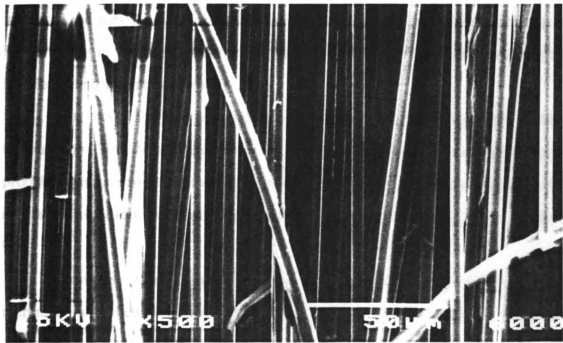


Figure 93. 500X SEM, 100GST transverse flexural fracture.

2.5

oxy

line

the

unt

trea

oxy

trea

surfa

corre

conc

thoug

incre

failur

interf

treatm

proba

increa

94.

increm

Artifac

size ma

2.5 IM6 CONCLUSIONS

Surface treatment of IM6 fibers produced an increase in chemisorbed surface oxygen. This increase occurred rapidly for the untreated fibers, and then at a lower, linear rate as surface treatment continued. This difference is probably attributable to the availability of reactive, edge, corner, and disordered carbon atom sites on the untreated fibers, compared with exclusively graphitic basal plane carbon atoms on the treated fibers.

The interfacial shear strength increased almost linearly with increasing surface oxygen percentage and with polar surface free energy, rapidly rising with 20% surface treatment compared to the untreated fiber and then increasing at a lower rate as surface treatment continued. Although these variables were shown to be closely correlated, actual causality is much more difficult to establish. It cannot be conclusively stated that there is a cause and effect relationship based upon these data, though such a relationship is strongly supported. The addition of the "G" size also increased the measured values of interfacial shear strength, and caused a change in failure mode in the fragmentation specimens from entirely interfacial to combined interfacial and interphase yielding.

The mode II fracture toughness increased with increasing fiber surface treatment and with the addition of the size. Sizing led to a particularly large increase, probably because of increased plastic deformation of the interphase region. This increase closely followed that of ISS, except for the sized case, as shown in Figure 94.

Transverse flexural strengths increased with the initial surface treatment increment and then remained approximately constant with additional treatment. Artifacts from fiber volume fraction differences, fiber bridging, and the aging of the size may have influenced the results for the 600%ST and 100GST fibers.

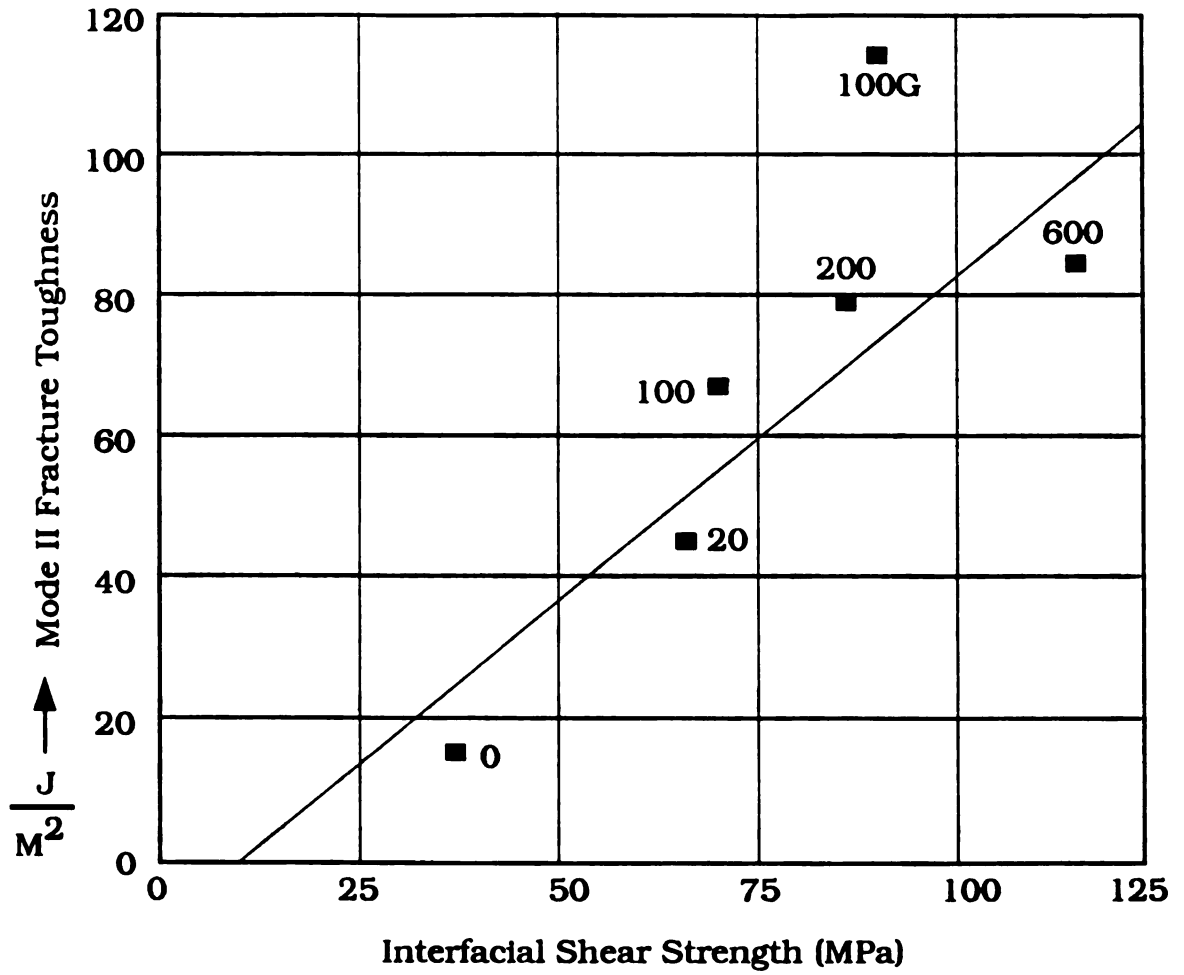


Figure 94. Mode II fracture toughness versus ISS.

the
siz
int
lin

wh
flex
fibe
incr
pro
resu
Add
the
the
fract
surfa
again

Interlaminar shear strengths increased with surface treatment compared with the untreated fibers, but increased at a low rate for all surface treated and treated and sized fibers. This was probably due to a matrix dominated failure mode with small interfacial effects. Nevertheless, the plot of ILSS versus ISS shows an approximately linear relationship, as seen in Figure 95.

The results of the mechanical testing program are summarized in Figure 96, which shows the interfacial shear strength, interlaminar shear strength, transverse flexural strength, and mode II fracture toughness for the surface treated but unsized fibers, plotted against surface treatment in each case. In all four cases, the initial increment of surface treatment increase the strength property substantially. This probably results from the removal of a weak surface layer from the fiber and a resultant change in failure mode from within the fiber to the interface or matrix. Additional surface treatment continues to increase the interfacial shear strength, but the transverse flexural and interlaminar shear strengths level off, apparently because the locus of failure has moved to the matrix, away from the interface. Mode II fracture toughness continues to increase with additional surface treatment until 200% surface treatment is reached, then levels off in the increment from 200% to 600%, again, because the mode of failure no longer involves the fiber/matrix interface.

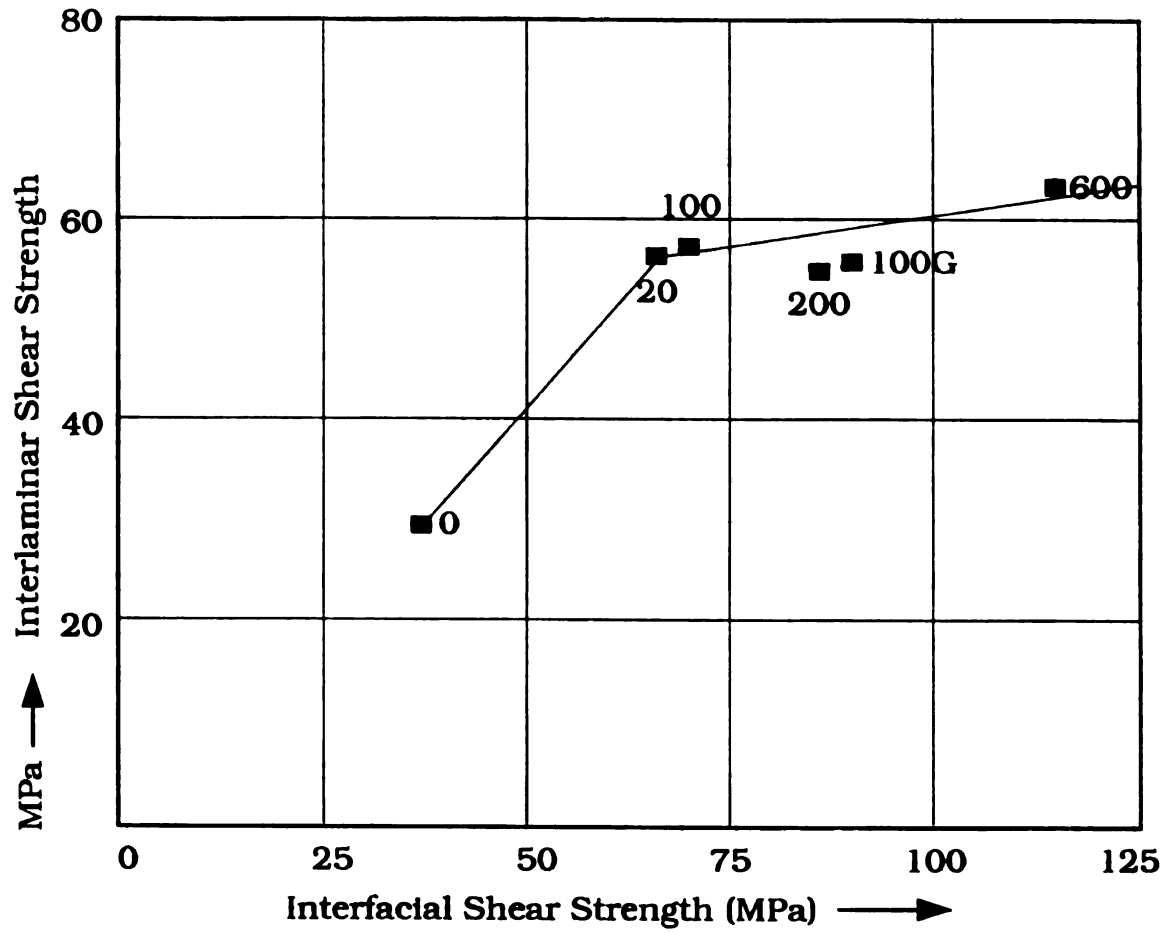
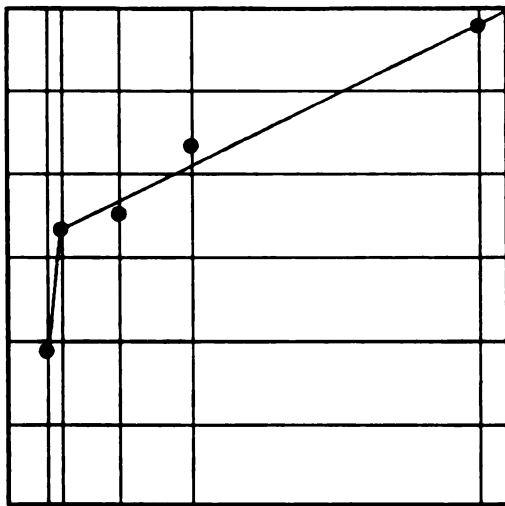
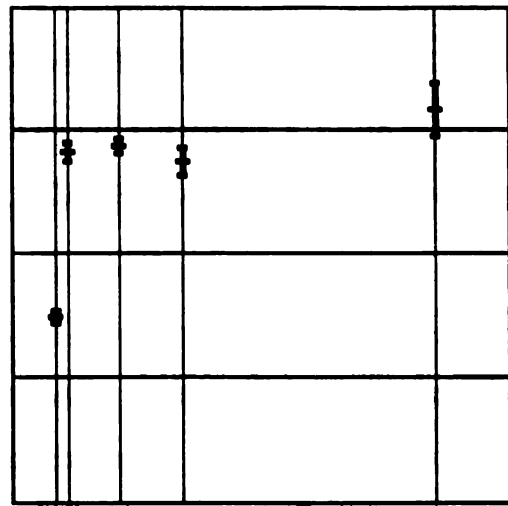


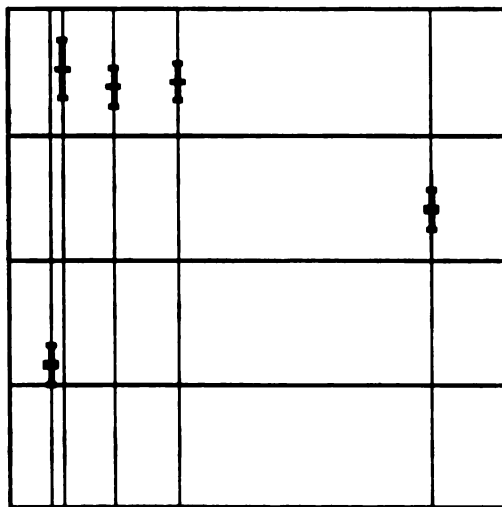
Figure 95. Interlaminar shear strength versus ISS.



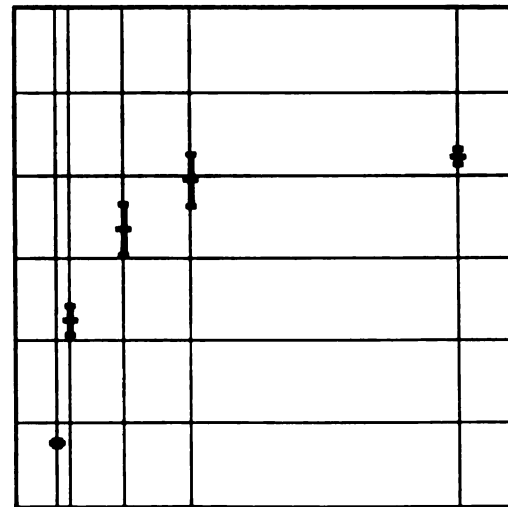
Interfacial Shear Strength



Interlaminar Shear Strength



Transverse Flexural Strength



Mode II Fracture Toughness

Figure 96. Summary of mechanical test results versus surface treatment.

CHAPTER 6
THE INFLUENCE OF PROCESSING TIME, TEMPERATURE, AND
COMPOSITION ON THE ADHESION OF CARBON FIBERS
TO BISPHENOL-A POLYCARBONATE

6.1 POLYCARBONATE SYNOPSIS

Interfacial shear strengths of AS4 and AU4 carbon fibers in pure BPA-polycarbonate and commercial Lexan 141 polycarbonate were measured with the single fiber fragmentation test. Specimens were prepared both by matrix deposition from methylene chloride followed by equilibration at temperatures below T_g and by hot pressing at temperatures above T_g , with and without solvent. Stress transfer in the hot pressed specimens showed substantial improvement over the weakly adhered solvent deposition specimens. Increasing consolidation time and temperature improved shear strength in the pure polycarbonate specimens. Lexan 141 matrix specimens, however, appeared to reach a lower, limiting shear strength which was not significantly changed by increasing consolidation time, temperature, or pressure, or by the presence of solvent.

6.2 POLYCARBONATE INTRODUCTION

Thermoplastic matrix composites are under intensive investigation in an effort to exploit potential advantages in toughness, fabrication speed, and environmental resistance. Optimization of these properties requires that a better understanding of fiber to thermoplastic matrix adhesion be developed. Amorphous thermoplastics, such as bisphenol-A polycarbonate, possess much greater fracture toughness than typical thermoset epoxy matrices, with a notched Izod impact strength of 801 J/m for Lexan[®] 141 [GE, 1988]. This toughness has not yet been fully translated into toughened composite systems, however, apparently because of problems with interfacial adhesion

[Parker, 1989], [Parker, 1988], [Bascom, 1987], [Lauke, 1988].

Understanding the mechanisms of adhesion between carbon fibers and thermoplastic matrices to improve composite performance has been the object of numerous studies [Kardos, 1973], [Di Landro, 1987], [Peacock, 1986]. While the thermoset epoxy matrix used in the work described in chapter 5 was applied to the fibers in the form of highly reactive monomers, dimers, and curing agent and subsequently polymerized, the polycarbonate thermoplastic investigated in this section was applied in a much less reactive polymerized form. The possibility of interfacial adhesion by the formation of primary chemical bonds is therefore considerably reduced. The microstructures of the matrices was also fundamentally different, with the epoxy polymerizing to form a three dimensional network of monomers linked by primary chemical bonds while the polycarbonate consists of an amorphous mass of linear polymer chains held together by secondary polar and dispersive bonds.

The possibility of fiber nucleation of crystallization introduces an additional microstructural variable by generating an anisotropic transcrystalline interphase with mechanical properties significantly different from the bulk matrix. The slow crystallization rate of polycarbonate allows this factor to be studied in isolation from other effects. The use of solvents in the pre-pregging steps of thermoplastic composite fabrication can lead to changes in crystallization and adsorption which can in turn influence fracture toughness and adhesion.

Along with the usual difficulties with the measurement of interfacial shear strengths, thermoplastic matrices present problems with specimen fabrication due to the high melt viscosities characteristic of these systems. These problems necessitated the development of special single fiber specimen production methods which allow testing in both amorphous and semi-crystalline thermoplastic materials. This paper describes these techniques and presents data which characterizes adhesion for this model amorphous thermoplastic matrix system.

6.3 POLYCARBONATE EXPERIMENTAL MATERIALS

Matrices investigated in this section included pure BPA-polycarbonate obtained from Polysciences Co. with a molecular weight range of 32-36,000, and an injection molding grade of polycarbonate, Lexan 141 from General Electric Co. which contains proprietary toughening agents and ultraviolet light stabilizers. Although the exact composition of the Lexan material is unknown because of its proprietary nature, it was chosen as one of the polycarbonate models for this investigation because it has been used as a matrix in a number of composite studies [Parker, 1988], and its mechanical properties are well characterized and available in product data sheets. These properties are summarized in Table 13.

The chemical structure of polycarbonate is shown in Figure 97. The alternation along each monomeric unit between bulky phenyl groups and methyl groups and the polar acetate, and ether linkages makes crystallization of this structure difficult. This produces a high entanglement density and an amorphous structure for kinetic reasons, i.e., the structure is not atactic and so may be crystallized, but the entanglement prevents crystallization except with extended annealing.

The fibers for this investigation were Hercules AS4 PAN-based carbon fibers, with the standard electrochemical oxidative surface treatment (type AS4) and without surface treatment (type AU4).

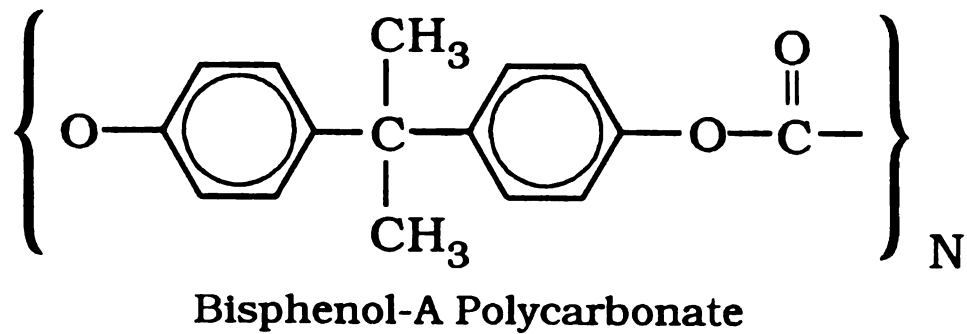


Figure 97. Chemical structure of BPA-Polycarbonate.

Table 13. Properties of Lexan 141 polycarbonate resin.

<u>Property</u>	<u>U.S. Units</u>	<u>SI Units</u>
Tensile Strength		
(yield)	9,000 psi	62 MPa
(ultimate)	10,000 psi	69 MPa
Shear Strength		
(yield)	9,000 psi	40 MPa
(ultimate)	10,000 psi	70 MPa
Shear Modulus	1.14 x 10 ⁵ psi	790 MPa
Izod Impact Strength (notched, 1/8" thick)	15 ft-lbs/in	801 J/m
Coefficient of Thermal Expansion	3.75 x 10 ⁻⁵ in/in °F	6.75 x 10 ⁻⁵ m/m °C

6.4 POLYCARBONATE EXPERIMENTAL PROCEDURE

The experimental procedure for thermoplastic matrix fragmentation specimen fabrication and testing are described in this section.

6.4.1 HOT PRESSED SPECIMEN PREPARATION

Thermoplastic matrix single fiber fragmentation test specimens were fabricated by hot pressing fibers between pairs of matrix sheets in the following manner.

Preform sheets, one half the thickness of the final specimens, were first produced by hot pressing pelletized material between aluminum foil sheets with the thickness controlled by a surrounding dam of RTV silicone material. Times and temperatures for this preliminary step were kept as low as possible to minimize chances of thermal degradation and the assembly was kept sealed in foil throughout the process to minimize oxidation. Aluminum foil pressing sheets were used to avoid the use of any release agents which might cause surface contamination and to allow the foil to be peeled away from the polycarbonate sheets without deforming them. One, 14 cm square by .8 mm thick preform sheet was then placed on a .1 mm aluminum sheet atop an outer aluminum foil sealing sheet and surrounded by a 1.6 mm thick high temperature RTV silicone frame (Figure 98).

Single, separated fibers were then draped across the sheet and surrounding gasket. Care was taken to avoid fiber contamination and damage during this layup process. Re-positioning the fibers after placement was avoided since this can lead to twisting and premature failure. Spacing strips of the same matrix material were placed on either side of the lower sheet to maintain separation and avoid fiber damage during the early heating stages before T_g was reached. The preform sheets and silicone gasket were carefully matched in size and thickness to produce minimal material flow which can produce bent and wavy fibers.

With enough isolated fibers laid in place, a razor knife was used to cut them into approximate 25 mm segments with minimal disturbance. This reduces fiber bending during matrix flow and contraction, and instead causes small rigid-body rotations and displacements which have no effect on final specimen yield. A pair of thermocouple wires were inserted at one corner of the sheet and insulated from the foil with teflon strips. The upper preform sheet was then laid over the spacer strips, followed by the top aluminum pressing sheet. The entire assembly was sealed in the outer aluminum foil and carefully placed between the hot press platens without

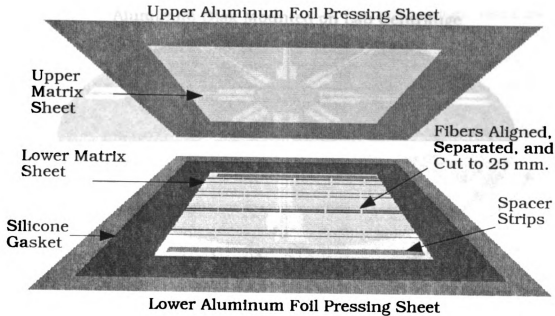


Figure 98. Fixture for hot pressing single fiber specimens.

disturbing the fibers, preforms, and gaskets.

Hot pressing then proceeded in the following manner. To ensure uniform heating, a light load, equal to the upper platen weight was applied during heating. This load was born by the spacer strips and did not produce fiber damage. A 1 hour soak at 125 °C was applied to dry the polycarbonate, which is sensitive to hydrolysis at elevated temperatures [Golovoy, 1989].

Following the 125 °C soak, the temperature was raised at approximately 5 °C/minute. Upon reaching the desired temperature, the load was applied and maintained throughout the pressing cycle. Cooling was accomplished by the standard platen water cooling system at approximately 1 °C/second for rapidly cooled specimens and 1 °C/minute for slow cooling.

Test coupons were die cut from the composite monolayers produced by this system with fibers aligned with the specimen gage sections.

Aluminum Disk Mounted on Lab Centrifuge

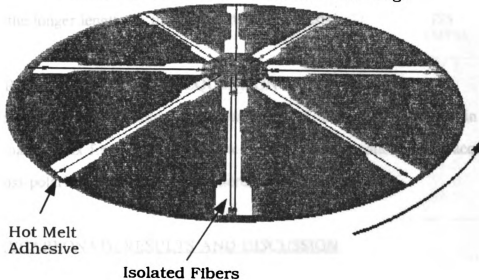


Figure 99. Spin coating fixture for solvent deposition specimen fabrication.

6.4.2. SOLVENT DEPOSITED SPECIMEN FABRICATION

Additional specimens were produced by embedding fibers in Lexan 141 polycarbonate deposited from a methylene chloride solution in the following manner, adapted from Bascom, et al [Bascom, 1987]. Isolated fibers were aligned on pre-cut polycarbonate coupons and secured with hot melt adhesive at the ends. These specimens were affixed radially to a disk atop a small centrifuge. A 5% solution of polycarbonate in methylene chloride was applied along the fiber length and the excess immediately spun off by briefly starting the centrifuge. This was repeated 4 times at 5 minute intervals to allow evaporation and the specimens were then equilibrated at the specified temperature for at least 24 hours prior to testing.

6.4.3 DATA ACQUISITION AND ANALYSIS

Fragment lengths were measured and a Poisson-Weibull analysis [Drzal, 1982] performed by using FiberTrack, [Waterbury, 1991]. Strengths were calculated using an average fiber diameter of 7.5 microns and a fiber strength of 5865 MPa for both

AS4 and AU4 fibers for the fragments in the elevated temperature tests, with a lower value for the longer lengths in the solvent deposition tests.

6.4.4 BIREFRINGENT IMAGE ACQUISITION

To document the failure characteristics of the failure modes in the polycarbonate matrix fragmentation specimens, birefringence patterns were acquired with a cross-polarized transmitted light microscope.

6.5 POLYCARBONATE RESULTS AND DISCUSSION

Three groups of single fiber fragmentation specimens were fabricated and tested, two employing Lexan 141 BPA-PC with and without solvent, and one group with pure polycarbonate with a molecular weight range of 32-36,000. The resultant fragment length/diameter ratios and interfacial shear strengths calculated from a Weibull-Poisson analysis appear in Tables 14 and 15 and in Figures 100 and 101.

6.5.1 SOLVENT PROCESSED SPECIMENS

The results from the first group of solvent deposition specimens (Table 14, Figure 100) with AS4 fibers in Lexan 141, show adhesion which increases with increasing equilibration temperature, reaching a limiting value at about 75 °C. With an ISS of only 27 MPa and L_c/D of 113/1, however, this level is inadequate for use in advanced composites.

The birefringence patterns of a solvent deposited specimen, equilibrated at 75 °C, appears in Figure 102. These patterns show an interfacial failure mode and very weak bonding as indicated by the weakness of the birefringence and the substantial crack advance distances in each stick-slip event.

Table 14. Matrix type, processing, L_c/D 's, and ISS for AS4 in Lexan 141.

Spec. Desig.	Fiber Type	Temp. (°C)	Time (min.)	Pres. (kPa)	Cooling Method	L_c/D	ISS (MPa)
MeCl1	AS4	25	1440	(atm)	-	173.9	17.1
MeCl2	AS4	60	1440	(atm)	Rapid	115.9	26.2
MeCl3	AS4	70	1440	(atm)	Rapid	112.8	27.3
MeCl4	AS4	230	15	475	Rapid	69.0	53.7
PC1	AS4	230	20	137	Rapid	60.2	53.5
PC2	AS4	230	20	689	Rapid	69.4	52.1
PC3	AS4	230	20	1379	Rapid	65.5	54.5
PC4	AS4	230	20	689	Slow	69.1	51.6
PC5	AS4	240	20	1370	Rapid	64.5	54.5

Specimens with methylene chloride present but hot pressed 15 minutes at 230 °C (MeCl4) showed greatly improved adhesion, with an ISS of 53.7 and L_c/D of 69, comparable to Lexan matrix specimens produced without solvent. The birefringence patterns for these specimens differ from those processed without solvent with much greater intensity, indicative of high ISS, and showing stick-slip behavior with much shorter crack advance distances (Figure 103). The initial presence of solvent did not appear to interfere with adhesion, provided that sufficient time and temperature were allowed for the solvent to diffuse away.

Thermogravimetric analysis of polycarbonate deposited from methylene chloride and equilibrated at 25, 50, and 75 °C for at least 24 hours showed weight loss over the temperature range from 25 °C to 150 °C (T_g) in the 25 and 50 °C samples but negligible loss in the 75 °C specimens. The small, methylene chloride molecules are apparently mobile within polycarbonate at this temperature. The ISS specimens equilibrated at 75 °C were therefore free of methylene chloride, producing the levelling off of ISS in the temperature range below T_g . Without consolidation of the polymer at a temperature at which the chains themselves are mobile, a porous, poorly consolidated microstructure existed. This poor microstructure also extends to the conformation of the polymer chains at the carbon fiber surface.

ISS (MPa) →

Figure

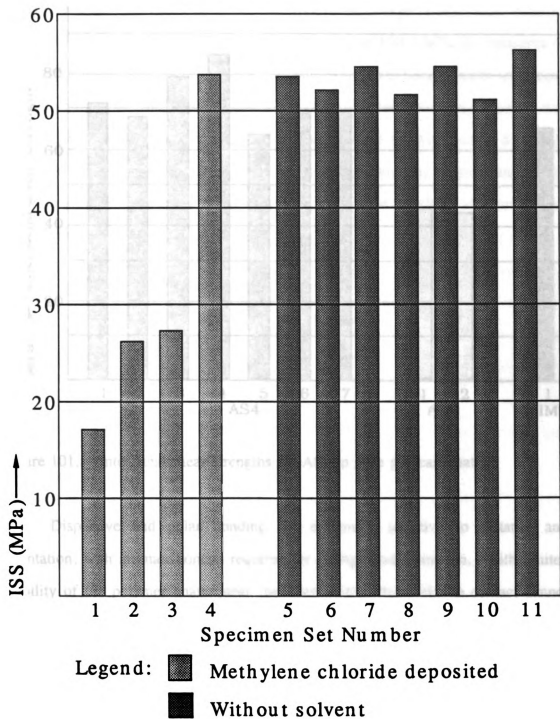


Figure 100. Interfacial shear strengths for AS4 in Lexan 141.

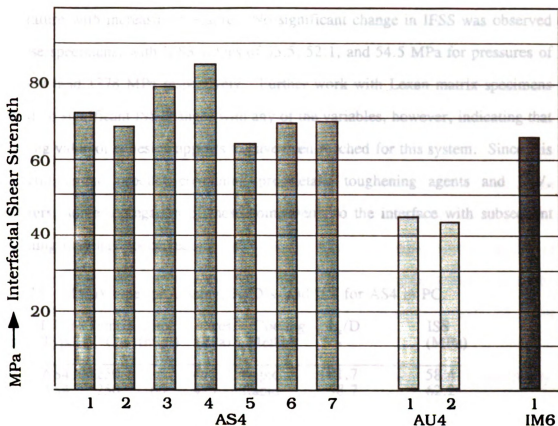


Figure 101. Interfacial shear strengths for AS4 in pure polycarbonate.

Dispersive and polar bonding are extremely sensitive to distance and orientation, with intimate contact required for strong bond formation. With limited mobility of the polymer chains near the fiber surface this intimate contact cannot occur.

These results may be summarized as indicating that adequate fiber/thermoplastic matrix adhesion requires that a sufficiently high temperature be attained for full relaxation of the polymer chains to occur.

6.5.2 SOLVENT FREE SPECIMENS

The influence of consolidation pressure was investigated with three sets of specimens, PC1, PC2, and PC3 (Table 15, Figure 100) produced at constant time and

temperature with increasing pressure. No significant change in IFSS was observed for these specimens, with IFSS values of 53.5, 52.1, and 54.5 MPa for pressures of 137, 689, and 1378 MPa respectively. Further work with Lexan matrix specimens showed no significant ISS changes with any of the variables, however, indicating that a limiting value of adhesion appears to have been reached for this system. Since this is a commercial product containing proprietary toughening agents and U.V. stabilizers, some segregation of these components to the interface with subsequent weakening may have occurred.

Table 15. Matrix type, processing, L_c/D 's, and ISS for AS4 in PC.

Spec. Desig.	Fiber Type	Temp. (°C)	Time (min.)	Pres. (kPa)	Cooling Method	L_c/D -	ISS (MPa)
PS2	AS4	250	15	475	Rapid	61.7	58.4
PS3	AS4	250	60	475	Rapid	58.7	62.2
PS6	AS4	250	120	475	Rapid	55.4	64.2
PS4	AS4	275	15	475	Rapid	60.5	59.2
PS9	AS4	275	30	475	Rapid	62.5	57.1
PS5	AS4	300	15	475	Rapid	52.7	67.8
PS1	AS4	275	15	475	Slow	61.7	57.5
PS7	AU4	250	15	475	Rapid	71.9	51.3

o

re

2.

1:

th

w

A

ga

pr

in

19

pro

the

me

sug

to p

1.2

proj

MPa

level

and

nearl

Consolidation time and temperature were found to have a significant influence on the pure polycarbonate specimens (Figure 101 and Table 15), with improvements resulting from increasing both. For specimens pressed 15, 60, and 120 minutes at 250 °C, ISS increased uniformly from 58.4 to 64.2 MPa. The specimens processed 15 and 30 minutes at 275 C showed a slight reduction from 59.2 to 57.1 MPa, but this is probably due to experimental scatter. A significant increase over these values was seen in the set pressed 15 minutes at 300 °C, with an ISS of 67.8 MPa. Attempts to repeat this test with longer press cycles were unsuccessful because of gasket failures but this is under continuing investigation. Matrix decomposition and property changes are problematic at such elevated temperatures and are under investigation.

These results are in general agreement with those of Brady and Porter [Brady, 1989], who investigated transverse toughness in carbon fiber/polycarbonate composites processed with different annealing times and temperatures. As they have pointed out, the temperatures at which improvements are seen are substantially greater than the melt crystallization temperature of 265 °C, thereby ruling out transcrystallinity, and suggesting an adsorption effect as the mechanism of variation.

It is also interesting to note that the minimum processing temperature found to produce maximum adhesion and elimination of solvent artifacts is approximately 1.2 times the polymer T_g (°K). Such processing temperature guidelines have been proposed based on polymer devolatilization studies [Mossner, 1988].

The untreated fibers AU4 had a lower ISS, 51.3 MPa compared with 58.4 MPa for identically processed AS4 fibers. Surface treatment evidently raises adhesion levels for this thermoplastic system, but the increase is not as great as that for AU4 and AS4 specimens in an epoxy matrix, which increased from less than 40 MPa to nearly 70 MPa with surface treatment.

This difference may arise from the formation of primary chemical bonds

between the chemisorbed surface oxygen attached to the carbon fiber during surface treatment and the reactive metaphenylene diamine curing agent. The absence of a similar reactive moiety in the polycarbonate precludes similar bond formation and limits adhesion increases to that resulting increases in the much-weaker polar bonds between the surface oxygen and the oxygen in the polycarbonate chains.

Another possible difference may result from the greater thermal compression stresses exerted by the thermoplastic on cooling from T_g than those produced in the thermoset cooling from its T_g . A greater compression may reduce the tendency for the weak surface layer in the carbon fiber to fail, producing an ISS of 50 MPa in the thermoplastic and < 40 MPa in the thermoset even though the locus of failure may be within the fiber in both cases.

6.5.3 INTERPRETATION OF BIREFRINGENCE PATTERNS

Four general types of birefringence patterns were observed among the different sets of specimens. Solvent deposited specimens displayed very faint patterns extended along several hundred microns of fiber (Figure 102), indicative of the weak bonding in these systems and an interfacial failure mode. Hot pressed and fast cooled Lexan 141 specimens showed interfacial failure by stick-slip cracking in the longer specimen fragments, particularly in those with methylene chloride present (Figure 103). These stick-slips were not as sharply defined as those present in epoxy matrix specimens, probably indicating a greater amount of plastic deformation accompanying the cracking.

Although the ISS of all Lexan matrix specimens consolidated above T_g were unaffected by time and temperature, one processing variable, cooling rate, did produce a change in the apparent failure mode. Slowly cooled Lexan matrix specimens showed evidence of shear band formation at sites some distance away from fiber breaks. These bands were visible under both polarized and non-polarized transmitted

light micrographs, as shown in Figure 104. The bands were never seen near the breaks, but always appeared some distance away. Apparently, a change in failure mode with distance from the breaks occurred, probably moving from interfacial to plastic shear deformation of the matrix.

Patterns in the pure polycarbonate specimens (PS series), were very strong, showing no evidence of stick-slip behavior or other variations (Figure 105). The intensity of these patterns indicates high ISS and a failure mode involving deformation of the matrix rather than interfacial cracking.

Although no evidence of crystallinity was observed in any of the actual fragmentation specimens produced under these processing conditions, extended annealing times (24 hours) for pure polycarbonate caused changes that appear to be crystallization related (Figure 106). Specially prepared specimens subjected to extended periods above T_g but below the melting temperature developed optically anisotropic regions in the vicinity of the fiber interphase (Figure 107). From these observations, however, sufficient time was not available for crystallization to occur under typical composite processing conditions.

In addition to the failure modes operative in the immediate vicinity of the fibers in the fragmentation specimens, crazing occurred within the matrix during testing for both Lexan 141 and pure polycarbonate specimens (Figure 108). The crazes did not appear to be nucleated by deformation near the fiber, but were completely independent of the fiber and breaks.



Figure 102. Solvent deposited Lexan matrix birefringence pattern.



Figure 103. Fast cooled Lexan matrix birefringence pattern.

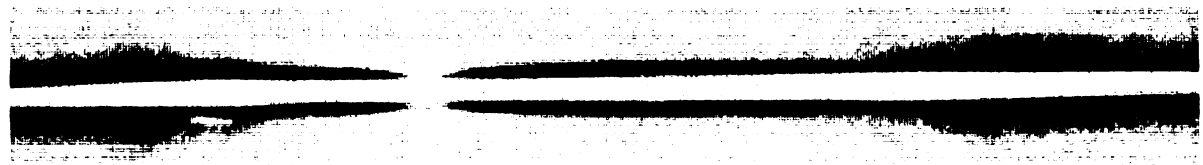


Figure 104. Slow cooled Lexan matrix birefringence pattern.



Figure 105. Pure polycarbonate matrix birefringence pattern.

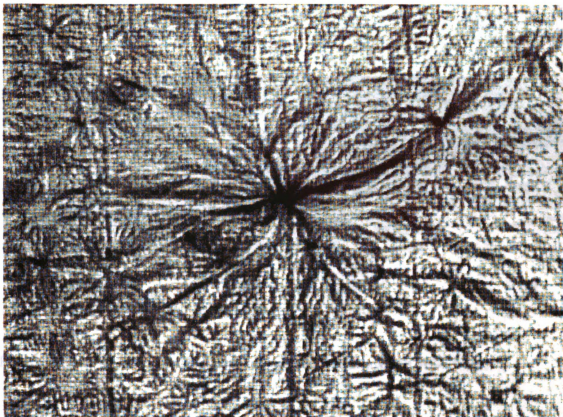


Figure 106. Surface of annealed polycarbonate.

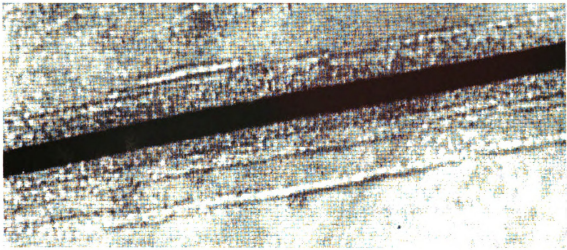


Figure 107. Possible polycarbonate crystalline sheath around AS4 fiber.

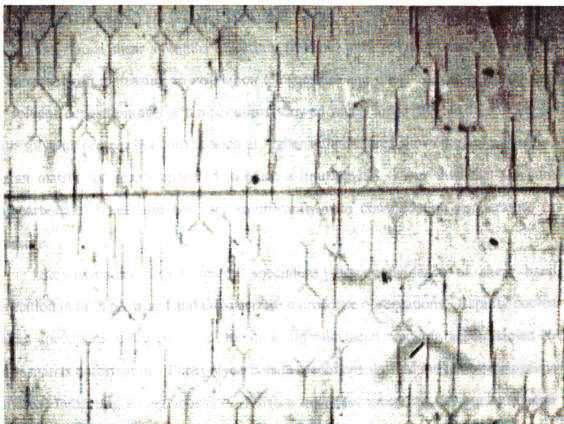


Figure 108. Crazed polycarbonate fragmentation specimen.

6.6

to in

by s

with

Lexa

poly

press

form

Lex

som

patt

exte

6.6 POLYCARBONATE CONCLUSIONS

Interfacial shear strengths of carbon fibers in pure polycarbonate were found to increase with increasing consolidation temperature and time. Specimens produced by solvent deposition at low temperatures showed much lower ISS while specimens with solvents present but consolidated at higher temperatures showed good adhesion. Lexan matrix specimens appeared to reach a limiting ISS, lower than that for pure polycarbonate, which did not vary significantly with consolidation temperature or pressure.

Slowly cooled Lexan matrix specimens showed evidence of shear band formation in both polarized and unpolarized microscope observations. Rapidly cooled Lexan specimens appeared to fail by stick-slip interfacial cracking accompanied by some matrix deformation. Pure polycarbonate specimens showed intense birefringence patterns, indicating strong adhesion. Surface treatment increased ISS but to a lesser extent than for thermoset epoxy matrix specimens.

CHAPTER 7

THE INFLUENCE OF FIBER NUCLEATED CRYSTALLIZATION ON INTERFACIAL SHEAR STRENGTHS AND FAILURE MODES OF CARBON FIBERS IN NYLON 6,6

7.1 NYLON 6,6 SYNOPSIS

Interfacial shear strengths of carbon fibers in a semicrystalline thermoplastic, Nylon 6,6, processed at various time, temperature, and pressure schedules were measured by single fiber fragmentation tests. The effects of processing conditions on fiber nucleation of crystallization, crystallite morphology, fiber-matrix stress transfer, and modes of failure were investigated by this technique. PAN-based Hercules AU4, AS4, and IM6 fibers were investigated. Interfacial shear strengths were calculated from a two parameter Weibull distribution treatment. Interphase microstructures and failure modes were evaluated by transmission optical microscopy and confocal scanning optical microscopy.

7.2 NYLON 6,6 INTRODUCTION

Fiber-matrix adhesion has been shown to play a critical role in composite performance for a wide variety of systems, ranging from thermoset polymer matrices through metal matrices, to brittle ceramics. Semicrystalline thermoplastic matrix composites are currently under intensive investigation in an effort to produce composites with improved toughness, environmental stability, and high temperature properties, and which may be rapidly and economically processed. The exploitation of these desirable properties requires that a full understanding of the nature of fiber-thermoplastic matrix adhesion be developed.

An additional variable is introduced for a semicrystalline thermoplastic, a complex interphase microstructure with mechanical properties which may substantially differ from the bulk material. This microstructure, often called "transcrystallinity", is generated when the fiber nucleates matrix crystal growth at numerous closely spaced sites, causing the normal, spherically symmetric growth habit to change to a radial, cylindrical symmetry, or two dimensional spherulitic structure [Kumamaru, 1983]. While this type of growth is often attained in very low V_f , it is less commonly observed in actual, high V_f composites [Zeng, 1986].

An extensive body of thermoplastic crystallization research has been performed on composites fabricated with poly(ether ether ketone) (PEEK) formulations usually obtained from Imperial Chemical Industries. Since this material is available only in proprietary compositions containing nucleating agents of an undisclosed nature, analysis of the literature is not entirely straightforward. The influence of thermal history on nucleant density has been the object of much of this work. Higher temperatures and longer durations of melt preheating have been shown to reduce the nucleant density in the bulk PEEK [Lee and Porter, 1986]. Reduced competition from nucleants in the matrix tends to increase the growth of the transcrystalline interphase. Transverse tensile strengths were found to double with increased preheat duration, and matrix retention on the fracture surfaces was correspondingly increased. For the case of ICI PEEK, then, the adhesion was found to increase with increasing transcrystallinity. Another conclusion that can be drawn from this work is that the nucleation agents in the matrix are more temperature sensitive than is the nucleation activity of the carbon fiber surface.

The effects of cooling rate on PEEK composites have been investigated to determine changes in degree of crystallinity and fracture toughness [Lee, 1987 A]. Crystallinity was found to decrease with increasing cooling rate. Axial tensile strength was unchanged, but both mode I and mode II fracture toughness decreased

with increasing degree of crystallinity. Further work showed that strengths and moduli of both the neat matrix and carbon fiber composites increased slightly with increasing degree of crystallinity while the fracture toughness and fracture energy decreased [Talbot, Springer, Berglund, 1987]. These properties were found to vary only with the final degree of crystallinity and not with the nature of the thermal history required to achieve that degree, i.e., slow cooling compared with rapid cooling and subsequent annealing.

The thermal prehistory of PEEK has been shown to involve a number of processes in addition to the destruction of nucleating agents [Deslandes, 1989]. Chain scission, chain branching, cross linking and nucleant formation were believed to occur at different rates and temperatures during preheating above the melt temperatures.

Epitaxial growth of polymers on fibers and fiber-like surfaces has been noted by a number of researchers, for example, [Tuinstra, 1970], [Kumamaru, 1983 (A) and (B)]. The general mechanisms involved in polymer nucleation, however, are not fully understood [Keller, 1977], [Binsbergen, 1977], [Stack, 1986] and the mechanisms involved in fiber nucleation may, or may not, involve epitaxy.

The embedded fiber fragmentation method for measuring interfacial shear strengths has been widely used with thermoset matrices because of its well documented consistency and sensitivity to interfacial properties and the relative ease of collecting a statistically significant data sample. The application of this valuable technique has generally depended upon the transparency of the matrix material for measurement of fragment lengths and observation of failure modes by optical birefringence. The development of methods to extend fragmentation testing to translucent semicrystalline materials was therefore made a goal of this research effort.

Observation of fragmentation test failure modes was facilitated by the availability of a new microscopy technique, confocal scanning optical microscopy (CSOM) which scans both the laser illumination source and the imaging optics to

produce an optical micrograph with high resolution and a very high rejection of interference from out of focal plane sources [Yatchmenoff, 1988] [Thomason, 1990].

This chapter describes the results of an investigation of the influence of fiber nucleated crystallization on the microstructure, shear strength and failure modes of Nylon 6,6, semicrystalline thermoplastic fragmentation specimens.

7.3 NYLON 6,6 EXPERIMENTAL PROCEDURE

Single fiber specimen fabrication with thermoplastic matrices and fragment length measurement for the translucent matrix presented special experimental problems which were addressed. Specimens were die cut from an isolated fiber sandwich which was produced by hot pressing a layer of aligned and separated single fibers between sheets of the matrix under an argon atmosphere without the use of solvents. Translucent matrix specimens were first strained to achieve the limiting fiber fragment length and then released, sanded and polished to reveal the fibers, and re-strained to expose breaks and transverse cracks for fragment measurement.

The experimental materials and methods used to study fiber-semicrystalline thermoplastic matrix adhesion are described in this section.

7.3.1 NYLON 6,6 EXPERIMENTAL MATERIALS

The model semicrystalline thermoplastic matrix chosen for this study was Nylon 6,6, poly(hexamethyl adipamide), (Figure 109). The choice was based upon the relative ease of processing compared with high temperature, high performance polymers such as PEEK and PPS and on the availability of the material without contamination by proprietary nucleating agents or other additives.

The fibers used include PAN-based Hercules types AU4, (untreated), AS4 (surface treated), and intermediate modulus IM6, (surface treated), which are described in chapter 4.

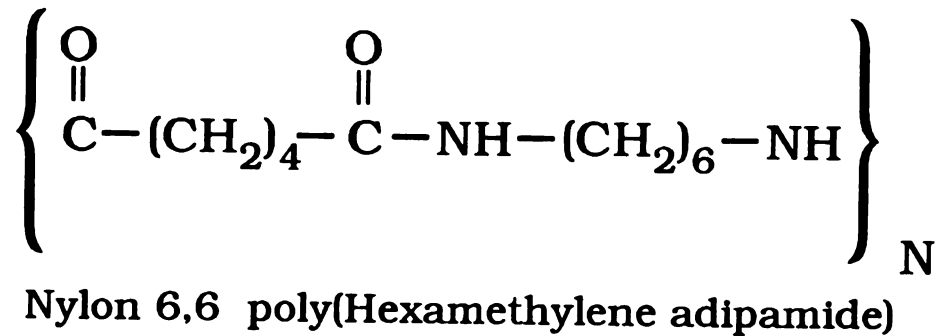


Figure 109. Chemical structure of Nylon 6,6 - poly(hexamethyl adipamide).

7.3.2 FABRICATION OF NYLON 6,6 ISS SPECIMENS

Thermoplastic matrix ISS specimens were fabricated by the following technique, similar to that used for polycarbonate matrices described in section 6.4.1. Sheets of the neat matrix material .5 mm thick x 14 cm square were produced by hot pressing between 0.1 mm thick aluminum sheets under an argon atmosphere at a temperature slightly above T_m to minimize thermal degradation. This thickness of acetone-washed aluminum pressing foil was selected to allow the foil to be peeled away from the specimens without causing deformation and to allow pressing to proceed without the use of a release agent which might cause surface contamination. Thickness and shape were controlled by the use of 0.5 mm thick RTV silicone strips which were arranged to form a dam.

After trimming to accurate dimensions, a bottom sheet was placed in the molding stack shown in Figure 98. Single fibers were draped across the sheet and the adjacent silicone frame and were straightened, aligned, and arranged in groups of two or three so that more than one fiber could be included in each specimen. When a sufficient set of fibers was laid in place they were then cut into segments approximately 2.5 cm in length with as little disturbance as possible.

A top sheet of matrix was then placed over the fibers and thermocouple, followed by the upper foil sheet. The aluminum foil was then sealed around the

assembly, taking care not to disrupt it. The packet was then placed in the hot press and an argon entry tube was affixed with tape. Following argon purging the press was heated to the required upper temperature and the desired load applied. Loads were monitored with an electronic hydraulic pressure transducer which was found to provide higher resolution than the Bourdon type gage supplied with the system.

Rapid cooling to the isothermal crystallization temperatures was accomplished by opening the press' water quenching valves for brief, predetermined periods of time. Although a precise step profile could not be achieved, the control was sufficient to allow for rapid cooling to a well defined temperature.

Following consolidation an outline of the specimen was placed over the straight segments of fibers and guide marks penciled on. Following the guide marks, specimen preforms were trimmed with scissors to sizes to allow entry into an arbor press die. Specimens were cut with with the arbor press and a sharp ASTM standard punch and die set leaving negligible deformation of the matrix within the gage length. The above procedure has been tested with Nylon 6,6 and BPA-polycarbonate and found to produce an acceptable yield of fibers which were sufficiently straight and aligned with the coupon.

7.3.3 NYLON 6,6 FRAGMENTATION TESTING

Interfacial shear strength testing proceeded as follows for the semi-crystalline nylon 6,6 matrix specimens. The translucence of the matrix precluded direct observations of fragment lengths through the full specimen thickness. The following method was therefore used.

Specimens were strained to approximately 6% strain, a level sufficient to ensure that the limiting fragment length was achieved. The coupons were then released, removed from the straining stage and sanded to closely approach the fiber surface. Since the fibers were generally very close to the coupon center, this could

generally be achieved by removing nearly half of the coupon thickness. If necessary, the depth of the fiber beneath the coupon surface was measured periodically by alternately focusing a microscope on the scattered fiber image and the surface during the latter stages of this approach. When the fiber was within 20-40 microns of the coupon surface the specimen was polished and remounted into the straining stage. Mineral oil was applied as a refractive index matching fluid and a cover slip applied to further improve image quality.

The specimens were then strained to separate the ends of the fiber fragments, making the break positions clearly visible and also allowing any matrix cracking to be observed. The positions of these breaks were recorded and analyzed with a computer interfaced translation stage utilizing FiberTrack [Waterbury, 1991].

7.4 NYLON 6,6 RESULTS AND DISCUSSION

Single fiber fragmentation ISS specimens were tested as described. The processing conditions, L_c/D ratios, interfacial shear strengths, and microstructure and failure mode observations are reported in this section and appear in Table 16 and Figure 110.

7.4.1 NYLON 6,6 ISS RESULTS

The AU4, untreated fibers showed substantially lower ISS, 44.8 and 45.8 MPa for sets U1 and U2 respectively, than the surface treated AS4 fiber specimens processed under the same conditions, 72.7 MPa for set N1. This difference may be attributed to the removal of a weak surface layer which may allow failure within the fiber, or to the addition of chemisorbed oxygen which may form polar or hydrogen bonds with polar groups in the nylon structure. As with the polycarbonate/AU4 specimens, the ISS of untreated fibers in this thermoplastic matrix was higher than that for AU4 fibers in thermoset epoxy. This effect is discussed in the conclusions,

in the conclusions, chapter 8.

Additional ISS improvements were achieved by slowly cooling at 1 degree °C/minute over those rapidly cooled at approximately 1 degree °C/second. Rapidly cooled specimens which were preheated at 300 °C to reduce nucleant density showed slightly reduced ISS compared with those consolidated at 275 °C.

The three sets of specimens consolidated at 382 KPa pressure showed lower adhesion than those processed at higher pressures, possibly due to inadequate consolidation and the persistence of a knit line. The best adhesion was shown by the set which was crystallized isothermally at the relatively low temperature of 225 °C.

Finally, the specimens with IM6, intermediate modulus fibers showed slightly lower adhesion than the comparable AS4 set.

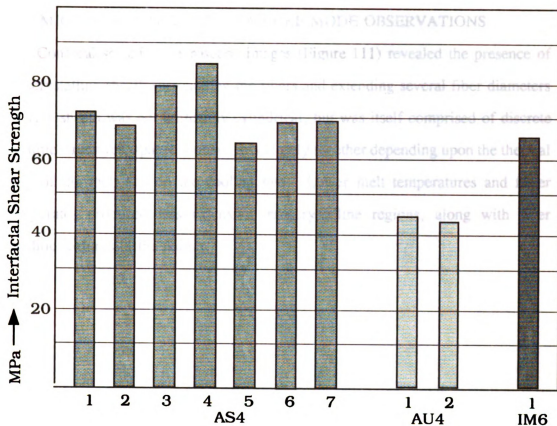


Figure 110. Interfacial shear strengths of carbon fibers in Nylon 6,6

Table 16. ISS and L_c/D of AU4, AS4, and IM6 fibers in Nylon 6,6.

Spec. Desig.	Fiber Type	Fab. Temp. °C	Fab. Pres. (KPa)	Cooling Method	L/D Ratio	ISS (MPa)	Crack Diameter (microns)
N1	AS4	275	657	Rapid	44.6	72.7	--
N2	AS4	300	657	Rapid	44.7	69.5	--
N3	AS4	275	657	225	36.4	85.8	--
N4	AS4	275	657	Slow	36.9	79.9	27
N5	AS4	275	382	245	48.1	65.1	27
N6	AS4	300	382	255	43.3	70.5	38
N7	AS4	300	382	250	42.7	70.6	45
U1	AU4	275	657	Rapid	75.7	45.8	13
U2	AU4	275	1313	Rapid	74.6	44.8	--
IM1	IM6	275	657	Rapid	54.1	66.9	--

7.4.2 MICROSTRUCTURE AND FAILURE MODE OBSERVATIONS

Confocal scanning microscope images (Figure 111) revealed the presence of a transcrystalline sheath surrounding the fibers and extending several fiber diameters out. This sheath was not uniformly cylindrical, but was itself comprised of discrete spherulitic structures, spaced more or less closely together depending upon the thermal history of the melt and on the cooling rate. Lower melt temperatures and faster cooling rates produced less extensive transcrystalline regions, along with finer spherulitic textures in the matrix.

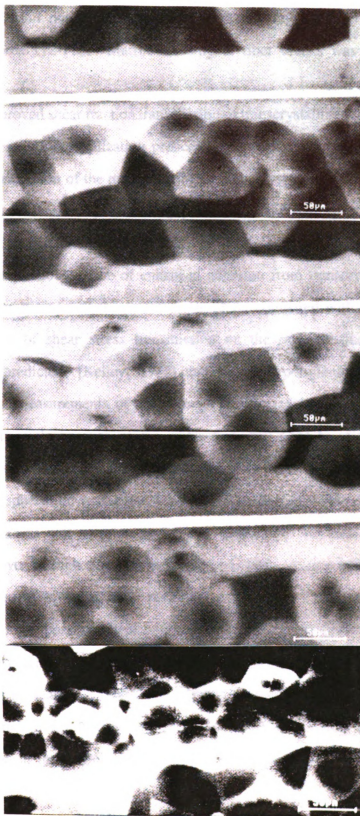


Figure 111. Four CSOM micrographs of transcrystallinity in Nylon 6,6.

Transmission optical micrographs (TOM) of fragmentation test breaks are shown in Figures 112-116. Matrix cracking at fiber breaks was observed in all samples.

The improved shear traction transmission of transcrystalline regions result from different factors. As crystallization proceeds compressive forces may increase due either to the contraction of the matrix during or after crystallization. These shrinkage stresses increase adhesion by increasing polar and dispersive interfacial forces and static and moving frictional coefficients.

Another possible source of enhanced adhesion from transcrystallinity results from the greater stiffness of the oriented interphase compared with the bulk matrix. The dependence of shear stress transmission on the ratio of fiber to interphase modulus was predicted, [Kelley, 1986] and shown experimentally, [Rao, 1990]. Although direct measurements of the stiffness of the transcrystalline interphase are probably not possible because of the small size, the strongly oriented crystalline material may be expected to have significantly greater shear modulus than either the amorphous or spherulitic crystalline forms of the material. Moreover, increasing interphase thickness will increase the overall stiffness of the local microstructure, since a thick layer of high shear modulus material has a greater stiffness than a thin layer surrounded by lower modulus material.

Yet another possible source of improved shear tractions associated with transcrystallinity arises from the intimate fiber/matrix contact achieved during the process of fiber nucleation of matrix crystallization. Strong dispersion bonding forces may be expected to result from the close fiber/matrix association resulting from coherence between the graphitic fiber structure and epitaxially crystallized polymer chains.

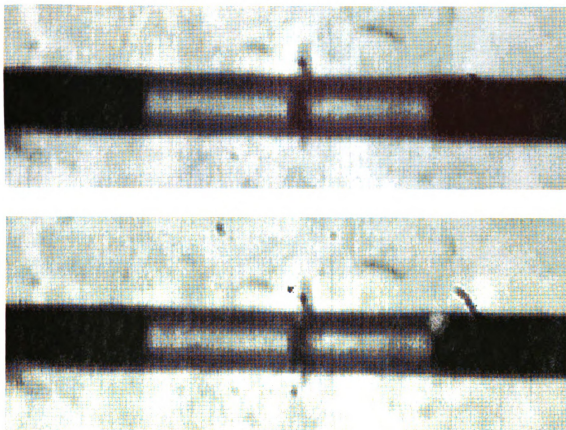


Figure 112. TOM of AU4 breaks in Nylon 6,6.

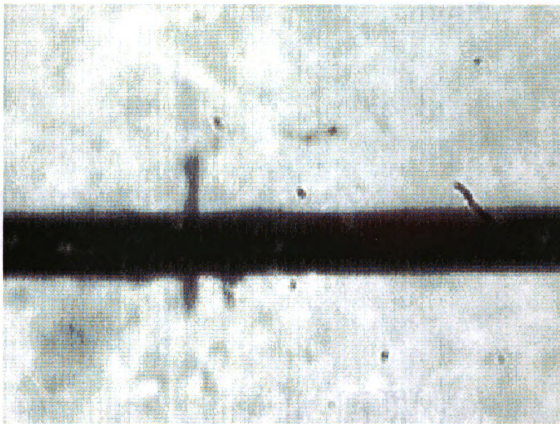


Figure 113. TOM of AS4 break in rapidly cooled Nylon 6,6.

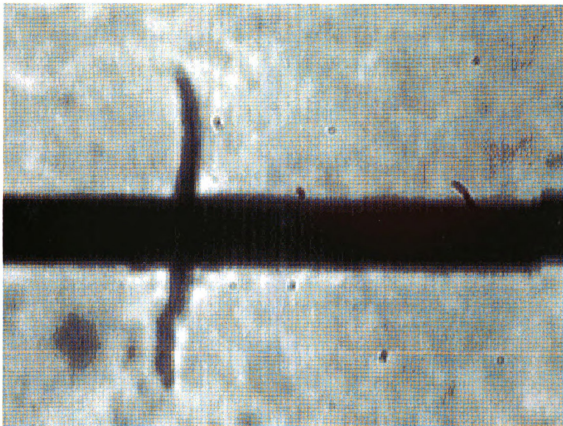


Figure 114. TOM of AS4 break in Nylon 6,6 slowly cooled from 275 °C.

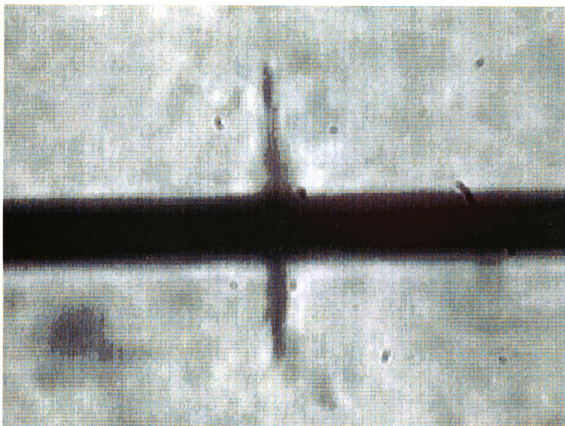


Figure 115. TOM of AS4 in Nylon 6,6 cons. @ 275 °C, iso-xtal @ 225 °C.

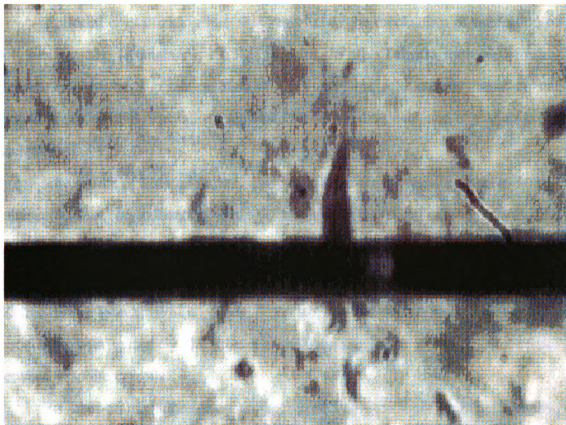


Figure 116. TOM of AS4 in Nylon 6,6 cons. @ 300 °C, iso-xtal @ 245 °C.

Epitaxial crystallization has been reported as the mechanism of nucleation of polymer crystals, [Kumamaru, 1983], [Tuinstra, 1970]. Tuinstra immersed freshly cleaved graphite basal plane surfaces in a polyethylene solution and found crystal growth at preferential orientations separated by 60° , strong evidence of true epitaxial nucleation.

The source of fiber nucleant activity may also arise from a "pseudo-epitaxial" enhancement of crystallization arising from the conjunction of molecularly flat graphitic basal planes [Hoffman, 1988] with the polymer melt. The spherulitic structures in polymer crystals are built up from flat, lamellar crystals [Keller, 1977], [Keith, 1986] [Stack, 1988]. These lamellae may be significantly stabilized by association with extremely flat surfaces, in particular in the presence of a corner between graphite crystals.

As fiber-matrix adhesion increased in moving from AU4 to AS4 fibers and with different processing conditions, a change occurred in failure mode from interfacial debonding with small radial matrix cracks to extensive matrix cracking with minimal debonding (Figures 112-116).

To investigate the relationship between interfacial shear strength and radial matrix cracking, measurements were made of some representative matrix cracks for five sets of specimens, reported in Table 16. The ISS is plotted against the average diameters of these cracks in Figure 117. Although the number of specimen types was limited, a correlation between higher ISS and greater radial crack diameter can be seen.

These cracks were more irregular than those in thermoset matrices, apparently due to the anisotropy of the matrix. The interaction of the transverse matrix cracks with the anisotropic interphase and matrix regions may be most clearly seen in the confocal scanning optical microscopy images (CSOM).

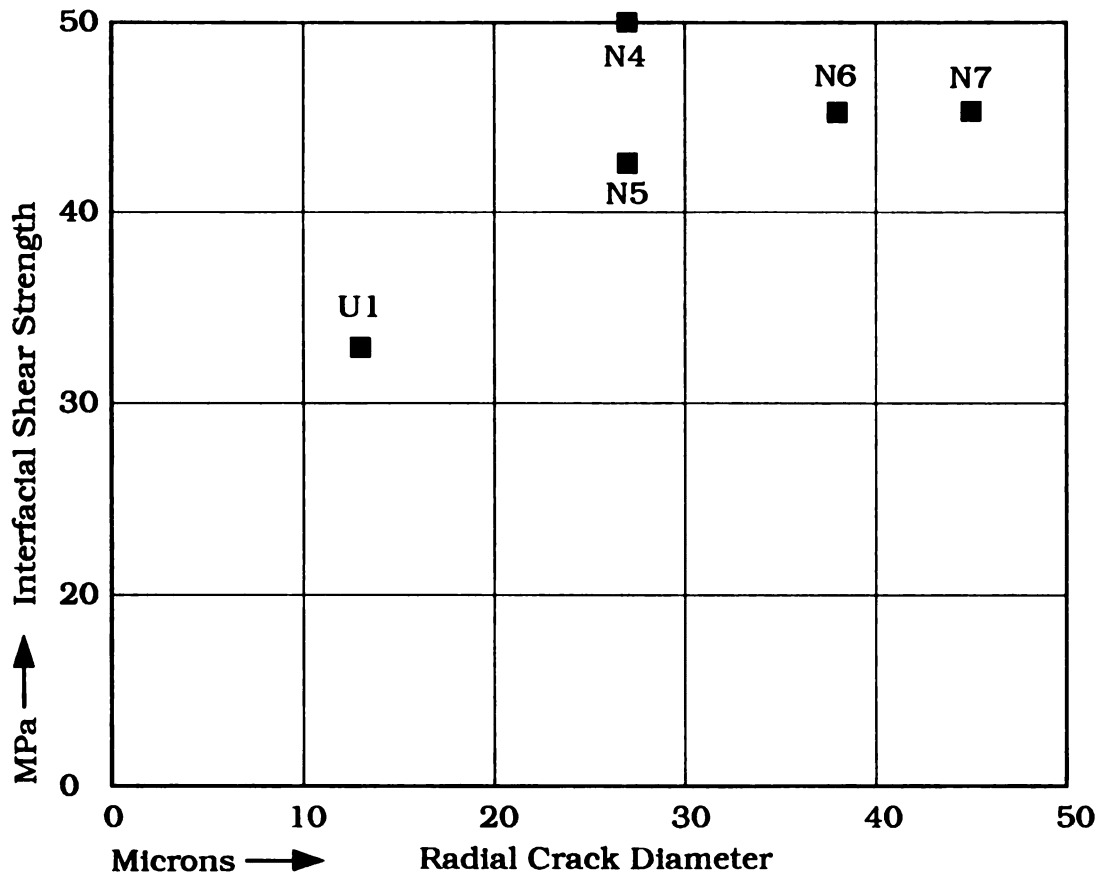


Figure 117. Interfacial shear strength versus radial crack diameter.

Cracks were initiated at random locations by breaks occurring at defects in the fiber. These cracks then propagated into the interphase along the preferred failure planes. For a spherulitic microstructure, this is either between spherulites (interspherulitic) or directly through the center of a spherulite (intra-spherulitic). By extension from spherulitic structures, the preferred failure plane for a strongly oriented transcrystalline interphase should be directly radially outward from the fiber. Examples of these kinds of cracks can be seen in Figures 118 and 119 (interspherulitic cracks), Figures 120 and 121 (intraspherulitic cracks), and Figure 122 (transcrystalline crack).

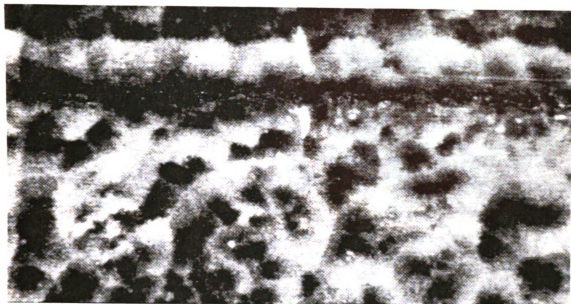


Figure 118. CSOM of AS4 break initiated interspherulitic crack #1.



Figure 119. CSOM of AS4 break initiated interspherulitic crack #2.

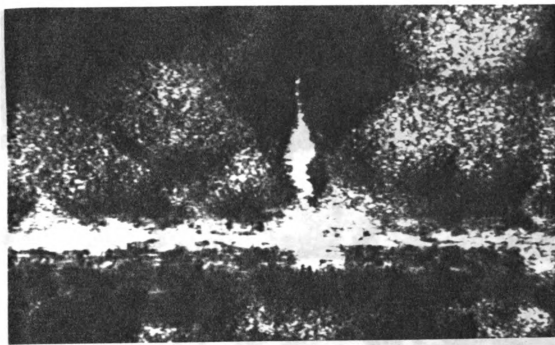


Figure 120. CSOM of AS4 break initiated intraspherulitic cracks #1.

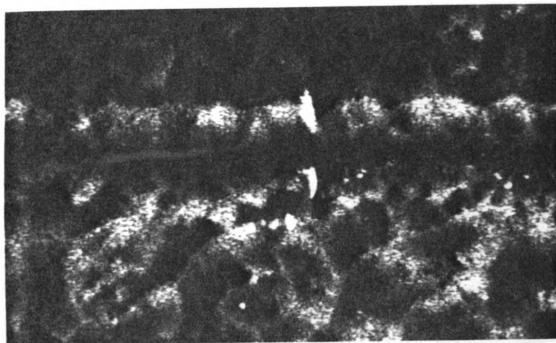


Figure 121. CSOM of AS4 break initiated intraspherulitic cracks #1

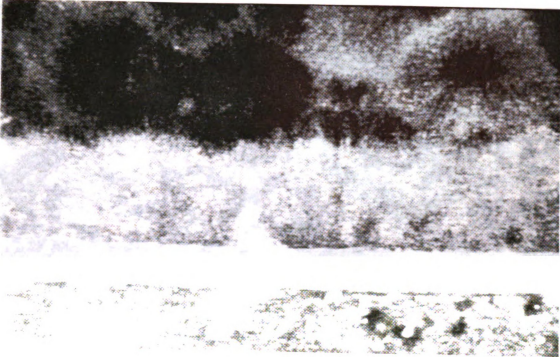


Figure 122. CSOM of AS4 break initiated transcrystalline crack #1.

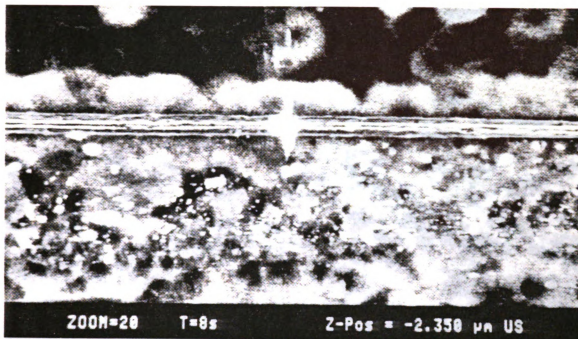


Figure 123. CSOM optical section of AS4 break in Nylon 6,6, Z= 2.35.

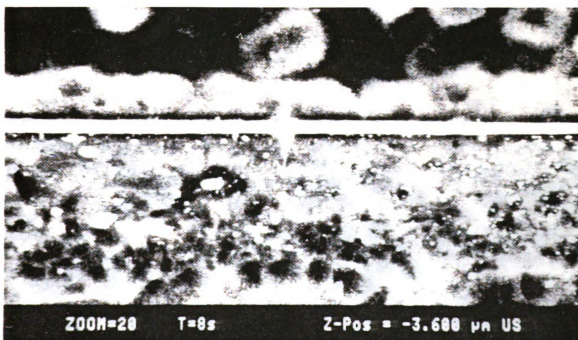


Figure 124. CSOM optical section of AS4 break in Nylon 6,6, Z= 3.6.

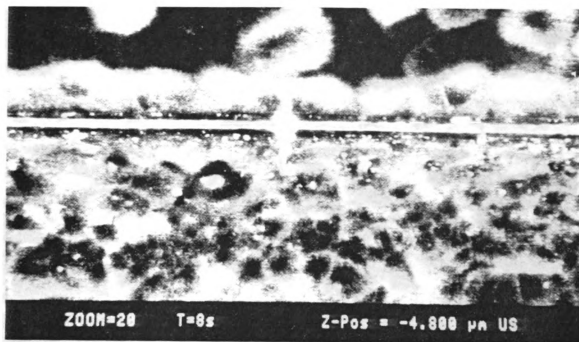


Figure 125. CSOM optical section of AS4 break in Nylon 6,6, Z= 4.8.

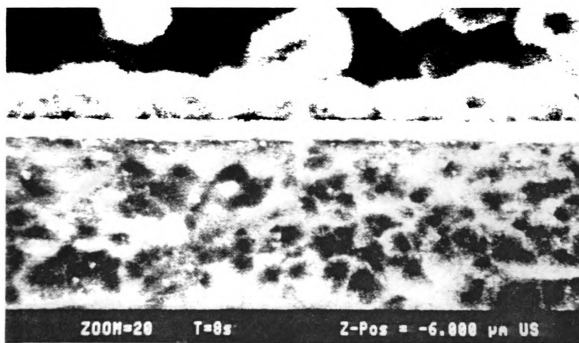


Figure 126. CSOM optical section of AS4 break in Nylon 6,6, Z= 6.0.

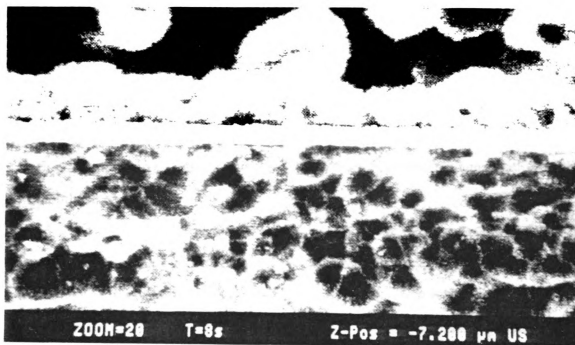


Figure 127. CSOM optical section of AS4 break in Nylon 6,6, Z= 7.2.

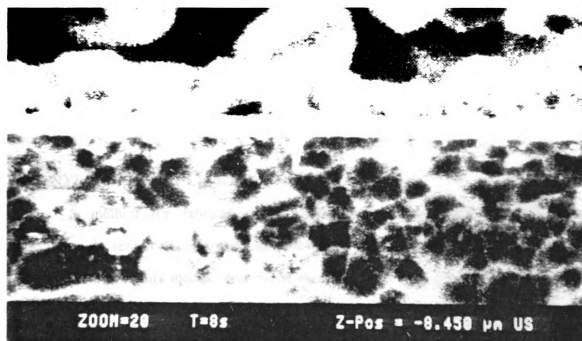


Figure 128. CSOM optical section of AS4 break in Nylon 6,6, Z= 8.45

7.4.3 HEATED STAGE MICROSCOPE OBSERVATIONS

Heated stage microscope observations showed that nucleation of crystallization at the fiber surface slightly preceded that in the bulk matrix. This nucleation took place in the absence of any shear deformations, which tend to additionally promote nucleation and which are likely to occur during processing of high V_f composites due to flow of the matrix material and thermal contraction of the melt in relation to the immobile fiber mass.

The fact that crystallization occurs as a result of nucleation at the fiber surface implies that extremely close contact exists at the fiber/matrix interface, closer than that which is likely to occur as a result of the growth of spherulites nucleated within the matrix eventually impinging upon the fiber. Since both polar and dispersive forces are strongly affected by distance, this close contact significantly increases adhesion.

Spherulite sizes were measured for specimens preheated at 275 and 300 °C and isothermally crystallized at 245, 250 and 255 °C on a microscope hot stage as a measure of the dependence of nucleant density on thermal treatment. Preheating at 300 °C was found to reduce this density by approximately 2 orders of magnitude compared with the 275 °C preheat. These temperatures were chosen for ISS specimen fabrication to investigate the influence of this variable.

7.5 NYLON 6,6 CONCLUSIONS

A method for fabricating and interrogating single fiber fragmentation specimens in semicrystalline thermoplastics has been developed that allows optical observations of failure modes. Interfacial shear strengths were found to increase with increases in the development of transcrystallinity at slower cooling rates and in specimens isothermally crystallized at low temperatures. CSOM observations of the interaction of fiber failure induced matrix cracks indicate that matrix cracks begin at random fiber breaks and migrate toward preferred failure planes within the matrix.

CHAPTER 8

CONCLUSIONS

8.1 FRAGMENTATION TEST CONCLUSIONS

The fragmentation test contains a wealth of potentially valuable information about the properties of the fiber-matrix interface and interphase, and the interaction of failure modes with all composite constituents. This information has only begun to be exploited, with numerous recordable and reproducible parameters that have received little or no attention in the literature. Some of these parameters extract information with less ambiguity than the critical length approach, since they involve a single mode of failure, analyzed by a single algorithm. The critical length approach, however, also has an advantage in that it allows for a single system for comparing all fragmentation test results.

Fiber failure strain energy release can significantly alter the failure modes and measured critical lengths in fragmentation tests. This effect has been largely ignored in the literature, and has clouded the interpretation of data. Other interfacial shear strength measurement methods do not include a contribution from fiber failure energy and so are fundamentally different measurements. In addition, these methods involve cracking with different symmetries, and therefore different potential crack growth habits and results.

8.3 ISFS CONCLUSIONS

The feasibility of determining fiber strengths at short gage lengths by in-situ fiber strength testing has been demonstrated. Results obtained from single-fiber fragmentation, in-situ fiber strength testing are in close agreement with those from short gage length fiber tension tests. The number of fiber flaws per unit length was found to increase exponentially with increasing strain increment.

The necessity of determining fiber prestrain produced during specimen fabrication was shown. A computerized weakest link model has been developed to analyze the experimentally determined fiber flaw distributions and to simulate the single-fiber fragmentation process.

8.4 ONVFA CONCLUSIONS

An optical method for the determination of composite volume fractions has been developed. The accuracy of the method is not influenced by small image variations because the data is extracted as a digital parameter, the number of fibers. The method is an absolute technique, which does not require calibration by any other test, and which provides fiber volume distribution information with unequalled spatial resolution.

8.5 IM6 CONCLUSIONS

Surface treatment of IM6 fibers produced an increase in chemisorbed surface oxygen. This increase occurred rapidly for the untreated fibers, and then at a lower, linear rate as surface treatment continued. This difference is probably attributable to the availability of reactive, edge, corner, and disordered carbon atom sites on the untreated fibers, compared with exclusively graphitic basal plane carbon atoms on the treated fibers.

The interfacial shear strength increased almost linearly with increasing surface

oxygen percentage and with polar surface free energy, rapidly rising with 20% surface treatment compared to the untreated fiber and then increasing at a lower rate as surface treatment continued. Although these variables were shown to be closely correlated, actual causality is much more difficult to establish. It cannot be conclusively stated that there is a cause and effect relationship based upon these data, though such a relationship is strongly supported. The addition of the toughened "G" size also increased the measured values of interfacial shear strength, and caused a change in failure mode in the fragmentation specimens from entirely interfacial to combined interfacial and interphase yielding.

The Mode II fracture toughness increased with increasing fiber surface treatment and with the addition of the size. Sizing led to a particularly large increase, probably because of increased plastic deformation of the interphase region. This increase closely followed that of ISS, except for the sized case.

Transverse flexural strengths were somewhat enigmatic and may have been influenced by fiber bridging artifacts or differences in fiber volume fraction.

Interlaminar shear strengths increased with surface treatment compared with the untreated fibers, but increased at a low rate for all surface treated and treated and sized fibers. This was probably due to a matrix dominated failure mode with small interfacial effects. Nevertheless, the plot of ILSS versus ISS shows an approximately linear relationship.

8.6 POLYCARBONATE CONCLUSIONS

Interfacial shear strengths of carbon fibers in pure polycarbonate were found to increase with increasing consolidation temperature and time. Specimens produced by solvent deposition at low temperatures showed much lower ISS while specimens with solvents present but consolidated at higher temperatures showed good adhesion. Lexan matrix specimens appeared to reach a limiting ISS which did not vary

significantly with consolidation temperature or pressure.

Slowly cooled Lexan matrix specimens showed evidence of shear band formation in both polarized and unpolarized microscope observations. Rapidly cooled Lexan specimens appeared to fail by stick-slip interfacial cracking accompanied by some matrix deformation. Pure polycarbonate specimens showed intense birefringence patterns, indicating strong adhesion.

8.7 NYLON 6,6 CONCLUSIONS

A method for fabricating and interrogating single fiber fragmentation specimens in semicrystalline thermoplastics has been developed that allows optical observations of failure modes. Interfacial shear strengths were found to increase with increases in the development of transcrystallinity. CSOM observations of the interaction of fiber failure induced matrix cracks indicate that matrix cracks begin at random fiber breaks and migrate toward preferred failure planes within the interphase and bulk matrix.

8.8 THERMOSET AND THERMOPLASTIC MATRIX CONCLUSIONS

The three classes of matrices studied in this investigation, thermoset, amorphous thermoplastic, and semicrystalline thermoplastic, differ in microstructure, reactivity of the melt, moduli, and other properties. The pattern of their adhesion to untreated and surface treated carbon fibers, however, is remarkably similar. The interfacial shear strength of untreated AU4 and surface treated, AS4 fibers in a thermoset epoxy, an amorphous thermoplastic, polycarbonate, and a semicrystalline thermoplastic, Nylon 6,6 are plotted in Figure 129. As can be seen, in all three matrices the AU4 fiber adhesion is significantly lower than the AS4 fiber. Moreover, the magnitude of the adhesion is approximately the same, with higher values for

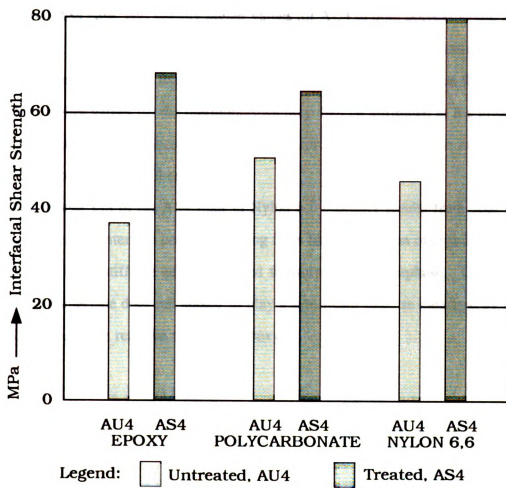


Figure 129. ISS of AU4 and AS4 fibers in thermoset and thermoplastic matrices.

the Nylon 6,6 AS4 case, and slightly higher values for AU4 in both polycarbonate and Nylon 6,6 than for epoxy. The similarity implies that a similar failure mechanism is involved for the AU4 fibers, that of failure within a weak surface layer in the fiber. The slightly higher values for the thermoplastics may then be attributed to the greater thermal contraction stresses increasing the normal force and therefore the maximum shear strength on this weak fiber layer.

The greater ISS of the AS4 fiber in Nylon 6,6 probably results from both the intimate fiber/matrix interface contact resulting from fiber nucleation of crystallization and from the higher stiffness of the oriented transcrystalline interphase. Chemical bonding at the interface does not appear to play a significant role, as indicated by the lower ISS of the more reactive thermoset epoxy.

APPENDIX A

SOURCE CODE FOR FIBERTRACK, FRAGMENTATION TEST DATA ACQUISITION AND ANALYSIS SYSTEM

The following program is the source code listing written compiled AmigaBasic (Absoft, AC-Basic) for the FiberTrack, fragmentation test data acquisition and analysis program described in chapter 7. Weibull calculation routines were translated and adapted from a mainframe Fortran program (author unknown). A list of subroutines and a brief description of their functions precedes the actual code. Long code lines have been reformatted, with leading hyphens attached to the second portions.

Main: Main program loop.

Start: Sets up menu interrupts and "sleeps" here until summoned by a menu call from the user.

StartupText: Displays copyright information and specifies df1: drive for all data diskettes.

ArrayDimensions: Defines all data arrays and allocates space to them.

Initialize: Sets all initial variables, file names, graphics colors, default moduli.

GammaData: Sets up a look-up table of the Gamma function.

InitializeMenu: Initializes the menu selections.

CheckMenu: Arrival point when user makes a menu selection. Finds column and routes to submenus.

Filemenu: Checks first column of menu items and routes to appropriate subroutine.

Graphics: Checks second column of menu items and routes to appropriate subroutine.

Tracking: Checks third column of menu items and routes to appropriate subroutine.

Calcs: Checks fourth column of menu items and routes to appropriate subroutine.

GammaLoader: Inputs Weibull shape and scale factors from user and performs Gamma function calculations.

FiberData: Inputs data on fiber diameter, modulus, etc. from user for all calculations.

MatrixData: Inputs data on matrix name, modulus, etc. from user for printouts.

LengthStrength: Simply sets fiber tensile strength at this point, intended to be upgraded to perform log-linear extrapolation to automatically find strength @ length.

GammaPlot: Produces a graphical plot of the Gamma function.

Dir: Lists directory of the df1: drive.

WriteTrack: Writes a file with the positions of all breaks, dial gage reading, strain, etc.

ReadTrack: Reads files written by WriteTrack.

ReadTracks: Reads a set of tracks with the same root file name and different track numbers.

PrintLengths: Prints out the fragment lengths, calculated from the break positions.

PrintBreakList: Prints out the break positions in a column format for a set of tracks.

WriteLengths: Writes a file with the fragment lengths, rather than positions.

WriteBreakList: Writes a file with the break positions for a set of tracks in column format.

WriteBreaks: Writes a file with the break positions, track by track.

ReadBreaks: Reads files written by WriteBreaks.

Tracker: Startup for tracking fiber break positions. Initializes file name, dial gage, asks if track should be destrained, sets up mouse interrupts.

Time0: Waits for joystick port input to note translation stage startup time and direction. Routes to "Loop".

Loop: Tracking routine loops here as long as the joystick port input is non-zero. Goes to "NewBreak" whenever user clicks mouse button, and when joystick port becomes zero at the moment the stage is halted. After stage stops prompts the user for the distance traversed and routes to "ScaleTrack", "WriteTrack", and "WeibullLoader".

NewBreak: Records the exact time of each mouse click, calculates the delta time from translation startup to that time, calculates a break position based on an assumed velocity that contains the correct sign for the stage motion direction, prints out the number of breaks, and generates an audio feedback tone to confirm that a break was recorded.

ScaleTrack: Rescales the track to the actual distance traversed, based on the user input. Destrains the track if desired.

ZeroTrack: Sets track to zero breaks and all break positions to zero.

ShowFibers: Displays a graphical representation of all break positions for one or more tracks. Allows user specification of breaks using mouse.

CheckMouse: Checks for mouse clicks and if on lower part of screen scrolls the break display to the left or right. If on upper part of screen checks to see which track

and
break is being selected and stores its index in the DataT() array.

DrawFibers: Performs the actual fiber display graphic output.

ListBreaks: Lists track and break numbers for selected breaks.

Cleanup: Clears the screen.

Quit: Resets menu and stops program operation.

Palet: Initializes screen, window, and pallettes.

WeibullLoader: Loads fragment lengths into Weibull routine. This version always Weibullizes track 1.

Weibull: Performs Weibull calculations, displays results, calls "LengthStrength" and "Gamma" routines.

Gamma: Performs Gamma function calculations based on lookup table and linear interpolation, prints out results.

FIBERTRACK 1.0 PROGRAM LISTING

```
'=====Single Fiber Critical Length Test=====
'=====Fiber Break Tracker - Data Input Program
```

```
'10/1/1989, Copyright Mark Waterbury
CLEAR ,25000
CLEAR ,70000&
```

```
Programloop:
GOSUB ArrayDimensions
GOSUB Initialize 'Sets Graphics and screen constants
GOSUB Palet' Sets palette, screen, and window
GOSUB StartupText
GOSUB InitializeMenu
```

```
Start:
ON MENU GOSUB CheckMenu : MENU ON
Unfinished = -1
WHILE Unfinished
SLEEP 'this program is event driven
WEND
```

```
StartupText:
CLS
LOCATE 10,1
PRINT "This program Copyrighted by Mark C. Waterbury
PRINT "10,1,1989 Licensed for use by the
PRINT "Composite Materials and Structures Center
PRINT "May not be reproduced or duplicated without the
```

```

PRINT "written consent of the author.
LOCATE 18,1
PRINT "Insert formatted data disk in df1:
PRINT "All track files will be saved to that disk.
RETURN

```

ArrayDimensions:

```

DIM X(30,200)
DIM NBreaks(30), Length(30), NewBreaks(30)
DIM DG(30),Strain(30), TStress(30)
DIM AveStrain(30) 'Ave. of track and the preceeding one
DIM FI$(30)
DIM DataT(200),DataB(200)
DIM Fiber(200),Stress(200)
DIM W(2000), WLog(2000) ' For Weibull Routine
DIM Gamma (205)
RETURN

```

Initialize:

```

WIDTH "LPT1:",255
Modulus = 34000000& 'modulus set to AS4 default
AS4Mod = 34000000& 'AS4 modulus, psi
IM6Mod = 40400000& IM6 modulus, psi
Pi = 3.14159
Scrx = 640:ScrY = 400
FT% = 160:FB% = FT% + 15
Gc% = 2 'gap color (integer)
Gap% = 4 'break gap
fc1% = 6 'fiber color 1
fc2% = 7 'fiber
Velocity = 200
FI$(0) = "00":FI$(1) = "01":FI$(2) = "02":FI$(3) = "03"
FI$(4) = "04":FI$(5) = "05":FI$(6) = "06":FI$(7) = "07"
FI$(8) = "08":FI$(9) = "09":FI$(10) = "10":FI$(11) = "11"
FI$(12) = "12":FI$(13) = "13":FI$(14) = "14":FI$(15) = "15"
FI$(16) = "16":FI$(17) = "17":FI$(18) = "18":FI$(19) = "19"
FI$(20) = "20":FI$(21) = "21":FI$(22) = "22":FI$(23) = "23"
FI$(24) = "24":FI$(25) = "25":FI$(26) = "26":FI$(27) = "27"
FI$(28) = "28":FI$(29) = "29":FI$(30) = "30"
GOSUB GammaData
RETURN

```

GammaData:

```

FOR I = 100 TO 200
READ Gamma(I)
NEXT I
DATA 1.00,.99433,.98884,.98355,.97844
DATA .9735,.96874,.96415,.95973,.95546
DATA .95135,.94740,.94359,.93993,.93642
DATA .93304,.92980,.92670,.92373,.92089
DATA .91817,.91558,.91311,.91075,.90852
DATA .90640,.90440,.90250,.90072,.89904
DATA .89747,.89600,.89464,.89338,.89222

```

```

DATA .89115,.89018,.88931,.88854,.88785
DATA .88726,.88676,.88636,.88604,.88581
DATA .88566,.88560,.88563,.88575,.88595
DATA .88623,.88659,.88704,.88757,.88818
DATA .88887,.88964,.89049,.89142,.89243
DATA .89352,.89468,.89592,.89724,.89864
DATA .90012,.90167,.90330,.90500,.90678
DATA .90864,.91057,.91258,.91466,.91683
DATA .91906,.92137,.92376,.92623,.92877
DATA .93138,.93408,.93685,.93989,.94261
DATA .94561,.94869,.95184,.95507,.95838
DATA .96177,.96523,.96877,.97240,.97610
DATA .97988,.98374,.98768,.99171,.99581,1!
  FOR I = 101 TO 200
    N = (I-100)/100
    Gamma(I-100) = Gamma(I)/N
  NEXT I

```

```
RETURN
```

InitializeMenu:

```

MENU 1,0,1,"File"
MENU 1,1,1,"Write Break File"
MENU 1,2,1,"Read Break File"
MENU 1,3,1,"Read Track"
MENU 1,4,1,"Read Set of Tracks"
MENU 1,5,1,"Dir"
MENU 1,6,1,"Quit, return to Basic"
MENU 2,0,1,"Calcs"
MENU 2,1,1,"Weibull Calcs"
MENU 2,2,1,"Gamma Calcs"
MENU 2,3,1,"Gamma Plot"
MENU 2,4,1,"Fiber Data"
MENU 2,5,1,"Matrix Data"
MENU 3,0,1,"Graphs"
MENU 3,1,1,"Show Fibers"
MENU 3,2,1,"Clear Screen"
MENU 3,3,1,"Write Break List"
MENU 3,4,1,"Write Length List"
MENU 3,5,1,"Print Break List"
MENU 3,6,1,"Print Length List"
MENU 4,0,1,"Tracker"
MENU 4,1,1,"Track Breaks"
MENU 4,2,1,"List Selected Breaks"

```

```
RETURN
```

CheckMenu:

```

MenuId = MENU(0)
MenuItem = MENU(1)
ON MenuId GOSUB Filemenu,Calcs,Graphics,Tracking
RETURN

```

Filemenu:

```
ON MenuItem GOSUB WriteBreaks,ReadBreaks,ReadTrack,
```

```
-ReadTracks,Dir,Quit
RETURN
```

Graphics:

```
ON MenuItem GOSUB ShowFibers,Cleanup,WriteBreakList, WriteLengths,
PrintBreakList, PrintLengths
RETURN
```

Tracking:

```
ON MenuItem GOSUB Tracker,ListBreaks
RETURN
```

Calcs:

```
ON MenuItem GOSUB WeibullLoader,GammaLoader,GammaPlot, FiberData,
MatrixData
RETURN
```

GammaLoader:

```
INPUT "File Name ",Fil$
INPUT "Alpha, Beta (set Alpha = 0 to quit) ",Alpha,Beta
IF Alpha = 0 THEN RETURN
GOSUB Gamma
GOTO GammaLoader
RETURN
```

FiberData:

```
CLS
INPUT "Fiber Designation ",FDesig$
INPUT "Fiber Diameter (microns) ",Diameter
INPUT "Fiber Strength @ 25 mm ",Strength0
INPUT "Fiber Modulus ",Modulus
RETURN
```

MatrixData:

```
CLS
INPUT "Matrix Designation",MDesig$
INPUT "Matrix Tensile Strength (psi) ",MTStrength
INPUT "Matrix Shear Strength (psi) ",MSStrength
INPUT "Matrix Tensile Modulus (psi) ",MTModulus
INPUT "Matrix Shear Modulus (psi) ",MSModulus
RETURN
```

LengthStrength:

```
Strength = Strength0
RETURN
```

GammaPlot:

```
PSET (0,10*Gamma(100)),1
FOR I = 0 TO 200
LINE -(I * 3,10 * Gamma(I)),1
NEXT I
FOR I = 0 TO 200 STEP 25
LINE (I * 3 ,180)-(I* 3,200),2
```

```

NEXT I
  INPUT "Printout? Y/N ",Pr$
  IF Pr$ <> "Y" THEN GOTO NoPrint
  LPRINT "Gamma Function for N = 0 to 2.00 in 1/100 ths"
  LPRINT
  FOR I = 0 TO 200 STEP 5
  LPRINT USING "###.#####";I/100;Gamma(I);Gamma(I+1);
  -Gamma(I+2);Gamma(I+3);Gamma(I+4)
  NEXT I
NoPrint:
RETURN

```

```

Dir:
  FILES "df1:"
RETURN

```

```

WriteTrack:
  FilT$ = Fil$ + Fl$(nT)
  OPEN FilT$ FOR OUTPUT AS 1
  WRITE #1, FilT$
  WRITE #1, nT
  WRITE #1,DG(nT),Strain(nT)
  WRITE #1,NBreaks(nT),Length(nT)
  FOR K = 1 TO NBreaks(nT)
  WRITE #1, X(nT,K)
  NEXT K
  CLOSE #1
  PRINT "File saved as ";FilT$
RETURN

```

```

ReadTrack:
  CLS
  INPUT "File name ",Fil$
  INPUT "Track ",nT
  IF nT = 0 THEN nT = 1
  IF nT > NTracks THEN NTracks = nT
  FilT$ = "df1:" + Fil$ + Fl$(nT)
  OPEN FilT$ FOR INPUT AS 1
  INPUT #1, F$
  INPUT #1, TT
  INPUT #1,DG(nT),Strain(nT)
  INPUT #1,NBreaks(nT),Length(nT)
  FOR K = 1 TO NBreaks(nT)
  INPUT #1, X(nT,K)
  NEXT K
  CLOSE #1
RETURN

```

```

ReadTracks:
  CLS
  INPUT "Parent File Name ",Fil$

```

```

INPUT "First and Last Tracks ",NFirst,NLast
NTracks = NLast - NFirst + 1
FOR nT = NFirst TO NLast
FilT$ = "df1:" + Fil$ + Fl$(nT)
OPEN FilT$ FOR INPUT AS 1
  INPUT #1, F$
  INPUT #1, Tn
  INPUT #1,DG(nT),Strain(nT)
  INPUT #1,NBreaks(nT),Length(nT)
  FOR K = 1 TO NBreaks(nT)
  INPUT #1, X(nT,K)
  NEXT K
CLOSE #1
NEXT nT
RETURN

```

PrintLengths:

```

LOCATE 1,1
LPRINT Fil$
LPRINT NTracks
FOR I = 1 TO NTracks-1
LPRINT USING "   ##";I;
NEXT I
LPRINT USING "   ##";I
FOR I = 1 TO NTracks - 1
LPRINT USING "   ###";DG(I);
NEXT I
LPRINT USING "   ###";DG(I)
FOR I = 1 TO NTracks -1
LPRINT USING " ##.####";Strain(I)-1;
NEXT I
LPRINT USING " ##.####";Strain(I)-1
FOR J = 1 TO NTracks -1
LPRINT USING "   ###";NBreaks(J);
NEXT J
LPRINT USING "   ###";NBreaks(J)
  MaxBreaks = NBreaks(1)
  FOR I = 2 TO NTracks -1
IF NBreaks(I) > MaxBreaks THEN MaxBreaks = NBreaks(I)
  NEXT I
FOR I = 2 TO MaxBreaks
FOR J = 1 TO NTracks -1
IF X(J,I) - X(J,I-1) > 0 THEN
Lx% = (X(J,I)-X(J,I-1))
LPRINT USING "   ####"; Lx%;
ELSE
LPRINT USING "   ####";X(J,I);
END IF
NEXT J
IF X(J,I) - X(J,I-1) > 0 THEN
Lx% = (X(J,I)-X(J,I-1))
LPRINT USING "   ####"; Lx%
ELSE

```

```

        LPRINT USING "    ####";X(J,I)
    END IF
NEXT I
RETURN

```

PrintBreakList:

```

LPRINT Fil$
LPRINT NTracks
FOR I = 1 TO NTracks-1
    LPRINT USING "    ## ";I;
NEXT I
LPRINT USING "    ##";I
FOR I = 1 TO NTracks - 1
    LPRINT USING "    ###";DG(I);
NEXT I
LPRINT USING "    ###";DG(I)
FOR I = 1 TO NTracks -1
    LPRINT USING " ##.####";Strain(I)-1;
NEXT I
LPRINT USING " ##.####";Strain(I)-1
FOR J = 1 TO NTracks -1
    LPRINT USING "    ### ";NBreaks(J);
NEXT J
LPRINT USING "    ###";NBreaks(J)
    MaxBreaks = NBreaks(1)
    FOR I = 2 TO NTracks -1
        IF NBreaks(I) > MaxBreaks THEN MaxBreaks = NBreaks(I)
    NEXT I
FOR I = 1 TO MaxBreaks
    FOR J = 1 TO NTracks -1
        XX% = X(J,I)
        LPRINT USING "    #####"; XX%;
    NEXT J
    XX% = X(J,I)
    LPRINT USING "    #####"; XX%
NEXT I
CLOSE #1
RETURN

```

WriteLengths:

```

LOCATE 1,1
INPUT "Save Lengths ",Fil$
Fil$ = "df1:" + Fil$
OPEN Fil$ FOR OUTPUT AS 1
WRITE #1, Fil$
WRITE #1, NTracks
FOR I = 1 TO NTracks-1
    PRINT #1, USING "    ##";I;
NEXT I
PRINT #1, USING "    ##";I
FOR I = 1 TO NTracks - 1
    PRINT #1, USING "    ###";DG(I);
NEXT I

```

```

PRINT #1, USING "   ###";DG(I)
FOR I = 1 TO NTracks -1
PRINT #1, USING " ##.####";Strain(I)-1;
NEXT I
PRINT #1, USING " ##.####";Strain(I)-1
  FOR J = 1 TO NTracks -1
  PRINT #1, USING "   ###";NBreaks(J);
  NEXT J
  PRINT #1, USING "   ###";NBreaks(J)
  MaxBreaks = NBreaks(1)
  FOR I = 2 TO NTracks -1
  IF NBreaks(I) > MaxBreaks THEN MaxBreaks = NBreaks(I)
  NEXT I
  FOR I = 2 TO MaxBreaks
  FOR J = 1 TO NTracks -1
  IF X(J,I) - X(J,I-1) > 0 THEN
  Lx% = (X(J,I)-X(J,I-1))
  PRINT #1, USING "   ####"; Lx%;
  ELSE
  PRINT #1, USING "   ####";X(J,I);
  END IF
  NEXT J
  IF X(J,I) - X(J,I-1) > 0 THEN
  Lx% = (X(J,I)-X(J,I-1))
  PRINT #1, USING "   ####"; Lx%
  ELSE
  PRINT #1, USING "   ####";X(J,I)
  END IF
  NEXT I
CLOSE #1
RETURN

```

WriteBreakList:

```

LOCATE 1,1
INPUT "Save Break List ",Fil$
Fil$ = "df1:" + Fil$
OPEN Fil$ FOR OUTPUT AS 1
WRITE #1, Fil$
WRITE #1, NTracks
FOR I = 1 TO NTracks-1
PRINT #1, USING "   ## ";I;
NEXT I
PRINT #1, USING "   ##";I
FOR I = 1 TO NTracks - 1
PRINT #1, USING "   ####";DG(I);
NEXT I
PRINT #1, USING "   ####";DG(I)
FOR I = 1 TO NTracks -1
PRINT #1, USING " ##.####";Strain(I)-1;
NEXT I
PRINT #1, USING " ##.####";Strain(I)-1
  FOR J = 1 TO NTracks -1
  PRINT #1, USING "   ## ";NBreaks(J);

```

```

NEXT J
PRINT #1, USING "   ###";NBreaks(J)
  MaxBreaks = NBreaks(1)
  FOR I = 2 TO NTracks -1
  IF NBreaks(I) > MaxBreaks THEN MaxBreaks = NBreaks(I)
  NEXT I
  FOR I = 1 TO MaxBreaks
  FOR J = 1 TO NTracks -1
  XX% = X(J,I)
  PRINT #1, USING "   #####"; XX%;
  NEXT J
  XX% = X(J,I)
  PRINT #1, USING "   #####"; XX%
  NEXT I
CLOSE #1
RETURN

```

WriteBreaks:

```

LOCATE 1,1
INPUT "Break File Name ",Fil$
Fil$ = "df1:" + Fil$
LOCATE 1,1:PRINT "
OPEN Fil$ FOR OUTPUT AS 1
WRITE #1, NTracks
FOR I = 1 TO NTracks
WRITE #1,T(I),DG(I),Strain(I)
NEXT I
  FOR J = 1 TO NTracks
  WRITE #1,NBreaks(J),Length(J)
  NEXT J
  FOR I = 1 TO NTracks
  FOR J = 1 TO NBreaks(I)
  WRITE #1,X(I,J)
  NEXT J
  NEXT I
CLOSE #1
RETURN

```

ReadBreaks:

```

LOCATE 1,1
INPUT "Read Breaks ",Fil$
Fil$ = "df1:" + Fil$
OPEN Fil$ FOR INPUT AS 1
INPUT #1, NTracks
FOR I = 1 TO NTracks
INPUT #1,Tn,DG(I),Strain(I)
NEXT I
  FOR J = 1 TO NTracks
  INPUT #1,NBreaks(J),Length(J)
  NEXT J
  FOR I = 1 TO NTracks
  FOR J = 1 TO NBreaks(I)

```

```

        INPUT #1,X(I,J)
        NEXT J
    NEXT I
CLOSE #1
RETURN

```

Tracker:

```

CLS
INPUT "File Name? ",Fil$
INPUT "Track Number (RETURN for single track) ",nT
IF nT = 0 THEN nT = 1
INPUT "De-Strain Tracks? 1/0 ",DStrain
IF DStrain THEN INPUT "Track Strain? ",Strain(nT)
PRINT "Set Newport drive to ZERO before starting"
Fil$ = "df1:" + Fil$
LOCATE 5,1:PRINT "Number of breaks = "
GOSUB ZeroTrack
ON MOUSE GOSUB NewBreak:MOUSE ON

```

Time0:

```

IF STICK(3) = 1 THEN
Tm# = TIMER
V = Velocity
GOTO Loop
END IF
IF STICK(3) = -1 THEN
Tm# = TIMER
V = -Velocity
GOTO Loop
END IF
GOTO Time0

```

Loop:

```

' Cycles through this loop while tracking,
' going to NewBreak on Mouse
WHILE STICK(3) <> 0
LOCATE 13,1:PRINT "Moving":LOCATE 13,1:PRINT " "
WEND
GOSUB NewBreak ' Records end of track as the last break
CLS
INPUT "Length traversed (microns) ",Length(nT)
IF Length(nT) = 0 THEN RETURN
GOSUB ScaleTrack
GOSUB WriteTrack
GOSUB WeibullLoader
IF NTracks = 0 THEN NTracks = 1
RETURN

```

NewBreak:

```

T# = TIMER
DeltaT# = TIMER - Tm#
NBreaks(nT) = NBreaks(nT) + 1
X(nT,NBreaks(nT)) = V * DeltaT#

```

```

LOCATE 5,20:PRINT NBreaks(nT)
SOUND 1024,.3
RETURN

```

ScaleTrack:

```

IF X(nT,NBreaks(nT)) = 0 THEN RETURN
Scale = ABS(Length(nT))/ABS(X(nT,NBreaks(nT)))
IF DStrain THEN Scale = Scale / (1 + Strain(nT))
FOR I = 1 TO NBreaks(nT)
X(nT,I) = X(nT,I) * Scale
NEXT I
IF V < 0 THEN
FOR I = 1 TO NBreaks(nT)
X(0,NBreaks(nT)-I+1) = Length(nT) + X(nT,I)
NEXT I
FOR I = 1 TO NBreaks(nT)
X(nT,I) = X(0,I)
NEXT I
END IF
RETURN

```

ZeroTrack:

```

IF nT = 0 THEN nT = 1
FOR I = 1 TO 200
X(nT,I) = 0
NEXT I
NBreaks(nT) = 0
RETURN

```

ShowFibers:

```

N = 0 'Number of data points
CLS
INPUT "Number Fibers? 1/0 ",PNumb
Shift% = -600
ON MOUSE GOSUB CheckMouse:MOUSE ON
GOSUB DrawFibers

```

InkL:

```

Ink$ = INKEY$
IF Ink$ = "0" THEN XOff% = 0:GOSUB DrawFibers
IF Ink$ = "9" THEN XOff% = Last% * Shift%:GOSUB DrawFibers
IF Ink$ = "1" THEN XOff% = Shift%:GOSUB DrawFibers
IF Ink$ = "2" THEN XOff% = 2 * Shift%:GOSUB DrawFibers
IF Ink$ = "3" THEN XOff% = 3 * Shift%:GOSUB DrawFibers
IF Ink$ = "4" THEN XOff% = 4 * Shift%:GOSUB DrawFibers
IF Ink$ = "5" THEN XOff% = 5 * Shift%:GOSUB DrawFibers
IF Ink$ = "6" THEN XOff% = 6 * Shift%:GOSUB DrawFibers
IF Ink$ = "7" THEN XOff% = 7 * Shift%:GOSUB DrawFibers
IF Ink$ = "8" THEN XOff% = 8 * Shift%:GOSUB DrawFibers
IF Ink$ = "Q" THEN :RETURN
IF Ink$ = "q" THEN :RETURN
GOTO InkL
RETURN

```

CheckMouse:

```

F = MOUSE(0)
Mx% = MOUSE(1):My% = MOUSE(2)
IF My% > 175 THEN
  IF Mx% < 160 THEN XOff% = XOff% - Shift% :GOTO MHop
  IF Mx% < 320 THEN XOff% = XOff% - Shift%/2 :GOTO MHop
  IF Mx% < 480 THEN XOff% = XOff% + Shift%/2 :GOTO MHop
  XOff% = XOff% + Shift%

```

MHop:

```

  GOSUB DrawFibers
  END IF
  IF My% < 170 THEN
    Dt = 0:DB = 0
    N = N + 1
    Dt = INT(My%/8)
    DataT(N) = Dt
    FOR I = 1 TO NBreaks(Dt)
      Lx = X(Dt,I)/10 + XOff%
      IF ABS(Lx + 3 - Mx%) < 3 THEN DB = I
    NEXT I
    IF DB = 0 THEN DataT(N) = 0:N = N - 1 :GOTO EndHop
    DataB(N) = DB
    Ly% = Dt * 8
    Lx = X(Dt,DB)/10 + XOff%
    LINE (Lx,Ly%)-(Lx+6,Ly%+2),4,bf
  EndHop:
  END IF
  RETURN

```

DrawFibers:

```

  CLS
  Last% = INT(-X(1,NBreaks(1))/(Shift%*10))
  FOR I = 1 TO NTracks
    Ly% = I * 8
    LINE (0,Ly%)-(640,Ly% + 2),3,bf
    FOR J = 1 TO NBreaks(I)
      Lx = X(I,J)/10 + XOff%
      IF Lx < 0 THEN GOTO NextJ
      IF Lx > 640 THEN GOTO NextJ
      LINE (Lx,Ly%)-(Lx+6,Ly%+2),2,bf
      L1 = I
      Px% = Lx/8
      IF Px% > 39 THEN Px% = 39
      IF Px% < 1 THEN Px% = 1
      IF Lx > 0 AND PNumb THEN LOCATE L1,Px%:PRINT USING "###";J
    NextJ: NEXT J
  NEXT I
  FOR I = 1 TO N
    Ly% = DataT(I) * 8
    Lx = X(DataT(I),DataB(I))/10 + XOff%
    IF Lx < 0 THEN GOTO DataHop
    IF Lx > 640 THEN GOTO DataHop

```

```

LINE (Lx,Ly%)-(Lx+6,Ly%+2),1,bf
DataHop: NEXT I
LINE (0,175)-(640,175),3
FOR I = 0 TO 63
LINE (I*10,175)-(I*10,170),3
NEXT I
FOR I = 0 TO 6
LINE (I*100,175)-(I*100+1,165),3 ,bf
NEXT I
LOCATE 23,1:PRINT -XOff%*10;:PRINT " Type Q to return";
RETURN

```

```

ListBreaks:
CLS
FOR I = 1 TO N
PRINT X(DataT(I),DataB(I))
NEXT I
RETURN

```

```

Cleanup:
CLS
RETURN

```

```

Quit:
MENU RESET
STOP

```

```

Palet:
SCREEN 1,640,200,3,2
WINDOW 1,"FiberTrack Single Fiber IFSS/ISFS Data
- Acquisition and Analysis M.C. Waterbury",,0,1
COLOR 3,0
PALETTE 0,0/15,0/15,2/15 :PALETTE 1,0/15,0/15,15/15
PALETTE 2,5/15,4/15,0/15 :PALETTE 3,15/15,15/15,15/15
PALETTE 4,15/15,12/15,0/15 :PALETTE 5,0/15,15/15,0/15
PALETTE 6,0/15,15/15,15/15 :PALETTE 7,2/15,2/15,2/15
RETURN

```

```

WeibullLoader:
CLS
N = 0
nT = 1 'Always does Track 1 in this version
FOR J = 2 TO NBreaks(nT) - 1
N = N + 1
W(N) = X(nT,J)-X(nT,J-1)
NEXT J
GOSUB Weibull
RETURN

```

```

Weibull:
REM====W(I) must contain the N values to be Weibullized
Sum1# = 0
FOR I = 1 TO N

```

```

WLog(I) = LOG(W(I))
Sum1# = Sum1# + WLog(I)
NEXT I
Sum1# = Sum1# / N
A = .1
FOR Iteration = 1 TO 100
  Sum2# = 0: Sum3# = 0: Sum4# = 0
  FOR I = 1 TO N
    xA = W(I) ^ A
    Sum2# = Sum2# + xA
    Sum3# = Sum3# + xA * WLog(I)
    Sum4# = Sum4# + xA * WLog(I) ^ 2
    Gola = WLog(I)
    PXE = EXP(A * Gola)
    Sum2# = Sum2# + PXE
    Sum3# = Sum3# + PXE * Gola
    Sum4# = Sum4# + PXE * Gola ^ 2
  NEXT I
  F = Sum3# / Sum2# - 1 / A - Sum1#
  Fp = (Sum4#*Sum2#-Sum3#*Sum3#)/(Sum2#*Sum2#)+1/(A*A)
  An = A - F / Fp
  IF ABS(A - An) < .0001 THEN GOTO Converged
  PRINT Iteration, A, An
  A = An
  NEXT Iteration
  PRINT "No Convergence"
RETURN
Converged:
  Beta = 0
  FOR I = 1 TO N
    Beta = Beta + EXP(An * WLog(I))
  NEXT I
  Beta = (Beta / N) ^ (1 / An)
  Alpha = An
  PRINT "Alpha = "; Alpha, "Beta = "; Beta
  PRINT "Number of Breaks = "; NBreaks(nT)
  GOSUB LengthStrength
  GOSUB Gamma
RETURN

Gamma:
'Performs linear interpolation using Gamma array values
IF Diameter = 0 THEN Diameter = 1
BetaD = Beta/Diameter
N = 1-1/Alpha
N100 = 100 * N
NInt = INT(N100)
NFrac = N100 - NInt
DeltaGamma = Gamma(NInt + 1) - Gamma(NInt)
GammaN = Gamma(NInt) + DeltaGamma * NFrac
Tau = (Strength/(2 * BetaD)) * GammaN
PRINT Fil$;" ";FDesig$;" in ";MDesig$
PRINT "   Alpha   Beta   Gamma   Strength

```

```

- Diameter IFSS"
PRINT USING "#####.## ";Alpha,Beta,GammaN,Strength,
-Diameter,Tau
PrintOut = 0
INPUT "Print out results? (Y/N) ";PO$
IF PO$ = "Y" THEN PrintOut = 1
IF PO$ = "y" THEN PrintOut = 1
IF PrintOut = 0 THEN GOTO GammaJump
LPRINT
LPRINT "Number of Breaks = ";NBreaks(nT)
LPRINT Fil$;" ";FDesig$;" in ";MDesig$
LPRINT " Alpha Beta Gamma Strength
- Diameter IFSS"
LPRINT USING "#####.## ";Alpha,Beta,GammaN,Strength,
-Diameter,Tau
LPRINT
GammaJump:
RETURN

```

APPENDIX B

SOURCE CODE FOR FIBERLINK, IN SITU FIBER STRENGTH, FRAGMENTATION TEST DATA ANALYSIS SYSTEM

The following program is the source code listing for the FiberLink, in situ fiber strength fragmentation test data acquisition and analysis program written in compiled AmigaBasic (Absoft, AC-Basic) described in chapter 7. Weibull calculation routines were translated and adapted from a mainframe Fortran program (author unknown). A list of subroutines and a brief description of their functions precedes the actual code. Long code lines have been reformatted, with leading hyphens attached to the second portions.

Main: Main program loop.

Start: Sets up menu interrupts and "sleeps" here until summoned by a menu call from the user.

StartupText: Displays copyright information and specifies df1: drive for all data diskettes.

ArrayDimensions: Defines all data arrays and allocates space to them.

LinkDims: Defines link-strength related arrays and allocates space to them.

InterLinkDims: Defines fragmentation test simulation related arrays and allocates space to them.

Initialize: Sets all initial variables, file names, graphics colors, default moduli.

GammaData: Sets up a look-up table of the Gamma function.

InitializeMenu: Initializes the menu selections.

CheckMenu: Arrival point when user makes a menu selection. Finds column and routes to submenus.

Filemenu: Checks first column of menu items and routes to appropriate subroutine.

Graphics: Checks second column of menu items and routes to appropriate subroutine.

LinkMenu: Checks third column of menu items and routes to appropriate subroutine.

InterLinkMenu: Checks fourth column of menu items and routes to appropriate subroutine.

GammaLoader: Inputs Weibull shape and scale factors from user and performs Gamma function calculations.

- ListLinks:** Prints out list of the strength assigned to each fiber link.
- FiberData:** Inputs data on fiber diameter, modulus, etc. from user for all calculations.
- MatrixData:** Inputs data on matrix name, modulus, etc. from user for printouts.
- LengthStrength:** Simply sets fiber tensile strength at this point, intended to be upgraded to perform log-linear extrapolation to automatically find strength @ length in future versions.
- GammaPlot:** Produces a graphical plot of the Gamma function.
- Dir:** Lists directory of the df1: drive.
- WriteTrack:** Writes a file with the positions of all breaks, dial gage reading, strain, etc.
- ReadTrack:** Read files written by WriteTrack.
- ReadTracks:** Reads a set of tracks with the same root file name and different track numbers.
- PrintLengths:** Prints out the fragment lengths, calculated from the break positions.
- PrintBreakList:** Prints out the break positions in a column format for a set of tracks.
- WriteLengths:** Writes a file with the fragment lengths, rather than positions.
- WriteBreakList:** Writes a file with the break positions for a set of tracks in column format.
- WriteBreaks:** Writes a file with the break positions, track by track.
- ReadBreaks:** Reads files written by WriteBreaks.
- ShowFibers:** Displays a graphical representation of all break positions for one or more tracks. Allows user specification of breaks using mouse.
- CheckMouse:** Checks for mouse clicks and if on lower part of screen scrolls the break display to the left or right. If on upper part of screen checks to see which track and break is being selected and stores its index in the DataT() array.
- DrawFibers:** Performs the actual fiber display graphic output.
- Cleanup:** Clears the screen.
- Quit:** Resets menu and stops program operation.
- Palet:** Initializes screen, window, and pallettes.
- BreakNumbers:** Reads in experimentally measure data on number of breaks in each strain interval for AS4 fibers in epoxy and solvent-deposited polycarbonate.

FiberModel: Core routine for fiber tensile test simulation. Initializes fiber, then goes to tensile test.

EditTest: Inputs specifications for tensile test simulation, number of samples, gage length, etc.

AddFlaws: Generates simulated fiber by adding flaws to links. Begins by initializing at 2 mpsi then adds correct numbers moving from smallest to largest flaws, (large flaws written over smaller ones since they control failure strength).

EPMod: Specifies AS4 in epoxy matrix data for fiber flaw populations.

PCMod: Specifies AS4 in epoxy matrix data for fiber flaw populations.

UserMod: Allows user-defined fiber flaw population data to be entered.

DrawFlaws: Draws a graphical representation of the fiber flaw distribution.

TensileStart: Entry point for tensile test simulation.

TensileTest: Performs simulated fiber tensile test. Cuts fiber at random point, checks links for weakest link in specified gage length, averages results.

PrintStrengths: Prints out results of simulated fiber tension test simulation.

SOURCE CODE LISTING FOR FIBERLINK

```
CLEAR ,40000&
CLEAR ,150000&
SCREEN 1,640,400,3,4
WINDOW 1,"Fiberlink/FiberTrack (C) SFF-ISFS",,0,1
```

```
Programloop:
GOSUB ArrayDimensions
GOSUB Initialize 'Sets Graphics and screen constants
GOSUB Palet' Sets palette, screen, and window
COLOR 2,0 'Specifies palette for screen outputs
GOSUB StartupText
GOSUB InitializeMenu
GOSUB BreakNumbers
```

```
Start: 'Main Program Loop, waits for menu inputs
ON MENU GOSUB CheckMenu : MENU ON
Unfinished = -1
WHILE Unfinished
SLEEP 'this program is event driven
WEND
```

```
StartupText:
CLS
LOCATE 10,1
PRINT "This program Copyrighted by Mark C. Waterbury
```

```

PRINT "FiberLink (C) Fiber Link Length Simulation
Program
PRINT "    May not be reproduced or duplicated
PRINT "    without the consent of the author.
LOCATE 18,1
PRINT "    Insert formatted data disk in df1:
PRINT "All track files will be saved to that disk.
RETURN

```

ArrayDimensions:

```

DIM X(21,500) 'Flaw Position Arrays
DIM NBreaks(21)
DIM Length(21)
DIM NewBreaks(21)
DIM DG(21)
DIM Strain(21)
DIM TStress(21)
DIM AveStrain(21) 'Ave of each track and preceding one
DIM FI$(21)
DIM T(21)
DIM DataT(500)
DIM DataB(500)
DIM Fiber(500)
DIM Stress(500)
DIM W(2000)
DIM WLog(2000) ' For Weibull Routine
DIM Gamma (205)

```

LinkDims:

```

DIM link%(10000) 'Strength of each fiber link
DIM Strength%(2000) 'Strength of each fiber sample
DIM NBr(21) 'Number of Breaks/25 mm @ (Strain)
DIM NBI(21),NBF(21)'Integral and Fractional Breaks/25 mm
DIM NbrEP(20) 'NBr/25 mm for AS4/Epoxy
DIM NbrPC(20) 'NBr/25 mm for AS4/PolyCarbonate
DIM NFibs(50) 'Numbers of Fibers to test
DIM Sample(50) 'Lengths of Fiber to test

```

InterLinkDims:

```

DIM Inter%(10000) 'Strength of each interface element
DIM BPos%(250) 'New Breaks array
DIM BPost(100)
DIM Transfer%(21)

```

Initialize:

```

Modulus = 34000000& 'AS4 default
AS4Mod = 34000000&
IM6Mod = 40400000&
Pi = 3.14159
Scrx = 640:ScrY = 400
FT% = 160:FB% = FT% + 15
Gc% = 2 'gap color (integer)
Gap% = 4 'break gap
fc1% = 6 'fiber color 1
fc2% = 7 'fiber
Velocity = 200 'default tracking speed

```

```

FI$(0) = "00" 'Appended to track file names
FI$(1) = "01":FI$(2) = "02":FI$(3) = "03":FI$(4) = "04"
FI$(5) = "05":FI$(6) = "06":FI$(7) = "07":FI$(8) = "08"
FI$(9) = "09":FI$(10) = "10":FI$(11) = "11":FI$(12) = "12"
FI$(13) = "13":FI$(14) = "14":FI$(15) = "15":FI$(16) = "16"
FI$(17) = "17":FI$(18) = "18":FI$(19) = "19":FI$(20) = "20"
FI$(21) = "21"
WIDTH "LPT1:",255 'Eliminates printer carriage returns
GOSUB GammaData
RETURN

```

GammaData: 'Loads the gamma function into Gamma(I)
RESTORE

```

FOR I = 100 TO 200
READ Gamma(I)
NEXT I
DATA 1.00,.99433,.98884,.98355,.97844
DATA .9735,.96874,.96415,.95973,.95546
DATA .95135,.94740,.94359,.93993,.93642
DATA .93304,.92980,.92670,.92373,.92089
DATA .91817,.91558,.91311,.91075,.90852
DATA .90640,.90440,.90250,.90072,.89904
DATA .89747,.89600,.89464,.89338,.89222
DATA .89115,.89018,.88931,.88854,.88785
DATA .88726,.88676,.88636,.88604,.88581
DATA .88566,.88560,.88563,.88575,.88595
DATA .88623,.88659,.88704,.88757,.88818
DATA .88887,.88964,.89049,.89142,.89243
DATA .89352,.89468,.89592,.89724,.89864
DATA .90012,.90167,.90330,.90500,.90678
DATA .90864,.91057,.91258,.91466,.91683
DATA .91906,.92137,.92376,.92623,.92877
DATA .93138,.93408,.93685,.93989,.94261
DATA .94561,.94869,.95184,.95507,.95838
DATA .96177,.96523,.96877,.97240,.97610
DATA .97988,.98374,.98768,.99171,.99581,1!
FOR I = 101 TO 200 'Calculates lower Gammas
N = (I-100)/100
Gamma(I-100) = Gamma(I)/N
NEXT I
RETURN

```

InitializeMenu:

```

MENU 1,0,1,"File"
MENU 1,1,1,"Write Break File  "
MENU 1,2,1,"Read Break File  "
MENU 1,3,1,"Read Track      "
MENU 1,4,1,"Read Set of Tracks"
MENU 1,5,1,"Dir              "
MENU 1,6,1,"Quit"
MENU 2,0,1,"Calcs"
MENU 2,1,1,"Weibull Calcs  "
MENU 2,2,1,"Gamma Calcs   "

```

```

MENU 2,3,1,"Gamma Plot  "
MENU 2,4,1,"Fiber Data  "
MENU 2,5,1,"Matrix Data  "
  MENU 3,0,1,"Graphs"
  MENU 3,1,1,"Show Fibers  "
  MENU 3,2,1,"Clear Screen  "
  MENU 3,3,1,"Write Break List  "
  MENU 3,4,1,"Write Length List  "
  MENU 3,5,1,"Print Break List  "
  MENU 3,6,1,"Print Length List  "
  MENU 3,7,1,"Track Breaks  "
  MENU 3,8,1,"List Selected Breaks  "
    MENU 4,0,1,"FiberLink"
    MENU 4,1,1,"Define Fiber Flaws  "
    MENU 4,2,1,"Generate Fiber  "
    MENU 4,3,1,"Draw Fiber  "
    MENU 4,4,1,"Tensile Test  "
    MENU 4,5,1,"Print Fiber Strengths"
    MENU 5,0,1,"InterLink"
    MENU 5,1,1,"InterLink Setup  "
    MENU 5,2,1,"InterLink Simulation  "
    MENU 5,3,1,"Print Link List  "
RETURN

CheckMenu:
  MenuId = MENU(0)
  MenuItem = MENU(1)
  ON MenuId GOSUB Filemenu,Calcs,Graphics,LinkMenu,
  -InterLinkMenu
RETURN

Filemenu:
  ON MenuItem GOSUB WriteBreaks,ReadBreaks,ReadTrack,
  -ReadTracks,Dir,Quit
RETURN

Graphics:
  ON MenuItem GOSUB ShowFibers,Cleanup,WriteBreakList,
  -WriteLengths,PrintBreakList,PrintLengths,Tracker,
  -ListBreaks
RETURN

LinkMenu:
  ON MenuItem GOSUB FiberModel,AddFlaws,DrawFlaws,
  -TensileStart,PrintStrengths
RETURN

InterLinkMenu:
  ON MenuItem GOSUB InterModel,InterLink,ListLinks
RETURN

Calcs:
  ON MenuItem GOSUB WeibullLoader,GammaLoader,GammaPlot,

```

```
-FiberData,MatrixData
RETURN
```

```
GammaLoader:
```

```
INPUT "File Name ",Fil$
INPUT "Alpha, Beta (set Alpha = 0 to quit) ",Alpha,Beta
IF Alpha = 0 THEN RETURN
GOSUB Gamma
GOTO GammaLoader
RETURN
```

```
ListLinks:
```

```
FOR I = 0 TO NLinks STEP 10
LPRINT link%(I);link%(I+1);link%(I+2);link%(I+3);
-link%(I+4);link%(I+5); link%(I+6);link%(I+7);
-link%(I+8);link%(I+9)
NEXT I
RETURN
```

```
FiberData:
```

```
CLS
INPUT "Fiber Designation ",FDesig$
INPUT "Fiber Diameter (microns) ",Diameter
INPUT "Fiber Strength @ 25 mm ",Strength0
INPUT "Fiber Modulus ",Modulus
RETURN
```

```
MatrixData:
```

```
CLS
INPUT "Matrix Designation",MDesig$
INPUT "Matrix Tensile Strength (psi) ",MTStrength
INPUT "Matrix Shear Strength (psi) ",MSStrength
INPUT "Matrix Tensile Modulus (psi) ",MTModulus
INPUT "Matrix Shear Modulus (psi) ",MSModulus
RETURN
```

```
LengthStrength:
```

```
Strength = Strength0
RETURN
```

```
GammaPlot:
```

```
PSET (0,10*Gamma(100)),1
FOR I = 0 TO 200
LINE -(I * 3,10 * Gamma(I)),1
NEXT I
FOR I = 0 TO 200 STEP 25
LINE (I * 3 ,180)-(I* 3,200),2
NEXT I
INPUT "Printout? Y/N ",Pr$
IF Pr$ <> "Y" THEN GOTO NoPrint
LPRINT "Gamma Function for N = 0 to 2.00 in 1/100 ths "
LPRINT
FOR I = 0 TO 200 STEP 5
```

```

LPRINT USING " ###.#####";I/100;Gamma(I);Gamma(I+1);
-Gamma(I+2);Gamma(I+3);Gamma(I+4)
NEXT I

```

```

NoPrint:
RETURN

```

```

Dir:
FILES "df1:"
RETURN

```

```

WriteTrack:
FilT$ = Fil$ + Fl$(nT)
OPEN FilT$ FOR OUTPUT AS 1
WRITE #1, FilT$
WRITE #1, nT
WRITE #1,DG(nT),Strain(nT)
WRITE #1,NBreaks(nT),Length(nT)
FOR k = 1 TO NBreaks(nT)
WRITE #1, X(nT,k)
NEXT k
CLOSE #1
PRINT "File saved as ";FilT$
RETURN

```

```

ReadTrack:
CLS
INPUT "File name ",Fil$
INPUT "Track ",nT
IF nT = 0 THEN nT = 1
IF nT > NTracks THEN NTracks = nT
FilT$ = "df1:" + Fil$ + Fl$(nT)
OPEN FilT$ FOR INPUT AS 1
INPUT #1, F$
INPUT #1, TT
INPUT #1,DG(nT),Strain(nT)
INPUT #1,NBreaks(nT),Length(nT)
FOR k = 1 TO NBreaks(nT)
INPUT #1, X(nT,k)
NEXT k
CLOSE #1
RETURN

```

```

ReadTracks:
CLS
INPUT "Parent File Name ",Fil$
INPUT "First and Last Tracks ",NFirst,NLast
NTracks = NLast - NFirst + 1
FOR nT = NFirst TO NLast
FilT$ = "df1:" + Fil$ + Fl$(nT)
OPEN FilT$ FOR INPUT AS 1
INPUT #1, F$

```

```

INPUT #1, Tn
INPUT #1, DG(nT), Strain(nT)
INPUT #1, NBreaks(nT), Length(nT)
  FOR k = 1 TO NBreaks(nT)
    INPUT #1, X(nT,k)
  NEXT k
CLOSE #1
NEXT nT
RETURN

```

PrintLengths:

```

LOCATE 1,1
LPRINT Fil$
LPRINT NTracks
  FOR I = 1 TO NTracks-1
    LPRINT USING "    ##";I;
  NEXT I
  LPRINT USING "    ##";I
  FOR I = 1 TO NTracks - 1
    LPRINT USING "    ###";DG(I);
  NEXT I
  LPRINT USING "    ###";DG(I)
  FOR I = 1 TO NTracks -1
    LPRINT USING " ##.####";Strain(I)-1;
  NEXT I
  LPRINT USING " ##.####";Strain(I)-1
  FOR J = 1 TO NTracks -1
    LPRINT USING "    ###";NBreaks(J);
  NEXT J
  LPRINT USING "    ###";NBreaks(J)
  MaxBreaks = NBreaks(1)
  FOR I = 2 TO NTracks -1
    IF NBreaks(I) > MaxBreaks THEN MaxBreaks = NBreaks(I)
  NEXT I
  FOR I = 2 TO MaxBreaks
    FOR J = 1 TO NTracks -1
      IF X(J,I) - X(J,I-1) > 0 THEN
        Lx% = (X(J,I)-X(J,I-1))
        LPRINT USING "    ####"; Lx%;
      ELSE
        LPRINT USING "    ####";X(J,I);
      END IF
    NEXT J
    IF X(J,I) - X(J,I-1) > 0 THEN
      Lx% = (X(J,I)-X(J,I-1))
      LPRINT USING "    ####"; Lx%
    ELSE
      LPRINT USING "    ####";X(J,I)
    END IF
  NEXT I
RETURN

```

PrintBreakList:

```

LPRINT Fil$
LPRINT NTracks
FOR I = 1 TO NTracks-1
  LPRINT USING "  ## ";I;
NEXT I
LPRINT USING "  ##";I
FOR I = 1 TO NTracks - 1
  LPRINT USING "   ###";DG(I);
NEXT I
LPRINT USING "   ###";DG(I)
FOR I = 1 TO NTracks -1
LPRINT USING " ##.####";Strain(I)-1;
NEXT I
LPRINT USING " ##.####";Strain(I)-1
FOR J = 1 TO NTracks -1
  LPRINT USING "   ### ";NBreaks(J);
NEXT J
LPRINT USING "   ###";NBreaks(J)
  MaxBreaks = NBreaks(1)
  FOR I = 2 TO NTracks -1
IF NBreaks(I) > MaxBreaks THEN MaxBreaks = NBreaks(I)
  NEXT I
  FOR I = 1 TO MaxBreaks
  FOR J = 1 TO NTracks -1
  XX% = X(J,I)
  LPRINT USING " #####"; XX%;
  NEXT J
  XX% = X(J,I)
  LPRINT USING " #####"; XX%
  NEXT I
CLOSE #1
RETURN

```

WriteLengths:

```

LOCATE 1,1
INPUT "Save Lengths ",Fil$
Fil$ = "df1:" + Fil$
OPEN Fil$ FOR OUTPUT AS 1
WRITE #1, Fil$
WRITE #1, NTracks
FOR I = 1 TO NTracks-1
  PRINT #1, USING "  ##";I;
NEXT I
PRINT #1, USING "  ##";I
FOR I = 1 TO NTracks - 1
  PRINT #1, USING "   ###";DG(I);
NEXT I
PRINT #1, USING "   ###";DG(I)
FOR I = 1 TO NTracks -1
PRINT #1, USING " ##.####";Strain(I)-1;
NEXT I
PRINT #1, USING " ##.####";Strain(I)-1
FOR J = 1 TO NTracks -1

```

```

PRINT #1, USING "   ###";NBreaks(J);
NEXT J
PRINT #1, USING "   ###";NBreaks(J)
  MaxBreaks = NBreaks(1)
  FOR I = 2 TO NTracks -1
IF NBreaks(I) > MaxBreaks THEN MaxBreaks = NBreaks(I)
  NEXT I
  FOR I = 2 TO MaxBreaks
  FOR J = 1 TO NTracks -1
  IF X(J,I) - X(J,I-1) > 0 THEN
  Lx% = (X(J,I)-X(J,I-1))
  PRINT #1, USING "   ####"; Lx%;
  ELSE
  PRINT #1, USING "   ####";X(J,I);
  END IF
  NEXT J
  IF X(J,I) - X(J,I-1) > 0 THEN
  Lx% = (X(J,I)-X(J,I-1))
  PRINT #1, USING "   ####"; Lx%
  ELSE
  PRINT #1, USING "   ####";X(J,I)
  END IF
  NEXT I
CLOSE #1
RETURN

```

WriteBreakList:

```

LOCATE 1,1
INPUT "Save Break List ",Fil$
Fil$ = "df1:" + Fil$
OPEN Fil$ FOR OUTPUT AS 1
  WRITE #1, Fil$
  WRITE #1, NTracks
  FOR I = 1 TO NTracks-1
  PRINT #1, USING "   ## ";I;
  NEXT I
  PRINT #1, USING "   ##";I
  FOR I = 1 TO NTracks - 1
  PRINT #1, USING "   ###";DG(I);
  NEXT I
  PRINT #1, USING "   ###";DG(I)
  FOR I = 1 TO NTracks -1
  PRINT #1, USING " ##.####";Strain(I)-1;
  NEXT I
  PRINT #1, USING " ##.####";Strain(I)-1
  FOR J = 1 TO NTracks -1
  PRINT #1, USING "   ## ";NBreaks(J);
  NEXT J
  PRINT #1, USING "   ##";NBreaks(J)
  MaxBreaks = NBreaks(1)
  FOR I = 2 TO NTracks -1
IF NBreaks(I) > MaxBreaks THEN MaxBreaks = NBreaks(I)
  NEXT I

```

```

FOR I = 1 TO MaxBreaks
  FOR J = 1 TO NTracks -1
    XX% = X(J,I)
    PRINT #1, USING " #####"; XX%;
  NEXT J
  XX% = X(J,I)
  PRINT #1, USING " #####"; XX%
NEXT I
CLOSE #1
RETURN

```

WriteBreaks:

```

LOCATE 1,1
INPUT "Break File Name ",Fil$
Fil$ = "df1:" + Fil$
LOCATE 1,1:PRINT " "
"
"
OPEN Fil$ FOR OUTPUT AS 1
WRITE #1, NTracks
FOR I = 1 TO NTracks
  WRITE #1,T(I),DG(I),Strain(I)
NEXT I
  FOR J = 1 TO NTracks
    WRITE #1,NBreaks(J),Length(J)
  NEXT J
  FOR I = 1 TO NTracks
    FOR J = 1 TO NBreaks(I)
      WRITE #1,X(I,J)
    NEXT J
  NEXT I
CLOSE #1
RETURN

```

ReadBreaks:

```

LOCATE 1,1
INPUT "Read Breaks ",Fil$
Fil$ = "df1:" + Fil$
OPEN Fil$ FOR INPUT AS 1
INPUT #1, NTracks
FOR I = 1 TO NTracks
  INPUT #1,Tn,DG(I),Strain(I)
NEXT I
  FOR J = 1 TO NTracks
    INPUT #1,NBreaks(J),Length(J)
  NEXT J
  FOR I = 1 TO NTracks
    FOR J = 1 TO NBreaks(I)
      INPUT #1,X(I,J)
    NEXT J
  NEXT I
CLOSE #1
RETURN

```

ShowFibers:

N = 0 'Number of data points

CLS

INPUT "Number Fibers? 1/0 ",PNumb

Shift% = -600

ON MOUSE GOSUB CheckMouse:MOUSE ON

GOSUB DrawFibers

InkL:

Ink\$ = INKEY\$

IF Ink\$ = "0" THEN XOff% = 0:GOSUB DrawFibers

IF Ink\$ = "9" THEN XOff% = Last% * Shift%:GOSUB

DrawFibers

IF Ink\$ = "1" THEN XOff% = Shift%:GOSUB DrawFibers

IF Ink\$ = "2" THEN XOff% = 2 * Shift%:GOSUB DrawFibers

IF Ink\$ = "3" THEN XOff% = 3 * Shift%:GOSUB DrawFibers

IF Ink\$ = "4" THEN XOff% = 4 * Shift%:GOSUB DrawFibers

IF Ink\$ = "5" THEN XOff% = 5 * Shift%:GOSUB DrawFibers

IF Ink\$ = "6" THEN XOff% = 6 * Shift%:GOSUB DrawFibers

IF Ink\$ = "7" THEN XOff% = 7 * Shift%:GOSUB DrawFibers

IF Ink\$ = "8" THEN XOff% = 8 * Shift%:GOSUB DrawFibers

IF Ink\$ = "Q" THEN :RETURN

IF Ink\$ = "q" THEN :RETURN

GOTO InkL

RETURN

CheckMouse:

F = MOUSE(0)

Mx% = MOUSE(1):My% = MOUSE(2)

IF My% > 175 THEN

IF Mx% < 160 THEN XOff% = XOff% - Shift% :GOTO MHop

IF Mx% < 320 THEN XOff% = XOff% - Shift%/2 :GOTO MHop

IF Mx% < 480 THEN XOff% = XOff% + Shift%/2 :GOTO MHop

XOff% = XOff% + Shift%

MHop:

GOSUB DrawFibers

END IF

IF My% < 170 THEN

Dt = 0:DB = 0

N = N + 1

Dt = INT(My%/8)

DataT(N) = Dt

FOR I = 1 TO NBreaks(Dt)

Lx = X(Dt,I)/10 + XOff%

IF ABS(Lx + 3 - Mx%) < 3 THEN DB = I

NEXT I

IF DB = 0 THEN DataT(N) = 0:N = N - 1 :GOTO EndHop

DataB(N) = DB

Ly% = Dt * 8

Lx = X(Dt,DB)/10 + XOff%

LINE (Lx,Ly%)-(Lx+1,Ly%+2),4,bf

EndHop:

END IF

RETURN

DrawFibers:

```

CLS
  Last% = INT(-X(1,NBreaks(1))/(Shift%*10))
  FOR I = 1 TO NTracks
    Ly% = I * 8
    LINE (0,Ly%)-(640,Ly% + 2),3,bf
    FOR J = 1 TO NBreaks(I)
      Lx = X(I,J)/10 + XOff%
      IF Lx < 0 THEN GOTO NextJ
      IF Lx > 640 THEN GOTO NextJ
      LINE (Lx,Ly%)-(Lx+2,Ly%+2),0,bf
      L1 = I
      Px% = Lx/8
      IF Px% > 39 THEN Px% = 39
      IF Px% < 1 THEN Px% = 1
      IF Lx > 0 AND PNumb THEN LOCATE L1,Px%:PRINT USING
      "##";J
    NextJ: NEXT J
  NEXT I
  FOR I = 1 TO N
    Ly% = DataT(I) * 8
    Lx = X(DataT(I),DataB(I))/10 + XOff%
    IF Lx < 0 THEN GOTO DataHop
    IF Lx > 640 THEN GOTO DataHop
    LINE (Lx,Ly%)-(Lx+6,Ly%+2),1,bf
  DataHop: NEXT I
  LINE (0,175)-(640,175),3
  FOR I = 0 TO 63
    LINE (I*10,175)-(I*10,170),3
  NEXT I
  FOR I = 0 TO 6
    LINE (I*100,175)-(I*100+1,165),3 ,bf
  NEXT I
  LOCATE 23,1:PRINT -XOff%*10;:PRINT "    Type Q to
  return";
  RETURN

```

ListBreaks:

```

CLS
  FOR I = 1 TO N
    PRINT X(DataT(I),DataB(I))
  NEXT I
  RETURN

```

Cleanup:

```

CLS
  RETURN

```

Quit:

```

  MENU RESET
  STOP

```

Palet:

```

PALETTE 0,0/15,0/15,0/15 :PALETTE 1,0/15,0/15,15/15
PALETTE 2,5/15,5/15,5/15 :PALETTE 3,15/15,15/15,15/15
PALETTE 4,6/15,6/15,6/15 :PALETTE 5,15/15,0/15,0/15
PALETTE 6,15/15,0/15,0/15 :PALETTE 7,0/15,15/15,0/15
RETURN

```

BreakNumbers:

. 'Breaks per 25 mm for Epoxy and PC matrix and AS4

Fibers

```

NbrPC(0) = 0 :NbrPC100(1) = 0 :NbrPC100(2) = 0
NbrPC(3) = 0 :NbrPC(4) = .4: NbrPC(5) = .13
NbrPC(6) = .99 :NbrPC(7) = 3.33 :NbrPC(8) = 6.2
NbrPC(9) = 12.16 :NbrPC(10) = 25 :NbrPC(11) = 50
NbrPC(12)=100:NbrPC(13)=200:NbrPC(14)=400:NbrPC(15)=800
NbrPC(16)=1600:NbrPC(17)=3200:NbrPC(18)=5000
NbrPC(19)=5000: NbrPC(20) = 5000
NbrEP(1) = 0 :NbrEP(2) = 0:NbrEP(3) = 0:NbrEP(4) = 1
NbrEP(5) = .53:NbrEP(6) = 2.22 : NbrEP(7) = 6.75
NbrEP(8) = 19.95:NbrEP(9) = 28.39:NbrEP(10) = 64.52
NbrEP(11) = 156:NbrEP(12) = 379:NbrEP(13) = 918
NbrEP(14) = 2224: NbrEP(15) = 5388:NbrEP(16) = 13054
NbrEP(17) = 31630:NbrEP(18) = 76638&: NbrEP(19) = 185689&
NbrEP(20) = 449916&

```

RETURN

FiberModel:

```

CLS
RANDOMIZE(TIMER/2)
Flawed = 0
Modulus = 340&'in .1 mpsi for AS4 for strain in %
INPUT "Model Length in links, 1 < L < 10000 ",NLinks
IF NLinks > 10000 THEN NLinks = 10000
IF NLinks = 0 THEN NLinks = 1000
INPUT "Link Length (microns) ",LinkLength
FiberLength = LinkLength * NLinks
MMpLink = LinkLength /1000
LinkC = FiberLength/25000 ' breaks/NLinks to B.Per 25 mm
INPUT "Epoxy, PC, or User? E/P/U ",EPC$
IF EPC$ = "P" THEN GOSUB PCMod
IF EPC$ = "E" THEN GOSUB EPMod
IF EPC$ = "U" THEN GOSUB UserMod
GOSUB EditTest
GOSUB AddFlaws
GOSUB TensileTest
RETURN

```

EditTest:

```

LOCATE 1,1:PRINT " "
LOCATE 1,1:INPUT "N Lengths ";NLengths
LOCATE 1,1:PRINT " "
LOCATE 1,1:INPUT "Draw Fiber? Y/N ",Flaw$:
LOCATE 1,1:PRINT " "
LOCATE 1,1:INPUT "Draw Breaks? Y/N ",Brk$

```

```

LOCATE 1,1:PRINT "
LOCATE 1,1:INPUT "Draw Cuts? Y/N ",Cut$
FOR k = 1 TO NLengths
LOCATE 1,1:PRINT "
LOCATE 1,1:PRINT k;" ";
INPUT "Length, N Fibers ",Sample(k),NFibs(k)
IF NFibs(k) > 2000 THEN NFibs(k)=2000 'Limit of Strength
Dim
NEXT k
RETURN

```

AddFlaws:

Saturation = 2000: ' Number of flaws/25 mm for limit case

Sat = 20

FOR I = 20 TO 1 STEP -1

IF NBr(I) > Saturation THEN Sat = I

Strain(I) = I * .25

TStress(I) = Modulus * Strain(I)

NEXT I

L0% = Sat * .25 * Modulus

FOR I = 1 TO NLinks

link%(I) = L0%

NEXT I

FOR I = Sat-1 TO 1 STEP -1

NBrks = NBr(I) * LinkC 'number in NLinks from 25 mm

FOR J = 1 TO NBrks

XT = RND * NLinks

link%(XT) = TStress(I)

NEXT J

Fract = NBrks - INT(NBrks)

IF RND < Fract THEN

XT = RND * NLinks

link%(XT) = TStress(I)

END IF

NEXT I

RETURN

EPMod: 'loads epoxy flaws into array

FOR I = 1 TO 20

NBr(I) = NbrEP(I)

NEXT I

RETURN

PCMod: 'loads PC flaws into array

FOR I = 1 TO 20

NBr(I) = NbrPC(I)

NEXT I

RETURN

UserMod:

CLS

FOR I = 1 TO 20

```

PRINT I;" strain = ";I * .25;" ";
INPUT "Breaks/25 mm = ",NBr(I)
NEXT I
Check: INPUT "All OK? (Y) ",Ch$
IF Ch$ = "Y" THEN RETURN
IF Ch$ = "y" THEN RETURN
GOTO UserMod

```

```

DrawFlaws:
CLS
LINE (0,0)-(640,400),3,bf
COLOR 2,0
FibWid = 24
FOR J = 0 TO 15
  Is = J * 625
  YS = (J+1) * FibWid
  FOR I = 1 TO 625
    Ix = Is + I
    Iy = link%(Ix)/85
    Ic = 5 + Iy/2
    LINE (I,YS)-(I,YS-Iy),0
  NEXT I
NEXT J
RETURN

```

```

TensileStart:
GOSUB EditTest
GOSUB TensileTest
RETURN

```

```

TensileTest:
INPUT "Print Flaw Distribution? (Y/N) ",PFD$
IF UCASE$(PFD$) <> "Y" THEN GOTO NoFLawPrints
LPRINT "FiberLink simulated fiber tensile test"
LPRINT "Number of breaks/25 mm"
FOR k = 1 TO 20 STEP 5
  LPRINT "NBr(";k;")=";NBr(k);" NBr(";k+1;")=";
  -NBr(k+1);" NBr(";k+2;")=";NBr(k+2);" NBr(";k+3;")=";
  -NBr(k+3);" NBr(";k+4;")=";NBr(k+4)
NEXT k
LPRINT "LinkLength = ";LinkLength
LPRINT "Total Length = ";FiberLength
LPRINT "Link constant = ";LinkC
LPRINT "Fiber Modulus = ";Modulus
NoFLawPrints:
FOR k = 1 TO NLengths
  IF Flaw$ = "Y" THEN GOSUB DrawFlaws
  PRINT Sample(k),NFibs(k)
  SSize = Sample(k) * 1000/LinkLength 'Scales to 100
  micron
IF SSize = 0 THEN RETURN
  Range = NLinks - SSize

```

```

WeakAve = 0
FOR I = 1 TO NFibs(k)
  XJ = RND * Range
  WeakL = 2000 'Initial Fiber Strength before flaws
  FOR J = 1 TO SSize
    IF link%(XJ+J) < WeakL THEN
      WeakL = link%(XJ+J)
      XJJ = XJ + J
    END IF
  NEXT J
  Strength%(I) = WeakL
  Is = INT(XJJ/625)
  YS = FibWid * (1 + Is)
  Xf = XJJ - 625 * Is
  Xc = XJ - 625 * Is
  IF Brk$ = "Y" THEN
    LINE(Xf-1,YS)-(Xf+1,YS-link%(XJJ)/85),2,bf
    IF Cut$ = "Y" THEN LINE (Xc,YS)-(Xc,YS-20),1
  'Cut

WeakAve = WeakAve + WeakL
NEXT I
WeakAve = WeakAve/NFibs(k)
DevSum = 0
FOR I = 1 TO NFibs(k)
  DevSum = DevSum + (WeakAve - Strength%(I))^2
NEXT I
DevSum = DevSum/NFibs(k)
StdDev = SQR(DevSum)
IF EPCS$ = "E" THEN LPRINT "AS4/Epoxy ";
IF EPCS$ = "P" THEN LPRINT "AS4/PC ";
IF EPCS$ = "U" THEN LPRINT "User ";
LPRINT NFibs(k);" Fibers ";Sample(k);" mm, Strength = ";
-WeakAve;" Std Deviation = ";StdDev
LOCATE 1,1:PRINT "
LOCATE 1,1
PRINT NFibs(k);" Fibers ";Sample(k);"mm, Strength = ";
-WeakAve;" Std Dev = ";StdDev;
NEXT k
RETURN

PrintStrengths:
LPRINT "FiberLink Tensile Test Simulation"
LPRINT "Strengths of ";FiberDesig$;" Fibers
LPRINT "Length ";Sample(1);" Strength"; WeakAve
FOR I = 1 TO NFibs(1) STEP 10
  FOR J = 0 TO 8
    LPRINT USING "#### "; Strength%(I+J);
  NEXT J
  LPRINT USING "#### "; Strength%(I+9)
NEXT I
RETURN

```

APPENDIX C

SOURCE CODE FOR OPTICAL NUMERIC VOLUME FRACTION ANALYSIS

The following program is the source code written in compiled Amiga Basic (AC-Basic) for the optical numeric volume fraction analysis system described in chapter 5. Image loading and saving routines are adapted and corrected from Carolynn Scheppner's (Commodore Business Machines) routines, provided on the Amiga "Extras" disk. A list of subroutines and a brief description of their functions precedes the actual listing. Long lines have been reformatted to fit the page, with leading hyphens attached to the second portion.

Main: Central routine that routes to all startup routines.

Start: Sets up menu interrupts and "sleeps" here until called.

Libs: Loads libraries of pointers to system calls.

ArrayDimensions: Defines arrays and allocates space to them.

Cycle: Routes to GetAddr which finds screen pallettes and sets up for color cycling.

ScreenSetup: Defines screen and window parameters.

Initialize: Initializes graphics variables, filenames, and defines grid sizes for statistics.

Cal1: Specifies default image size calibration.

Cal2: Specifies second default image size.

SetCal: Allows user specified image size calibration.

InitializeMenu: Initializes menu selections.

CheckMenu: Checks menu interrupts and routes to each menu.

Filemenu: Checks file menu and routes to selection.

Calcs: Checks calculations menu and routes to selection.

Graph: Checks graph menu and routes to selection.

Batch: Checks Batch menu and routes to selection.

Dist: Checks Statistics menu and routes to selection.

Region: Draws crosshairs and marks starting corner for defining a region within an image. Passes to "Square" routine when the mouse button is clicked and held.

Square: Defines the ending corner for a box started by "Region" routine then finds number of fibers in the box, determines volume fraction, and displays it in menu.

Distribution: Counts number of fibers in each box in a grid of small boxes on the screen.

stats2: Finds number of boxes with few fibers, finds average fibers/box and standard deviation. Called by "ReadDist".

Stats: Same as "Stats2", called during fiber counting.

Histogram: Plots number of boxes vs. fiber/box.

WriteStats: Writes a disk file named "FileName" + ".STA" containing the number of boxes vs. fibers/box, the average fibers/box, and the standard deviation.

ReadStats: Reads files written by "WriteStats" for concatenation with new data.

ReadDist: Reads files written by "WriteDist" for displaying block maps or concatenation with new data. Variables K and L designate starting indices for positioning inputted data into a larger array.

WriteDist: Writes block map data of fibers/box for grids of boxes on screen.

Map: Draws block maps with gray scales proportioned to fibers/box. Uses indices inputted in "ReadDist".

PrintDist: Prints out distribution data determined by "Stats" routines.

BarGraph: Displays bar graphs in grid boxes with heights proportioned to number fibers/box.

SmallBar: Same as "BarGraph" except all bars are squeezed to the left of the screen.

BlockGraph: Displays a small block graph with gray scale proportioned to fibers/box.

Grid: Displays a grid of hollow boxes with outline gray scale proportioned to fibers/box.

Palet1: Sets colors of each of 32 screen pallettes. Colors in top 16 for easy viewing.

Palet2: Sets colors to gray scale for top 16 pallettes.

AutoCounter: Automated fiber counting routine. This is the core routine of the program that identifies fibers, checks to see if they have been counted previously, assigns their coordinates to arrays in columns, calculates the volume fractions, and saves the results to disk and the menu.

FiberCounter: A manual fiber counter using the mouse. May be used for correcting auto counts. May confuse AutoCounter if used during its processing.

Dir0: Displays directory of drive df0:.

Dir1: Displays directory of drive df1:.

Rad: Displays directory of drive Rad:, a recoverable RAM disk used in some systems.

Brt: Sets brightness threshold for fibers.

Cali: Sets horizontal and vertical calibration data for number of pixels per 100 microns. Converts to microns per pixel and determines overall screen area.

FibArea: Inputs cross-sectional area of average fiber.

Distance: Sets up "MeasureRadius" which measures any dimension on the screen with a mouse-dragged line.

MeasureRadius: Measure dimensions on the screen, converting number of pixels with horizontal and vertical calibration data to X, Y and total distances. Can be used to measure fibers for setting counting radius.

FindDiameter: An attempt to automatically measure fiber diameters. Not very successful so far.

WriteMenu: Writes the counting radius and fiber brightness threshold to a menu.

PalBar: Displays a bar with each of the pallettes in it. Clicking the mouse on these colors can be an aid to setting the fiber brightness threshold.

BatchRead: Reads in the numbers of fibers in a previously counted batch. Finds average volume fraction for the batch.

BatchPrint: Prints out the numbers of fibers for each image in a batch and the average for the whole.

RResults: Reads in the number of fibers/image files written by WResults.

WResults: Writes a file with the number of fibers/image.

BatchGraph: Produces a graph with line heights proportioned to the number of fibers/image.

Notice: Displays program information and copyright.

BatchCounter: Counts batches of previously save fiber images. Writes fibers/image, fiber coordinates, and statistics and map files to disk.

BCalc: Calculates the volume fraction results for a batch of counted images.

VoidCalcs: Calculates the approximate void volume fraction from the fiber volumes and the composite, fiber, and matrix densities.

BPrint: Prints out the results of a counted batch.

BWrite: Writes a disk file with the results of a counted batch.

WriteFibers: Writes the coordinates of the fibers in an image to a disk file named "FileFibers"

ReadFibers: Reads in the files written by "WriteFibers".

DrawTags: Draws tags on counted fibers after "ReadFibers".

TagMap: Draws a map of fibers with one white pixel representing each fiber position, 1/3 scale.

Cleanup: Clears the screen.

Histogram: Performs an areal analysis by determining the number of pixels assigned to each palette.

MouseTograph: Momentarily changes the color of all pixels assigned to a given palette so that they may be seen.

Diameter: Assigns the position of a fiber to a vertical column array form.

Quit: Closes libraries, ends program.

ReadImage: Interfaces menu with PictureLI subprogram.

GetAddr: Returns screen addresses and information.

WriteImage: Interfaces menu with PictureSI subprogram.

EnterImageName: Enters save file name for PictureSI.

SUB PictureSI Saves IFF images (C. Scheppner, CBM).

GetScrAddrSI: Returns information on screen data to the PictureSI subprogram.

SUB PictureLI Loads IFF images (C. Scheppner, CBM)

GetScrAddrLI: Returns information on screen data to the PictureLI subprogram.

SUB InvertVideo Switches to reverse video for crosshairs.

SUB NormalVideo Returns to normal video after crosshairs.

PROGRAM LISTING

```
'=====Fiber End Counter- Volume Fraction Calculator=
'Copyright 12/3/88, Mark Waterbury
'Optical Numeric Volume Fraction Analysis (ONVfA)
'Fiber volume determination by plotting fiber end
' positions
GOSUB ScreenSetup
GOSUB Notice
CLEAR ,35000& 'clears basic stack
CLEAR ,120000& 'clears data memory space
DEFINT I,J,K,X,Y 'defines these variables as integers Main:
GOSUB Libs 'Initializes Amiga LIBRARYs and FUNCTIONS
GOSUB ArrayDimensions 'Sets sizes of array variables
GOSUB InitializeMenu 'Sets screen menu system
GOSUB Initialize 'Sets Graphics and other constants
```

Start:

```
CLS
ON MENU GOSUB CheckMenu : MENU ON
Unfinished = -1
WHILE Unfinished
  SLEEP ' event driven
WEND
```

Libs:

```
DECLARE FUNCTION xOpen& LIBRARY
DECLARE FUNCTION xRead& LIBRARY
DECLARE FUNCTION xWrite& LIBRARY
DECLARE FUNCTION AllocMem&() LIBRARY
LIBRARY "dos.library"
LIBRARY "exec.library"
LIBRARY "graphics.library"
RETURN
```

ArrayDimensions:

```
DIM X(3000),Y(3000) 'X, Y coordinates of fibers
DIM Xc(120,60),Yc(120,60),Xn(120)
DIM Fl$(20),FileName$(20),FileName$(20) 'images (2 disks)
DIM FName$(10,40)
DIM CMap%(31) 'Palettes to brightness values 0 to 15
DIM MapC%(31) 'Brightness to Palettes
DIM Histo(31) 'Histogram of percent each palette
DIM HistoSum(31),SumHisto(31)
DIM Fibers(10,40) 'Number of fibers in each picture
DIM FibDist(20,20),DistNumb(100) 'Number of fibers/square
DIM DistMap%(15,15,10,5)
DIM RE(31),GR(31),BL(31) 'Color Palettes
DIM BPlaneSI&(5),BPlaneLI&(5) 'For PicLI and PicSI
DIM NFirst(10),NLast(10),Drv$(4) 'Batch numbers and drive
DIM Total(10),NPics(10),Average(10)
DIM AveFibres(10),DComposite(10)
```

```

DIM NFibres(20)
DIM cTab%(32)
RETURN

```

```

Cycle:
GOSUB GetAddr
RETURN

```

```

ScreenSetup:
  SMode = 1: Depth = 5: WMode = 16 'Lo-res, 5 bit planes
  ScreenX = 320:ScreenY = 200 'Screen dimensions in pixels
  SCREEN 2,ScreenX,ScreenY,Depth,SMode
  WINDOW 2,"",WMode,2
  PALETTE 0,0,0,0
RETURN

```

```

Initialize:
  GOSUB Palet1
  GOSUB Cal2
  XEnd = 311: YEnd = 195
  XScreen = 312: YScreen = 190
  TC% = 16 'Tag color
  VC% = 18 'Void color
  MC% = 17 'Map color
  Ch% = 16
  NXGroups = 12 'sample area groups per 312 X pixels
  NYGroups = 10 'sample area groups per 190 Y pixels
  NX = NXGroups/XScreen 'groups per X pixel
  NY = NYGroups/YScreen 'groups per Y pixel
  Xn = XScreen/NXGroups 'Pixels per X group
  YN = YScreen/NYGroups 'Pixels per Y group
  FI$(0) = "0":FI$(1) = "1":FI$(2) = "2":FI$(3) = "3":FI$(4) = "4"
  FI$(5) = "5":FI$(6) = "6":FI$(7) = "7":FI$(8) = "8"
  FI$(9) = "9":FI$(10) = "10":FI$(11) = "11":FI$(12) = "12"
  FI$(13) = "13":FI$(14) = "14":FI$(15) = "15":FI$(16) = "16"
  FI$(17) = "17":FI$(18) = "18":FI$(19) = "19":FI$(20) = "20"
RETURN

```

```

Call1:
  HCalib = 179.33:VCalib = 159 '20X ULWD, 6.7X, CCD
  FiberArea = 40.5375 'AS4 microns squared
  DFibers = 1.8: DMatrix = 1.206 'AS4, DER331/MPDA
  Thd% = 11 'fiber brightness threshold
  RadiusY = 11 'counting diameter
  MENU 4,7,2," 20X-6.7X-CCD "
  MENU 4,8,1," 20X-3.3X-CCD "
  GOSUB SetCal
RETURN

```

```

Call2:
  HCalib = 91:VCalib = 78 '20X ULWD, 3.3X, CCD
  FiberArea = 40.5375 'microns squared for AS4 batch
  DFibers = 1.8: DMatrix = 1.206 'AS4, DER331/MPDA

```

```

Thd% = 11 'fiber brightness threshold
RadiusY = 5.1 'counting diameter
MENU 4,7,1," 20X-6.7X-CCD "
MENU 4,8,2," 20X-3.3X-CCD "
GOSUB SetCal
RETURN

```

SetCal:

```

HCal = 100/HCalib:VCal = 100/VCalib 'Microns per pixel
ScreenX = 316 * HCal:ScreenY = 202 * VCal
Screenarea = ScreenX * ScreenY 'Area in microns square
= FiberArea/Screenarea
RETURN

```

Calibration

InitializeMenu:

```

MENU 1,0,1,"File"
MENU 1,1,1,"Read image      "
MENU 1,2,1,"Read Fiber Coordinates "
MENU 1,3,1,"Write Fiber Coordinates"
MENU 1,4,1,"Directory of drive 0  "
MENU 1,5,1,"Directory of drive 1  "
MENU 1,6,1,"Write image      "
MENU 1,7,1,"Write Image Name    "
MENU 1,8,1,"Read Statistics     "
MENU 1,9,1,"Write Statistics    "
MENU 1,10,1,"Quit"
  MENU 2,0,1,"Calcs"
  MENU 2,1,1,"Test Count       "
  MENU 2,2,1,"Batch Count      "
  MENU 2,3,1,"Manual Count     "
  MENU 2,4,1,"Calculate Distribution "
  MENU 2,5,1,"Calculate statistics "
  MENU 2,6,1,"Histogram       "
  MENU 2,7,1,"FIBER AREA CALIBRATION "
  MENU 2,8,1,"SCREEN AREA CALIBRATION "
  MENU 2,9,1,"FIBER BRIGHTNESS ADJUST "
  MENU 2,10,1,"COUNTING RADIUS ADJUST "
  MENU 3,0,1,"Graph"
  MENU 3,1,1,"Draw Fiber Tags"
  MENU 3,2,1,"Color Palet     "
  MENU 3,3,1,"Gray Palet      "
  MENU 3,4,1,"Palette Bar     "
  MENU 3,5,1,"Clear Screen    "
  MENU 3,6,1,"[Data Output]   "
MENU 4,0,1,"Batch"
MENU 4,1,1,"Read Batch      "
MENU 4,2,1,"Graph Batch     "
MENU 4,3,1,"Print Batch     "
MENU 4,4,1,"Read Distrib    "
MENU 4,5,1,"Write Distrib   "
MENU 4,6,1,"Print Distrib   "
  MENU 5,0,1,"Stats"
  MENU 5,1,1,"Grid      "

```

```

    MENU 5,2,1,"Bar  "
    MENU 5,3,1,"Block "
    MENU 5,4,1,"NBar  "
    MENU 5,5,1,"Map   "
    MENU 5,6,1,"TagMap "
    MENU 5,7,1,"Area  "
    MENU 5,8,1,"Distance"
    MENU 5,9,1,"Diameter"
RETURN

CheckMenu:
  MenuId = MENU(0)
  MenuItem = MENU(1)
  ON MenuId GOSUB Filemenu,Calcs,Graph,Batch,Dist
RETURN

Filemenu:
  ON MenuItem GOSUB ReadImage,ReadFibers,WriteFibers,Dir0,
  Dir1,WriteImage,EnterImageName,ReadStats,WriteStats,Quit
RETURN

Calcs:
  ON MenuItem GOSUB AutoCounter,BatchCounter,FiberCounter,
  Distribution,Stats,Histogram,FibArea,Cali,Brt,Rad
RETURN

Graph:
  ON MenuItem GOSUB DrawTags,Palet1,Palet2,PalBar,Cleanup
RETURN

Batch:
  ON MenuItem GOSUB BatchRead,BatchGraph,BatchPrint,
  ReadDist,WriteDist,PrintDist,Cal1,Cal2
RETURN

Dist:
  ON MenuItem GOSUB Grid,BarGraph,BlockGraph,SmallBar,Map,
  TagMap,Region,Distance,FindDiameter
RETURN

Region:
  MOUSE OFF
  InvertVideo
  ScX% = 320:ScY% = 200
  f% = MOUSE(0)
  f% = MOUSE(0)
  WHILE MOUSE(0) = 0
  f% =MOUSE(0)
  CX% =MOUSE(1)
  CY% =MOUSE(2)
  LINE (0,CY%)-(ScX%,CY%),Ch%
  LINE (CX%,0)-(CX%,ScY%),Ch%
  LINE (0,CY%)-(ScX%,CY%),Ch%
  LINE (CX%,0)-(CX%,ScY%),Ch%
  WEND
  GOSUB Square
RETURN

```

Square:

```

f% = MOUSE(0)
SX% = MOUSE(3)
SY% = MOUSE(4)
WHILE MOUSE(0) = -1
EX% = MOUSE(5)
EY% = MOUSE(6)
LINE (SX%,SY%)-(EX%,EY%),Ch%,B
LINE (SX%,SY%)-(EX%,EY%),Ch%,B
WEND

```

NormalVideo

```

LINE (SX%,SY%)-(EX%,EY%),17,B
dX = (EX%-SX%)
dY = (EY% - SY%)
BoxArea = dX * dY * HCal * VCal
NBox = 0
FOR I = 1 TO NFibers
IF X(I) > SX% THEN
IF X(I) < EX% THEN
IF Y(I) > SY% THEN
IF Y(I) < EY% THEN
PSET(X(I),Y(I)),17
CIRCLE (X(I),Y(I)),1,17
NBox = NBox + 1
END IF
END IF
END IF
END IF
NEXT I
NFib$ = "NFibers " + STR$(NBox)
MENU 3,7,1,NFib$
VFib = 100 * FiberArea * NBox/BoxArea
VFib$ = "Fiber Vf " + STR$(VFib)
MENU 3,8,1,VFib$
MenuString$ = "dX =" + STR$(dX) + " dY =" + STR$(dY)
MENU 3,9,1,MenuString$
MenuString$ = "Microns^2 = " + STR$(BoxArea)
MENU 3,10,1,MenuString$
MOUSE ON
RETURN

```

Distribution:

```

MaxFib = 0
FOR I = 0 TO NXGroups - 1
FOR J = 0 TO NYGroups - 1
FibDist(I,J) = 0
NEXT J
NEXT I
FOR I = 1 TO NFibers
IF Y(I) < 6 THEN GOTO NeI
XI = INT(X(I) * NX)
YI = INT((Y(I)-6) * NY)
FibDist(XI,YI) = FibDist(XI,YI) + 1

```

```

NeI: NEXT I
  FOR J = 0 TO NYGroups - 1
    FOR I = 0 TO NXGroups - 1
      IF FibDist(I,J) > MaxFib THEN MaxFib = FibDist(I,J)
    NEXT I
  NEXT J
  SOUND 2000,10
RETURN

```

```

stats2:
MaxFiberSet = 30
FibAlarm = 15
NBelow = 0
Sum = 0
SumSq = 0
NGroups = NXGroups * NYGroups
FOR J = 0 TO NYGroups - 1
  FOR I = 0 TO NXGroups - 1
    Sum = Sum + DistMap%(I,J,K,l)
    DistNumb(DistMap%(I,J,K,l)) = DistNumb(DistMap%(I,J,K,l)) + 1
    IF DistMap%(I,J,K,l) <= FibAlarm THEN NBelow = NBelow + 1
  NEXT I
NEXT J
Ave = Sum/NGroups
FOR J = 0 TO NYGroups - 1
  FOR I = 0 TO NXGroups - 1
    SumSq = SumSq + (Ave - DistMap%(I,J,K,l))^2
  NEXT I
NEXT J
SumSq = SumSq/NGroups
Deviation = SQR(SumSq)
SOUND 3000,8
GOSUB Histogram
RETURN

```

```

Stats:
MaxFiberSet = 30
FibAlarm = 15
NBelow = 0
Sum = 0
SumSq = 0
NGroups = NXGroups * NYGroups
FOR J = 0 TO NYGroups - 1
  FOR I = 0 TO NXGroups - 1
    Sum = Sum + FibDist(I,J)
    DistNumb(FibDist(I,J)) = DistNumb(FibDist(I,J)) + 1
    IF FibDist(I,J) <= FibAlarm THEN NBelow = NBelow + 1
  NEXT I
NEXT J
Ave = Sum/NGroups
FOR J = 0 TO NYGroups - 1
  FOR I = 0 TO NXGroups - 1
    SumSq = SumSq + (Ave - FibDist(I,J))^2
  NEXT I
NEXT J

```

```

    NEXT I
  NEXT J
  SumSq = SumSq/NGroups
  Deviation = SQR(SumSq)
  SOUND 3000,8
  GOSUB Histogram
RETURN

```

Histogram:

```

  BotY = 180
  FOR I = 1 TO MaxFiberSet
  LINE (I * 4,BotY)-(I*4+4,BotY-DistNumb(I)),1,bf
  NEXT I
RETURN

```

WriteStats:

```

  StatName$ = Fil$ + ".STA"
  OPEN StatName$ FOR OUTPUT AS 1
  WRITE #1, Fil$
  WRITE #1, MaxFiberSet
  WRITE #1, Sum,Ave,Deviation
  FOR I = 1 TO MaxFiberSet
  WRITE #1, DistNumb(I)
  NEXT I
  CLOSE #1
RETURN

```

ReadStats:

```

  INPUT "Enter Stats Name ",Fil$
  StatName$ = Fil$ + ".STA"
  OPEN StatName$ FOR INPUT AS 1
  INPUT #1, Fil$
  INPUT #1, MaxFiberSet
  INPUT #1, Sum,Ave,Deviation
  FOR I = 1 TO MaxFiberSet
  INPUT #1, DistNumb(I)
  NEXT I
  CLOSE #1
RETURN

```

ReadDist:

```

  INPUT "Distribution Name (.Map) ",Fil$
  INPUT "Enter K, L ",K,l
  StatName$ = Fil$ + ".Map"
  OPEN StatName$ FOR INPUT AS 1
  INPUT #1, VoidFraction
  FOR J = 0 TO NYGroups - 1
  FOR I = 0 TO NXGroups - 1
  INPUT #1,DistMap%(I,J,K,l)
  IF DistMap%(I,J,K,l) > MaxFib THEN MaxFib=DistMap%(I,J,K,l)
  NEXT I
  NEXT J
  CLOSE #1

```

```

IF K > KMax THEN KMax = K
IF l > LMax THEN LMax = l
GOSUB stats2
RETURN

```

WriteDist:

```

MapName$ = Fil$ + ".Map"
OPEN MapName$ FOR OUTPUT AS 1
WRITE #1, VoidFraction
FOR J = 0 TO NYGroups - 1
  FOR I = 0 TO NXGroups - 1
    WRITE #1, FibDist(I,J)
  NEXT I
NEXT J
CLOSE #1
RETURN

```

Map:

```

BlockX = 5:BlockY = 4
FOR K = 1 TO KMax
  FOR l = 1 TO LMax
    IF MaxFib = 0 THEN RETURN
    FirstX = (K - 1) * (NXGroups * BlockX + 1)
    FirstY = 5 + (l - 1) * NYGroups * BlockY
    FOR J = 0 TO NYGroups - 1
      FOR I = 0 TO NXGroups - 1
        LeftX = FirstX + I * BlockX
        RightX = LeftX + BlockX
        TopY = FirstY + J * BlockY
        BotY = TopY + BlockY
        FD = 16 + 15 * DistMap%(I,J,K,l)/MaxFib
        IF FD > 31 THEN FD = 31
        LINE(LeftX,TopY)-(RightX,BotY),FD,bf
      NEXT I
    NEXT J
  NEXT l
NEXT K
RETURN

```

PrintDist:

```

LPRINT Fil$
FOR J = 0 TO NYGroups - 1
  FOR I = 0 TO NXGroups - 1
    LPRINT FibDist(I,J); " ";
    IF FibDist(I,J) > MaxFib THEN MaxFib = FibDist(I,J)
  NEXT I
LPRINT
NEXT J
RETURN

```

BarGraph:

```

IF MaxFib = 0 THEN RETURN
LeftX = 0:RightX = 0

```

```

TopY = 0:BotY = 0
BarWidth = 4
FOR J = 0 TO NYGroups - 1
  FOR I = 0 TO NXGroups - 1
    LeftX = I * Xn
    RightX = LeftX + BarWidth
    BotY = 5 + (J+1) * YN
    FD = 16 + 15 * FibDist(I,J)/MaxFib
    LINE(LeftX,BotY)-(RightX,BotY-FibDist(I,J)+5),FD,bf
  NEXT I
NEXT J
RETURN

```

SmallBar:

```

IF MaxFib = 0 THEN RETURN
LeftX = 0:RightX = 0
TopY = 0:BotY = 0
BarWidth = 4
FOR J = 0 TO NYGroups - 1
  FOR I = 0 TO NXGroups - 1
    LeftX = I * BarWidth
    RightX = LeftX + BarWidth
    BotY = 5 + (J+1) * YN
    FD = 16 + 15 * FibDist(I,J)/MaxFib
    LINE(LeftX,BotY)-(RightX,BotY-FibDist(I,J)+5),FD,bf
  NEXT I
NEXT J
RETURN

```

BlockGraph:

```

IF MaxFib = 0 THEN RETURN
LeftX = 0:RightX = 0
TopY = 5:BotY = 0
FOR J = 0 TO NYGroups - 1
  FOR I = 0 TO NXGroups - 1
    LeftX = I * 6
    RightX = LeftX + 6
    TopY = J * 5
    BotY = TopY + 5
    FD = 16 + 15 * FibDist(I,J)/MaxFib
    LINE(LeftX,TopY)-(RightX,BotY),FD,bf
  NEXT I
NEXT J
RETURN

```

Grid:

```

IF MaxFib = 0 THEN RETURN
LeftX = 0:RightX = 0
TopY = 6:BotY = 0
FOR J = 0 TO NYGroups - 1
  BotY = TopY + YN
  FOR I = 0 TO NXGroups - 1
    RightX = LeftX + Xn

```

```

    FD = 16 + 15 * FibDist(I,J)/MaxFib
    LINE(LeftX,TopY)-(RightX-1,BotY-1),FD,B
    LeftX = RightX
  NEXT I
  LeftX = 0
  TopY = BotY
NEXT J
RETURN

```

Palet1:

```

PALETTE 16,15/15,0/15,0/15 : PALETTE 17,0/15,0/15,10/15
PALETTE 18,0/15,10/15,0/15 : PALETTE 19,15/15,10/15,0/15
PALETTE 20,0/15,0/15,5/15 : PALETTE 21,12/15,12/15,12/15
PALETTE 22,2/15,0/15,0/15 : PALETTE 23,4/15,0/15,0/15
PALETTE 24,7/15,0/15,0/15 : PALETTE 25,10/15,0/15,0/15
PALETTE 26,15/15,0/15,0/15 : PALETTE 27,15/15,15/15,0/15
PALETTE 28,0/15,15/15,0/15 : PALETTE 29,0/15,15/15,15/15
PALETTE 30,0/15,0/15,15/15:PALETTE 31,15/15,15/15,15/15
RETURN

```

Palet2:

```

FOR I = 24 TO 31
  Gray = I * 2 - 47
  PALETTE I,Gray/15,Gray/15,Gray/15
NEXT I
RETURN

```

AutoCounter:

```

GOSUB FiberCounter
XEnd = 311:YEnd = 195
IF RadiusY = 0 THEN RadiusY = 11
NTh% = RadiusY/3
RadiusX = RadiusY*1.2: RadiusSq = 1.44*RadiusY^2
CC% = RadiusX/1.5
FOR I = 1 TO XEnd/CC% + 1
  Xn(I) = 0
NEXT I
NFibers = 0
FOR J = 0 TO YEnd
  FOR I = 0 TO XEnd
    IF CMap%(POINT(I,J)) < Thd% THEN NThd% = 0:GOTO NexI
    NThd% = NThd% + 1
    IF NThd% > NTh% THEN
      Ix = I/CC% + 1
      FOR K = Ix - 1 TO Ix + 1
        IF ABS(I - Xc(K,Xn(K))) > RadiusX THEN GOTO NexK
        IF ABS(J - Yc(K,Xn(K))) > RadiusY THEN GOTO NexK
        IF (I-Xc(K,Xn(K)))^2 + 1.44*(J-Yc(K,Xn(K)))^2 < RadiusSq THEN GOTO NexI
      NEXT K
    END IF
  NEXT I
NEXT J

```

NexK: NEXT K

```

  Xn(Ix) = Xn(Ix) + 1
  Xc(Ix,Xn(Ix)) = I:Yc(Ix,Xn(Ix)) = J
  CIRCLE (I,J),1,16

```

```

    PSET (I,J),16
    NThd% = 0
  END IF
NexI:NEXT I
  NThd% = 0
  NEXT J
  K = 0
  FOR I = 1 TO XEnd/CC% + 1
    FOR J = 1 TO Xn(I)
      K = K + 1
      X(K) = Xc(I,J):Y(K) = Yc(I,J)
    NEXT J
  NEXT I
  NFibers = K
  VFract = NFibers * Calibration
  MenuString$ = "NFibers = " + STR$(NFibers)
  MENU 3,7,1,MenuString$
  MenuString$ = "Vf = " + LEFT$(STR$(VFract*100),4)
  MENU 3,8,1,MenuString$
RETURN

```

FiberCounter:

```

ON MOUSE GOSUB CountMouse:MOUSE ON
RadiusX = RadiusY * 1.2

```

RETURN

CountMouse:

```

f = MOUSE(0)
A = MOUSE(3)
B = MOUSE(4)
IF A < 2 THEN IF B < 2 THEN J = YEnd :RETURN
IF CC% = 0 THEN CC% = RadiusX/1.5
Ix = A/CC% + 1
Xn(Ix) = Xn(Ix) + 1
NFibers = NFibers + 1
Xc(Ix,Xn(Ix)) = A:Yc(Ix,Xn(Ix)) = B
X(NFibers) = A:Y(NFibers) = B
CIRCLE (A,B),1,17
PSET (A,B),17
NFib$ = "NFibers = " + STR$(NFibers)
MENU 3,7,1,NFib$
VFib = 100 * NFibers * Calibration
VFib$ = "Fiber Vf = " + LEFT$(STR$(VFib),4)
MENU 3,8,1,VFib$

```

RETURN

Dir0:

```

FILES "df0:"

```

RETURN

Dir1:

```

FILES "df1:"

```

RETURN

Rad:

```
LOCATE 24,1:INPUT "Fiber-pixel radius ",RadiusY
RETURN
```

Brt:

```
LOCATE 24,1:INPUT "Brightness threshold",ThdSet% RETURN
```

Cali:

```
LastHCalib = HCalib :LastVCalib = VCalib
LOCATE 22,1:PRINT "
PRINT "
LOCATE 22,1
PRINT "Horizontal =";HCalib;" Vertical =";VCalib
LOCATE 23,1
INPUT "Horizontal, Vertical ",HCalib,VCalib
IF HCalib = 0 THEN HCalib = LastHCalib
IF VCalib = 0 THEN VCalib = LastVCalib
HCal = 100/HCalib:VCal = 100/VCalib 'Microns per pixel
ScreenX = 316 * HCal:ScreenY = 202 * VCal
Screenarea = ScreenX * ScreenY 'Area in microns square
Calibration = FiberArea/Screenarea
LOCATE 22,1
PRINT "
PRINT "
PRINT "
RETURN
```

FibArea:

```
LastFiberArea = FiberArea
LOCATE 22,1
PRINT "
PRINT "
LOCATE 22,1:PRINT "Current fiber area = ";FiberArea
LOCATE 23,1
INPUT "Fiber area (square microns) =",FiberArea
LOCATE 22,1
PRINT "
PRINT "
IF FiberArea = 0 THEN FiberArea = LastFiberArea
RETURN
```

Distance:

```
ON MOUSE GOSUB MeasureRadius
MOUSE ON
FD = 0
RETURN
```

MeasureRadius:

```
InvertVideo
f% = MOUSE(0)
SX% =MOUSE(3)
SY% =MOUSE(4)
WHILE MOUSE(0) = -1
EX% = MOUSE(5)
```

```

EY% = MOUSE(6)
LINE (SX%,SY%)-(EX%,EY%),Ch%
LINE (SX%,SY%)-(EX%,EY%),Ch%
WEND
NormalVideo
dX = EX%-SX%: dY = EY%-SY%
dMX = dX * HCal
dMY = dY * VCal
Distance = SQR(dMX^2 + dMY^2)
IF FD = 0 THEN LINE (SX%,SY%)-(EX%,EY%),Ch%
MenuString$="X pix =" + STR$(dX) + " Y pix =" + STR$(dY)
MENU 3,9,1,MenuString$
MenuString$ = "Microns = " + STR$(Distance)
MENU 3,10,1,MenuString$
RETURN

FindDiameter:
TH% = 8
f = MOUSE(0)
f = MOUSE(0)
MOUSE OFF
InvertVideo
WHILE MOUSE(0) = 0
SX% = MOUSE(1)
SY% = MOUSE(2)
LINE (SX%,SY%)-(SX% + 20,SY%),16
LINE (SX%,SY%)-(SX% + 20,SY%),16
WEND
NormalVideo
SX% = MOUSE(3)
SY% = MOUSE(4)
NT% = 0
BAve = 0
FOR I = 0 TO 20
B% = CMap%(POINT(SX% + I,SY%))
IF B% > TH% THEN
NT% = NT% + 1
BAve = BAve + B%
PSET (SX% + I,SY%),19
END IF
IF B% < TH% THEN
IF NT% > 3 THEN
BAve = BAve/NT%
RadiusY = NT%/1.2
Thd% = BAve - 2
GOSUB WriteMenu
END IF
NT% = 0
PSET(SX% + I,SY%),0
END IF
NEXT I
MOUSE ON
RETURN

```

WriteMenu:

```
MenuString$ = "Diam =" + STR$(NT%) + " Brt =" + STR$(BAve)
MENU 3,11,1,MenuString$
RETURN
```

PalBar:

```
FOR I = 0 TO 31
  LINE(I*3,180)-(I*3+3,178),I,bf
NEXT I
RETURN
```

BatchRead:

```
Nb = Nb + 1
Total(Nb) = 0
Reader = 1
CLS
BFlag = 1
INPUT "Enter first file number ",NFirst(Nb)
INPUT "Enter last file number ",NLast(Nb)
INPUT "File Name with disk ",FileName1$
NPics(Nb) = NLast(Nb) - NFirst(Nb) + 1
FOR I = NFirst(Nb) TO NLast(Nb)
  FName$(Nb,I) = FileName1$ + FI$(I)
NEXT I
  Total = 0
  FOR I = NFirst(Nb) TO NLast(Nb)
    Fil$ = FName$(Nb,I)
    GOSUB ReadFibers
    Fibers(Nb,I)=NFibers
    Total(Nb) = Total(Nb) + NFibers
  NEXT I
  OverAllSum = OverAllSum + Total(Nb)
  OverAllNPics = OverAllNPics + NPics(Nb)
  OverallAverage = OverAllSum/OverAllNPics
  Average(Nb) = Total(Nb)/NPics(Nb)
BFlag = 0
Reader = 0
NBatches = Nb
RETURN
```

BatchPrint:

```
PRINT "File Name ";FileName1$
PRINT "Total = ";Total(Nb)
PRINT "Average = ";Average(Nb)
PRINT
  FOR J = NFirst(Nb) TO NLast(Nb)
    PRINT FName$(Nb,J);
    PRINT USING " #### ";Fibers(Nb,J)
  NEXT J
INPUT "Printout desired? ",POS$
IF POS$ = "Y" OR POS$ = "y" THEN
  LPRINT "File Name ";FileName1$
```

```

LPRINT "Total = ";Total(Nb)
LPRINT "Average = ";Average(Nb)
LPRINT
FOR J = NFirst(Nb) TO NLast(Nb)
LPRINT FIName$(Nb,J);
LPRINT USING "      #### ";Fibers(Nb,J)
NEXT J
END IF
RETURN

```

RResults:

```

INPUT " Enter Results Name ",ResultFile$
OPEN ResultFile$ FOR INPUT AS 1
INPUT #1,NBatches
SumStart = 0
FOR I = 1 TO NBatches
FOR J = NFirst(I) TO NLast(I)
INPUT #1,FIName$(I,J),Fibers(I,J)
NEXT J
NEXT I
CLOSE #1
RETURN

```

WResults:

```

INPUT " Enter Results Name ",ResultFile$
OPEN ResultFile$ FOR OUTPUT AS 1
WRITE #1,NBatches
SumStart = 0
FOR I = 1 TO NBatches
FOR J = NFirst(I) TO NLast(I)
WRITE #1,FIName$(I,J),Fibers(I,J)
NEXT J
NEXT I
CLOSE #1
RETURN

```

BatchGraph:

```

N = 0
CLS
R = .1
RX = 4
ZO = 200
FOR I = 1 TO NBatches
FOR J = NFirst(I) TO NLast(I)
N = N + 1
CIRCLE(N*RX,ZO-Fibers(I,J)*R),1,I
LINE(N*RX,ZO-Average(I)*R)-((N+1)*RX,ZO-Average(I)*R),I
NEXT J
NEXT I
LINE(0,ZO-0*R)-(300,ZO-0*R),1
LINE(0,ZO-500*R)-(300,ZO-500*R),1
LINE(0,ZO-1000*R)-(300,ZO-1000*R),1
LINE(0,ZO-1500*R)-(300,ZO-1500*R),1

```

RETURN

Notice:

```
CLS
LOCATE 5,1
PRINT "      Optical Numeric Volume
PRINT "      Fraction Analysis
PRINT "      ONVfA"
PRINT
PRINT " Licensed for use by the Composite
PRINT " Materials and Structures Center
PRINT " Michigan State University
PRINT " Serial No. 1050
PRINT " Copyright October 13, 1989
PRINT " Mark C. Waterbury
PRINT
PRINT "      Version 1.1
RETURN
```

BatchCounter:

```
BFlag = 1 'Indicates that a batch is being counted
INPUT "Number of Batches ",NDrives
INPUT "Printout desired? Y/N ",YN$
Printout = 0
IF YN$ = "Y" THEN Printout = 1
IF YN$ = "y" THEN Printout = 1
FOR D = 1 TO NDrives
INPUT "File Name with drive ",FileName$(D)
INPUT "First and last file numbers ",NFirst(D),NLast(D)
INPUT "Composite density (for voids) ",DComposite(D)
INPUT "Matrix density ",DMat
IF DMat < > 0 THEN DMatrix = DMat
INPUT "Fiber density ",DFib
IF DFib < > 0 THEN DFibers = DFib
NEXT D
FOR D = 1 TO NDrives
FOR I = NFirst(D) TO NLast(D)
FilName$(I) = Drv$(D) + FileName$(D) + FI$(I)
NEXT I
NPic = 0
FOR M = NFirst(D) TO NLast(D)
NPic = NPic + 1
Fil$ = FilName$(M)
PicNameLI$ = Fil$
PictureLI PicNameLI$
GOSUB GetAddr$
GOSUB Palet1
GOSUB AutoCounter
NFibres(NPic) = NFibers
Vf = NFibers * Calibration
LOCATE 1,1:PRINT Fil$;" NFibers = ";NFibers
PRINT "Fiber Vf = ";100 * Vf
```

```

    PRINT FileName$(M); " Data being written"
    GOSUB Distribution
    GOSUB Stats
      GOSUB WriteFibers
      GOSUB WriteDist
      GOSUB WriteStats
    NEXT M
    NPics = NPic
    GOSUB BCalc
    GOSUB BWrite
    IF Printout THEN GOSUB BPrint
  NEXT D
  BFlag = 0
RETURN

BCalc:
TotalFibres = 0
FOR NPic = 1 TO NPics
  TotalFibres = TotalFibres + NFibres(NPic)
NEXT NPic
AveFibres(D) = TotalFibres/NPics
Vf = AveFibres(D) * Calibration
Vm = (DComposite(D)-Vf * DFibers)/DMatrix
Vv = 1 - Vf - Vm
VFib = 100 * Vf:Vmatr = 100 * Vm: Vvoid = 100 * Vv
RETURN

VoidCalcs:
Vm = -(Vf * DFibers - DComposite)/DMatrix
Vv = 1 - Vf - Vm
RETURN

BPrint:
LPRINT "Optical Numeric Volume Fraction Analysis"
LPRINT
LPRINT "Volume fractions for ";FileName$(D);" set."
LPRINT "Fiber density = ";DFibers;
LPRINT " Matrix density = ";DMatrix
LPRINT "Composite density = ";DComposite(D)
LPRINT
LPRINT "Fiber area = ";FiberArea
LPRINT "Screen area = ";Screenarea
LPRINT
LPRINT "Image #   Fibers   Vf"
NPic = 0
FOR I = NFirst(D) TO NLast(D)
  NPic = NPic + 1
  VfPic = NFibres(NPic) * Calibration
  LPRINT USING "####.#  ";I;NFibres(NPic);VfPic*100
NEXT I
LPRINT
LPRINT "Average number of fibers = ";AveFibres(D)
LPRINT

```

```

LPRINT "Fiber Vf = ";;PRINT USING "##.#";VFib
LPRINT "Matrix Vm = ";;PRINT USING "##.#";Vmatr
LPRINT "Void Vv = ";;PRINT USING "##.#";Vvoid
RETURN

```

BWrite:

```

Fil$ = Drv$(D) + FileName$(D) + ".res"
OPEN Fil$ FOR OUTPUT AS 1
PRINT #1, "Optical Numeric Volume Fraction Analysis"
PRINT #1, "Average volume fractions for ";FileName$(D);" set."
PRINT #1, "Fiber density = ";DFibers;" Matrix density = ";DMatrix
PRINT #1, "Composite density = ";DComposite(D)
PRINT #1, "Fiber area = ";FiberArea
PRINT #1, "Screen area = ";Screenarea
PRINT #1, "Image #   Fibers   Vf"
  NPic = 0
  FOR I = NFirst(D) TO NLast(D)
    NPic = NPic + 1
    VfPic = NFibres(NPic) * Calibration
    PRINT #1,I,NFibres(NPic),VfPic * 100
  NEXT I

```

```

PRINT #1, "Average number of fibers = ";AveFibres(D)
PRINT #1, "Fiber volume fraction = ";VFib
PRINT #1, "Matrix volume fraction = ";Vmatr
PRINT #1, "Void volume fraction = ";Vvoid
CLOSE #1
RETURN

```

WriteFibers:

```

IF NFibers = 0 THEN PRINT "Fibers not counted ":RETURN
FibFil$ = Fil$ + "Fibers"
OPEN FibFil$ FOR OUTPUT AS 1
WRITE #1,Fil$,Note$
WRITE #1,NFibers
  FOR I = 1 TO NFibers
    WRITE #1,X(I),Y(I)
  NEXT I
CLOSE #1
RETURN

```

ReadFibers:

```

FibFil$ = Fil$ + "Fibers"
OPEN FibFil$ FOR INPUT AS 1
INPUT #1,f$,Note$
INPUT #1,NFibers
IF Reader = 1 THEN GOTO FibJump
FOR I = 1 TO NFibers
  INPUT #1,X(I),Y(I)
NEXT I
FibJump: CLOSE #1
RETURN

```

DrawTags:

```

FOR I = 1 TO NFibers
  CIRCLE(X(I), Y(I)), 1, TC %
  PSET(X(I), Y(I)), TC %
NEXT I
RETURN

```

TagMap:

```

MapScale = 3
Factor = 313/MapScale
YFactor = 198/MapScale
INPUT "File name with drive ", FibFI$
INPUT "First and last file numbers ", FirstFib, LastFib
CLS
FOR M = FirstFib TO LastFib
  NY = 0
  N = M - FirstFib
  NCheck: IF N > MapScale-1 THEN N=N-MapScale: NY=NY+1: GOTO NCheck
  FibFil$ = FibFI$ + FI$(M) + "Fibers"
  OPEN FibFil$ FOR INPUT AS #1
  INPUT #1, Fil$, Note$
  INPUT #1, NFibers
  FOR I = 1 TO NFibers
    INPUT #1, X(I), Y(I)
  NEXT I
  CLOSE #1
  NShift = N * Factor
  NYShift = NY*YFactor
  FOR I = 1 TO NFibers
    PSET (NShift + X(I)/MapScale, NYShift + Y(I)/MapScale), MC %
  NEXT I
NEXT M
RETURN

```

Cleanup:

```

CLS
RETURN

```

Histogram:

```

MaxHisto = 0
FOR I = 0 TO 15
  Histo(I) = 0
NEXT I
XSample = 2: YSample = 2 'Sample rate for Areal Analysis
FOR J = 0 TO YEnd STEP YSample
  FOR I = 0 TO XEnd STEP XSample
    Histo(POINT (I,J)) = Histo(POINT (I,J)) + 1
  NEXT I
NEXT J
SXa = (XEnd+1)/XSample: SYa = (YEnd+1)/YSample
FOR I = 0 TO 15
  Histo(I) = 100 * Histo(I)/(SXa * SYa)
  IF Histo(I) > MaxHisto THEN MaxHisto = Histo(I)

```

```

NEXT I
Sum = Histo(MapC%(0))
HistoSum(MapC%(0)) = Sum
FOR I = 1 TO 15
Sum = Sum + Histo(MapC%(I))
HistoSum(MapC%(I)) = Sum
NEXT I
Sum = Histo(MapC%(15))
SumHisto(MapC%(15)) = Sum
FOR I = 14 TO 0 STEP -1
Sum = Sum + Histo(MapC%(I))
SumHisto(MapC%(I)) = Sum
NEXT I
LOCATE 1,1
FOR I = 0 TO 15
PRINT USING "## ";I;
PRINT USING " ##.##";Histo(MapC%(I));HistoSum(MapC%(I));
PRINT USING " ##.##";SumHisto(MapC%(I))
LINE(I*10,180)-(I*10+8,180-Histo(MapC%(I))),MapC%(I),bf
NEXT I
INPUT "Type Y for printout ";Y$
IF Y$ = "Y" THEN GOTO Pr
IF Y$ = "y" THEN GOTO Pr
GOTO Nope
Pr:
FOR I = 0 TO 15
LPRINT USING "## ";I;
LPRINT USING "##.##";Histo(MapC%(I));HistoSum(MapC%(I));
_SumHisto(MapC%(I))
NEXT I
Nope: ON MOUSE GOSUB MouseTograph
MOUSE ON
RETURN

MouseTograph:
f = MOUSE(0)
SX% =MOUSE(3)
SY% =MOUSE(4)
Pal = POINT (SX%,SY%)
PALETTE Pal,0,0,1
FOR I = 1 TO 20000
NEXT I
PALETTE Pal,CMap%(Pal)/15, CMap%(Pal)/15, CMap%(Pal)/15
RETURN

Diameter:
ND = ND + 1
IF ND > 100 THEN RETURN
Xc(ND,J) = NT%
Yc(0,J) = ND
RETURN

```

```
Quit:
MENU RESET
LIBRARY CLOSE
STOP
```

```
ReadImage:
INPUT "Enter file name ",PicNameLI$
PictureLI PicNameLI$
Fil$ = PicNameLI$
FilMen$ = "File Name " + Fil$
GOSUB GetAddr$
GOSUB Palet1
ON MOUSE GOSUB MouseTograph
MOUSE ON
NFibers = 0
RETURN
```

```
GetAddr$:
sWindow& = WINDOW(7)
sScreen& = PEEKL(sWindow& + 46)
sViewPort& = sScreen& + 44
sRastPort& = sScreen& + 84
sColorMap& = PEEKL(sViewPort& + 4)
colorTab& = PEEKL(sColorMap& + 4)
sBitMap& = PEEKL(sRastPort& + 4)
scrDepth% = PEEK(sBitMap& + 5)
nColors% = 2^scrDepth%
FOR kk = 0 TO 15
  cTab%(kk) = PEEKW(colorTab&+(kk*2))
  CMap%(kk) = INT(cTab%(kk)/256)
  MapC%(CMap%(kk)) = kk
NEXT
RETURN
```

```
WriteImage:
PictureSI WritePicName$
RETURN
```

```
EnterImageName:
LOCATE 24,1: INPUT "Image Name ",WritePicName$
RETURN
```

```
SUB PictureSI (WritePicName$) STATIC
  SHARED BPlaneSI&()
  saveError$ = ""
  AvailRam& = FRE(-1)
  NeededRam& = ((W/8)*h*(D+1))+5000
  IF AvailRam& < NeededRam& THEN
    PRINT "Not enough free ram"
    GOTO McleanupSI
  END IF
  GOSUB GetScrAddr$SI
  ccrtDir% = 1:ccrtStart% = 1:ccrtEnd% = nColors% - 1
```

```

ccrtSecs& = 0:ccrtMics& = 2000
cReg% = ccrtStart% :fHandle& = 0:mybuf& = 0
FileName$ = WritePicName$ + CHR$(0)
fHandle& = xOpen&(SADD(FileName$),1006)
IF fHandle& = 0 THEN
  saveError$ = "Can't open output file"
  GOTO ScleanupSI
END IF
ClearPublic& = 65537&
mybufsize& = 120
mybuf& = AllocMem&(mybufsize&,ClearPublic&)
IF mybuf& = 0 THEN
  saveError$ = "Can't alloc buffer"
  GOTO ScleanupSI
END IF
cbuf& = mybuf&
GOSUB GetScrAdrsSI
zero& = 0: pad% = 0:aspect% = &HA0B:BMHDsize& = 20
CMAPsize& = (2^scrDepth%) * 3:CAMGsize& = 4:CCRTsize& = 14
BODYsize& = (scrWidth%/8) * scrHeight% * scrDepth%
FORMsize& = BMHDsize& + CMAPsize& + CAMGsize& + CCRTsize& +
BODYsize& + 44
tt$ = "FORM"
wLen& = xWrite&(fHandle&,SADD(tt$),4)
wLen& = xWrite&(fHandle&,VARPTR(FORMsize&),4)
tt$ = "ILBM"
wLen& = xWrite&(fHandle&,SADD(tt$),4)
IF wLen& <= 0 THEN
  saveError$ = "Error writing FORM header"
  GOTO ScleanupSI
END IF
tt$ = "BMHD"
wLen& = xWrite&(fHandle&,SADD(tt$),4)
wLen& = xWrite&(fHandle&,VARPTR(BMHDsize&),4)
wLen& = xWrite&(fHandle&,VARPTR(scrWidth%),2)
wLen& = xWrite&(fHandle&,VARPTR(scrHeight%),2)
wLen& = xWrite&(fHandle&,VARPTR(zero&),4)
temp% = (256 * scrDepth%)
wLen& = xWrite&(fHandle&,VARPTR(temp%),2)
wLen& = xWrite&(fHandle&,VARPTR(zero&),4)
wLen& = xWrite&(fHandle&,VARPTR(aspect%),2)
wLen& = xWrite&(fHandle&,VARPTR(scrWidth%),2)
wLen& = xWrite&(fHandle&,VARPTR(scrHeight%),2)
IF wLen& <= 0 THEN
  saveError$ = "Error writing BMHD"
  GOTO ScleanupSI
END IF
tt$ = "CMAP"
wLen& = xWrite&(fHandle&,SADD(tt$),4)
wLen& = xWrite&(fHandle&,VARPTR(CMAPsize&),4)
FOR kk& = 0 TO nColors% - 1
  regTemp% = PEEKW(colorTab& + (2*kk&))
  POKE(cbuf& + (kk&*3)),(regTemp% AND &HF00) / 16

```

```

    POKE(cbuff + (kk*3) + 1), (regTemp% AND &HF0)
    POKE(cbuff + (kk*3) + 2), (regTemp% AND &HF) * 16
NEXT
    wLen& = xWrite&(fHandle&, cbuff, CMAPsize&)
    IF wLen& <= 0 THEN
        saveError$ = "Error writing CMAP"
        GOTO ScleanupSI
    END IF
    tt$ = "CAMG"
    wLen& = xWrite&(fHandle&, SADD(tt$), 4)
    wLen& = xWrite&(fHandle&, VARPTR(CAMGsize&), 4)
    vpModes& = PEEKW(sViewPort& + 32)
    wLen& = xWrite&(fHandle&, VARPTR(vpModes&), 4)
    IF wLen& <= 0 THEN
        saveError$ = "Error writing CAMG"
        GOTO ScleanupSI
    END IF
    tt$ = "CCRT"
    wLen& = xWrite&(fHandle&, SADD(tt$), 4)
    wLen& = xWrite&(fHandle&, VARPTR(CCRTsize&), 4)
    wLen& = xWrite&(fHandle&, VARPTR(ccrtDir%), 2)
    temp% = (256*ccrtStart%) + ccrtEnd%
    wLen& = xWrite&(fHandle&, VARPTR(temp%), 2)
    wLen& = xWrite&(fHandle&, VARPTR(ccrtSecs&), 4)
    wLen& = xWrite&(fHandle&, VARPTR(ccrtMics&), 4)
    wLen& = xWrite&(fHandle&, VARPTR(pad%), 2)
    IF wLen& <= 0 THEN
        saveError$ = "Error writing CCRT"
        GOTO ScleanupSI
    END IF
    tt$ = "BODY"
    wLen& = xWrite&(fHandle&, SADD(tt$), 4)
    wLen& = xWrite&(fHandle&, VARPTR(BODYsize&), 4)
    scrRowBytes% = scrWidth% / 8
    FOR rr& = 0 TO scrHeight% - 1
        FOR pp& = 0 TO scrDepth% - 1
            scrRow& = BPlaneSI&(pp&) + (rr&*scrRowBytes%)
            wLen& = xWrite&(fHandle&, scrRow&, scrRowBytes%)
            IF wLen& <= 0 THEN
                saveError$ = "Error writing BODY"
                GOTO ScleanupSI
            END IF
        NEXT
    NEXT
NEXT
saveError$ = ""
ScleanupSI:
IF fHandle& <> 0 THEN CALL xClose&(fHandle&)
IF mybuff& <> 0 THEN CALL FreeMem&(mybuff&, mybuffsize&)
EXIT SUB
McleanupSI:
IF loadError$ <> "" THEN PRINT loadError$
IF saveError$ <> "" THEN PRINT saveError$
EXIT SUB

```

GetScrAdrsSI:

```

sWindow& = WINDOW(7)
sScreen& = PEEKL(sWindow& + 46)
sViewPort& = sScreen& + 44
sRastPort& = sScreen& + 84
sColorMap& = PEEKL(sViewPort& + 4)
colorTab& = PEEKL(sColorMap& + 4)
sBitMap& = PEEKL(sRastPort& + 4)
scrWidth% = PEEKW(sScreen& + 12)
scrHeight% = PEEKW(sScreen& + 14)
scrDepth% = PEEK(sBitMap& + 5)
nColors% = 2^scrDepth%
FOR kk& = 0 TO scrDepth% - 1
    BPlaneSI&(kk&) = PEEKL(sBitMap& + 8 + (kk&*4))
NEXT
RETURN
END SUB

```

SUB PictureLI (PicNameLI\$) STATIC
 SHARED BPlaneLI&()

```

CLS
loadError$ = ""
f$ = PicNameLI$
MENU 1,11,0,PicNameLI$
ccrtDir% = 0:ccrtStart% = 0:ccrtEnd% = 0:ccrtSecs& = 0
ccrtMics& = 0:fHandle&=0:mybuf&=0:foundBMHD&=0
foundCMAP&=0:foundCAMG&=0:foundCCRT&=0:foundBODY& = 0
FileName$ = f$ + CHR$(0)
fHandle& = xOpen&(SADD(FileName$),1005)
IF fHandle& = 0 THEN
    loadError$ = "Can't open/find pic file"
    GOTO LcleanupLI
END IF
ClearPublic& = 65537&
mybufsize& = 360
mybuf& = AllocMem&(mybufsize&,ClearPublic&)
IF mybuf& = 0 THEN
    loadError$ = "Can't alloc buffer"
    GOTO LcleanupLI
END IF
inbuf& = mybuf&
cbuf& = mybuf& + 120
cTab& = mybuf& + 240
rlen& = xRead&(fHandle&,inbuf&,12)
tt$ = ""
FOR kk& = 8 TO 11
    tt% = PEEK(inbuf& + kk&)
    tt$ = tt$ + CHR$(tt%)
NEXT
IF tt$ <> "ILBM" THEN
    loadError$ = "Not standard ILBM pic file"
    GOTO LcleanupLI

```

```

END IF
ChunkLoopLI:
  rLen& = xRead&(fHandle&,inbuf&,8)
  icLen& = PEEKL(inbuf& + 4)
  tt$ = ""
  FOR kk& = 0 TO 3
    tt% = PEEK(inbuf& + kk&)
    tt$ = tt$ + CHR$(tt%)
  NEXT
IF tt$ = "BMHD" THEN 'BitMap header
  foundBMHD& = 1
  rLen& = xRead&(fHandle&,inbuf&,icLen&)
  iWidth% = PEEKW(inbuf&)
  iHeight% = PEEKW(inbuf& + 2)
  iDepth% = PEEK(inbuf& + 8)
  iCompr% = PEEK(inbuf& + 10)
  scrWidth% = PEEKW(inbuf& + 16)
  scrHeight% = PEEKW(inbuf& + 18)
  iRowBytes% = iWidth% / 8
  scrRowBytes% = scrWidth% / 8
  nColors% = 2^(iDepth%)
  AvailRam& = FRE(-1)
  NeededRam& = ((scrWidth%/8)*scrHeight%*(iDepth% + 1))+5000
  IF AvailRam& < NeededRam& THEN
    loadError$ = "Not enough free ram"
    GOTO LcleanupLI
  END IF
  kk& = 1
  IF scrWidth% > 320 THEN kk& = kk& + 1
  IF scrHeight% > 200 THEN kk& = kk& + 2
  GOSUB GetScrAddrLI
ELSEIF tt$ = "CMAP" THEN
  foundCMAP& = 1
  rLen& = xRead&(fHandle&,cbuf&,icLen&)
  FOR kk& = 0 TO nColors% - 1
    Red% = PEEK(cbuf&+(kk&*3))
    gre% = PEEK(cbuf&+(kk&*3)+1)
    blu% = PEEK(cbuf&+(kk&*3)+2)
    regTemp% = (Red%*16)+(gre%)+(blu%/16)
    POKEW(cTab&+(2*kk&)),regTemp%
  NEXT
ELSEIF tt$ = "CAMG" THEN 'Amiga ViewPort Modes
  foundCAMG = 1
  rLen& = xRead&(fHandle&,inbuf&,icLen&)
  camgModes& = PEEKL(inbuf&)
ELSEIF tt$ = "CCRT" THEN 'Graphicraft color cycle info
  foundCCRT& = 1
  rLen& = xRead&(fHandle&,inbuf&,icLen&)
  ccrtDir% = PEEKW(inbuf&)
  ccrtStart% = PEEK(inbuf& + 2)
  ccrtEnd% = PEEK(inbuf& + 3)
  ccrtSecs& = PEEKL(inbuf& + 4)
  ccrtMics& = PEEKL(inbuf& + 8)

```

```

ELSEIF tt$ = "BODY" THEN 'BitMap
  foundBODY& = 1
  IF iCompr% = 0 THEN 'no compression
    FOR rr& = 0 TO iHeight% -1
      FOR pp& = 0 TO iDepth% -1
        scrRow& = BPlaneLI&(pp&)+(rr&*scrRowBytes%)
        rLen& = xRead&(fHandle&,scrRow&,iRowBytes%)
      NEXT pp&
    NEXT rr&
  ELSEIF iCompr% = 1 THEN 'cmpByteRun1
    FOR rr& = 0 TO iHeight% -1
      FOR pp& = 0 TO iDepth% -1
        scrRow& = BPlaneLI&(pp&)+(rr&*scrRowBytes%)
        bCnt% = 0
        WHILE (bCnt% < iRowBytes%)
          rLen& = xRead&(fHandle&,inbuf&,1)
          inCode% = PEEK(inbuf&)
          IF inCode% < 128 THEN
            rLen& = xRead&(fHandle&,scrRow& + bCnt%, inCode% +1)
            bCnt% = bCnt% + inCode% + 1
          ELSEIF inCode% > 128 THEN
            rLen& = xRead&(fHandle&,inbuf&,1)
            inByte% = PEEK(inbuf&)
            FOR kk& = bCnt% TO bCnt% + 257 - inCode%
              POKE(scrRow&+kk&),inByte%
            NEXT
            bCnt% = bCnt% + 257 - inCode%
          END IF
        WEND
      NEXT
    NEXT
  ELSE
    loadError$ = "Unknown compression algorithm"
    GOTO LcleanupLI
  END IF
ELSE
  FOR kk& = 1 TO icLen&
    rLen& = xRead&(fHandle&,inbuf&,1)
  NEXT
  IF (icLen& OR 1) = icLen& THEN
    rLen& = xRead&(fHandle&,inbuf&,1)
  END IF
END IF
IF foundBMHD& AND foundCMAP& AND foundBODY& THEN
  GOTO GoodLoadLI
END IF
IF rLen& > 0 THEN GOTO ChunkLoopLI
IF rLen& < 0 THEN 'Read error
  loadError$ = "Read error"
  GOTO LcleanupLI
END IF
IF (foundBMHD&=0) OR (foundBODY&=0) OR (foundCMAP&=0) THEN
  loadError$ = "Needed ILBM chunks not found"

```

```
GOTO LcleanupLI
END IF
```

```
GoodLoadLI:
```

```
loadError$ = ""
```

```
IF foundCMAP& THEN
```

```
    CALL LoadRGB4&(sViewPort&,cTab&,nColors%)
```

```
END IF
```

```
LcleanupLI:
```

```
IF fHandle& < > 0 THEN CALL xClose&(fHandle&)
```

```
IF mybuf& < > 0 THEN CALL FreeMem&(mybuf&,mybufsize&)
```

```
EXIT SUB
```

```
McleanupLI:
```

```
IF loadError$ < > "" THEN PRINT loadError$
```

```
IF saveError$ < > "" THEN PRINT saveError$
```

```
EXIT SUB
```

```
GetScrAddrLI:
```

```
sWindow& = WINDOW(7)
```

```
sScreen& = PEEKL(sWindow& + 46)
```

```
sViewPort& = sScreen& + 44
```

```
sRastPort& = sScreen& + 84
```

```
sColorMap& = PEEKL(sViewPort& + 4)
```

```
colorTab& = PEEKL(sColorMap& + 4)
```

```
sBitMap& = PEEKL(sRastPort& + 4)
```

```
scrWidth% = PEEKW(sScreen& + 12)
```

```
scrHeight% = PEEKW(sScreen& + 14)
```

```
scrDepth% = PEEK(sBitMap& + 5)
```

```
nColors% = 2^scrDepth%
```

```
FOR kk& = 0 TO scrDepth% - 1
```

```
    BPlaneLI&(kk&) = PEEKL(sBitMap& + 8 + (kk&*4))
```

```
NEXT
```

```
RETURN
```

```
END SUB
```

```
SUB InvertVideo STATIC
```

```
    CALL SetDrMd& (WINDOW(8),3)
```

```
END SUB
```

```
SUB NormalVideo STATIC
```

```
    CALL SetDrMd& (WINDOW(8),1)
```

```
END SUB
```

APPENDIX D

SOURCE CODE FOR WILHELMY WETTING BALANCE DATA ACQUISITION SYSTEM

The following program is the source code listing for the micro-Wilhelmy balance control and data acquisition program written in compiled MicroSoft QuickBasic, and the Wilhelmy data analysis program written in compiled AmigaBasic (ABSoft AC-Basic), described in chapter 2. The routines for controlling the PC21 Compumotor, Omega A/D conversion card, and the Cole-Parmer temperature controller were adapted from code provided by the respective manufacturers.

A list of subroutines and a brief description of their functions precedes the actual code. Long code lines have been reformatted, with leading hyphens attached to the second portions.

The first program listing is for controlling the Wilhelmy balance and acquiring data, the second for further analysing that data.

Main: Main program loop.

Dims: Defines all data arrays and allocates space to them.

MenuRefresh: Writes a menu line at the bottom of the screen. Typing the first letter in each word directs the program to that subroutine.

InLoop: The main menu "INKEY" loop. Checks user keyboard entries and directs program flow to the appropriate subroutine.

DataEntry: Inputs data on the fiber, liquid, temperatures, etc.

StageMove: Moves the stage upward 1/100 inch.

Wilhelmy: Main Wilhelmy routine. Immerses fiber in steps, pauses, records balance weight then saves data.

FindAverage: Averages several voltages measured from A/D converter in "Logger" after each immersion increment.

Calculations: Calculates wetting angle from immersion force and fiber perimeter.

ArcCosine: Returns the inverse cosine to the calculations routine.

LogStart: Begins logging force data.

Logger: Accesses the A/D card and logs force data.

ReadVolts: Calls A/D card 100 times to smooth out noise and returns average result.

SetZero: Sets the input with the fiber out of the liquid to zero to cancel the tare weight of the fiber and hook.

SetMass: Sets the ratio between the change in mass measured and the change in A/D card output voltage.

LoadCalib: Loads a previously stored A/D card calibration.

PrintData: Prints out mass and angle data.

Initialize: Initializes all constants, sets mnemonic variables to appropriate CompuMotor command strings.

SetCMD: Concatenates CompuMotor command strings from parts.

Reminders: A list of CompuMotor command strings that may be used by users wishing to customize code.

Helper: A sarcastic reference to the complete absence of online user help.

DriveParameters: Prints out the current status of the CompuMotor commands.

DriveProgram: Allows the user to edit the Wilhelmy sequence.

FileSave: Saves data to file.

ReadFile: Reads previously saved data for re-analysis with different diameter, etc.

Stoppit: Halts the CompuMotor motion.

Reader: Reads position information from the CompuMotor to the system bus, one character at a time.

CMDWriter: Sends commands stored in CMD\$ to CompuMotor via the "Transmitter" routine 1 character at a time.

Transmitter: Actually transmits each character sent by the CMDWriter routine.

InitializePC21: Initializes the CompuMotor by sending a command string that prepares it for further instructions.

ReadStatus: Reads the status of the temperature regulator.

ReadTemp: For Cole Parmer Model 20B with 134 ADC, reads temperatures and setpoint.

ReadVolt: The general A/D card reading routine, provided for reading temperatures.

LinearizeE: Converts the A/D card voltages into temperatures for use with type E thermocouples.

LinearizeJ: Converts the A/D card voltages into temperatures for use with type J thermocouples.

WILHELMY BALANCE CONTROL AND DATA ACQUISITION SOURCE CODE

```

REM === Wilhelmy Balance Control Program =====
REM === Copyright April 10, 1989 Mark Waterbury, for the
REM Composite Materials and Structures Center, Michigan
State University
DEFINT I-K

```

Main:

```

  GOSUB Dims
  GOSUB Initialize
  GOSUB InitializePC21:
  GOSUB MenuRefresh
  GOSUB InLoop
END

```

Dims:

```

  DIM Mass(20, 100), AveMass(20), Deviation(20), Angle(20), Energy(20)
RETURN

```

MenuRefresh:

```

  CLS
  PRINT "Data entry, Wilhelmy, Save file, Read file, Quit"
  PRINT "Zero, Calibrate, Load calibration, Arithmetic"
RETURN

```

InLoop:

```

  M$ = INKEY$
  IF M$ = "W" THEN GOSUB Wilhelmy
  IF M$ = "w" THEN GOSUB Wilhelmy
  IF M$ = "q" THEN GOSUB Stoppit: END
  IF M$ = "Q" THEN GOSUB Stoppit: END
  IF M$ = "z" THEN GOSUB SetZero
  IF M$ = "Z" THEN GOSUB SetZero
  IF M$ = "C" THEN GOSUB SetMass
  IF M$ = "c" THEN GOSUB SetMass
  IF M$ = "D" THEN GOSUB DataEntry
  IF M$ = "d" THEN GOSUB DataEntry
  IF M$ = "F" THEN GOSUB FileSave
  IF M$ = "f" THEN GOSUB FileSave
  IF M$ = "R" THEN GOSUB ReadFile
  IF M$ = "r" THEN GOSUB ReadFile
  IF M$ = "S" THEN GOSUB FileSave
  IF M$ = "s" THEN GOSUB FileSave
  IF M$ = "L" THEN GOSUB LoadCalib
  IF M$ = "l" THEN GOSUB LoadCalib
  IF M$ = "A" THEN GOSUB Calculations
  IF M$ = "a" THEN GOSUB Calculations
  IF M$ = "P" THEN GOSUB PrintData
  IF M$ = "p" THEN GOSUB PrintData
  IF M$ = "M" THEN GOSUB StageMove
  IF M$ = "m" THEN GOSUB StageMove

```

```
GOTO InLoop
RETURN
```

```
DataEntry:
```

```
CLS
INPUT "Fiber name ", Fiber$
INPUT "Fiber diameter (microns) ", Diameter
INPUT "Liquid name", Liquid$
INPUT "Liquid Surface Tension (mJ/M^2) ", Elv
INPUT "Liquid temperature ", Temperature
```

```
RETURN
```

```
StageMove:
```

```
A$ = "1": V$ = ".5": D$ = "60000" 'Up 1/100 inch
CMD$ = " MN A" + A$ + " V" + V$ + " D" + D$ + " G
''Preset move
GOSUB CMDWriter
RETURN
```

```
Wilhelmy:
```

```
MoveTime2& = 60 'Seconds to complete stage moves
J = 0
Samples = 25
CLS
LINE (0, 200)-(640, 200), 1
LINE (0, 350)-(640, 350), 1
INPUT "Data file name ", Fil$
INPUT "Initial immersion distance (inches ) ", Immersion
IF Immersion > 1 THEN Immersion = 0
MoveTime1& = 60
D$ = "-500000"
IF Immersion = 0 THEN D$ = "0"
IF Immersion = .1 THEN D$ = "-100000"
IF Immersion = .2 THEN D$ = "-200000"
IF Immersion = .3 THEN D$ = "-300000"
IF Immersion = .4 THEN D$ = "-400000"
IF Immersion = .5 THEN D$ = "-500000"
A$ = "1": V$ = "1"
CMD$ = " MN A" + A$ + " V" + V$ + " D" + D$ + " G ''Preset move
GOSUB LogStart
GOSUB FindAverage
GOSUB CMDWriter
StartTime& = TIMER
Waiter: WHILE (TIMER - StartTime&) < MoveTime1&
GOTO Waiter
WEND
A$ = "1": V$ = ".1": D$ = "-20000" 'Down 1/100 inch
CMD$ = " MN A" + A$ + " V" + V$ + " D" + D$ + " G ''Preset move
FOR J = 1 TO 15
GOSUB CMDWriter
StartTime& = TIMER
Waiter2: WHILE (TIMER - StartTime&) < MoveTime2&
```

```

GOTO Waiter2
WEND
GOSUB LogStart
GOSUB FindAverage
NEXT J
A$ = "1": V$ = ".1": D$ = "60000" 'Up 1/100 inch
  CMD$ = " MN A" + A$ + " V" + V$ + " D" + D$ + " G ""Preset move
FOR J = 16 TO 20
GOSUB CMDWriter
  StartTime& = TIMER
Waiter3: WHILE (TIMER - StartTime&) < MoveTime2&
GOTO Waiter3
WEND
GOSUB LogStart
GOSUB FindAverage
NEXT J
GOSUB Calculations
CMD$ = " S "
GOSUB CMDWriter
TIMER OFF
GOSUB FileSave
GOSUB MenuRefresh
RETURN

```

FindAverage:

```

Sum = 0
FOR K = 1 TO Samples
  Sum = Sum + Mass(J, K)
NEXT K
  AveMass(J) = Sum / Samples
Sum = 0
FOR K = 1 TO Samples
  Sum = Sum + (AveMass(J) - Mass(J, K)) ^ 2
NEXT K
  Sum = Sum / Samples
  Deviation(J) = SQR(Sum)
RETURN

```

Calculations:

```

FOR J = 0 TO 20
  Force = 9.807 * AveMass(J) / 1000000
  Perimeter = Diameter * Pi / 1000000
  ElvKg = Elv / 1000
  CosTheta = Force / (Perimeter * ElvKg)
GOSUB ArcCosine
  Angle(J) = 180 * ArcCos / Pi
NEXT J
RETURN

```

ArcCosine:

```

IF CosTheta < 0 THEN RETURN
  ArcCos = -ATN(CosTheta / SQR(-CosTheta * CosTheta + 1)) + 1.5708
RETURN

```

LogStart:

```

K = 0
ON TIMER(1) GOSUB Logger
TIMER ON
x = INP(ADC) 'Starts first conversion
WHILE K < Samples + 1
WEND
TIMER OFF
RETURN

```

Logger:

```

K = K + 1
GOSUB ReadVolts
LOCATE 5, 1
PRINT Count, Count2, Volts, Mass(J, K)
Graph = Volts * 10000
IF J < 11 THEN PSET (J * (Samples + 5) + K, 200 -
Graph), 1
IF J > 10 THEN PSET ((J - 11) * (Samples + 5) + K, 350 - Graph), 1
RETURN

```

ReadVolts:

```

Sum = 0
FOR N = 1 TO 100
Count = INP(ADC + 1)
Count2 = INP(ADC)
Sum = Sum + Count * 256 + Count2
NEXT N
Ave = Sum / 100
Volts = (Ave - 32768!) * .0001522588# - Volts0
Mass(J, K) = Volts * VtoMFactor
RETURN

```

SetZero:

```

Sum = 0
FOR N = 1 TO 5000
x = INP(ADC)
Count = INP(ADC + 1)
Count2 = INP(ADC)
Sum = Sum + Count * 256 + Count2
NEXT N
Ave = Sum / 5000
Volts0 = (Ave - 32768!) * .0001522588#'Scale in
volts
PRINT Volts0
RETURN

```

SetMass:

```

CLS
PRINT "Remove calibration weight and hook"
INPUT "Hit RETURN when ready to zero", F
GOSUB SetZero
PRINT "Apply calibration weight to pan B"

```

```

INPUT "Calibration weight (milligrams) ", CalibWeight
INPUT "Hit RETURN when ready to calibrate", F
Sum = 0
  FOR N = 1 TO 5000
    x = INP(ADC)
    Count = INP(ADC + 1)
    Count2 = INP(ADC)
    Sum = Sum + Count * 256 + Count2
  NEXT N
  Ave = Sum / 5000
  VoltsM = (Ave - 32768!) * .0001522588#'Scale in volts
  DeltaV = VoltsM - Volts0
  VtoMFactor = (CalibWeight / 5) / DeltaV
  PRINT "Voltage with Calibration Mass = "; VoltsM
  PRINT "Volts to Milligrams Factor = "; VtoMFactor
  OPEN "Calibrat.ion" FOR OUTPUT AS 1
  WRITE #1, Volts0, VoltsM, VtoMFactor
  CLOSE #1
RETURN

LoadCalib:
  OPEN "Calibrat.ion" FOR INPUT AS 1
  INPUT #1, Volts0, VoltsM, VtoMFactor
  CLOSE #1
  PRINT Volts0, VoltsM, VtoMFactor
RETURN

PrintData:
  LPRINT Fil$
  LPRINT "Fiber  Liquid  E (lv)  Diameter
Temperature"
  LPRINT Fiber$, Liquid$, Elv, Diameter, Temperature
  LPRINT " J      Mass (mg)   Angle"
  FOR J = 1 TO 20
    LPRINT USING " ###.#### "; J; AveMass(J), Angle(J)
  NEXT J
RETURN

Initialize:
  SCREEN 11
  WIDTH 80, 60
  ADC = 797 'A/D Converter IBM bus location
  Status = ADC - 1 'Digital Input bus location
  Channel = 0 'Specify ADC channel
  OUT ADC, Channel * 16' Select channel
  Pi = 3.14159
  Q = 1: REM number of thermometers - 1
  G(0) = .8: G(1) = .8: K(0) = 11.4: K(1) = 11.4'Thermocouple calibrations
  Interval = 1 'Seconds between weight samples
  NormalMove$ = " MN "
  AltMove$ = " MA "
  ConMove$ = " MC "
  LoopM$ = " L"

```

```

TDelay$ = " T"
EndLoop$ = " N "
Vel$ = " V"
Acc$ = " A"
Dest$ = " D"
Go$ = " G "
Cease$ = " S "
Reverse$ = " H"
A$ = ".1": V$ = ".2": D$ = "50000": H$ = "+": L$ = "1": T$ = "0"
Move$ = AltMove$: LpM$ = LoopM$: TDel$ = TDelay$: EndLp$ = EndLoop$
GOSUB SetCMD
SlowLoop$ = CMD$
WilhelmyCMD$ = CMD$
V$ = ".4"
GOSUB SetCMD
MedLoop$ = CMD$
V$ = "1"
GOSUB SetCMD
FastLoop$ = CMD$
Move$ = NormalMove$: LpM$ = "": TDel$ = "": T$ = "": EndLp$ = ""
V$ = ".1"
GOSUB SetCMD
UpSlow$ = CMD$
V$ = ".4"
GOSUB SetCMD
UpMed$ = CMD$
V$ = "1"
GOSUB SetCMD
UpFast$ = CMD$
A$ = "1": V$ = ".1": D$ = "-20000"
StepDown$ = " MN A" + A$ + " V" + V$ + " D" + D$ + " G "'Preset move
RETURN

```

SetCMD:

```

CMD$ = Move$ + Acc$ + A$ + Vel$ + V$ + Reverse$ + H$ +
Dest$ + D$ + LpM$ + L$ + TDel$ + T$ + EndLp$ + Go$
RETURN

```

Reminders:

```

REM A$ = Acceleration Rev/Sec Sec, V$ = Velocity Rev/Sec
REM H$ = Direction "+" or "-" D$ = Distance/ motor steps 25000/rev
REM L$ = Number of Loop moves, T$ = Time of delay between loops
REM CMD$=" MC A"+A$+" V"+V$+" H"+H$+" G " 'Continuous move
REM CMD$=" S " 'Stop
REM CMD$=" MN A"+A$+" V"+V$+" D"+H$+D$+" G " 'Preset move
REM CMD$=" MA A"+A$+" V"+V$+" D"+H$+D$+" G " 'Alternating
move
REM CMD$=" MN A"+A$+" V"+V$+" D"+H$+D$+" L"+L$+" G " 'Loop
- Function
REM CMD$=CMD$+"T"+T$+" N " ELSE CMD$=CMD$+" N " 'Loop w
delay
RETURN

```

Helper:

```
CLS
PRINT "The Lord Helps Those That Helps Themselves"
RETURN
```

DriveParameters:

```
CLS
PRINT " Daedal Drive Programming"
PRINT
PRINT "Velocity (RPS) = "; V$
PRINT " Acceleration (RPS^2) ="; A$
PRINT "Distance (25000/Rev) = "; D$

PRINT "Looping ";
IF Looping THEN PRINT "ON" ELSE PRINT "OFF"
IF Looping THEN PRINT "Number of Loops = "; L$
IF Move$ = NormalMove$ THEN PRINT "Normal Move Mode"
IF Move$ = AltMove$ THEN PRINT "Alternating Move Mode"
IF Move$ = ConMove$ THEN PRINT "Continuous Move Mode"
PRINT "Direction = "; H$
RETURN
```

DriveProgram:

```
CMDL$ = CMD$
GOSUB DriveParameters
MoveL$ = Move$: VL$ = V$: AL$ = A$: DL$ = D$: HL$ = H$
PRINT "Enter new values or hit RETURN"
PRINT
INPUT "New Velocity ", V$
IF V$ = "" THEN V$ = VL$
INPUT "Distance (with + or -) ", D$
IF D$ = "" THEN D$ = DL$
INPUT "Acceleration ", A$
IF A$ = "" THEN A$ = AL$
INPUT "Looping? Y/N ", LP$
LpM$ = "": TDel$ = "": EndLp$ = ""
IF LP$ = "Y" OR LP$ = "y" THEN
INPUT "Number of Loops ", L$
LpM$ = LoopM$: TDel$ = TDelay$: EndLp$ = EndLoop$
END IF
GOSUB SetCMD
INPUT "Make this the Wilhelmy Cycle? Y/N ", WilCyc$
IF WilCyc$ = "Y" THEN WilhelmyCMD$ = CMD$
IF WilCyc$ = "y" THEN WilhelmyCMD$ = CMD$
GOSUB MenuRefresh
RETURN
```

FileSave:

```
OPEN Fi$ FOR OUTPUT AS 1
WRITE #1, Fi$
WRITE #1, Volts0, VoltsM, CalibWeight, VtoMFactor
WRITE #1, Fiber$, Liquid$, Elv, Diameter, Temperature
WRITE #1, Samples
```

```

FOR J = 0 TO 20
WRITE #1, J, Angle(J), Energy(J), AveMass(J),
Deviation(J)
NEXT J
FOR J = 0 TO 20
FOR I = 1 TO Samples
WRITE #1, Mass(J, I)
NEXT I
NEXT J
CLOSE #1
RETURN

```

ReadFile:

```

INPUT "File Name ", Fil$
OPEN Fil$ FOR INPUT AS 1
INPUT #1, Fil$
INPUT #1, Volts0, VoltsM, CalibWeight, VtoMFactor
INPUT #1, Fiber$, Liquid$, Elv, Diameter, Temperature
INPUT #1, Samples
FOR J = 0 TO 20
INPUT #1, J, Angle(J), Energy(J), AveMass(J),
Deviation(J)
NEXT J
FOR J = 0 TO 20
FOR I = 1 TO Samples
INPUT #1, Mass(J, I)
NEXT I
NEXT J
CLOSE #1
RETURN

```

Stoppit:

```

CMD$ = " S "
GOSUB CMDWriter
RETURN

```

Reader: REM + + + + + = = = = Transfer from PC21 to IBM bus, 1 character at a time

```

BYTE = INP(ADDRESS% + 1)
IF MESSAGE AND NOT BYTE THEN RETURN
answer = INP(ADDRESS%)
OUT ADDRESS% + 1, (CONTROL OR RECEIVED)
MessByte: BYTE = INP(ADDRESS% + 1)
IF MESSAGE AND BYTE THEN GOTO MessByte
OUT ADDRESS% + 1, (CONTROL AND NOT RECEIVED)
CHAR$ = CHR$(answer)
answer$ = answer$ + CHAR$
IF CHAR$ = CHR$(13) THEN RETURN ELSE GOTO Reader
RETURN

```

CMDWriter: 'Sends instructions to PC21 1 character at a time

```

FOR I = 1 TO LEN(CMD$)

```

```

CHAR$ = MIDS(CMD$, I, 1)
GOSUB Transmitter
NEXT I
CHAR$ = CHR$(13)
GOSUB Transmitter
RETURN

```

Transmitter:

```

BYTE = INP(ADDRESS% + 1)
IF IDBREADY AND NOT BYTE THEN GOTO Transmitter
OUT ADDRESS%, ASC(CHAR$)
OUT ADDRESS% + 1, (CONTROL OR IDBREADY)
IDByte: BYTE = INP(ADDRESS% + 1)
IF IDBREADY AND BYTE THEN GOTO IDByte
OUT ADDRESS% + 1, (CONTROL AND NOT IDBREADY)
RETURN

```

InitializePC21:

```

ADDRESS% = 768 ' PC21 IBM bus address
CONTROL = 96 'This is the normal state of the Control Byte
STOPPED = 2 ' (is the motor moving)
CRASH = 4 ' Control Bit 2
LOADRDY = 4 ' Status Bit 2
INTACK = 8 'Control Bit 3
MESSAGE = 8 'Status Bit 3
IDBREADY = 16 'Control Bit 4
FAULT = 32 'Control Bit 5
INTERRUPT = 64 ' Control Bit 6
RECEIVED = 128 ' Control Bit 7
OUT ADDRESS% + 1, (CONTROL OR CRASH) 'Control Bit 2 high
OUT ADDRESS% + 1, (CONTROL AND NOT CRASH) 'Control Bit 2 low
FOR Y = 1 TO 1000
NEXT 'wait for BMA
OUT ADDRESS% + 1, (CONTROL AND NOT FAULT) 'Control Bit 5 low
OUT ADDRESS% + 1, (CONTROL OR FAULT) 'Control Bit 5 high
RETURN

```

ReadStatus:

```

IF INP(Status) AND 128 THEN DigInp = 1 ELSE DigInp = 0
'For digital Input
RETURN

```

ReadTemp: 'For Cole Parmer Model 20B with 134 ADC

```

OUT ADC, 0
FOR J = 0 TO NThermometers
FOR N = 0 TO 7
GOSUB ReadVolt
V(N) = V
NEXT N
C = (V(3) - V(0)) / K(J) - 273
FOR N = 1 TO 7
IF N = 3 THEN GOTO NextN

```

```

      V = (V(N) - V(0)) * G(J)
GOSUB LinearizeE
      LOCATE 10, 1
      PRINT "Thermometer #"; J, "T.C. #"; N -INT(N / 3) + INT(N / 6)
      PRINT USING "####.#"; T;
NextN:  NEXT N
      NEXT J
RETURN

```

ReadVolt:

```

      OUT ADC, J * 16 + N 'Select Channel
      x = INP(ADC)      'Start conversion
      TOT = 0
      AVERAGE = 10    'Set average larger for smoother data
      FOR x = 1 TO AVERAGE
      TOT = TOT + INP(ADC + 1) * 256 + INP(ADC)
      NEXT x
      TOT = TOT / AVERAGE
      V = (TOT - 32768!) * .152588
RETURN

```

LinearizeE:

```

      V = V + C * 6.1
      IF V < 366 THEN T = V / 6.1: RETURN
      IF V < 836 THEN T = 60 + (V - 366) / 6.72: RETURN
      IF V < 1487 THEN T = 130 + (V - 836) / 7.223: RETURN
      IF V < 2494 THEN T = 220 + (V - 1487) / 7.74: RETURN
      IF V < 5633 THEN T = 350 + (V - 2494) / 8.049: RETURN
      IF V < 6878 THEN T = 740 + (V - 5633) / 7.785: RETURN
      T = 900 + (V - 6878) / 7.6: RETURN

```

LinearizeJ:

```

      V = V + C * 5.2
      IF V < 411 THEN T = V / 5.2: RETURN
      IF V < 2738 THEN T = 79 + (V - 411) / 5.527: RETURN
      IF V < 3367 THEN T = 500 + (V - 2738) / 5.72: RETURN
      IF V < 3911 THEN T = 610 + (V - 3367) / 6.05: RETURN
      T = 700 + (V - 3911) / 6.33: RETURN

```

The following list describes the functions of the subroutines in the Wilhelmy balance data analysis program written in AmigaBasic.

Main: Main program loop.

Start: Program "sleeps" here until called by user's menu interrupt.

Libs: Loads libraries of system calls.

ArrayDimensions: Defines all data arrays and allocates space to them.

ScreenSetup: Sets up screen, window, and pallettes.

Initialize: Initializes all constants.

InitializeMenu: Initializes the menu selections.

CheckMenu: Arrival point when user makes a menu selection. Finds column and routes to submenus.

Filemenu: Checks first column of menu items and routes to appropriate subroutine.

Calcs: Checks second column of menu items and routes to appropriate subroutine.

Graph: Checks third column of menu items and routes to appropriate subroutine.

NSamples: Inputs the number of samples.

GraphData: Produces a graph of force data.

DataEntry: Inputs data on fiber designation and diameter.

Calculations: Calculates contact angles from force and perimeter.

WriteFile: Writes out data files.

ReadFile: Reads in data files.

Palet: Sets the screen pallettes.

Dir: Displays the directory of the current directory.

Dir0: Displays directory of drive df0:.

Dir1: Displays directory of drive df1:.

Cleanup: Clears the screen.

FindAverage: Finds average and standard deviation of a set of data points.

Quit: Closes libraries, resets menu, ends program operation.

WriteImage: Saves screen image to disk file.

EnterImageName: Inputs file name for saving image of graphed data.

WILHELMY BALANCE DATA ANALYSIS PROGRAM SOURCE CODE

```

REM === Wilhelmy Balance Calculations Program
REM === Copyright April 10, 1989 Mark Waterbury, for the
REM Composite Materials and Structures Center
REM Michigan State University
GOSUB ScreenSetup
CLEAR ,25000& 'clears basic stack
CLEAR ,50000& 'clears data memory space
DEFINT I,J,k 'defines these variables as integers
Main:
GOSUB Libs 'Initializes Amiga LIBRARYs and FUNCTIONS
GOSUB ArrayDimensions 'Sets sizes of array variables
GOSUB Initialize 'Sets Graphics and other constants
GOSUB InitializeMenu 'Sets screen menu system

Start:
CLS
ON MENU GOSUB CheckMenu : MENU ON
Unfinished = -1
WHILE Unfinished
    SLEEP ' event driven
WEND

Libs:
DECLARE FUNCTION xOpen& LIBRARY
DECLARE FUNCTION xRead& LIBRARY
DECLARE FUNCTION xWrite& LIBRARY
DECLARE FUNCTION AllocMem&() LIBRARY
LIBRARY "dos.library"
LIBRARY "exec.library"
LIBRARY "graphics.library"
RETURN

ArrayDimensions:
DIM Mass(20, 100), AveMass(20), Deviation(20), Angle(20), Energy(20)
DIM BPlaneSI&(5),BPlaneLI&(5) 'For picture Loader and Saver
DIM cTab%(32)
RETURN

ScreenSetup:
SMode = 4: Depth = 4: WMode = 0
WindowTitle$ = ""
ScreenX = 640:ScreenY = 400
SCREEN 1,ScreenX,ScreenY,Depth,SMode
WINDOW 1,WindowTitle$,,WMode,1
RETURN

Initialize:
GOSUB Palet

```

```

COLOR 10,0
Samples = 10
RETURN

```

InitializeMenu:

```

MENU 1,0,1,"File"
MENU 1,1,1,"Directory"
MENU 1,2,1,"Directory of drive 0"
MENU 1,3,1,"Directory of drive 1"
MENU 1,4,1,"Read File"
MENU 1,5,1,"Write File"
MENU 1,6,1,"Read image"
MENU 1,7,1,"Write image"
MENU 1,8,1,"Write Image Name"
MENU 1,9,1,"Quit"
MENU 2,0,1,"Calcs"
MENU 2,1,1,"Number of Samples"
MENU 3,0,1,"Graph"
MENU 3,1,1,"Graph Data"
MENU 3,2,1,"Palet Reset"
MENU 3,3,1,"Clear Screen"

```

```
RETURN
```

CheckMenu:

```

MenuId = MENU(0)
MenuItem = MENU(1)
ON MenuId GOSUB Filemenu,Calcs,Graph,Batch,Dist
RETURN

```

Filemenu:

```

O N M e n u I t e m G O S U B D i r
,Dir0,Dir1,ReadFile,WriteFile,ReadImage,WriteImage,EnterImageName,Quit
RETURN

```

Calcs:

```

ON MenuItem GOSUB NSamples,Calculations
RETURN

```

Graph:

```

ON MenuItem GOSUB GraphData,Palet,Cleanup
RETURN

```

NSamples:

```

INPUT "Number of samples per set ",Samples
RETURN

```

GraphData:

```

LINE (0,200)-(640,200),1
FOR J = 0 TO 20
  FOR I = 1 TO Samples
    PSET (J * (Samples + 5) + I,200 - Mass(J,I) * 500),1
  NEXT I
NEXT J
RETURN

```

DataEntry:

```

CLS
INPUT "Fiber name ", Fiber$
INPUT "Fiber diameter (microns) ", Diameter
INPUT "Liquid name", Matrix$
INPUT "Liquid Surface Tension (mJ/M^2) ", Elv
INPUT "Liquid temperature ", Temperature

```

RETURN

Calculations:

```

FOR J = 0 TO 20
  Newtons = 9.807 * AveMass(J) / 1000000&
  Perimeter# = Diameter * Pi / 1000000&
NEXT J
RETURN

```

WriteFile:

```

INPUT "File Name ", Fil$
OPEN Fil$ FOR OUTPUT AS 1
  WRITE #1, Fil$
  WRITE #1, Volts0, VoltsM, CalibWeight, VtoMFactor
  WRITE #1, Fiber$, Liquid$, Elv, Diameter, Temperature
  WRITE #1, Samples
  FOR J = 0 TO 20
    WRITE #1, J, Angle(J), Energy(J), AveMass(J), Deviation(J)
  NEXT J
  FOR J = 0 TO 20
    FOR I = 1 TO Samples
      WRITE #1, Mass(J, I)
    NEXT I
  NEXT J
CLOSE #1
RETURN

```

ReadFile:

```

INPUT "Change Sign? 1/0 ", ChangeSign
INPUT "File name ", Fil$
OPEN Fil$ FOR INPUT AS 1
  INPUT #1, Fil$
  INPUT #1, Volts0, VoltsM, CalibWeight, VtoMFactor
  INPUT #1, Fiber$, Liquid$, Elv, Diameter, Temperature
  INPUT #1, Samples
  FOR J = 0 TO 20
    INPUT #1, J, Angle(J), Energy(J), AveMass(J), Deviation(J)
  NEXT J
  FOR J = 0 TO 20
    FOR I = 1 TO Samples
      INPUT #1, Mass(J, I)
    IF ChangeSign THEN Mass(J,I) = -Mass(J,I)
  NEXT I
NEXT J
CLOSE #1

```

RETURN

Palet:

```
FOR I = 2 TO 9
  PALETTE I,I/9,I/9,I/9
NEXT I
PALETTE 10,1,1/2,0
PALETTE 11,1,0,1
PALETTE 12,0,1,1
PALETTE 13,1,1,0
PALETTE 14,0,1,0
PALETTE 15,0,0,1
PALETTE 0,1,1,1
PALETTE 1,0,0,0
```

RETURN

Dir:

```
FILES
RETURN
```

Dir0:

```
FILES "df0:"
RETURN
```

Dir1:

```
FILES "df1:"
RETURN
```

Cleanup:

```
CLS
RETURN
```

FindAverage:

```
Sum = 0
FOR k = 1 TO Samples
  Sum = Sum + Mass(J, k)
NEXT k
  AveMass(J) = Sum / Samples
Sum = 0
FOR k = 1 TO Samples
  Sum = Sum + (AveMass(J) - Mass(J, k)) ^ 2
NEXT k
  Sum = Sum / Samples
  Deviation(J) = SQR(Sum)
RETURN
```

Quit:

```
MENU RESET
LIBRARY CLOSE
STOP
```

ReadImage:

```

INPUT "Enter file name ",PicNameLI$
PictureLI PicNameLI$
Fil$ = PicNameLI$
FilMen$ = "File Name " + Fil$
GOSUB GetAddr$
GOSUB Palet1
NFibers = 0
RETURN

```

GetAddr\$:

```

sWindow& = WINDOW(7)
sScreen& = PEEKL(sWindow& + 46)
sViewPort& = sScreen& + 44
sRastPort& = sScreen& + 84
sColorMap& = PEEKL(sViewPort& + 4)
colorTab& = PEEKL(sColorMap& + 4)
sBitMap& = PEEKL(sRastPort& + 4)
scrDepth% = PEEK(sBitMap& + 5)
nColors% = 2^scrDepth%
FOR kk = 0 TO nColors% -1
  cTab%(kk) = PEEKW(colorTab& +(kk*2))
  CMap%(kk) = INT(cTab%(kk)/256)
NEXT
RETURN

```

WriteImage:

```

PictureSI WritePicName$
RETURN

```

EnterImageName:

```

LOCATE 24,1: INPUT "Image Name ",WritePicName$
RETURN

```

BIBLIOGRAPHY

BIBLIOGRAPHY

Ashbee, K.H.G., Ashbee, E., Photoelastic Study of Epoxy Resin/Graphite Fiber Load Transfer, *J. of Composite Mat.*, 22, Jul. 1988, pp. 602-615.

Asloun, El. M., Donnet, J.B., Guilpain, G., Nardin, M., Schultz, J., On the Estimation of the Tensile Strength of Carbon Fibers at Short Lengths, *J. of Materials Science*, 24, 1989, pp. 3504-3510.

ASTM D 3171 - 76, ASTM Standards and Literature References for Composite Materials, 1987 (A), pp. 169-172.

ASTM E 562 - 83, ASTM Standards and Literature References for Composite Materials, 1987 (B), pp. 511-517.

Atkinson, C., On Stress Singularities and Interfaces in Linear Elastic Fracture Mechanics, *Int. J. of Fracture*, 13, Dec. 1977, pp. 807-820.

Bailey, J.E., Parvizi, A., On Fibre Debonding Effects and the Mechanism of Transverse-Ply failure in Cross-Ply Laminates of Glass Fibre/Thermoset Composites, *J. Mat. Science*, 16, Jan. 1981, pp. 649-659.

Bascom, W.D., Boll, D.J., Fuller, B., Phillips, P.J., Fractography of the Interlaminar Fracture of Carbon-Fibre Epoxy Composites, *J. Mater. Sci.*, 20, 1985, 3184.

Bascom, W.D., Gweon, S.Y., Fractography and Failure Mechanisms of Carbon Fiber-Reinforced Composite Materials, in *Fractography and Failure Mechanisms of Polymers and Composites*, Elsevier, 1989, pp. 351-385.

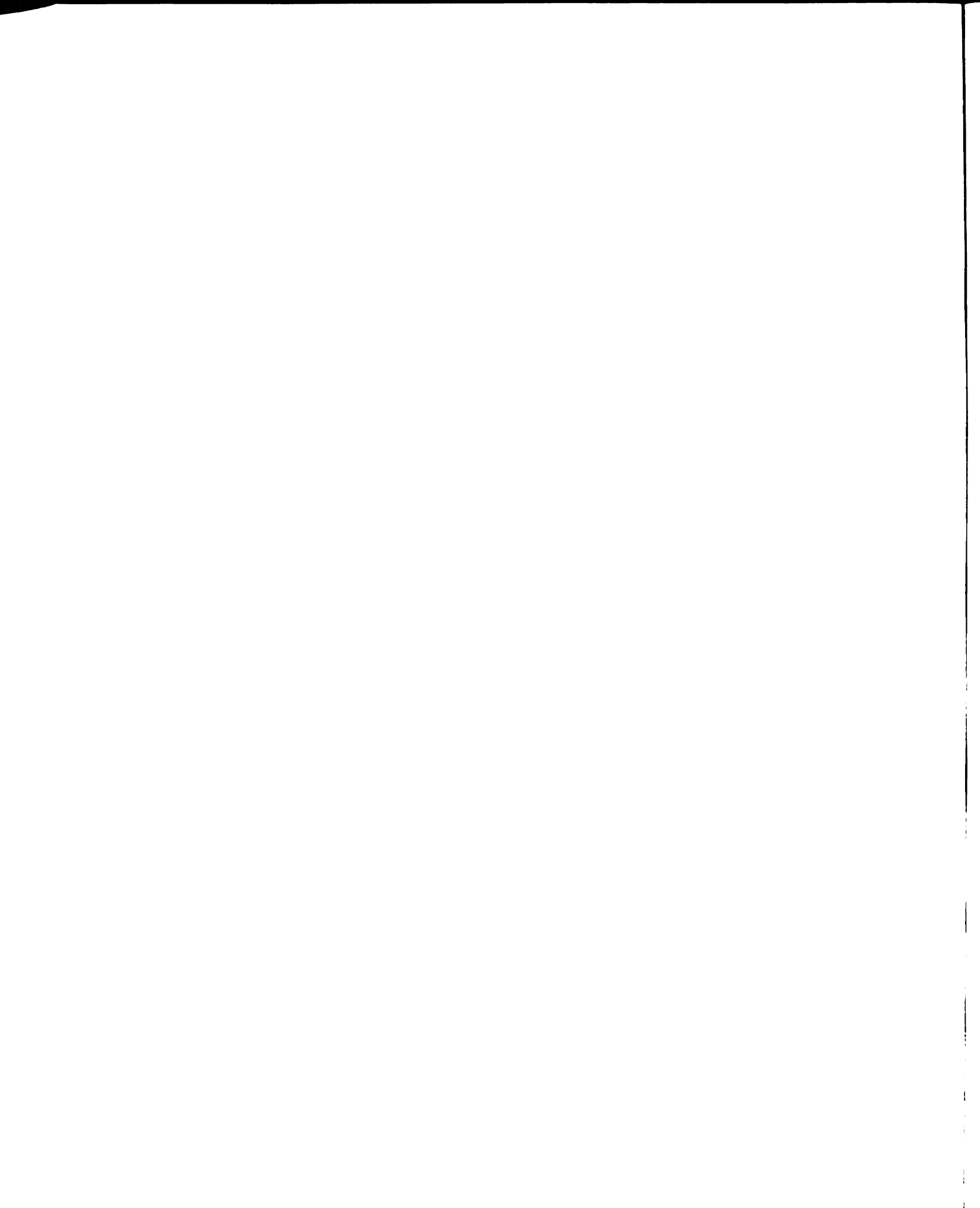
Bascom, W.D., Jensen, R.M., Stress Transfer in Single Fiber/Resin Tensile Tests, *J. Adhesion*, 19, Jan. 1986, pp. 219-239.

Bascom, W.D., Interfacial Adhesion of Carbon Fibers, NASA CR-178306, Aug. 1987.

Bascom, W.D., NASA Report No. CR-178306, Aug. 1987.

Bascom, W.D., Yon, K-J., Jensen, R.M., Cordner, L., The Adhesion of Carbon Fibers to Thermoset and Thermoplastic Polymers, *J. Adhesion*, 34, 1991, pp. 79-98.

Binbergen, F.L., Natural and Artificial Heterogeneous Nucleation in Polymer Crystallization, *J. of Polymer Science Symposium*, 59, 1977, pp. 11-29.



- Brady, R.L., Porter, R.S., Interfacial Crystallization and Adsorption in Polycarbonate/Carbon Fiber Composites, *J. Thermo. Comp. Mat*, 2, Jul. 1989, pp. 164-171.
- Broutman, L.J., Measurement of the Fiber-Polymer Matrix Interfacial Strength, *ASTM STP 452*, Jan. 1969, pp. 27-41.
- Cantwell, W.J., Roulin-Moloney, A.C., Fractography and Failure Mechanisms of Unfilled and Particulate Filled Epoxy Resins, in *Fractograph and Failure Mechanisms of Polymers and Composites*, Elsevier, 1989, 233-290.
- Cebe, P., Hong, S., Crystallization Behaviour of Poly(ether-ether-ketone), *Polymer*, 27, Aug. 1986, pp. 1183-1192.
- Chai, H., Interlaminar Shear Fracture of Laminated Composites,, *Int. J. of Fracture*, 43, 1990, pp. 117-131.
- Cilley E., Roylance D., Schneider N., Composite Materials, Testing and Design (Third Conference), *ASTM STP 546*, 1974, pp. 237-249.
- Cooke, T.F., High Performance Fiber Composites With Special Emphasis on the Interface, *J. Polymer Eng.*, 7, (3), Jan. 1987, pp. 197-254.
- Crasto, A.S., Corey, R., Dickinson, J.T., Subramanian, R.V., Eckstein, Y., Correlation of Photon and Acoustic Emission with Failure Events in Model Composites, *Comp. Sci. Tech.*, 30, 1987, pp. 35-58.
- Crosby, J.M., Drye, T.R., Fracture Studies of Discontinuous Fiber Reinforced Thermoplastic Composites, *J. Reinforced Plastics*, 6, Apr. 1987, pp. 162-169.
- Curtin, W.A., Fiber Fragmentation in a Single-Filament Composite, *Physical Review Lett*, (In press).
- Curtis, P.T., An Investigation of the Mechanical Properties of Improved Carbon Fibre Composites Materials, *J. of Composite Materials*, 21, Dec. 1987, pp. 1118-1144.
- Dave, R., Lorenzo, L., A Note on Polymeric Inner-Layered Single Fiber Interfacial Strength Determination, *Polymer Composites*, 10, (3), Jun. 1989, pp. 199-201.
- Denison, P., Jones, F.R, Watts, J.F., A Quantification and Investigation of Surface Micro-porosity in Carbon-Fibres Using Labelling and XPS, *Surface Interface Analysis*, 12, 1988, pp. 455-460.
- Deslandes, Y., Day, M., Sabir, N.-F., Suprunchuk, T., Crystallization of Poly(Aryl-Ether-Ether-Ketone): Effect of Thermal History of the Melt on Crystallization Kinetics, *Polymer Composites*, 10, (5), Oct. 1989, pp. 360-366.
- Di Landro L., Pegoraro M., Carbon Fiber Thermoplastic Matrix Adhesion, *J. of Materials Science*, 22, 1987, pp. 1980-1986.
- Dilangro, L., Dibenedetto, A.T., Groeger, J., The Effect of Fiber-Matrix Stress Transfer on the Strength of Fiber-Reinforced Composite Materials, *Polymer Composites*, 9, (3), Jun. 1988, pp. 209-221.

- DeBenedetto, A.T., Nicolais, L., *Plast*, 10, (5), 1979, p. 83.
- DiBenedetto, Evaluation of Fiber Surface Treatments in Composite Materials, *Pure & Appl. Chem.* 57, (11), 1985, pp. 1659-1665.
- DiBenedetto A.T, Nicolais L., Ambrosio L., Groeger J., Stress Transfer and Fracture in Single Fiber/Epoxy Composites, *ICCI I*, Jul. 1986, pp. 47-54.
- Drzal, L.T., Rich, M.J., Camping, J.D., Park, W.J., Interfacial Shear Strength and Failure Mechanisms in Graphite Fiber Composites, *Reinforced Plastics/Composites Institute Proc.* 1980 (A), Sect. 20-C, pp. 1-7.
- Drzal, L. T., Rich, M. J., Camping, J. P., Park, W. J., "A Single Filament Technique for Determining Interfacial Shear Strength and Failure Mode in Composite Materials", *Proceedings of 1980 Conference, Reinforced Plastics and Composites Institute, SPI, Paper 20C*, 1980 (B).
- Drzal, L.T., Hammer, G.E., Graphite Fiber Surface Analysis by X-Ray Photoelectron Spectroscopy and Polar/Dispersive Free Energy Analysis, *Applications of Surface Science*, 4, 1980, pp. 340-355.
- Drzal L.T., Rich, M.J., Lloyd, P.F., Adhesion of Graphite Fibers to Epoxy Matrices: II. The Effect of Fiber Finish, *J. Adhesion*, 16, Jan. 1983, pp. 133-152.
- Drzal, L.T., Rich, M.J., Lloyd, P.F., Adhesion of Graphite Fibers to Epoxy Matrices: I. The Role of Fiber Surface Treatment, *J. Adhesion*, 16, Jan. 1982, pp. 1-30.
- Drzal, L.T., Rich, M.J., Progress report, "Improved Materials for Composite and Adhesive Joints", period 9/1/81 - 8/31/82, Contract # F33615-81-C-5056, Dayton Research Institute, U. Dayton Report # UDR-TR-82-118.
- Farinato, R.S., Kaminski, S.S., Courter, J.L., Acid-Base Character of Carbon Fiber Surfaces, *J. Adh. Sci. Tech.*, 1990, (in press).
- Favre J.P., Perrin J., Carbon Fibre Adhesion to Organic Matrices, *J. Mater. Sci.*, 7, Jan. 1972, pp. 1113-1118.
- Figueroa, J.C., Schadler, L.S., Campbell, L., Filament Fragmentation Phenomena, *Mat. Res. Soc. Symp. Proc.*, 170, 1990, pp. 65-70.
- Folkes, M.J., Wong, W.K., Determination of Interfacial Shear Strength in Fibre-Reinforced Thermoplastic Composites, *Polymer*, 28, Jul. 1987, pp. 1309-1314.
- Fraser, W.A., Ancker, F.H., DiBenedetto, A.T., Elbirli, B., Evaluation of Surface Treatments for Fibers in Composite Materials, *Polymer Composites*, 4, (4), 1983, pp. 238-248.
- Galiotis, C., Melanitis, N., Batchelder, D.N., Robinson, I.M., Residual Strain Mapping in Carbon Fibre/PEEK Composites, *Composites*, 19, (4), July 1988, pp. 321-324.

Galiotis, C., Melanitis, N., Tetlow, P. L., and Davies, C. K. L., "Interfacial Shear Stress Mapping in Model Composites," Technomic Publishing Co., E. Lansing, MI, Jun. 1990, pp. 276-286.

Garton A., Stevenson W.T., Crosslinking of Epoxy Resins at Interfaces. IV. Anhydride-Cured Resins at Carbon and Graphite Surfaces, *J. of Polym. Sci: Pt. A*, 26, Jan. 1981, pp. 541-557.

Gaur, U., Desio, G., Miller, B., Measuring Fiber/Matrix Adhesion in Thermoplastics Composites, *Plastics Engineering*, Oct. 1989, pp. 43-45.

GE, Lexan Polycarbonate Resin Properties Guide, GE Plastics, 1988.

Golovoy, A., Zinbo, M., Water Sorption and Hydrolytic Stability of Polycarbonates, *Polymer Eng. and Science*, 29, (24), Dec. 1989, pp. 1733-1737.

Griffith, A.A., *Phil. Trans. R. Soc.*, A221, 1921, p. 163.

Griffith, A.A., *Proc. 1st Int. Congr. Appl. Math.*, Delft, Holland, 1924, p. 55.

Gutowski, W., Physico-Chemical Criteria for Maximum Adhesion. Part I: Theoretical Concepts and Experimental Evidence, *J. Adhesion*, 19, Jan. 1985, pp. 29-49.

Hamstad M.A., Moore R.L., Acoustic Emission from Single and Multiple Kevlar 49 Filament Breaks, *J. Comp. Mater.*, 20, Jan. 1986, pp. 46-66.

Henstenburg, R.B., Phoenix, S.L., Interfacial Shear Strength Studies Using the Single-Filament-Composite Test. Part II: A Probability Model and Monte Carlo Simulation, *Polymer Composites*, 10, (5), Dec 1989, pp. 389-408.

Hibbs, M.F., Bradley, W.L., Correlations Between Micromechanical Failure Processes and the Delamination Toughness of Graphite/Epoxy Systems, *ASTM STP 948*, 1987, p. 389.

Hinkley, J.A., Bascom, W.D., Allred, R.E., Interlaminar Fracture in Carbon Fiber/Thermoplastic Composites, *Mat. Res. Soc. Symp.*, 170, Jan. 1990, pp. 351-356.

Hodge, D.J., Middlemiss, B.A, Peacock, J.A., Correlation Between Fibre Surface Energetics and Fibre-Matrix Adhesion in Carbon Fibre Reinforced PEEK Composite, *Mat. Res. Symp. Proc*, 170, Jan. 1990, pp. 327-339.

Hoffman, W.P., Elings V.B., Gurley J.A., Scanning Tunneling Microscopy on Carbon Fibers, *Carbon*, 26, Jul. 1988, pp. 754-757.

Hooke, K.J., Agrawal, R.K., Drzal, L.T., *J. of Adhesion*, 32, 1990, pp. 157-170.

Hsiao, B.S., Chen, E.J.H., Study of Transcrystallization in Polymer Composites, *Mat. Res. Symp. Proc*, 170, Jan. 1990, pp. 117-121.

Hughes, J.D.H., The Carbon Fibre/Epoxy Interface - A Review, *Composites Science and Technology*, 41, 1991, pp. 13-45.

Ishitani A., Application of X-Ray PhotoElectron Spectroscopy to Surface Analysis of Carbon Fiber, *Carbon*, 19, (4), 1981, pp. 261-275.

Ismail M.K., Structure and Active Surface Area of Carbon Fibers, *Carbon*, 25, (5), 1987, pp. 653-662.

Jang, B., Liu, C.W., Wang, C.Z., Shih, W.K., Mechanical Properties and Morphology of Crystalline Polymers and Their Continuous Fiber Composites, *J. of Thermoplastic Composite Materials*, 1, Jul. 1988, pp. 242-275.

Jaworske, D.A., Gaier, J.R., Hung, C.C., Banks, B.A., Properties and Potential Applications of Brominated P-100 Carbon Fibers, *SAMPE Quarterly*, 18, (1), Oct. 1986, pp. 9-14.

Jaworske, D.A., Maciag, C., Improving the Interlaminar Shear Strength of Carbon Fiber-Epoxy Composites Through Carbon Fiber Bromination, *Nasa Tech. Mem.* 100248, Dec 1987.

Jeronimidis, G., Parkyn, A.T., Residual Stresses in Carbon Fibre-Thermoplastic Matrix Laminates, *J. Comp. Mats.*, 22, May 1988, pp. 401-415.

Jock, C.P., Quantitative Optical Microscopy Fiber Volume Methods for Composites, *J. Reinf. Plast. and Comps.*, 5, Apr. 1986, pp. 110-119.

Johannesson, T., Sjoblom, P., Selden, R., The Detailed Structure of Delamination Fracture Surfaces in Graphite/Epoxy Laminates, *J. Mat. Science*, 19, Jan. 1984, pp. 1171-1177.

Kardos J.L., Regulating the Interface in Graphite/Thermoplastic Composites, *J. Adhesion*, 5, 1973, pp. 119-138.

Katagiri, G., Ishida, Hid., Ishitani, A., Raman Spectra of Graphite Edge Planes, *Carbon*, 26, 4, Jan. 1988, pp. 565-571.

Kavanagh, A., Schlogl R., The Morphology of Some Natural and Synthetic Graphites, *Carbon*, 26, 1, Jan. 1988, pp. 23-32.

Keith H.D., Padden F.J., A Discussion of Spherulitic Crystallization and Spherulitic Morphology in High Polymers, *Polymer*, 27, Jan. 1986, pp. 1463-1471.

Keller, A., Polymer Crystallization: A Survey and Salient Current Issues, *J. Poly. Sci. P. Sym*, 59, Jan 1977, pp. 1-10.

Kelley, A., Tyson, W.R., *J. Mech. Phy. Solids*, 13, 1965, p. 329.

Kelley, A., Macmillan, N.H., *Strong Solids*, Clarendon Press, 1986.

Kinloch, A.J., Kodokian, G.K.A., On the Calculation of Dispersion and Polar Force Components of the Surface Free Energy, *J. Adhesion*, 34, 1991, pp. 41-44.

Kolle, J.J., Lin, K.Y., Mueller, A.C., A Micro/Macro Approach to Fracture in Composites, *Polymer Composites*, 11, (6), 1990, pp. 314-321.

Kumamaru, F., Oono, T., Kajiyama, T., Suehiro, K., Takayanagi, M., Epitaxial Crystallization of Nylon 6 Cast from Solution on the Surface of Poly(p-phenylene Terephthalamide Filament, *Polymer Composites*, 4, (2), Apr. 1983 (A), pp. 135-140.

Kumamaru, F. Oono, T., Kajiyama, T., Takayanagi, M., Interfacial Interaction between Poly(p-phenylene Terephthalamide) Filament and Nylon 6 Matrix Crystallized from the Melt, *Polymer Composites*, 4, (2), April, 1983 (B), pp. 141-148.

Lauke B., W. Pompe, Relation Between Work of Fracture and Fracture Toughness of Short-Fibre Reinforced Polymers, *Comp. Sci. Tech.*, 31, Jan. 1988, pp. 25-33.

Lee W.I., Talbott M.F., Springer G.S., Berglund, L.A., Effects of Cooling Rate on the Crystallinity and Mechanical Properties of Thermoplastic Composites, *J. of Reinf. Plastics and Comps.*, 6, Jan. 1987, pp. 2-12.

Lee Y., Porter R.S., Crystallization of Poly(etheretherketone) (PEEK) in Carbon Fiber Composites, *Polym. Eng. Sci.*, 26, (9), May 1986, pp. 633-639.

Lee, R.N., Carbon-Fiber Surface Properties, *Encyc. of Composites*, In Press.

Lhymn, C., Schultz, J.M., Strength and Toughness of Fibre-Reinforced Thermoplastics: Effect of Temperature and Loading Rate, *Composites*, 18, (4), Sep 1987, pp. 287-292.

Li S.K., Smith R.P., Neumann A.W. Wilhelmy Technique and Solidification Front Technique to Study the Wettability of Fibres, *J. Adhesion*, 17, 1984, pp. 105-122.

Ma, B.T. Schadler, L.S., Laird, C., Figueroa, J.C., Acoustic Emission in Single Filament Carbon/Polycarbonate and Kevlar/Polycarbonate Composites Under Tensile Deformation, *Polymer Composites*, 11, (4), Aug. 1990, pp. 211-216.

Maekawa, Z., Hamada, H., Yoshioka, S., Fiber Fragment Distribution in Embedded Single Filament Test, *ICCI II*, Jun. 1988, pp. 553-565.

Mahishi J.M., An Integrated Michromechanical and Macromechanical Approach to Fracture Behavior of Fiber-Reinforced Composites, *Eng. Fracture Mech.*, 25, (2), Jan. 1986, pp. 197-228.

Medellin-Rodrig, Phillips, P.J., Crystallization and Structure-Mechanical Property Relations in Poly(Aryl Ether Ether Ketone) [PEEK], *Poly. Eng. and Sci.*, 30, (14), Jul. 1990, pp. 860-889.

Medrano R.E, Gillis P.P., Weibull Statistics: Tensile and Bending Tests, *J. Am. Ceram. Soc.*, 70, (10), Oct. 1987, pp. 230-232.

Miller, B., Muri, P., Rebenfeld, L, A Microbond Method for Determination of the Shear Strength of a Fiber/Resin Interface, *Comp. Sci. Tech.*, 28, Jan. 1987, pp. 17-32.

Miller, A.G., Wingert, A.L., Fracture Surface Characterization of Commercial Graphite/Epoxy Systems, Nondestructive Evaluation and Flaw Criticality for Composite Materials, *ASTM STP 696*, 1979, pp. 223-273.

- Moore, G.A., Applications of Modern Metallographic Techniques, ASTM STP 480, 1970, pp. 3-48.
- Morris, G.E., Determining Fracture Directions and Fracture Origins on Failed Graphite/Epoxy Surfaces, Nondestructive Evaluation and Flaw Criticality for Composite Materials, ASTM STP 696, 1979, pp. 274-297.
- Mossner, L.S., Grulke, E.A., Effects of Thermodynamic Models on the Predictions of Free Volume Diffusion Theory for concentrated Polymer Solutions, J. of Applied Polymer Science, 35, 1988, pp. 923-936.
- Narkis, M., Chen, E.J.H., Review of Methods for Characterization of Interfacial Fiber-Matrix Interactions, Polymer Composites, 9, (4), Aug 1989, pp. 245-251.
- Netravali, A.N., Henstenburg, R., Phoenix, S.L., Schwartz, P., Interfacial Shear Strength Studies Using the Single-Filament-Composite Test. I: Experiments on Graphite Fibers in Epoxy, Polymer Composites, 10, (4), Aug 1989.
- Netravali, A.N., Schwartz, P., Phoenix, S.L., Study of Interfaces of High-Performance Glass Fibers and DGEBA-based Epoxy Resins Using Single-Fiber-Composite Test, Polymer Composites, 10, (6), Dec 1989, pp. 385-388.
- Netravali, A.N., Topoleski, L.T.T., Sachse, W.H., Phoenix, S.L., An Acoustic Emission Technique for Measuring Fiber Fragment Length Distributions in the Single-Fiber-Composite Test, 35, 1989, pp. 13-29.
- Norita T., Junichi M., Matsuda H., Effect of Surface Treatment of Carbon Fiber on Mechanical Properties of CFRP, ICCI I, Jul. 1986, pp. 123-132.
- Palley, I., Signorelli, A.J., New Method for Evaluation of Fiber/Matrix Adhesion, J. Adhesion, 25, 1988, pp. 161-167.
- Parker, D.S., Yee, A.F., Factors Influencing the Mode I Interlaminar Fracture Toughness of a Rubber Toughened Thermoplastic Matrix Composite, J. Thermo. Comp. Mat, 2, Jan. 1989, pp. 2-18.
- Parker, D.S., Yee, A.F., Toughening of a Thermoplastic Matrix Composite: Processing Issues, Adv. in Mat. and Process Engineering, 1988, pp. 270-279.
- Peacock J. A., Fife B., Nield E., Crick R. A., Examination of the Morphology of Aromatic Polymer Composite (APC-2) Using an Etching Technique, ICCI I, Jul. 1986, pp. 299-306.
- Peacock, J.A., Fife, B., Nield, E., Barlow, C.Y., A Fibre-Matrix Interface Study of Some Experimental PEEK/Carbon-Fibre Composites, Composite Interfaces, ICCI II, 1986, pp. 143-149.
- Penn, L.S., Lee, S.M., Interpretation of Experimental Results in the Single Pull-out Filament Test, J. of Composites Technology and Research, 11, (1), Spring 1989, pp. 23-30.
- Peters, P.W.M., Springer, G.S., Effects of Cure and Sizing on Fiber-Matrix Bond Strength, J. Comp. Mats., 21, Feb. 1987, pp. 157-171.

- Phani, K.K., The Strength-Length Relationship for Carbon Fibres, *Composites Science and Technology*, 30, 1987, pp. 59-71.
- Piggott, M.R., The Effect of the Interface/Interphase on Fiber Composite Properties, *Polymer Composites*, 8, (5), Oct. 1987, pp. 291-297.
- Piggott M.R., Sanadi A., Chua P.S., Andison D., Mechanical Interactions in the Interphasial Region of Fibre Reinforced Thermosets, *Composite Interfaces, ICCI I*, 1986, pp. 109-121.
- Piggott M.R., Expressions Governing Stress-Strain Curves in Short Fibre Reinforced Polymers, *J. Mater. Sci.*, 13, Jan. 1978, pp. 1709-1716.
- Piggott M.R., Dai S.R., Debonding and Friction at Fibre-Polymer Interfaces. II: Macroscopic Model Experiments, *Comp. Sci. Tech.*, 31, Jan. 1988, pp. 15-24.
- Piggott, M.R., Andison, D., The Carbon Fibre-Epoxy Interface, *J. Reinf. P. & Comps*, 6, Jul. 1987, pp. 290-302.
- Piggott, M.R., Debonding and Friction at Fibre-Polymer Interfaces. I: Criteria for Failure and Sliding, *Comp. Sci. and Tech.*, 30, Jan. 1987, pp. 295-306.
- Plueddemann, E.P., Adhesion Through Silane Coupling Agents, *J. Adhesion*, 2, Jul. 1970, pp. 184-201.
- Purslow, D., Matrix Fractography of Fibre-Reinforced Thermoplastics, Part 1. Peel Failures, *Composites*, 18, 5, pp. 365-380.
- Reedy, E.D., Fiber Stress Concentrations in Kevlar/Epoxy Monolayers, *J. of Comp. Materials*, 19, Nov. 1985, pp. 533-543.
- Rich, M.J., Drzal, L.T., Interfacial Properties of Some High-Strain Carbon Fibers in an Epoxy Matrix, *J. Reinf. Plas. Comp*, 7, Mar. 1988, pp. 145-154.
- Rich.-Frاند. R., Naerheim, Y., Fracture Morphology of Graphite/Epoxy Composites, *J. Comp. Materials*, 17, Mar. 1983, pp. 105-113.
- Roche, E.J., Lavin, J.G., Parrish, R.G., The Mosaic Nature of the Graphite Sheet in Pitch-Based Carbon Fibers, *Carbon*, Sep. 1988, pp. 911-912.
- Sanadi A R., Piggott M.R., Interfacial Effects in Carbon-Epoxy: Part 2 Strength and Modulus With Short Random Fibres, *J. Mater. Sci.*, 20, Jan. 1987, pp. 431-437.
- Sargent J.P., Ashbee K.H.G., Detection and Measurement of Very Small Interfacial Gaps in GRP, *Composites Science and Technology*, 22, 1985, pp. 135-152.
- Schadler, L.S., Ma, B.T., Laird, C., Acoustic Emission in Single Filament Carbon/Polycarbonate and Kevlar/Polycarbonate Composites Under Tensile Deformation, *Polymer Composites*, 11, (4), Aug. 1990, pp. 211-216.
- Schultz, J., Lavielle, L., Martin, C., The Role of the Interface in Carbon Fibre-Epoxy Composites, *Adhesion Soc. Proc.*, 10, Feb. 1987, pp. 513-528.

- Shih G.C., Ebert E.J., Interface Strength Effects on the Compressive-Flexural/Shear Failure Mode Transition of Composites subjected to Four-Point Bending, *J. Mater. Sci.*, 21, Jan. 1986, pp. 3957-3965.
- Sideridis, E., The In-Plane Shear Modulus of Fibre Reinforced Composites as Defined by the Concept of Interphase, *Comp. Sci. and Technology*, 31, 1988, pp. 35-53.
- Stack G.M., Mandelkern L., On the Crystallization of High Molecular Weight Normal Hydrocarbons, *Macromolecules*, 21, Jan. 1988, pp. 510-514.
- Stringer, L.G., Comparison of the Shear Stress-Strain Behavior of Some Structural Adhesives, *J. Adhesion*, 18, 1985, pp. 185-196.
- Takemori, M.T., Polymer Fatigue Fracture Diagrams: BPA Polycarbonate, *Polymer Eng. and Science*, 28, 10, May 1988, pp. 641-647.
- Talbott M F., Springer G.S., Berglund, L.A., The Effects of Crystallinity on the Mechanical Properties of PEEK Polymer and Graphite Fiber Reinforced PEEK, *J. Comp. Mater.*, 21, Nov. 1987, pp. 1056-1081.
- Theocaris P.S., The Concept and Properties of Mesophase in Composites, *Composite Interfaces*, ICCI I, 1986, pp. 329-349.
- Theocaris P.S., Philippi T., Theoretical Evaluation of the Extent of the Mesophase in Particulate and Fibrous Composites, *J. Rein. Plas. Comp.*, 4, Jan. 1985, pp. 173-185.
- Thomason, J.L., Knoester, A., Application of Confocal Scanning Optical Microscopy to the Study of Fibre-Reinforced Polymer Composites, *J. of Mat. Sci. Let.*, 9, Mar. 1990, pp. 258-262.
- Tong Y., Jasiuk I., The Effect of Interface on the Mechanical Properties of Composites, *ICCI II*, 1988, *Composite Interfaces*, pp. 757-764.
- Tuinstra, F., Baer, E., Epitaxial Crystallization of Polyethylene on Graphite, *Polymer Letters*, 8, 1970, pp. 861-865.
- Underwood, F.M., Batchelder, D.N, Sharpe, D.J., The Raman Optomechanical Strain Gauge Adapted for Use in Carbon Fibre Composite Laminates, pp. 69-73.
- Wagner H.D., Steenbakkens L., Microdamage Analysis of Fibrous Composite Monolayers Under Tensile Stress, *J. of Materials Science*, 24, 1989.
- Wagner, H.D., Statistical Concepts in the Study of Fracture Properties of Fibres and Composites, *Application of Fracture Mechanics to Composite Materials*, Elsevier, 1988.
- Wagner, H. D. and Eitan, A., "Interpretation of the Fragmentation Phenomenon in Single-Filament Composite Experiments", *Journal of Materials Science*, 1990, (in press).

- Waterbury, M. C. and Drzal, L. T., "Interfacial Shear Strengths of Carbon Fibers in Bisphenol A Polycarbonate", ICCI III, Elsevier Science Publishing, New York, May, 1990.
- Waterbury, M. C., FiberTrack, Single fiber fragmentation data acquisition and analysis computer program, Copyright, M. C. Waterbury, 1990.
- Weibull, W., in Proceedings of the Royal Swedish Institute for Engineering Research, 151, 1939.
- Weibull, W., A Statistical Distribution Function of Wide Applicability, J. Applied Mech., 18, 1951, p. 293.
- Weinberg, M., Shear Testing of Neat Thermoplastic Resins and Their Unidirectional Graphite Composites, Composites, Nov. 1987, pp. 386-392.
- Wesson, S.P., Allred, R.E., Acid-Base Properties of Carbon and Graphite Fiber Surfaces, J. Adhes. Sci. Tech., 4, 4, Jan 1990, pp. 277-301.
- Wimolkiatisak A, Bell J.P., Interfacial Shear Strength and Failure Modes of Interphase-Modified Graphite-Epoxy Composites, Polymer Composites, 10, (3), Jun. 1989, pp. 162-172.
- Wright, W.W., The Carbon Fibre/Epoxy Resin Interphase - A Review - Part II, Composite Polymers, 3, 1990, pp. 360-401.
- Yatchmenoff, B., A New Confocal Scanning Optical Microscope, American Laboratory, Apr. 1988, pp. 58-66.
- Yip, P.W., Lin, S.S., Effect of Surface Oxygen on Adhesion of Carbon Fiber Reinforced Composites, Mat. Res. Soc. Symp. Proc., 170, 1990, pp. 339-344.
- Zeng H., Kong B., Investigations on the Structure and Properties of the Carbon Fiber/Nylon-10,10 Composites, Composite Interfaces, ICCI I, 1986, pp. 55-64.
- Zhu, Y., Zhou, B., He, G., Zheng, Z., A Statistical Theory of Composite Materials Strength, J. of Composite Materials, 23, Mar. 1989, pp. 280-287.

MICHIGAN STATE UNIV. LIBRARIES



31293007815834